# Reactions of Hydrogen and Oxygen Atoms on Interstellar Grain Analogues

A thesis submitted for the degree of Doctor of Philosophy

Michael David Ward

Department of Chemistry

University College London

2012

*To my grandparents, Dee and Brian*

I, Michael David Ward, confirm that the work presented in this thesis is my own. Where information has been derived from other sources, I confirm that this has been indicated in the thesis.

Signed,

# Abstract

The region of space between stars, the interstellar medium, has been found to contain over 160 chemical species to date. These molecules are contained within regions of gas and dust, measuring several light years across, known as interstellar dust clouds. Many of these molecular species are formed in the gas phase, for example, *via* the reactions of molecules with ions. However, some critical gas phase processes are often slow due to the low temperatures and pressures found in the interstellar medium and cannot readily account for the abundances of some species. Consequently reactions on the surfaces of interstellar dust grains are often invoked to explain the abundances some molecules. These dust grains represent approximately 1 % of the mass of a typical interstellar dust cloud and typically consist of carbon, silicates or metal oxides. The temperature of these interstellar dust grains is low enough (~ 10 K) that over time icy mantles consisting of simple atomic and molecular species can build up on their surfaces. Whether and how these simple species can be processed to form more complex molecules such as alcohols, simple sugars and potentially amino acids is a key astrochemical problem.

One way in which astrophysical ices can be processed to form more complex species is *via* the reactions of species within the ice with simple free radicals such as H, C, N and O. This thesis therefore presents experimental studies of the reactions of atomic species with some astrophysically relevant molecular ices under interstellar conditions. Since hydrogen and oxygen are the first and third most abundant elements in the interstellar medium respectively, these experiments have specifically focussed upon the reactions of hydrogen and oxygen atoms. In addition to the characterization of surface reactions between key astrochemical species, kinetic parameters for use in astrochemical models are derived from these experiments.

# Acknowledgements

Completing a PhD can either be an extremely stressful process or one of the most fulfilling experiences in life. I would like to thank the following people for helping to ensure that, in my case, it was the latter.

Firstly, I would like to thank my supervisor, Steve Price. His supervision, support and encouragement, both during my PhD and before, have been simply excellent. I would also like to thank my second supervisor, Wendy Brown, for all of her support and encouragement.

All of the members of the Price group who have helped to make these past four years so enjoyable. In particular, Elspeth Latimer, for showing me the way around the Cosmic Dust Lab, and Mike Parkes for all of his help, and, especially, for allowing me to put his early starts to good use!

All of my friends outside of the Price group, especially Andy Smith. Andy has been uniquely willing to listen to my physical chemistry related problems over the years and always gives a good impression of understanding them.

Finally, to my wife, Esther Radley. It's hard to imagine how this would have happened without you. Thank you.

# List of Publications

Listed below are the previous and expected future publications of the work presented in this thesis.

*Thermal Reactions of Oxygen Atoms with Alkenes at Low Temperatures on Interstellar Dust.*

Ward, M. D., Price, S. D., *Ap. J.*, 2011, **741**, *121*.

*Thermal Reactions of Oxygen Atoms with Carbon Disulfide at Low Temperatures on Interstellar Dust.*

Ward, M. D., Hogg, I. A., Price, S. D., *Mon. Not. R. Astron. Soc.* In print.

*Thermal Reactions of Hydrogen Atoms with Sulfur-Bearing Molecules at Low Temperatures on Interstellar Dust.*

Ward, M. D., Price, S. D., In preparation.

*A Thermal Route to Interstellar Hydroxylamine.*

Ward, M. D., Leong, K. M., Price, S. D., In preparation.

*Experimental Studies of the Astrochemical Reactivity of C—C and C—N Multiple Bonds.*

Ward, M. D., Watson, R. E., Price, S. D., In preparation.

# List of Acronyms and Abbreviations

| | |
|---|---|
| 2D | Two-dimensional |
| ASW | Amorphous Solid Water |
| BBO | β-Barium Borate |
| CFD | Constant Fraction Discriminator |
| DC | Direct Current |
| DFT | Density Functional Theory |
| EI | Electron Ionization |
| ER | Eley-Rideal |
| HOPG | Highly Oriented Pyrolitic Graphite |
| HV | High Vacuum |
| IR | Infra-red |
| ISM | Interstellar Medium |
| KD*P | Potassium Dideuterium Phosphate |
| LH | Langmuir-Hinshelwood |
| ML | Monolayer |
| MPI | Multi-photon Ionization |
| Nd:YAG | Neodymium-doped Yttrium Aluminium Garnet |
| np-ASW | Non-porous Amorphous Solid Water |
| PC | Personal Computer |
| PCI | Peripheral Component Interconnect |
| PICS | Partial Ionization Cross-Section |
| PTFE | Polytetrafluoroethylene |

| | |
|---|---|
| RAIRS | Reflection-absorption Infra-red Spectroscopy |
| REMPI | Resonance Enhanced Multi-photon Ionization |
| TDC | Time to Digital Converter |
| TMP | Turbomolecular Pump |
| TPD | Temperature Programmed Desorption |
| TOF | Time of Flight |
| TOFMS | Time of Flight Mass Spectrometer |
| UCL | University College London |
| UHV | Ultra High Vacuum |
| UV | Ultra-violet |
| YAG | Yttrium Aluminium Garnet |

# Table of Contents

# List of Figures

# List of Tables

# Chapter 1 - Introduction

## 1.1 Overview

The region of space between stars is known as the interstellar medium. It is naïvely tempting to consider this region to be 'empty space', however, in reality the interstellar medium contains vast clouds of gas and dust which are the precursors for star formation. These interstellar dust clouds vary widely in density, with number densities of atoms and molecules ranging from $10^7$ to $10^{10}$ $m^{-3}$.[1] As will be discussed in detail later in this chapter, the more diffuse interstellar clouds largely consist of atomic hydrogen, whilst the denser clouds contain molecular hydrogen as well as other molecular species. These interstellar dust clouds undergo gravitational collapse leading, eventually, to star formation. Molecules within in the dust clouds are crucial in this star forming process since they act as coolants, radiating away excess energy as a cloud collapses. Indeed, over 160 molecules have been detected to date in the interstellar medium, primarily in the denser interstellar clouds.[2] Yet interstellar clouds, with their conditions of low temperatures and pressures, represent a deeply unfavourable environment for chemical reactions. Consequently, the abundances of many of the molecules which have been observed in the gas phase cannot be explained by gas phase chemistry alone. Instead, it is believed that these molecules form *via* reactions on the surfaces of the dust grains which exist within interstellar clouds. These dust grains are of a similar diameter to the wavelengths of visible light, and are composed of materials such as carbon, silicates, metals and metal oxides. Typically dust grains represent approximately 1 % of the mass of an interstellar cloud.[1] In the denser interstellar clouds these dust grains are coated in icy mantles consisting of volatile species which either freeze out onto the grain surface from the gas phase or are formed *in situ* on the surface. These icy mantles predominantly consist of water ice but also contain a variety of minor components such as simple organics, ammonia and the sulfur bearing molecules carbonyl sulfide and sulfur dioxide. Thus, given this mixture of chemical species present on the dust grain surfaces, it is clear that there is the potential for a rich solid state chemistry in dense interstellar clouds. This chemistry can either consist of reactions involving radicals which have minimal activation energies or can be initiated by energetic processing of the ice, for example, by cosmic rays. This thesis presents the results of experimental investigations of the former type of reactions; the reactions of

free radicals with molecular ices of astrophysical interest. In particular this thesis focuses on the surface reactions of oxygen and hydrogen atoms with the aforementioned molecular ices on interstellar grain analogues. This chapter will outline the important role that chemistry plays in the interstellar medium and introduce key concepts relevant to the study of chemistry of the interstellar medium. Additionally, an overview of previous studies which have investigated the reactions of oxygen and hydrogen atoms on interstellar grain analogues is also provided.

## 1.2 The Chemical Composition of the Universe

Approximately $10^{-5}$ seconds after the 'Big Bang' the Universe had cooled sufficiently for the formation of the first ingredients of the chemical elements, electrons, protons and neutrons.[3,4] In chemical terms, the Universe at this time contained only ionized hydrogen atoms. The formation of nuclei of deuterium and helium occurred after several minutes, with the former arising from the fusion of protons with neutrons, whilst the latter was a product of the fusion of these nascent deuterium nuclei. Hydrogen and helium persisted in a state of complete ionization for approximately $10^5$ years, after which time electrons began to recombine, initially with helium nuclei, and then with protons, to form neutral helium and hydrogen atoms.[5] The formation of neutral helium atoms can be said to represent the beginning of chemistry in the Universe, with very simple ion chemistry now being possible:

$$He + H^+ \rightarrow HeH^+ + h\nu \qquad 1.1$$

$$He + He^+ \rightarrow He_2^+ + h\nu \qquad 1.2$$

Once neutral atomic hydrogen had started to form, the first $H_2$ molecules could be produced. However, hydrogen atoms were not able to recombine efficiently *via* a simple two body reaction, since there are no allowed dipole transitions *via* which the nascent $H_2$ molecules could radiate away the 4.5 eV of energy released upon forming the H—H bond. Nor was there any significant possibility of a three body reaction occurring under the low pressure conditions of the early Universe. Instead the very first hydrogen molecules were formed *via* the helium catalysed reactions 1.1, 1.3 and 1.4.[5]

$$HeH^+ + H \rightarrow H_2^+ + He \quad 1.3$$

$$H_2^+ + H \rightarrow H^+ + H_2 \quad 1.4$$

These first hydrogen molecules were quickly destroyed by the cosmic background radiation.[5] It is now widely accepted that with the increasing abundance of atomic hydrogen in the early Universe, $H_2$ was primarily formed *via* the electron and proton catalysed reactions 1.5 to 1.8:[5-7]

$$H + e^- \rightarrow H^- + h\nu \quad 1.5$$

$$H^- + H \rightarrow H_2 + e^- \quad 1.6$$

$$H + H^+ \rightarrow H_2^+ \quad 1.7$$

$$H_2^+ + H \rightarrow H_2 + H^+ \quad 1.8$$

The formation of molecular hydrogen was crucial to the evolution of the Universe as these $H_2$ molecules provided a cooling mechanism for pre-galactic gas clouds as they underwent gravitational collapse. The chemistry of the early Universe was therefore extremely important in the formation of structure and thus, ultimately, in the formation of the first stars.

It was not until the formation of the first stars that elements heavier than hydrogen and helium could be formed in any appreciable quantity. The heavier elements, up to iron and nickel, are produced in stars *via* various nuclear fusion reactions starting from hydrogen and helium. However, nuclear fusion of iron nuclei, as well as those elements heavier than iron, is endothermic and so rapidly leads to the gravitational collapse of a star at the end of its life cycle. The elements heavier than iron and nickel are formed predominantly in supernova explosions.[8] Nevertheless, hydrogen and helium still constitute 99.9 % of atoms in the known Universe with the other elements making up the remaining 0.1 %. Carbon, nitrogen and oxygen represent the majority of this final 0.1 % with the heavier elements being even less abundant. However, despite the

relatively low abundance of elements heavier than helium, an extremely rich chemistry is observed in the interstellar medium.

To date, over 160 molecules and ions have been detected in the interstellar medium, from simple diatomics to large organic molecules.[2] Furthermore, the rate of detection of species in the interstellar medium has been approximately constant since 1970 (Figure 1.1), thus, with new, more sensitive, telescopes coming online in the next decade, it is very likely that many more ions and molecules will be detected over the coming years.

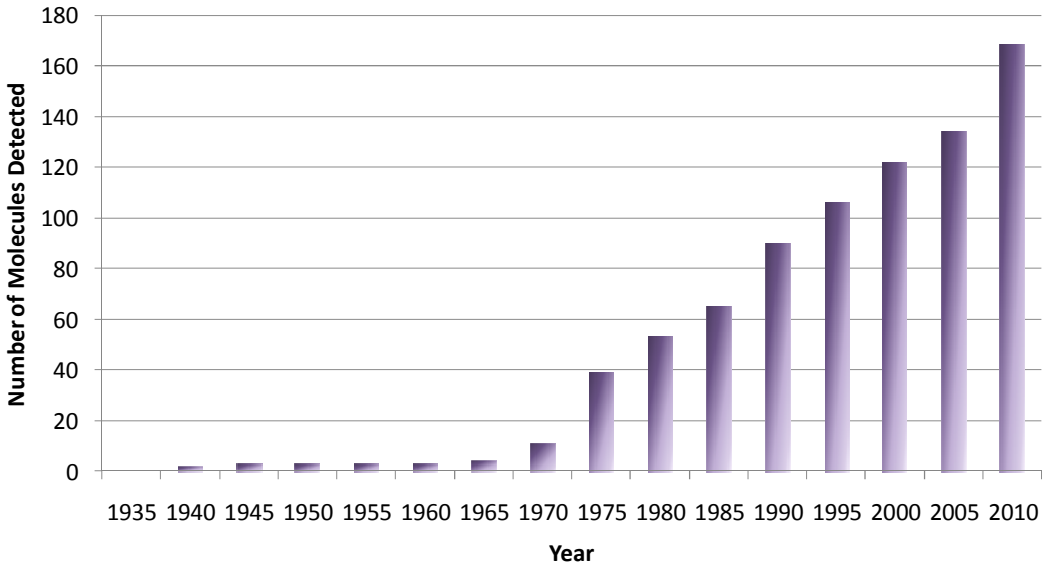


Figure 1.1 The total number of molecules detected to date in the interstellar medium.

It is clear, given the number and complexity of interstellar molecules detected so far, that the interstellar medium has a very rich chemistry. Understanding the formation mechanisms of interstellar species, as well as the reactions which they may undergo, has therefore attracted considerable interest, not only due to the fact that such interstellar chemical reactions determine the materials available for the formation of planetary systems, but also because of the potential for prebiotic molecules to be formed in the interstellar medium.

## 1.3 Interstellar Clouds

Interstellar clouds are vast regions of gas and dust, typically measuring several light-years in diameter. These clouds are also where the vast majority of interstellar molecules are formed. The gas in interstellar clouds is comprised primarily of hydrogen and helium as well as trace quantities of species containing heavier elements. Carbon

monoxide, for example, is the second most abundant molecule in interstellar clouds after molecular hydrogen, $H_2$, and has an abundance relative to $H_2$ of approximately $1 \times 10^{-5}$.[1] The ratio of gas phase species to dust grains is of the order of $10^{12}$ and appears to be approximately constant across measured regions.[1] Nevertheless, the range of interstellar clouds and conditions found within them is extremely broad. For convenience, interstellar clouds may be loosely categorized as either 'dense' or 'diffuse' according to the number density of species within them. Diffuse clouds are characterised by number densities of $10^7 - 10^9$ $m^{-3}$ and have typical gas temperatures in the region of 100 K and dust temperatures of approximately 10 K.[1,9] As a result of their low densities, diffuse clouds are readily penetrated by high energy photons and cosmic rays, and most molecular species are rapidly dissociated. Dense clouds typically have number densities of $10^9 - 10^{10}$ $m^{-3}$ and gas and dust temperatures of approximately 10 K.[1,9] In contrast with diffuse clouds, dense clouds are self-shielding from ultraviolet radiation; meaning that a large proportion of such radiation incident upon the clouds is absorbed by molecules on the periphery of the cloud and so does not penetrate the cloud's centre. Consequently, dense clouds contain a much larger proportion of molecular species than diffuse clouds.[1,9]

## 1.4 Interstellar Dust Grains

Interstellar dust grains were first observed indirectly by William Herschel around 1784.[10] Herschel observed that there existed regions of the sky which were completely devoid of stars. However, the cause of these apparently starless regions was not clear at the time; were they indeed regions without stars or was the starlight in fact being blocked by something between the stars and the Earth? It is now clear that these dark regions of the sky are a consequence of dust grain containing interstellar clouds which absorb and scatter radiation from stars.[10] Today the evidence for interstellar dust grains comes from several sources, which are discussed below.

The first piece of evidence for the existence of interstellar dust clouds is in fact the observation by Herschel that radiation from stars is blocked in certain directions. This effect is more formally known as extinction.[1,10] Interstellar extinction curves are often plotted for particular lines of sight and show the variation of the extinction with $1/\lambda$, where $\lambda$ is the wavelength measured in μm. Most of these extinction curves share similar key features, including a section in the visible region where the extinction is

approximately proportional to $1/\lambda$, a 'hump' at approximately 4.6 $\mu m^{-1}$ (217 nm), and strongly increasing extinction with $1/\lambda$ in the far UV region.[1] However, the most important piece of evidence for the existence of interstellar dust grains comes from the proportionality between extinction and $1/\lambda$ in the visible region. It can be shown that such behaviour can be expected when light is scattered by particles which have a similar radius to the wavelengths of that light.[1] Thus the average interstellar extinction curve indicates the presence of interstellar dust particles which are similar in size to the wavelengths of visible light.

Secondly the depletion of elements in the gas phase in interstellar clouds provides an important indication of the existence of interstellar grains.[1,10] Such elemental depletions are measured with respect to the Sun, which, as a typical star, is assumed to have elemental abundances typical of the Galaxy. However, when the elemental abundances of interstellar clouds are measured, it is found that some elements are heavily depleted with respect to their abundance in the Sun. Furthermore the depletion of elements appears to generally increase with increasing condensation temperature. An element's condensation temperature is the temperature below which it can form a solid which is stable at interstellar pressures.[1] This observation strongly suggests that high condensation temperature elements in the gas moving away from a star form stable solids as the gas cools, and are thus removed from the gas, leading to their observed depletions.

Further evidence for interstellar dust grains comes from the diffuse light in the interstellar medium.[1,10] Diffuse light is light which does not appear to originate from one particular source but instead comes from every direction. The only way in which this can be explained is that starlight is scattered by material in the interstellar medium. One candidate for such material is the gas in interstellar clouds. However, the cross section for Rayleigh scattering of light by H atoms is several orders of magnitude too small to explain the amount of diffuse light observed.[1] The diffuse light can, however, be more satisfactorily explained by Rayleigh scattering from dust grains.

Spectral lines can also be observed in the infrared spectra of background stars which are attributed to absorptions by solid state species in the foreground.[1,10] For example a common feature in such spectra is a broad absorption at approximately 9.7 μm which arises from Si—O bonds in amorphous silicates. Additionally, in regions associated

with very strong extinctions (i.e dense clouds), features corresponding to solid state CO, $CO_2$ and $H_2O$ are observed[1] in addition to much weaker features associated with other solid state molecules.[11]

Two final pieces of evidence for dust grains in the interstellar medium are luminescence from grains and the partial polarization of starlight.[1,10] The former is observed as a broad emission feature in the infrared region. This emission feature is attributed to luminescence from materials with band gap energies of approximately 2 eV.[1] One class of material with such a band gap energy is, for example, amorphous hydrocarbons which are rich in hydrogen. The partial polarization of starlight arises from the preferential extinction of light linearly polarized in one direction over that polarized in the perpendicular direction. Such an effect can arise if dust grains which either have anisotropic crystal structures (such as graphite) or are geometrically anisotropic (i.e. elongated in one direction) preferentially align with each other. A possible mechanism for the alignment of dust grains involves paramagnetic grains preferentially rotating such that their axis of rotation is aligned with any background magnetic field in the interstellar medium.[1]

In light of the evidence discussed above, it is clear that interstellar clouds contain dust grains consisting of elements observed to be depleted in the gas phase and which form stable solid materials under interstellar conditions. Such materials include carbon, silicates, metals and metal oxides.[1] As outlined in the previous section, interstellar grains typically represent a fraction of approximately $10^{-12}$, by number, of species in an interstellar cloud or 1 % of the cloud by mass.[10] As will be described in detail in the following sections it is now widely believed that interstellar dust grains play a crucial role in molecule formation in the interstellar medium.

## 1.5 Molecule Formation in the Interstellar Medium

The conditions of the interstellar medium appear, upon initial inspection, to be deeply unfavourable to chemical reactions. The low temperatures typical of interstellar dust grains rule out all endothermic reactions in addition to exothermic reactions which have any significant reaction barrier. Furthermore, the low number densities in interstellar clouds mean that, even in dense clouds, an atom or molecule undergoes a collision approximately once every two weeks.[12] Therefore, even reactions which are both exothermic and barrierless can only proceed very slowly. Nevertheless, there are some

mitigating factors which must also be considered. For example, the lifetime of a typical interstellar cloud is approximately $10^5$ – $10^6$ years, thus, whilst the collisional rate is slow by terrestrial standards, it is still sufficiently fast on an astronomical timescale for reactions to occur efficiently. Additionally, many of the chemical species which exist within interstellar clouds are ions or radicals. Both radical-radical and ion-neutral reactions often proceed with no activation energy.[12] Furthermore, the rate of collisions between ions and neutral species is typically a factor of 10 – 100 larger than the corresponding rate for two neutral species.[12] This enhanced collisional rate for ions with neutral species is a consequence of the attractive ion-induced dipole interactions between the ion and neutral species. In view of the above arguments, it is clear that gas phase reactions can, in some cases, proceed efficiently even under the conditions of the interstellar medium. Indeed, the observed abundances of many species observed in the interstellar medium are well explained by gas phase reaction networks. Nevertheless, some interstellar molecules, such as methanol and water, are observed to be more abundant than predicted by gas phase models.[13] In these cases reactions at the surface of the interstellar dust grains described in Section 1.4 are invoked to explain the observed abundances.

## 1.6 Surface Chemistry in Diffuse Interstellar Clouds

As already discussed, the destruction rates of molecules in diffuse interstellar clouds are high relative to the formation rates due to penetration of such clouds by high energy photons. Consequently, the gas in diffuse interstellar clouds is predominantly atomic hydrogen and the dust grains do not possess the icy molecular mantles they do in dense clouds. The low abundances of molecules in diffuse clouds means that the only chemical reactions occurring on dust grain surfaces tend to be those involving the recombination of atomic species. In particular, the high abundance of atomic hydrogen results in its reactions, both with itself and with other atomic species, being dominant. Indeed the most significant chemical reaction in diffuse clouds is the recombination of H atoms on dust grain surfaces to form molecular hydrogen, $H_2$. The recombination reaction of atomic hydrogen has been extensively studied, both experimentally (see refs [14-29]) and theoretically (see refs [19,20,30-53]). Some examples of these studies are discussed in the 'Previous Studies' section below.

## 1.7 Surface Chemistry in Dense Interstellar Clouds

Dense interstellar clouds are characterized by having a sufficient number density that the core of the cloud is shielded from stellar ultraviolet radiation by the outer layers of the cloud. In this case the destruction of molecules in the core of the cloud is limited to that induced by cosmic rays. Consequently, over time, polyatomic molecules can be formed *via* sequential reactions of simpler building blocks either in the gas phase or on grain surfaces. The net formation of molecules in dense interstellar clouds leads to the development of icy mantles on the surfaces of dust grains in dense clouds. In addition to CO, which is formed in the gas phase before accreting onto the grain surface, the major molecular constituents of these icy mantles are $H_2O$, $NH_3$, $CH_4$ and $CH_3OH$, which can be formed on the grain surface *via* successive reactions of H atoms with O, N, C and CO respectively.[54-57] Additionally, $CO_2$, as well as other minor molecular components have been identified in interstellar ices such as, OCS and $SO_2$.[58-60] This rich mixture of molecules in the condensed phase gives rise to the potential for a range of chemical reactions to occur both within the ice and at the solid-gas interface. These reactions can broadly be categorized into two groups: thermal reactions and suprathermal reactions.

### 1.7.1 Thermal Chemistry

Thermal reactions are those which occur between two species which are in thermal equilibrium with their surroundings, in this case the interstellar gas or ice. Given the very low temperatures typical of interstellar clouds there is very little thermal energy available to overcome reaction barriers. Since reactions between closed shell species usually exhibit large activation energies, thermal reactions in the interstellar medium tend to be limited to those reactions in which at least one of the reactants is a free radical. Some examples of these radical reactions include the sequential hydrogenation of O, N, C and CO by H atoms. It is the thermal reactions of H and O atoms with various molecular ices of astrophysical relevance which are investigated in the experiments discussed in this thesis.

### 1.7.2 Suprathermal Chemistry

Whilst it is beyond the scope of this thesis to discuss suprathermal solid state chemistry in the interstellar medium in detail, it is mentioned here for the purpose of comparison with thermal chemistry. Suprathermal reactions are those initiated by high energy particles such as protons or electrons or by UV light. The processing of the ice by these

energetic species causes the dissociation of molecules within the ice to produce suprathermal fragments which can then overcome activation energies to reactions not accessible *via* thermal mechanisms. A simple example would be the energetic processing of methane ice to form more complex hydrocarbons such as $C_2H_4$ and $C_2H_6$.[61] Suprathermal reactions in astrophysical ice analogues have been the subject of extensive experimental investigation, whilst, as discussed in the following section, thermal reactions have received relatively little attention.

## 1.8 Previous Studies

Previous studies of the thermal surface reactions of hydrogen are overwhelmingly dominated by studies of the recombination of two H atoms to form $H_2$. This emphasis on hydrogen atom recombination is both a consequence of the astrophysical importance of this reaction as well as the fact that its simplicity allows for very detailed studies, both theoretically and experimentally. Thus, this simple reaction between two H atoms can be investigated to lay the foundations for understanding more complicated surface reactions, which are less easily modelled. Indeed, thermal surface reactions of hydrogen atoms with other species, or of oxygen atoms, have received relatively little attention either experimentally or theoretically. In this section, an overview of previous studies which investigate the thermal surface reactions of either hydrogen or oxygen atoms under interstellar conditions is presented.

### 1.8.1 Recombination Reactions of Hydrogen Atoms

The recombination of hydrogen atoms on the surface of water ice which contained impurities such as hydrogen, methane and ammonia, amongst other species, was first shown to be efficient, at temperatures relevant to the ISM, by Gould and Salpeter[30]. According to these authors' work, there is a window of efficient recombination for grain surface temperatures between 5 and 20 K, depending upon the depth of the physisorption well. The upper and lower limits on the grain surface temperature arise from the need for gas phase hydrogen atoms to be able to 'stick' to the surface without immediately desorbing and the requirement that nascent hydrogen molecules desorb from the surface rather than building up a monolayer of $H_2$ over time. It is estimated that the recombination efficiency in this temperature window is between 0.1 and 1. Hollenbach and Salpeter ([31]) later extended the Gould and Salpeter ([30]) study to non-

ideal surfaces and found that at temperatures below 25 K the recombination efficiency was close to 100 %.

The two studies discussed above consider the recombination of hydrogen atoms which are pre-adsorbed onto, and thermalised with, the dust grain surface. Such a surface recombination process is known as the Langmuir-Hinshelwood (LH) mechanism. Alternatively, a reaction at a surface can proceed *via* the Eley-Rideal (ER) mechanism. In the ER mechanism, only one of the precursor atoms is adsorbed onto, and thermalised with, the surface. A second, gas phase, atom then collides and reacts directly with the adsorbed atom to form a product molecule which desorbs from the surface. A third, intermediate, mechanism known as the 'hot atom' mechanism may be considered as similar to the LH mechanism but with one atom not fully thermalised with the surface. In real-world surface reactions, each of these mechanisms are likely to take place to greater or lesser degrees. However, in the case of the recombination of hydrogen atoms in the interstellar medium, it is believed that the LH mechanism is likely to dominate as the flux of H atoms impinging upon the surface is small. This low flux means that the probability of an incoming H atom either immediately colliding with an adsorbed atom, or not having time to thermalise with the surface before colliding with an adsorbed atom, is low. Nevertheless, the majority of theoretical studies of hydrogen atom recombination on surfaces analogous to interstellar dust grains have considered the Eley-Rideal mechanism.[35,36,39-44,47-50,62]

One of the earliest theoretical studies to consider the distribution of the 4.5 eV H—H binding energy released upon the formation of a hydrogen molecule on a perfect graphite surface was carried out by Parneix and Brechignac[47]. In this study molecular dynamics calculations were used to determine the vibrational, rotational and translational energy of the nascent $H_2$ molecule, assuming formation *via* an ER type mechanism. The results of this study showed that approximately 3.4 eV of the H—H binding energy was transferred to the $H_2$ molecules.

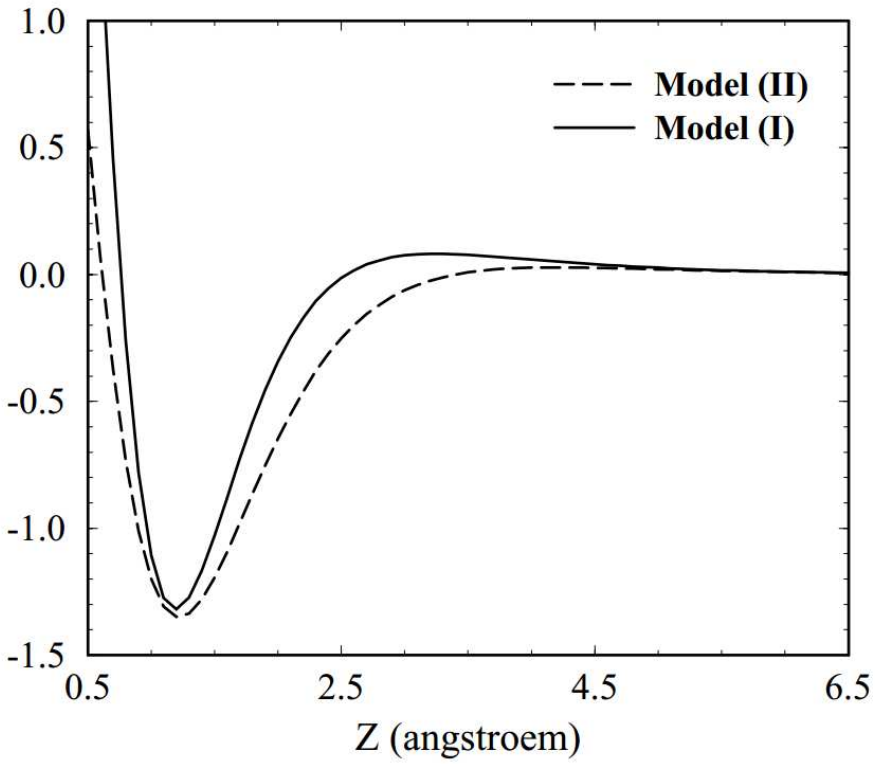


Figure 1.2 Models of the H-graphite interaction potential from Parneix and Brechignac.[47]

Two H – graphite interaction potentials were used in this study, shown in Figure 1.2. Model I results in approximately 50 % of the 3.4 eV of energy transferred to the nascent $H_2$ going into the translational excitation of the molecule, 31 % contributing to vibrational excitation, and the remaining 19 % to the rotational mode. Alternatively, model II results in the distribution of the energy transferred to the nascent $H_2$ between the translational, vibrational and rotational modes of $H_2$ as 41 %, 38 % and 21 % respectively. Parneix and Brechignac's work also shows that such transfer of energy into the vibrational excitation of the nascent molecular hydrogen would give rise to $H_2$ in vibrational states up to $v = 7$.

Two years later, Farebrother *et al* [35] reported a two dimensional density functional theory (DFT) study of the recombination of hydrogen atoms on a graphite analogue. This study again assumed an ER type mechanism in which the secondary H atom collides with the primary H atom adsorbed on the graphite surface collinearly with the C—H bond. Rotational excitation was disregarded in this study and the results were reported for the $J = 0$ rotational state. The authors calculate that in such a reaction scheme the $H_2$ would be formed with considerable vibrational excitation. They find that vibrational states up to and including $v = 6$ are populated with the most populated state

being $v$ = 2. The same authors later extended the this study by carrying out a three dimensional DFT study on the same system.[40] This study considered the rotational excitation of the nascent molecular hydrogen in addition to the vibrational and translational excitation and found that the hydrogen was formed highly rotationally excited, with rotational states up to $J$ = 20 being populated. However, including rotational degrees of freedom in the calculations was found to significantly reduce the vibrational excitation of the nascent $H_2$, whilst the translational excitation was largely unchanged.

Rutigliano *et al*[48] have also studied the recombination of H atoms *via* the ER mechanism using a semi-classical method. In this study, an H atom was initially chemisorbed onto a graphite surface at 10 K. The authors then model gas phase H atoms, with a range of kinetic energies between 0 and 0.1 eV, colliding and reacting with the pre-adsorbed H atom. The recombination efficiency for hydrogen atoms reacting in this way was found to be unity at kinetic energies above 0.05 eV and to decrease rapidly below this energy. Additionally, the authors find that when $H_2$ is formed *via* the ER mechanism, it is formed both vibrationally and rotationally excited. Specifically, a broad peak in the vibrational distribution is observed between $v$ = 3 and $v$ = 6, and in the rotational distribution between $J$ = 8 – 11.

Another study, very similar in scope to that carried out by Rutigliano *et al,* was undertaken by Morrisset *et al*.[43] In this study, the authors again consider H atom recombination at a surface *via* the ER mechanism. Morrisset *et al*[43] consider coronene as a graphite analogue and vary the kinetic energy of the gas phase hydrogen atom between 0.3 meV and 500 meV. It is again found that a large proportion of the 4.5 eV of binding energy released upon the formation of an H—H bond goes into the vibrational excitation of the nascent $H_2$ molecule. Further studies were also carried out by Morrisset *et al* to investigate the distribution of the H—H binding energy when molecular hydrogen is formed on a graphite surface *via* the LH mechanism.[45,46] These studies of the LH mechanism also find that the nascent $H_2$ molecules are considerably rotationally and vibrationally excited.

Sha and co-workers have used quantum scattering calculations to estimate the reaction cross section for hydrogen atom recombination on a graphite surface in three different situations.[50] The three scenarios considered are each based upon an ER type

mechanism; in the first case the pre-adsorbed H atom is chemically bonded (chemisorbed) to a surface carbon atom which is held rigidly in a tetrahedral geometry throughout the reaction, in the second case the H atom is still chemisorbed onto the surface but this time the surface is allowed to relax as the reaction proceeds, and finally, in the third case, the H atom is physisorbed onto the surface. In each of the cases where the pre-adsorbed H atom is chemisorbed, the reaction cross-section is approximately constant for gas phase H atom kinetic energies above 0.4 eV but falls to zero at low kinetic energies due to small barriers of a few tenths of an eV in the entry channel. Conversely, in the physisorbed case, the shallow physisorption well gives rise to large reaction cross-sections when the kinetic energy of the impinging H atom is small, but at kinetic energies above 0.05 eV the reaction cross section drops away toward zero. The authors attribute the low reaction cross section at high collision energies in the physisorbed case to the incoming H atom having enough kinetic energy to eject the adsorbed H atom from the physisorption well and into the gas phase without a reaction taking place. The study also calculated the expected distribution of the H—H binding energy between the vibrational, rotational and translational modes of the nascent molecular hydrogen, and found that whilst it is formed in vibrationally excited states there is little rotational excitation. Furthermore, whilst in the scenarios where the H atom is chemisorbed onto the surface the product $H_2$ molecules are formed with approximately 1 eV of translational energy, in the physisorbed case the nascent molecular hydrogen had almost no translational energy.

All of the studies discussed above have considered the recombination of hydrogen atoms taking place on an otherwise clean surface. It is clear that this could lead to some discrepancies between theoretical and experimental work as such a situation is impossible to achieve experimentally. Meijer *et al* [41] have studied the effect of the surface coverage with H atoms on the final energy distribution of the recombined $H_2$ molecules using a time dependent wave packet method. The model the authors used is that of a graphite surface with a monolayer of hydrogen atoms adsorbed onto it. It is found that this inclusion of spectator hydrogen atoms on the surface significantly reduces the vibrational excitation of the nascent $H_2$.

Most recently Bachellerie *et al* [32] have studied the effect of collisions between nascent hydrogen molecules and the walls of pores in a carbonaceous dust grain immediately following their formation on a graphene surface. The authors justify their use of

classical trajectory simulations on the basis that previous studies by Morriset *et al* [45,46] had found that quasi-classical simulations (which include the H-surface zero point energy) were in good agreement with full quantum mechanical simulations. Bachellerie *et al* find that collisions between the nascent $H_2$ molecules and the surface do not significantly alter the total amount of energy of the $H_2$ molecules. Instead such collisions have the effect of transferring some of the vibrational energy of the molecules into the rotational mode. As an example, the authors find that after 10 – 15 collisions the vibrational distribution shifts from the range $5 \leq v \leq 15$ to $0 \leq v \leq 10$. The rotational distributions are simultaneously shifted from $5 \leq J \leq 20$ to $10 \leq J \leq 30$.

The recombination of atomic hydrogen on astrophysically relevant surfaces, under conditions similar to those in the ISM, has also been studied experimentally. Several of these experimental studies have been carried out by Pirronello and co-workers.[25-27,37,63,64] These studies have investigated the recombination of hydrogen atoms on graphite surfaces, on olivine (silicate) surfaces and also on amorphous solid water surfaces.

In the first of the experimental studies by Pirronello and co-workers [27], the authors use temperature programmed desorption (TPD) to determine the recombination efficiency of hydrogen and deuterium atoms on an olivine surface held at temperatures between 5 and 20 K. It was found that the yield of HD produced on the surface decreases with increasing surface temperature over the range of temperatures investigated. The authors attribute this temperature dependence to the hydrogen atoms only residing on the surface for short periods of time at higher temperatures and thus only having a low probability of recombination. The recombination efficiency was found to be between 0.03 and 0.05 for surface temperatures between 10 and 15 K; a value that is considerably lower than the 0.3 calculated by Hollenbach and Salpeter.[31,65] The discrepancy between the recombination efficiency calculated by Hollenbach and Salpeter [31,65] and that determined by Pirronello *et al* [27] is attributed to the fact that in the earlier theoretical study a perfect surface was assumed, whereas in reality the surface will inevitably have defects. The authors of the TPD study contend that this heterogeneity may reduce the rate of tunnelling or alter the sticking probability for H atoms. Further comparison was made between the recombination rate calculated from the recombination efficiency determined experimentally and the recombination rate inferred from observations by Jura.[66] Pirronello *et al* [27] suggest that their recombination

rate and that of Jura ($1 \times 10^{-17}$ - $3 \times 10^{-17}$ $cm^{-3}$ $s^{-1}$) may be reconciled if the surface area of dust grains in the ISM is five to ten times larger than previously considered in models.

The study by Pirronello and co-workers described above [27] was extended by further TPD experiments by Pirronello *et al* [25]. In this follow up study, second order desorption kinetics were observed for HD when the H and D atom coverage was low and the surface temperature was approximately 6 K. Second order desorption kinetics are characteristic of a recombination reaction taking place during the TPD process, thus implying in this case that the H and D atoms initially do not recombine in the low coverage regime. Conversely, under conditions of higher H and D atom coverage (although still less than a monolayer) first order desorption kinetics were observed, implying that the H and D atoms recombine prior to the desorption process but remain adsorbed on the surface as HD molecules. These results have two important implications for hydrogen recombination in the interstellar medium: firstly that H and D atoms are immobile on the surface at low surface temperatures, and secondly that the 4.5 eV of binding energy released upon recombination does not necessarily lead to desorption of the nascent molecule.

Later, the Pirronello group moved on to study the recombination of hydrogen and deuterium atoms on an amorphous carbon surface [26]. The authors found that at surface temperatures relevant to the interstellar medium, hydrogen recombination on amorphous graphite surfaces was more efficient by a factor of between 1.5 and 2 than on the olivine surface studied previously.

The formation of molecular hydrogen on amorphous water ice surfaces has also been studied by the Pirronello group.[63,64] In the first study, the recombination efficiency of hydrogen was investigated on both high density amorphous ice ($\rho = 1.1 \pm 0.1$ g $cm^{-3}$) and on low density amorphous ice ($\rho = 0.94 \pm 0.3$ g $cm^{-3}$).[63] The high density amorphous ice was formed by depositing water vapour onto a copper substrate at 10 K directly from a capillary. Low density amorphous ice was formed *via* two methods in this study. Firstly, high density ice was produced, as before, and thermally annealed to produce low density amorphous ice by heating the substrate to 90 K and holding it at that temperature for 5 minutes. Alternatively, the UHV chamber was filled with background water vapour which was then deposited on the copper substrate at 77 K.

The authors found that hydrogen recombination was more efficient on low density amorphous ice than on high density amorphous ice at 10 K, with the difference between the two surfaces becoming less marked with increasing temperature to 18 K. The second study sought to determine the kinetic energy of $D_2$ molecules following their formation on, and desorption from, the amorphous ice surface. The authors found that the desorbing $D_2$ atoms had the same kinetic temperature as the temperature of the ice surface (16 K).

The formation of molecular hydrogen on carbonaceous surfaces has also been studied by Gough *et al* [16]. In this study, two types of graphite surface were prepared on the walls of their experimental cell; one by depositing carbon onto the cell walls by sublimation from a graphite filament, the other by producing an electrical discharge in 0.25 Torr of methane. The structures of the two types of carbon surface were studied by scanning electron microscopy. The surface prepared using the graphite filament was found to be mostly smooth with some localised soot deposits whilst the surface prepared by electrical discharge in methane was much rougher. The authors then determined the rovibrational distribution of $H_2$ formed *via* the recombination of hydrogen atoms on each surface using dissociative low energy electron attachment, represented by Equation 1.9.

$$H_2\,(v, J) + e^- \rightarrow H_2^-\,(^2\Sigma_u^+) \rightarrow H^- + H \qquad 1.9$$

The electron energy is scanned and those hydride ions produced with zero kinetic energy, that is to say at threshold, are detected using a quadrupole mass analyser and ion optics. The population of vibrational states could then be derived from the intensities of successive peaks in a plot of $H^-$ intensity against electron energy. The rotational energy of the nascent $H_2$ molecules could also be estimated from the width of the peaks. The authors observed that hydrogen molecules were formed in vibrational states up to $v = 7$ with the most populated states being $v = 3 – 5$ depending upon the surface temperature. Conversely the rotational excitation of the recombined molecular hydrogen was found to be low. Despite the fact that these experiments were carried out at surface temperatures higher than those found in the ISM, Gough and co-workers nevertheless conclude that their results support the hypothesis that molecular hydrogen is formed in vibrationally excited states in the ISM.

Hornekær *et al* have studied the formation of HD and $D_2$ on porous and non-porous amorphous solid water surfaces in order to elucidate the effect of surface morphology on the recombination of H atoms on interstellar dust grains.[17,18] Through the use of TPD techniques the authors find that the nascent molecules readily desorb from the non-porous surfaces as they are formed, but only desorb from the porous surfaces when the surface is heated. The authors suggest that this difference between the two surface types is due to the newly formed molecules being trapped within the pore network of the porous surfaces and thus thermalising with the surface, whereas on non-porous surfaces the molecules desorb without thermalising and are thus likely to have considerable excitation, as predicted by theory.

Hornekær and co-workers have also studied the chemisorption of hydrogen and deuterium atoms on graphite surfaces using scanning tunnelling microscopy and TPD.[19] Processes involving chemisorption of hydrogen atoms on graphite are not generally considered important in the ISM as there is a 0.2 eV (≈ 1550 K) barrier to chemisorption which cannot readily be overcome by hydrogen atoms under normal interstellar conditions.[49,67] However, the authors suggest that, in photo-dissociation regions and in post-shock regions, the small fraction of hydrogen atoms in the high energy tail of the Maxwell-Boltzmann distribution have enough energy to overcome the barrier to chemisorption. Furthermore, Hornekær *et al* [19] find that the barrier to chemisorption is reduced at adsorption sites *ortho* or *meta* to a pre-adsorbed atom or even eliminated entirely for sites *para* to the pre-adsorbed atom. The authors therefore conclude that the resulting clustering of H atoms on the graphite surface can provide a mechanism for molecular hydrogen formation in higher temperature regions of the ISM, either by dimer formation or by an ER type mechanism.

### *Previous Results from the UCL Cosmic Dust Experiment*

Previous experiments in the UCL Cosmic Dust lab have investigated the distribution in the nascent HD molecules of the binding energy released following the recombination of H and D atoms.[21,22,24] This was achieved by measuring the rovibrational distribution for HD molecules formed on a cold highly oriented pyrolitic graphite (HOPG) surface.

The HOPG surface was cooled to temperatures in the region of 15 – 20 K. Both H and D atoms are transported to the surface via separate PTFE tubes and impinge on this surface constantly throughout the experiments. By the time the atoms reached the

surface they had thermalised with the PTFE tubes and, thus, had a temperature of approximately 300 K. The vibrational and rotational populations of product HD molecules desorbing from the surface were then probed using resonance enhanced multi-photon ionization (REMPI) and time of flight mass spectrometry (TOFMS), as described in detail in Chapter 2.

The results of these experiments showed HD molecules are formed in excited vibrational states following the recombination of H and D atoms on an HOPG surface; the peak in the vibrational distribution was found to be at $v = 4$ with states up to $v = 7$ being populated. In contrast, the peak in the rotational distribution of each vibrational state was found to occur at $J = 1$. The finding that the HD is formed with significant vibrational excitation, but little rotational excitation, implies that a significant proportion of the 4.5 eV of binding energy goes into the vibrational mode of the nascent HD molecules. The rovibrational distribution determined from these experiments can be seen in Figure 1.3.

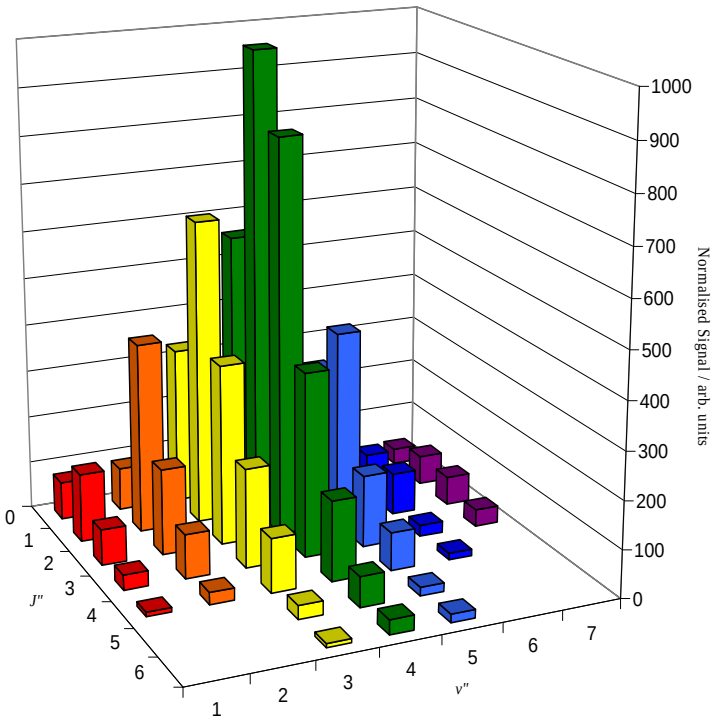


Figure 1.3 The rovibrational distribution of nascent HD previously measured using the Cosmic Dust experiment. The HD molecules were formed from the H + D recombination reaction on an HOPG surface at 15 K .

### 1.8.2 Reactions of Oxygen Atoms with Hydrogen Atoms

Experimentally investigating the reaction between oxygen atoms and hydrogen atoms presents particular difficulties. These problems stem from the fact that hydrogen atoms react with all three $O_x$ ($x = 1 – 3$) species (atomic oxygen, molecular oxygen and ozone) and yet it is extremely difficult to produce atomic oxygen which is free from molecular oxygen. One of the most common ways to form oxygen atoms is to generate a discharge in molecular oxygen, but, given that the dissociation efficiency is always less than 100 %, the oxygen atom beam will always contain some $O_2$. In order to minimize this problem other oxygen containing precursors have been used to produce O atoms in a discharge, most common amongst these being nitrous oxide ($N_2O$).[68-72] Nevertheless, whilst it is known that a microwave discharge in $N_2O$, for example, produces O atoms in abundance,[73] it does not completely eliminate the problem of $O_2$ contamination as O atoms readily recombine in the atom transport tubes and on the surface of the dust grain analogue. In order to exclusively study the reaction between oxygen atoms and hydrogen atoms, oxygen atoms would therefore need to be produced *in situ* on the surface.

Despite the above experimental challenges, Dulieu *et al* [74] have attempted to study the reaction between hydrogen and oxygen atoms. Whilst in their experiments, the authors use a microwave discharge in molecular oxygen to produce O atoms, in order to circumvent some of the problems discussed above, they have used a statistical argument to disentangle the contributions to water formation from the atomic and molecular oxygen pathways.

In the Dulieu *et al* [74] experiments, $D_2O$ formation is studied on a surface of amorphous solid water ($H_2O$) (ASW) by dosing the ASW with D and O atoms which have been produced by microwave discharges in $D_2$ and $O_2$ respectively. Temperature programmed desorption (TPD) experiments were then carried out to detect any products formed. In an initial set of experiments both $D_2O$ and HDO were observed during this temperature programmed desorption in addition to $H_2O$ from the original ASW layer. It is clear that the $D_2O$ is formed from the reaction of D atoms with O and $O_2$. The authors then attribute the HDO signal to isotope exchange between the $H_2O$ ASW layer and the product $D_2O$, a process which is known to occur at approximately 130 K. In order to provide a more quantitative insight into the reaction, the authors carried out further

experiments in which the ASW surface was irradiated with D and $^{18}O$ atoms. This reaction would be expected to produce $D_2{}^{18}O$, however, due to the isotope exchange process described above, $HD^{18}O$ and $H_2{}^{18}O$ are also observed. In order to determine the contributions to water formation from the reaction of D atoms with atomic and molecular oxygen, the authors firstly measure the total number of $^{18}O$ nuclei in terms of ion counts and scale this number according the flux of $^{18}O_2$. The authors are therefore able to obtain a ratio, $\alpha$, of the total number of $^{18}O$ nuclei accounted for in the three water isotopologues to the total number of $^{18}O$ nuclei available. The value of $\alpha$ is 0.76 with the authors attributing the 'missing' $^{18}O$ nuclei to atoms or molecules which have desorbed throughout the experiment, to atoms which have formed $^{18}OH$ or to molecules which have reacted to form $D_2{}^{18}O_2$ and its isotopologues. The last suggestion could have been simply confirmed by searching for signals at *m*/*z* 40 but unfortunately no such observations are reported. If D atoms reacted only with $O_2$ then the dissociation efficiency of $O_2$ (40 %) would place an upper limit on $\alpha$ of 0.60. The authors therefore attribute the remaining water products to formation from the reaction of D with $^{18}O$. Any contribution from the reaction of D with ozone, which is formed from the reaction of $O + O_2$, is disregarded in these calculations due to the low O concentrations used in these experiments and the low mobility of O and $O_2$ at the surface temperatures investigated. In summary, these experiments indicate that water formation from the surface hydrogenation reactions of O atoms would be an efficient process in the interstellar medium.

The recombination of oxygen atoms with hydrogen atoms to form water on a grain surface has also been widely studied theoretically.[75-79] For example Papoular[75] used a semi-empirical method, which used quantum mechanical calculations along with parameters previously measured experimentally, to study the successive hydrogen addition reactions to an O atom on a hydrocarbon rich surface. One of the main findings of this work was that the exothermicity of both the O + H reaction and the OH + H reaction combined with their weak physisorption energies on the surface leads to the product OH and $H_2O$ molecules being ejected into the gas phase. Papoular therefore concludes that the first layer of water ice on a dust grain surface must arise from accretion of water molecules formed in the gas phase with grain surface formation mechanisms becoming more important in the for subsequent layers. Indeed, quasi-classical calculations by Bergeron *et al*[78] also find that the nascent OH molecule,

formed from the recombination of H and O atoms physisorbed on graphite, possesses a significant amount of internal energy, ultimately leading to desorption. This finding thus supports Papoular's hypothesis that the first water layer must be formed *via* accretion. However, this conclusion does not take into account the situation on other surfaces such as silicates onto which the reactants and/or intermediates may chemisorb without having to surmount a barrier. Goumans *et al*, for example, studied the reaction between hydrogen and oxygen atoms on a forsterite (a magnesium silicate) (010) surface using an embedded cluster approach.[77] In such embedded cluster calculations, a region of the surface around the site of interest is treated quantum mechanically using density functional theory (DFT) whilst the surrounding bulk surface is treated classically using molecular mechanics calculations, in order to reduce the computational cost. The authors find that hydrogen atoms can chemisorb onto the pristine forsterite (010) surface with no barrier. Furthermore, the existence of a smooth reaction pathway between the gas phase hydrogen atom and the chemisorbed state *via* a physisorbed state is taken to imply that hydrogen atoms would predominantly chemisorb on such a surface. Interestingly the chemisorption mechanism is found to involve a proton binding to a silicate oxygen atom whilst an electron is detached from an adjacent Mg atom forming a surface electron. This surface electron site can strongly bind an O $^3$P atom giving rise to the preferential formation of H and O atom pairs in adjacent sites. Thus, water formation can proceed on a silicate surface *via* the reaction of chemisorbed H and O atoms. Furthermore the fact that the reactants and intermediates are chemisorbed means that a substantial part of the exothermicity of the recombination reactions can be dissipated into the surface, allowing the product water molecules to remain bound to the surface. Therefore, it seems clear that in the interstellar medium, providing that there are available chemisorption sites, it is not necessary to resort to accretion of water molecules from the gas phase in order to account for the formation of the first water layer on the grain surface. Furthermore, it is perhaps unrealistic to consider the reaction occurring on an otherwise bare surface as it is likely that other accreted species such as $H_2$ and CO would be present. It has been found previously that the many adsorbate surface bonds present when a grain surface is partially covered with adsorbates can act as an energy sink for the H + H recombination reaction.[41] Thus even when the reactants are physisorbed onto the surface it may still be that the product water molecules can be stabilized on the surface.

### 1.8.3 Other Reactions of Oxygen Atoms

#### *O + CO*

The reaction between O atoms and CO has been studied experimentally by Roser *et al*, [80] who carried out two separate sets of experiments. In the first set of experiments $^{13}CO$ was co-deposited onto a copper substrate at 5 K together with oxygen atoms formed in a microwave discharge of $O_2$. The CO/O ratio used was varied between 5.6 and 21, with an excess of CO being used in order to minimize the interaction of O atoms with each other and with residual $O_2$ from the microwave discharge. Temperature programmed desorption spectra were taken following the co-deposition of $^{13}CO$ molecules and O atoms, however no $^{13}CO_2$ was observed. In a second set of experiments the same procedure was followed but this time a cap of approximately 100 layers of $H_2O$ ice was deposited over the top of the CO/O ice. The role of this cap was to delay the desorption of CO molecules and O atoms so that they interacted with each other at higher temperatures than was possible with CO and O alone. In these experiments $^{13}CO_2$ was produced, indicating the existence of a small reaction barrier which the authors estimate to be equivalent to 290 K.

In similar experiments on the reaction of O atoms with CO, Raut and Baragiola do observe the formation of a small amount of $CO_2$ at 20 K using RAIRS.[81] These authors attribute the discrepancy between their results and those of Roser and co-workers to their higher signal to noise ratio compared with that achieved in the earlier experiments. In any case it seems that whilst the reaction may be enhanced at higher temperatures in the presence of water ice, at 20 K the reaction either does not proceed or proceeds slowly.

The reaction of CO ice with O atoms has also received some theoretical attention.[82] In their study Goumans and Andersson used harmonic quantum transition state theory to investigate the possible role of tunnelling in the CO + O reaction. The authors find that whilst tunnelling can enhance the classical rate of the reaction at the low temperatures of the interstellar medium, the classical rate is already very low. Consequently the authors conclude that the O + CO reaction is not an efficient route to $CO_2$ formation on interstellar dust grains, as indicated by the experimental studies discussed above.

In view of the results obtained in these experimental and theoretical studies, it appears that the reaction of CO with O atoms may not fully explain the formation of $CO_2$ under interstellar conditions. In fact it is now widely believed that $CO_2$ formation on grain surfaces predominantly proceeds *via* the reaction of CO with OH.[83-85]

### 1.8.4 Other Reactions of Hydrogen Atoms

#### $H + O_2$

It has been found experimentally that hydrogen atoms readily react with molecular oxygen ices to form water and hydrogen peroxide as outlined above. Both Iopollo *et al*[86] and Miyauchi *et al*[87] have studied the reactions of H (or D) atoms with $O_2$ experimentally and confirmed the formation of $H_2O$ and $H_2O_2$ ($D_2O$ and $D_2O_2$) at astrophysically relevant temperatures.

Iopollo *et al* studied the reaction on a gold surface at seven different temperatures between 12 and 28 K using IR spectroscopy.[86] In these experiments the authors react both H atoms and D atoms, produced *via* thermally cracking $H_2$ and $D_2$, with $O_2$ to form $H_2O$ and $H_2O_2$ or $D_2O$ and $D_2O_2$ respectively. It is found that the column densities of the products increase with fluence to a maximum level at each temperature. Once this maximum level is reached the column density remains constant with increasing fluence. The column density maxima increase with increasing temperature, whereas the initial rate of change of column density is independent of temperature. This implies that the rate of reaction is temperature independent but that there is more $O_2$ ice available for reaction at higher temperature. The authors explain this as being due to the H (D) atoms being able to penetrate deeper into the $O_2$ ice at higher temperatures. This is perhaps due to the $O_2$ ice taking on a more open structure as the temperature increases towards its desorption temperature.

Very similar experiments were also carried out by Miyauchi *et al*, this time on an aluminium substrate at 10 K.[87] In these experiments the H and D atoms were produced in a microwave discharge in $H_2$ and $D_2$ respectively. As in the Iopollo *et al*[86] experiments, the authors find that the column density of both $H_2O$ ($D_2O$) and $H_2O_2$ ($D_2O_2$) increase to a maximum during dosing of H (D) atoms before reaching a steady state. However, in contrast to the Iopollo *et al*[86] experiments, the authors observe an isotope effect in that the rate of formation of $H_2O$ is faster than that for $D_2O$. The

appearance of an isotope effect in the formation of $H_2O/D_2O$ and not in the formation of $H_2O_2/D_2O_2$ suggests that there is a barrier for the reaction of $H_2O_2$ with H atoms to produce $H_2$ and $H_2O$ through which the H atoms tunnel, however it is not clear from either study why this effect was observed in the Miyauchi *et al*[87] experiments and not in the Iopollo *et al*[86] experiments.

### $H + O_3$

Mokrane *et al* have investigated the reaction of D atoms and $O_3$ molecules on a non-porous amorphous solid water (np-ASW) surface.[88] In order to produce the np-ASW, $H_2O$ is deposited on a copper substrate at 120 K before being cooled to 10 K. Ozone was produced in these experiments *via* one of two techniques. Either $O_2$ gas was subjected to a radio frequency discharge to form ozone which was then condensed by immersion in liquid nitrogen and the $O_2$ gas pumped away, or it was prepared *in situ* by exposing a layer of $O_2$ ice to a beam of O atoms. In either case some $O_2$ inevitably remains on the surface, either due to the dissociation of ozone during transport to the surface in the former case or due to the incomplete reaction of $O_2$. In order to distinguish the $H + O_3$ reaction mechanism from the $H + O_2$ reaction mechanism, this $O_2$ must be removed. This is achieved by heating the sample to 50 K, a temperature below the desorption temperature of ozone but above that of molecular oxygen. The sample was then irradiated with D atoms produced from a microwave discharge in $D_2$ and the products detected using temperature programmed desorption.

Following the sequential deposition of ozone and D atoms on the np-ASW surface at 10 K the authors observe a desorption peak at *m*/*z* 19 for HDO molecules in their TPD spectra. In order to confirm that this is not due to reaction of D atoms with the underlying $H_2O$ molecules in the np-ASW layer, an experiment was also carried out in which D atoms were dosed directly onto the np-ASW surface with no ozone present. In this latter case no HDO desorption was observed. The appearance of HDO in the experiments with ozone is therefore attributed to the reaction of D atoms with $O_3$ molecules to produce $D_2O$ followed by the isotope exchange reaction:

$$H_2O + D_2O \rightarrow 2HDO \qquad 1.10$$

This reaction is known to proceed efficiently at temperatures greater than 130 K, as discussed above. The authors mention in conclusion that the destruction rate of ozone was similar to that of O atoms in the Dulieu *et al*[74] experiments, indicating that, where ozone is available, its reaction with H atoms is likely to be an important water formation mechanism. Specifically, ozone is expected to form in dense clouds where the number density of O atoms is greater than that of H atoms.

The reaction of pure $O_3$ ice with H and D atoms has also been investigated by Romanzin *et al*.[55] These authors observe the production of both $H_2O$ ($D_2O$) and $H_2O_2$ ($D_2O_2$) with the peroxide isotopomers being formed in slightly greater yield than those of water at 25 K, whilst at 50 K the water isotopologues are slightly more abundant. At the intermediate temperature investigated, 40 K, the yields of both peroxide and water were approximately equal.

It is clear then that whilst solid ozone has not been detected in the interstellar medium, it may, if present, provide an important contribution to the formation of water ice *via* reactions with hydrogen atoms. In fact, Romanzin *et al* suggest that the non-detection of ozone in interstellar ices may be a consequence of its efficient consumption *via* reactions with hydrogen atoms.

### *H + CO*

The earliest astrochemical study of the reaction of thermal H atoms with solid CO ice at interstellar temperatures was carried out by Hiraoka and co-workers.[89] In this study, the authors consecutively dosed 10 monolayers (ML) of CO onto the metallic surface of the cold head of a cryocooler at 12 K, followed by 5 minutes of dosing of H atoms produced in a direct current (DC) glow discharge. This process was repeated 100 times, after which the authors carried out TPD experiments in order to detect any products formed. It was found that thermal H atoms did indeed react with solid CO at 12 K to form formaldehyde, $H_2CO$, and methanol, $CH_3OH$, in approximately a 5:1 ratio. However, the overall conversion efficiency of CO to $H_2CO$ was found to be rather low; only 0.06 %. The explanation the authors provide for the low product yield is that there may be a competing hydrogen abstraction reaction in which an H atom reacts with the intermediate HCO radical to reform CO along with $H_2$. The authors also note that the high ratio of $H_2CO$ to $CH_3OH$ implies that H atoms preferentially react with CO at the C atom rather than the O atom, because attack of an H atom on the O atom of the CO

molecule would result in the formation of an O—H bond, and consequently the preferential formation of $CH_3OH$.

However, in a later study by the Hiraoka group, the reaction of CO ice with thermal H atoms was found to produce $H_2CO$ but no $CH_3OH$.[90] The explanation provided by the authors for the discrepancy between this work and their previous investigation of this reaction is that in the earlier study ultraviolet photons produced by the hydrogen discharge were allowed to impinge upon the CO ice surface and consequently methanol was produced by UV processing of product $H_2CO$ molecules. Additionally, CO molecules in the vacuum chamber during dosing were found to enter the hydrogen discharge tube and adsorb on to the inner walls of the tube, potentially leading to reactions between CO and excited hydrogen species in the discharge which could then be deposited onto the cold surface. The lack of methanol formation observed in this more recent study then is attributed to these experimental short comings having been addressed.

The above results from Hiraoka and co-workers are in contrast to those obtained by Watanabe *et al*.[91] In their investigation of the CO + H reaction taking place on an aluminium substrate at 10 K, Watanabe *et al* observe the formation of both $H_2CO$ and $CH_3OH$. Furthermore the conversion efficiency of CO is found to be 6 % for $H_2CO$ and 4 % $CH_3OH$; an overall conversion efficiency of 10 %. These high conversion efficiencies are in marked contrast to the less than 0.1 % yield obtained by Hiraoka *et al*.[89] Watanabe and co-workers conclude that the difference must be attributable to the higher H atom flux in their experiments ($\sim 10^{15}$ $cm^{-2}$ $s^{-1}$) compared with those in the Hiraoka experiments ($\sim 10^{13}$ $cm^{-2}$ $s^{-1}$).[91-93]

A more recent study by Fuchs *et al* agrees with Watanabe and co-workers that methanol is indeed produced *via* the reaction of thermal H atoms with CO ice at 10 – 15 K.[54] Furthermore these authors investigate the effect of fluence on product yield and confirm that the discrepancy between the results of the Watanabe group and those of the Hiraoka group was in fact a consequence of the different H atom fluxes used, as suggested by Hidaka *et al*.[94] Additionally, Fuchs *et al* have fitted their experimental data using a Monte Carlo simulation of the hydrogenation process and thus derived reaction barriers for reactions 1.11 and 1.12.

$$H + CO \rightarrow HCO \quad 1.11$$

$$H + H_2CO \rightarrow H_3CO \quad 1.12$$

At 12 K the barriers ($E/R$) for reactions 1.11 and 1.12 were estimated to be 390 ± 40 K and 415 ± 40 K respectively. The non-observation of the intermediate radicals HCO and $CH_3O$ using reflection absorption infra-red spectroscopy (RAIRS) indicates that the reaction of these radicals with an H atom is barrierless. On the basis of these reaction barriers, the authors conclude that the majority of methanol in the interstellar medium can be explained by the surface reaction of thermal H atoms with CO ice.

The surface reaction of hydrogen atoms with CO has also been treated theoretically. For example, Awad *et al*[95] use a kinetic model in order to derive rate constants for the successive hydrogenation reactions of CO in a mixed $H_2O$/CO ice from the experimental data of Watanabe *et al*[92]. This model initially assumes that H atoms do not penetrate the surface of the ice but does allow for cracks in the ice which increase the overall surface area for reaction. The model fits the experimental results of Watanabe *et al* well at early times. However, at later times, the model fails to predict the gradual decrease in the CO column density which is observed experimentally. Instead, the model predicts that the column density of CO should reach a constant positive value. This discrepancy is attributed by Awad *et al* to penetration of the ice by H atoms becoming more important at later times. The authors then use the deviation of the experimental results from those predicted by the kinetic model to estimate a rate constant for H atom diffusion in the ice. This diffusion constant is found to be $2.5 \times 10^{-21}$ cm$^2$ s$^{-1}$. Clearly then H atom diffusion into the mixed $H_2O$/CO ice is rather slow, especially when compared with the rate constant for H atom diffusion into hexagonal water ice (~$10^{-16}$ cm$^2$ s$^{-1}$).[96,97] However, the authors note that it has long been known that the surface mobility of H atoms on crystalline ice is substantially larger than on amorphous ice due to the highly irregular potential energy surface in the latter case, and therefore the same arguments may be expected to hold for H atom diffusion into the ice.[95,98] The rate constants derived by the authors again imply that much of the interstellar methanol can be accounted for by hydrogenation of CO on grain surfaces.

The reaction barriers for each reaction step in the sequential hydrogenation of CO to form methanol taking place on a silica surface have also been calculated by Goumans *et al* [99] using an embedded cluster model similar to that used in their study of the reactions of O and H atoms as described above.[77] The authors consider the reaction proceeding *via* a gas phase hydrogen atom reacting with a CO molecule adsorbed at three different reactive sites on an edingtonite (a barium aluminosilicate) (100) surface. These sites are a silanol, SiOH site, a silanolate, $SiO^-$ site, and a radicaloid SiO site. Both CO and reaction intermediates are weakly physisorbed at the SiOH site, thus the reaction barriers are found to be very similar to those in the gas phase: approximately 16 kJ $mol^{-1}$ for the addition of H to CO and approximately 22 – 23 kJ $mol^{-1}$ for the addition of H to $H_2CO$. The remaining two steps are barrierless radical-radical recombination reactions as for the gas phase. By contrast, when the reaction takes place at the $SiO^-$ site, the negative charge weakens the C≡O triple bond in CO and the C=O double bond in $H_2CO$. Consequently this silanolate site does show some catalytic behaviour with the reaction barriers reduced to 9.5 kJ $mol^{-1}$ and 18.5 kJ $mol^{-1}$ respectively for the addition of a hydrogen atom to CO and $H_2CO$ respectively. Finally the radicaloid site alters the reaction barriers for each step dramatically. This effect arises from the fact that CO can chemisorb without a barrier to the radicaloid site to form an SiO-C$^{\cdot}$=O radical which can then undergo a barrierless reaction with an H atom to form SiO-C(H)=O. However, the reaction of this closed shell intermediate with a further H atom now has a barrier of approximately 41 kJ $mol^{-1}$. A similar effect is seen for the third and fourth addition reactions: the addition of the third hydrogen atom is barrierless whilst addition of the final H atom to produce methanol has a barrier of 144 kJ $mol^{-1}$. A further effect of chemisorption discovered by the authors is that the final hydrogen addition step is mildly endothermic (0.9 kJ $mol^{-1}$). This endothermicity appears to arise from the breaking of the chemisorption bond when going from $CH_3O$ ($E_{ads}$ = 414.4 kJ $mol^{-1}$) to $CH_3OH$ ($E_{ads}$ = 13.1 kJ $mol^{-1}$). The authors conclude that whilst the SiO site shows a strong catalytic effect for addition of the first and third H atoms to CO removing the barriers completely, the introduction of barriers for the second and fourth addition steps renders this site a poor catalyst for methanol formation in the interstellar medium. Conversely the silanolate ($SiO^-$) site is predicted to catalyse methanol formation effectively, albeit still requiring quantum mechanical tunnelling at the low temperatures of the interstellar medium. These silanolate sites may be expected to be abundant in the interstellar medium due to the average negative charge of interstellar dust grains.[100]

### *H + Hydrocarbons*

The reactions of hydrogen atoms with ices of acetylene, $C_2H_2$, ethene, $C_2H_4$, ethane, $C_2H_6$ [101] and propene, $C_3H_6$, [102] have been studied by Hiraoka and co-workers. In the earlier study investigating the hydrogenation reactions of the $C_2$ hydrocarbons at 10 K, the authors find that both $C_2H_2$ and $C_2H_4$ are readily hydrogenated to $C_2H_6$ with similar saturation yields.[101] For example, for a 10 ML thick hydrocarbon reactant ice and a one hour hydrogen atom dosing time, the yield of $C_2H_6$ from $C_2H_2$ is approximately 30 % while that from $C_2H_4$ is approximately 40 %. It is interesting to note also that in the experiments on the hydrogenation of $C_2H_2$, no evidence of $C_2H_4$ could be observed, implying that the reaction of $C_2H_2$ with hydrogen atoms is the rate determining step while the reaction of $C_2H_4$ with hydrogen atoms is much faster. Indeed, the hydrogenation of $C_2H_4$ was reported to be approximately 6000 times faster than the that of $C_2H_2$ at 77 K by Bennett & Mile.[103] It is perhaps surprising then that the product yields are very similar for both reactions. The authors attribute this similarity in yields, despite the large difference in rates, to an increased sticking probability for hydrogen atoms on $C_2H_2$ ice compared to $C_2H_4$.

In the study of the reaction of $C_3H_6$ with hydrogen atoms, Hiraoka *et al* find, as expected, that the main product was propane, $C_3H_8$.[102] Additionally, other minor products were observed resulting from the reactions of radical intermediates, formed from the addition of hydrogen atoms to propene molecules, reacting with surrounding propene molecules. For example one of these minor products was found to be 2-methylpentane, $C_6H_{14}$, which can be formed from the reaction of a propyl ($C_3H_7$) radical with a $C_3H_6$ molecule, followed by addition of a hydrogen atom to the resulting 2-methylpentyl radical.

### *H + Other Oxygen Containing Molecules*

There has been some experimental attention devoted to the surface reactions of thermal H atoms with other oxygen containing molecules, especially those containing the carbonyl (C=O) bond. This focus on the reactions of carbonyl-containing species has perhaps been prompted by the reactivity of CO molecules towards H atoms, as discussed above. In particular the reactions of H atoms with ices of carbon dioxide ($CO_2$)[104], formic acid (HCOOH)[104], acetaldehyde ($CH_3CHO$)[104], acetone ($CH_3C(O)CH_3$)[105], and 2-propanol ($CH_3CH(OH)CH_3$)[105] have been studied.

Bisschop *et al* studied the reactions of hydrogen atoms with ices of $CO_2$, HCOOH and $CH_3CHO$ using both RAIRS and TPD. The authors found no evidence that $CO_2$ reacts with H atoms in the temperature range 12 – 60 K.[104] The reaction of $CO_2$ with two hydrogen atoms to form HCOOH is exothermic. Therefore, the authors conclude that the $HCO_2$ intermediate must be too high in energy to be formed efficiently at the temperatures investigated experimentally. Furthermore it was found that the presence of water ice did not catalyse the reaction, at least not substantially enough for any reaction products to be observed experimentally.

Bisschop and co-workers also studied the reaction of HCOOH ice with thermal H atoms. The product of sequential hydrogen atom addition reactions to HCOOH would be methylene glycol ($CH_2(OH)_2$), however none could be observed in RAIRS or TPD experiments. Furthermore no products involving breaking the bonds in the HCOOH molecule (e.g $H_2CO$, $CH_3OH$, $CO_2$, CO) could be observed.

The study by Bisschop *et al* also included an investigation of the reactivity of $CH_3CHO$ ice with H atoms. Using RAIRS, the authors could observe the formation of $H_2CO$, $CH_3OH$ and $CH_4$. However, the hydrogenation product, ethanol ($C_2H_5OH$), could not be observed using RAIRS. Nevertheless, ethanol was observed in the TPD spectra along with the aforementioned products. This finding indicates that the major mechanistic pathway for the reaction of H atoms with acetaldehyde ice involves the cleavage of the C—C bond of the acetaldehyde molecule, with simple hydrogenation of the carbonyl group to produce ethanol being a minor pathway. At temperatures around 15 K the authors determine rate constants in the region of $10^{-15}$ $cm^2$ $s^{-1}$ for the reaction of acetaldehyde ice with H atoms.

Hiraoka *et al* have investigated the reactions of H atoms with ices of acetone and 2-propanol at 13 – 100 K using TPD.[105] In the case of the acetone reaction, it was found that whilst no 2-propanol was formed, methane and methanol or ethanol, were both detected. The authors have difficulty in distinguishing between methanol and ethanol due to their very similar fragmentation patterns and desorption temperatures. The yield of methane after a reaction time of 60 minutes was approximately 10 % at 13 K, increasing towards 11 % at 40 K, above which temperature it started to desorb. The yield of methanol or ethanol was much lower at approximately 1 % and was largely independent of temperature, showing only a small increase at 100 K. The products of

the 2-propanol reaction with H atoms were found to be methane, methanol or ethanol, and acetone with yields (after 60 minutes reaction time) of approximately 17 %, 8 % and 7 % respectively at 13 K. These yields were found to be approximately constant for reaction temperatures up to 60 K (40 K for methane), above which the yields of alcohols and acetone increase to maxima of approximately 12 % and 15 % respectively. The authors attribute this increase at higher temperatures to the increased mobility of the organic reactant molecules in the ice, thus allowing the surface layers to be replenished by unreacted molecules from the bulk ice.

### *H + N, CN and HCN*

The reactions of hydrogen atoms with some nitrogen containing species which are considered likely to be present in interstellar ices has also received some experimental attention.[56,106-108] The earliest of these studies, performed by Hiraoka *et al*, investigated the reaction of N atoms trapped in an $N_2$ matrix with hydrogen atoms at 15 K using TPD.[106] The authors found that this reaction produced ammonia, albeit in low yield. However in a later study by the Hiraoka group investigating the reaction of D atoms with the cyano (CN) radical at 10 K to produce the deuterium cyanide isomers DCN and DNC, the authors see no evidence of $ND_3$ formation.[107] Given the group's earlier results on the reaction of N and H atoms, this finding is surprising because the CN radicals in these experiments were produced in a direct current discharge of a 50:1 mixture of $N_2$ and HCN which might also be expected to produce N atoms. In light of this result the authors conclude that the addition reactions NH + H and $NH_2$ + H must be inefficient under interstellar conditions. However, another explanation for the discrepancy between may simply be the inefficient formation of N atoms when there is an 'impurity' of HCN present in the $N_2$ discharge. Some circumstantial evidence for this explanation comes from the authors' observation of tholin films appearing on the walls of the discharge tube over time. Specifically, the formation of these tholins, which are essentially poorly characterised nitrogen rich organic materials, may occur *via* the reaction of nitrogen atoms with hydrocarbon radicals produced from HCN in the discharge. Alternatively CN radicals may simply out-compete N atoms for hydrogen atoms.

A more recent study by Hidaka *et al* investigated ammonia formation *via* the surface hydrogenation of N atoms using RAIRS.[56] In these experiments the authors confirm the formation of ammonia at 10 K but see no ammonia formation at 20 K, implying that the

reaction must proceed *via* an LH mechanism. The absence of an ER mechanism is unsurprising given the dilution of N atoms in the $N_2$ matrix. These experiments therefore appear to support the explanation that the presence of HCN in the $N_2$ discharge inhibits the production of N atoms, probably through their reaction with hydrocarbon fragments to produce tholins.

As previously mentioned, the primary purpose of the latter study by Hiraoka and co-workers[107] was to investigate the reaction of D atoms with CN radicals produced from a discharge in a mixture of HCN in $N_2$. After discounting any reaction of CN radicals with $D_2$, the authors conclude that this reaction does indeed proceed efficiently at 10 – 20 K. Both DCN and DNC were found to be produced with DNC being approximately 3 times higher in yield than DCN. Whist DNC is thermodynamically less stable than DCN, the barrier to isomerisation is sufficiently large (for example 127 kJ $mol^{-1}$ for HNC/HCN)[109] that isomerisation of DNC to DCN is practically forbidden at 10 – 20 K. It is therefore reasonable to take the ratio DNC to DCN observed in these experiments as representative of the ratio in which they are originally formed. The yield of both DCN and DNC was found to be largest at 10 K, decreasing to an almost negligible level at 20 K, an effect the authors attribute to the decreased sticking probability of H atoms at 20 K. This explanation implies that no product is formed *via* the Eley-Rideal mechanism, again unsurprising, given the low concentration of CN radicals in the $N_2$ matrix. Whilst no quantative evaluation of the efficiency of this surface reaction route to HCN/HNC formation with respect to other mechanisms was provided, the authors note that the high abundance of CN radicals in the interstellar medium implies that these surface reactions may be important in interstellar clouds.

More recently the reaction of the HCN molecule itself with H atoms was studied by Theule *et al.*[108] The reactions of other unsaturated bonds, such as C=C, C≡C, and C=O bonds, with H atoms has been widely studied as discussed above. Consequently the reactions of C≡N bonds with hydrogen atoms are of significant astrophysical interest, especially given their potential for forming amine containing prebiotic molecules such as amino acids. In these experiments HCN was deposited onto a polished copper surface at 15 K. The HCN ice was then dosed with a total H atom fluence of typically $10^{18}$ $cm^{-2}$. The H atoms in these experiments were produced in a microwave discharge of $H_2$. Following the irradiation of the HCN ice with H atoms, no products were observable using IR spectroscopy, however methylamine, $CH_3NH_2$ was detected using TPD. From

this finding it is clear that methylamine is produced from the hydrogenation of HCN in rather low yield. The authors also searched for the intermediate imine species, $H_2C$=NH, however it was not detected, implying that the hydrogenation of the imine group proceeds much more rapidly than that of the nitrile group and thus that the formation of the imine from HCN is the rate determining step. The non-observation of the imine could also be explained if the reaction proceeded *via* a carbene (HC—$NH_2$) or a nitrene ($H_3C$—N) intermediate. However, it appears unlikely that the formation of such biradical species would be preferred over that of the closed shell imine.

## 1.9 The UCL Cosmic Dust Experiment

As discussed above, experimental studies of the heterogeneous thermal reactions of oxygen atoms are somewhat limited, covering only three reactions; O + H, O + CO and O + $O_2$.[57,74,80,81,110] Consequently, our current understanding of the reactions of thermal oxygen atoms in interstellar ices is severely limited. Furthermore, given that oxygen is the third most abundant element in the Universe, the chemistry of oxygen atoms in the interstellar medium is of significant interest. Furthermore, the importance of oxygen in forming prebiotic molecules such as simple amino acids and sugars gives extra significance to the chemistry of oxygen in the interstellar medium. One of the aims of the current work is therefore to further our understanding of surface reactions that are available to thermal oxygen atoms as well as to derive kinetic data for such reactions. Such data can be used in astrochemical models.

Whilst the surface reactions of thermal hydrogen atoms have been more widely studied, the majority of these studies have focussed on $H_2$ formation *via* the surface catalysed recombination of two hydrogen atoms. The surface reactions of hydrogen atoms with other molecules, such as CO, O, $O_2$, $O_3$, $CO_2$ and HCOOH to name a few, have been studied experimentally. However, there are still many hydrogenation reactions which are astrophysically relevant but have received little attention. For example, little attention has been paid to the reactions of hydrogen atoms with ices of sulfur-bearing molecules. In fact, no previous astrochemical studies of the thermal reactions of sulfur-bearing molecules in interstellar ices have reported in the literature. This neglect of sulfur bearing molecules is surprising for two reasons: firstly OCS and $SO_2$ have already been detected in interstellar ices, and secondly, the observed depletion of sulfur in the gas phase implies that a substantial proportion of sulfur in the interstellar medium

is frozen out onto interstellar dust grain surfaces. A second aim of the work presented in this thesis is therefore to elucidate some of the, as yet unstudied, thermal reactions of hydrogen atoms. In particular, those reactions relevant to sulfur chemistry, which may take place on interstellar grain surfaces, are investigated. Again kinetic data is derived for use in astrochemical models.

As described above, the UCL cosmic dust experiment was originally designed to probe the fate of the 4.5 eV of binding energy released upon the recombination of two hydrogen atoms on the surface of an interstellar dust grain analogue. However, as will be described in detail in the next chapter, the experimental setup has been modified significantly to allow the study of the reactions of species heavier than hydrogen. In particular this modification has involved adapting the experimental apparatus to allow temperature programmed desorption (TPD) experiments to be carried out.

## 1.10 Summary

This Chapter has introduced, and provided an overview, of the field of astrochemistry and outlined the astrophysical motivation for studying the chemistry of the interstellar medium. In particular, a presentation of the current understanding of chemistry in the interstellar medium has been provided as well as a detailed review of previous experimental and theoretical studies of the thermal heterogeneous reactions of hydrogen and oxygen atoms in the interstellar medium. Furthermore the aims of the experimental investigations presented in this thesis have been set out. The following chapters will discuss the experimental setup and the method employed for deriving kinetic parameters from the experimental data. Later chapters will discuss the results of experimental investigations of particular reactions of hydrogen and oxygen atoms.

## 1.11 References


(1) Dyson, J. E.; Williams, D. A. *The Physics of the Interstellar Medium*, 2nd ed.; Institute of Physics: Bristol, 1997.
(2) Kwok, S.; Zhang, Y. *Nature* **2011**, *479*, 80.
(3) Kallman, C. G. *Physics Letters B* **1982**, *112*, 213.
(4) Olive, K. A. *Nuclear Physics B* **1981**, *190*, 483.
(5) Lepp, S.; Stancil, P. C.; Dalgarno, A. *Journal of Physics B-Atomic Molecular and Optical Physics* **2002**, *35*, R57.
(6) Latter, W. B.; Black, J. H. *Astrophysical Journal* **1991**, *372*, 161.
(7) Glover, S. C. O. *Astrophysical Journal* **2003**, *584*, 331.
(8) Hoyle, F.; Fowler, W. A. *Astrophysical Journal* **1960**, *132*, 565.
(9) Snow, T. P.; McCall, B. J. *Annual Review of Astronomy and Astrophysics* **2006**, *44*, 367.
(10) Williams, D. A.; Herbst, E. *Surface Science* **2002**, *500*, 823.
(11) Tielens, A.; Hagen, W. *Astronomy and Astrophysics* **1982**, *114*, 245.
(12) Herbst, E. *Chemical Society Reviews* **2001**, *30*, 168.
(13) Burke, D. J.; Brown, W. A. *Physical Chemistry Chemical Physics* **2010**, *12*, 5947.
(14) Baouche, S.; Gamborg, G.; Petrunin, V. V.; Luntz, A. C.; Baurichter, A.; Hornekaer, L. *Journal Of Chemical Physics* **2006**, *125*.
(15) Creighan, S. C.; Perry, J. S. A.; Price, S. D. *Journal Of Chemical Physics* **2006**, *124*.
(16) Gough, S.; Schermann, C.; Pichou, F.; Landau, M.; Cadez, I.; Hall, R. I. *Astronomy and Astrophysics* **1996**, *305*, 687.
(17) Hornekaer, L.; Baurichter, A.; Petrunin, V. V.; Field, D.; Luntz, A. C. *Science* **2003**, *302*, 1943.
(18) Hornekaer, L.; Baurichter, A.; Petrunin, V. V.; Luntz, A. C.; Kay, B. D.; Al-Halabi, A. *Journal of Chemical Physics* **2005**, *122*.
(19) Hornekaer, L.; Rauls, E.; Xu, W.; Sljivancanin, Z.; Otero, R.; Stensgaard, I.; Laegsgaard, E.; Hammer, B.; Besenbacher, F. *Physical Review Letters* **2006**, *97*.
(20) Hornekaer, L.; Sljivancanin, Z.; Xu, W.; Otero, R.; Rauls, E.; Stensgaard, I.; Laegsgaard, E.; Hammer, B.; Besenbacher, F. *Physical Review Letters* **2006**, *96*.
(21) Islam, F.; Latimer, E. R.; Price, S. D. *Journal Of Chemical Physics* **2007**, *127*, 064701.
(22) Latimer, E. R.; Islam, F.; Price, S. D. *Chemical Physics Letters* **2008**, *455*, 174.
(23) Manico, G.; Raguni, G.; Pirronello, V.; Roser, J. E.; Vidali, G. *Astrophysical Journal* **2001**, *548*, L253.
(24) Perry, J. S. A.; Gingell, J. M.; Newson, K. A.; To, J.; Watanabe, N.; Price, S. D. *Measurement Science & Technology* **2002**, *13*, 1414.
(25) Pirronello, V.; Biham, O.; Liu, C.; Shen, L. O.; Vidali, G. *Astrophysical Journal* **1997**, *483*, L131.

(26) Pirronello, V.; Liu, C.; Roser, J. E.; Vidali, G. *Astronomy and Astrophysics* **1999**, *344*, 681.
(27) Pirronello, V.; Liu, C.; Shen, L. Y.; Vidali, G. *Astrophysical Journal* **1997**, *475*, L69.
(28) Vidali, G.; Roser, J. E.; Manico, G.; Pirronello, V. *Journal of Geophysical Research-Planets* **2004**, *109*.
(29) Vidali, G.; Roser, J. E.; Manico, G.; Pirronello, V. Experimental study of the formation of molecular hydrogen and carbon dioxide on dust grain analogues. In *Space Life Sciences: Steps toward Origin(S) of Life*, 2004; Vol. 33; pp 6.
(30) Gould, R. J.; Salpeter, E. E. *Astrophysical Journal* **1963**, *138*, 393.
(31) Hollenbach, D. J.; Salpeter, E. E. *Astrophysical Journal* **1971**, *163*, 155.
(32) Bachellerie, D.; Sizun, M.; Aguillon, F.; Sidis, V. *Journal of Physical Chemistry A* **2009**, *113*, 108.
(33) Bachellerie, D.; Sizun, M.; Aguillon, F.; Teillet-Billy, D.; Rougeau, N.; Sidis, V. *Physical Chemistry Chemical Physics* **2009**, *11*, 2715.
(34) Biham, O.; Furman, I.; Katz, N.; Pirronello, V.; Vidali, G. *Monthly Notices of the Royal Astronomical Society* **1998**, *296*, 869.
(35) Farebrother, A. J.; Meijer, A. J. H. M.; Clary, D. C.; Fisher, A. J. *Chemical Physics Letters* **2000**, *319*, 303.
(36) Jackson, B.; Lemoine, D. *Journal of Chemical Physics* **2001**, *114*, 474.
(37) Katz, N.; Furman, I.; Biham, O.; Pirronello, V.; Vidali, G. *Astrophysical Journal* **1999**, *522*, 305.
(38) Kim, Y. H.; Ree, J.; Shin, H. K. *Chemical Physics Letters* **1999**, *314*, 1.
(39) Meijer, A.; Farebrother, A. J.; Clary, D. C. *Journal of Physical Chemistry A* **2002**, *106*, 8996.
(40) Meijer, A.; Farebrother, A. J.; Clary, D. C.; Fisher, A. J. *Journal of Physical Chemistry A* **2001**, *105*, 2173.
(41) Meijer, A.; Fisher, A. J.; Clary, D. C. *Journal of Physical Chemistry A* **2003**, *107*, 10862.
(42) Morisset, S.; Aguillon, F.; Sizun, M.; Sidis, V. *Chemical Physics Letters* **2003**, *378*, 615.
(43) Morisset, S.; Aguillon, F.; Sizun, M.; Sidis, V. *Physical Chemistry Chemical Physics* **2003**, *5*, 506.
(44) Morisset, S.; Aguillon, F.; Sizun, M.; Sidis, V. *Journal of Physical Chemistry A* **2004**, *108*, 8571.
(45) Morisset, S.; Aguillon, F.; Sizun, M.; Sidis, V. *Journal of Chemical Physics* **2004**, *121*, 6493.
(46) Morisset, S.; Aguillon, F.; Sizun, M.; Sidis, V. *Journal of Chemical Physics* **2005**, *122*, art. no.
(47) Parneix, P.; Brechignac, P. *Astronomy and Astrophysics* **1998**, *334*, 363.
(48) Rutigliano, M.; Cacciatore, M.; Billing, G. D. *Chemical Physics Letters* **2001**, *340*, 13.

(49) Sha, X. W.; Jackson, B. *Surface Science* **2002**, *496*, 318.
(50) Sha, X. W.; Jackson, B.; Lemoine, D. *Journal of Chemical Physics* **2002**, *116*, 7158.
(51) Ree, J.; Kim, Y. H.; Shin, H. K. *Chemical Physics Letters* **2002**, *353*, 368.
(52) Takahashi, J.; Masuda, K.; Nagaoka, M. *Monthly Notices of the Royal Astronomical Society* **1999**, *306*, 22.
(53) Takahashi, J.; Masuda, K.; Nagaoka, M. *Astrophysical Journal* **1999**, *520*, 724.
(54) Fuchs, G. W.; Cuppen, H. M.; Ioppolo, S.; Romanzin, C.; Bisschop, S. E.; Andersson, S.; van Dishoeck, E. F.; Linnartz, H. *Astronomy & Astrophysics* **2009**, *505*, 629.
(55) Romanzin, C.; Ioppolo, S.; Cuppen, H. M.; van Dishoeck, E. F.; Linnartz, H. *Journal of Chemical Physics* **2011**, *134*.
(56) Hidaka, H.; Watanabe, M.; Kouchi, A.; Watanabe, N. *Physical Chemistry Chemical Physics* **2011**, *13*, 15798.
(57) Hiraoka, K.; Miyagoshi, T.; Takayama, T.; Yamamoto, K.; Kihara, Y. *Astrophysical Journal* **1998**, *498*, 710.
(58) Boogert, A. C. A.; Schutte, W. A.; Helmich, F. P.; Tielens, A.; Wooden, D. H. *Astronomy and Astrophysics* **1997**, *317*, 929.
(59) Palumbo, M. E.; Geballe, T. R.; Tielens, A. *Astrophysical Journal* **1997**, *479*, 839.
(60) Gerakines, P. A.; Whittet, D. C. B.; Ehrenfreund, P.; Boogert, A. C. A.; Tielens, A.; Schutte, W. A.; Chiar, J. E.; van Dishoeck, E. F.; Prusti, T.; Helmich, F. P.; de Graauw, T. *Astrophysical Journal* **1999**, *522*, 357.
(61) Bennett, C. J.; Jamieson, C. S.; Osamura, Y.; Kaiser, R. I. *Astrophysical Journal* **2006**, *653*, 792.
(62) Martinazzo, R.; Tantardini, G. F. *Journal Of Chemical Physics* **2006**, *124*.
(63) Roser, J. E.; Manico, G.; Pirronello, V.; Vidali, G. *Astrophysical Journal* **2002**, *581*, 276.
(64) Roser, J. E.; Swords, S.; Vidali, G.; Manico, G.; Pirronello, V. *Astrophysical Journal* **2003**, *596*, L55.
(65) Hollenbach, D.; Salpeter, E. E. *Journal of Chemical Physics* **1970**, *53*, 79.
(66) Jura, M. *Astrophysical Journal* **1975**, *197*, 575.
(67) Jeloaica, L.; Sidis, V. *Chemical Physics Letters* **1999**, *300*, 157.
(68) Piper, L. G.; Rawlins, W. T. *Abstracts of Papers of the American Chemical Society* **1982**, *184*, 63.
(69) Piper, L. G.; Rawlins, W. T. *Journal of Physical Chemistry* **1986**, *90*, 320.
(70) Sol, V. M.; Louw, R.; Mulder, P. *Recueil Des Travaux Chimiques Des Pays-Bas-Journal of the Royal Netherlands Chemical Society* **1990**, *109*, 346.
(71) Sol, V. M.; Vandrunen, M. A.; Louw, R.; Mulder, P. *Journal of the Chemical Society-Perkin Transactions 2* **1990**, 937.

(72) Tsuji, M.; Kumagae, J.; Nakano, K.; Matsuzaki, T.; Tsuji, T. *Applied Surface Science* **2003**, *217*, 134.
(73) Ung, A. Y. M. *Chemical Physics Letters* **1975**, *32*, 351.
(74) Dulieu, F.; Amiaud, L.; Congiu, E.; Fillion, J. H.; Matar, E.; Momeni, A.; Pirronello, V.; Lemaire, J. L. *Astronomy & Astrophysics* **2010**, *512*, 5.
(75) Papoular, R. *Monthly Notices of the Royal Astronomical Society* **2005**, *362*, 489.
(76) Cazaux, S.; Cobut, V.; Marseille, M.; Spaans, M.; Caselli, P. *Astronomy & Astrophysics*, *522*, 14.
(77) Goumans, T. P. M.; Catlow, C. R. A.; Brown, W. A.; Kastner, J.; Sherwood, P. *Physical Chemistry Chemical Physics* **2009**, *11*, 5431.
(78) Bergeron, H.; Rougeau, N.; Sidis, V.; Sizun, M.; Teillet-Billy, D.; Aguillon, F. *Journal of Physical Chemistry A* **2008**, *112*, 11921.
(79) Cuppen, H. M.; Herbst, E. *Astrophysical Journal* **2007**, *668*, 294.
(80) Roser, J. E.; Vidali, G.; Manico, G.; Pirronello, V. *Astrophysical Journal* **2001**, *555*, L61.
(81) Raut, U.; Baragiola, R. A. *Astrophysical Journal Letters* **2011**, *737*.
(82) Goumans, T. P. M.; Andersson, S. *Monthly Notices of the Royal Astronomical Society* **2010**, *406*, 2213.
(83) Ioppolo, S.; van Boheemen, Y.; Cuppen, H. M.; van Dishoeck, E. F.; Linnartz, H. *Monthly Notices of the Royal Astronomical Society* **2011**, *413*, 2281.
(84) Noble, J. A.; Dulieu, F.; Congiu, E.; Fraser, H. J. *Astrophysical Journal* **2011**, *735*.
(85) Oba, Y.; Watanabe, N.; Kouchi, A.; Hama, T.; Pirronello, V. *Physical Chemistry Chemical Physics* **2011**, *13*, 15792.
(86) Ioppolo, S.; Cuppen, H. M.; Romanzin, C.; van Dishoeck, E. F.; Linnartz, H. *Astrophysical Journal* **2008**, *686*, 1474.
(87) Miyauchi, N.; Hidaka, H.; Chigai, T.; Nagaoka, A.; Watanabe, N.; Kouchi, A. *Chemical Physics Letters* **2008**, *456*, 27.
(88) Mokrane, H.; Chaabouni, H.; Accolla, M.; Congiu, E.; Dulieu, F.; Chehrouri, M.; Lemaire, J. L. *Astrophysical Journal Letters* **2009**, *705*, L195.
(89) Hiraoka, K.; Ohashi, N.; Kihara, Y.; Yamamoto, K.; Sato, T.; Yamashita, A. *Chemical Physics Letters* **1994**, *229*, 408.
(90) Hiraoka, K.; Sato, T.; Sato, S.; Sogoshi, N.; Yokoyama, T.; Takashima, H.; Kitagawa, S. *Astrophysical Journal* **2002**, *577*, 265.
(91) Watanabe, N.; Kouchi, A. *Astrophysical Journal* **2002**, *571*, L173.
(92) Watanabe, N.; Shiraki, T.; Kouchi, A. *Astrophysical Journal* **2003**, *588*, L121.
(93) Watanabe, N.; Nagaoka, A.; Shiraki, T.; Kouchi, A. *Astrophysical Journal* **2004**, *616*, 638.
(94) Hidaka, H.; Watanabe, N.; Shiraki, T.; Nagaoka, A.; Kouchi, A. *Astrophysical Journal* **2004**, *614*, 1124.
(95) Awad, Z.; Chigai, T.; Kimura, Y.; Shalabiea, O. M.; Yamamoto, T. *Astrophysical Journal* **2005**, *626*, 262.

(96) Bartels, D. M.; Han, P.; Percival, P. W. *Chemical Physics* **1992**, *164*, 421.
(97) Strauss, H. L.; Chen, Z.; Loong, C. K. *Journal of Chemical Physics* **1994**, *101*, 7177.
(98) Smoluchowski, R. *Journal of Physical Chemistry* **1983**, *87*, 4229.
(99) Goumans, T. P. M.; Richard, C.; Catlow, A.; Brown, W. A. *Journal of Chemical Physics* **2008**, *128*, 6.
(100) Gail, H. P.; Sedlmayr, E. *Astronomy and Astrophysics* **1975**, *41*, 359.
(101) Hiraoka, K.; Takayama, T.; Euchi, A.; Handa, H.; Sato, T. *Astrophysical Journal* **2000**, *532*, 1029.
(102) Hiraoka, K.; Sato, T.; Sato, S.; Takayama, T.; Yokoyama, T.; Sogoshi, N.; Kitagawa, S. *Journal of Physical Chemistry B* **2002**, *106*, 4974.
(103) Bennett, J. E.; Mile, B. *Journal of the Chemical Society-Faraday Transactions I* **1973**, *69*, 1398.
(104) Bisschop, S. E.; Fuchs, G. W.; van Dishoeck, E. F.; Linnartz, H. *Astronomy & Astrophysics* **2007**, *474*, 1061.
(105) Hiraoka, K.; Yamashita, A.; Miyagoshi, T.; Oohashi, N.; Kihara, Y.; Yamamoto, K. *Astrophysical Journal* **1998**, *508*, 423.
(106) Hiraoka, K.; Yamashita, A.; Yachi, Y.; Aruga, K.; Sato, T.; Muto, H. *Astrophysical Journal* **1995**, *443*, 363.
(107) Hiraoka, K.; Ushiama, S.; Enoura, T.; Unagiike, H.; Mochizuki, N.; Wada, A. *Astrophysical Journal* **2006**, *643*, 917.
(108) Theule, P.; Borget, F.; Mispelaer, F.; Danger, G.; Duvernay, F.; Guillemin, J. C.; Chiavassa, T. *Astronomy & Astrophysics* **2011**, *534*.
(109) Gazdy, B.; Musaev, D. G.; Bowman, J. M.; Morokuma, K. *Chemical Physics Letters* **1995**, *237*, 27.
(110) Grim, R. J. A.; Dhendecourt, L. B. *Astronomy and Astrophysics* **1986**, *167*, 161.

# Chapter 2 – Experimental Methodology and Data Analysis

## 2.1 Overview

The UCL Cosmic Dust experiment was initially designed to probe the recombination of atomic hydrogen atoms, to form $H_2$, on the surface of an interstellar dust grain analogue, under astrophysically relevant conditions.[1] The aim of the experiment was to determine the fate of the 4.5 eV of energy released following the formation of an H—H bond. Specifically, the rovibrational distribution of the nascent $H_2$ molecules was measured resonance enhanced multi-photon ionization (REMPI). For experimental reasons, the recombination of hydrogen and deuterium atoms to form hydrogen deuteride (HD) was studied and a complete rovibrational distribution for HD formed in this manner was obtained before the start of the work discussed here. Following the HD experiments, several modifications have been made to the experimental setup in order to allow the study of the chemistry of heavier species on interstellar dust grain analogues. The principal experimental difference between studying HD formation and studying the chemistry of heavier species is that HD desorbs from the surface spontaneously upon formation due to the exothermicity of the recombination reaction; in contrast to HD, heavier species remain bound to the surface. A means of desorbing any reaction products into the gas phase for detection is therefore required. The experiments discussed here therefore employ a TPD technique to probe such reaction products formed following the dosing of astrophysically relevant species onto an HOPG surface which is held at temperatures relevant to the interstellar medium. Typically, potential reactants are dosed for one hour onto the surface which is then warmed in order to desorb all species on the surface into the gas phase. A consequence of using this TPD technique is that a means of efficiently ionizing the desorbed molecules, regardless of their rovibrational state, is required. The desorbing species are therefore ionized using electrons and detected by a time of flight mass spectrometer.

The interstellar dust grain analogue used in these experiments is a slab of highly oriented pyrolitic graphite (HOPG) measuring 20 mm × 10 mm × 2 mm. The ordering of the atomic layers in graphite is represented by the ‘mosaic spread’, measured in degrees; a lower value for the mosaic spread indicates a more ordered structure. The mosaic spread of the sample of HOPG used in these experiments is 3.5 ° ± 1.5 °. A more defective graphite surface, or even amorphous carbon, would perhaps represent more astrophysically realistic substrate upon which to study reactions. However, in

order to allow for comparison with theoretical studies, which have predominantly used graphene as a model for carbonaceous dust grains surfaces, HOPG has been used as the analogue of an interstellar grain surface.

## 2.2 Vacuum Setup

The present experiment is housed in two differentially pumped stainless steel vacuum chambers sealed with conflat flanges. Two identical microwave discharge cells are installed in a high vacuum (HV) "source" chamber whilst a second ultra high vacuum (UHV) "target" chamber contains a cryogenically cooled HOPG substrate mounted adjacent to the source region of a time-of-flight mass spectrometer (TOFMS). The base pressure in the source chamber is typically $1 \times 10^{-7}$ Torr, whilst in the target chamber the base pressure is $1 \times 10^{-10}$ Torr. Under normal experimental conditions the pressure in the source chamber is in the region of $1 \times 10^{-6}$ Torr whilst in the target chamber during dosing it is $1 \times 10^{-8}$ Torr. These elevated operating pressures are due to the reactant gases present in the chambers. For comparison, dense interstellar clouds typically have a number density of $10^{10}$ $m^{-3}$ and a gas temperature of 10 K, which is equivalent to a pressure of approximately $1 \times 10^{-14}$ Torr.[2] Nevertheless, the pressures used in the present experiments allow astrophysical reactions to be studied on a laboratory timescale whilst still being sufficiently low that gas phase interactions of species are negligible. Additionally, the very low collisional fluxes under UHV conditions allow surface experiments to be carried out at low temperatures over several hours without significant contamination arising from adsorption of background gases.

The operating pressures in each chamber are maintained by separate turbomolecular pumps (TMPs) with pumping speeds of 400 l $s^{-1}$ for $N_2$. These TMPs are each backed by two-stage rotary pumps. In the target chamber a titanium sublimation pump is also installed which can be used to enhance the pumping speed of hydrogen, a gas which, due to its low molecular mass, is less efficiently removed by momentum transfer pumps such as TMPs. The pressure in the source chamber is monitored by means of a Penning gauge, whilst that in the target chamber is monitored using an ion gauge. A schematic diagram of the entire experimental apparatus is shown in Figure 2.1.

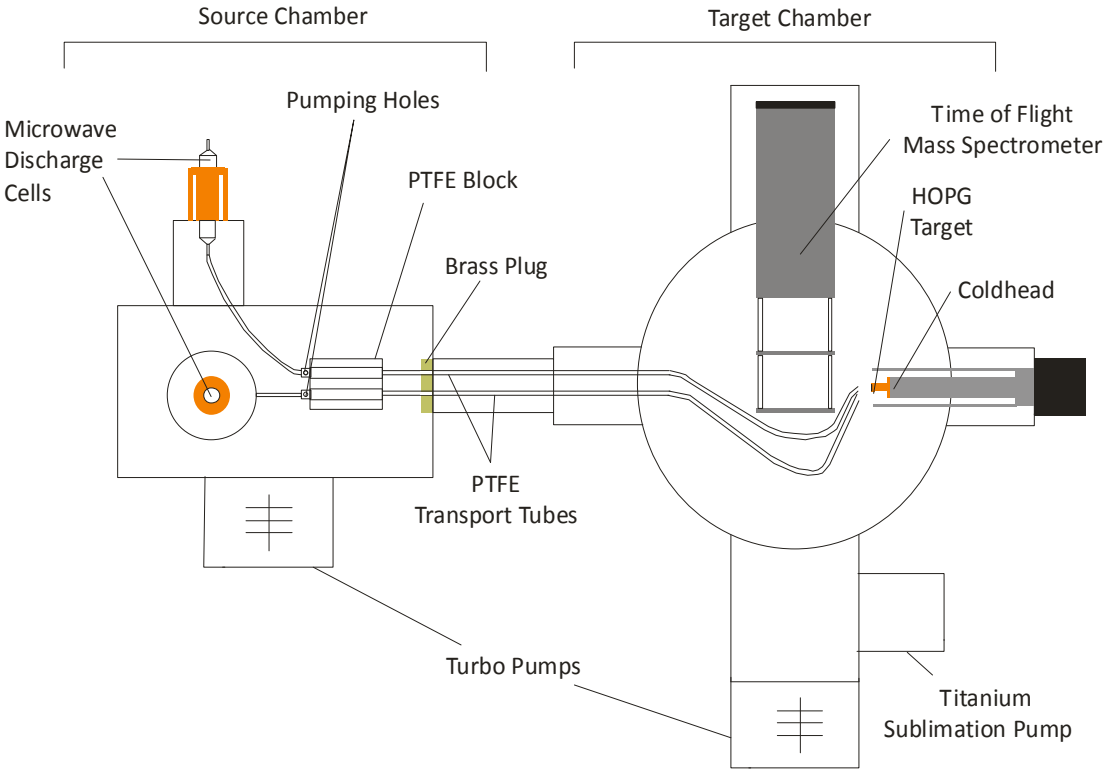


Figure 2.1 A schematic diagram of the experimental arrangement.

## 2.3 Generation of Atomic Species

In the current experimental setup two separate microwave discharge sources are available for generating atoms or free radicals. Each source consists of a Pyrex discharge cell, measuring 260 mm long with an outer diameter of 25.5 mm, surrounded by a two-piece cylindrical copper radiator based upon the design of McCullough *et al.*[3,4] The Pyrex discharge cells are pre-treated with *ortho*-phosphoric acid for a minimum of 12 hours in order to reduce the atomic recombination efficiency on the Pyrex surface.[5] The two pieces of each copper radiator are designed to fit together such that there is a minimum clearance between the copper radiator and the Pyrex cell, thus ensuring the efficient coupling of the microwaves into the plasma whilst avoiding any strain on the Pyrex cell. Each piece of the copper radiator has two pairs of 2 mm wide slots cut into it which link to a female type-N connector (see Figure 2.2). When microwaves are applied to the copper radiator a potential difference is induced across the walls of these slots. The superposition of the potential differences from the four pairs of radiator slots gives rise to an oscillating electric field between the radiators. Therefore, when some of the gas molecules in the Pyrex discharge cell are ionized, for example by touching the high voltage tip of a Tesla coil to the outside of the discharge cell, the resulting free electrons oscillate in the electric field produced by the microwave radiator and collide with other

gas molecules. These electron-molecule collisions result in further ionization of the gas resulting in a ‘cascade’ effect. This ionization cascade produces a plasma in the discharge tube. This type of plasma is known as a ‘low temperature plasma’ because, whilst electrons in the plasma are excited by the microwave frequency electric field, neutral species and ions (which are too heavy to respond to the rapidly oscillating electric field) remain relatively close to the ambient temperature. The electron-molecule collisions in the plasma also promote the dissociation of the gas in the discharge cell, thus allowing atoms and radicals to be generated from appropriate precursor gases.

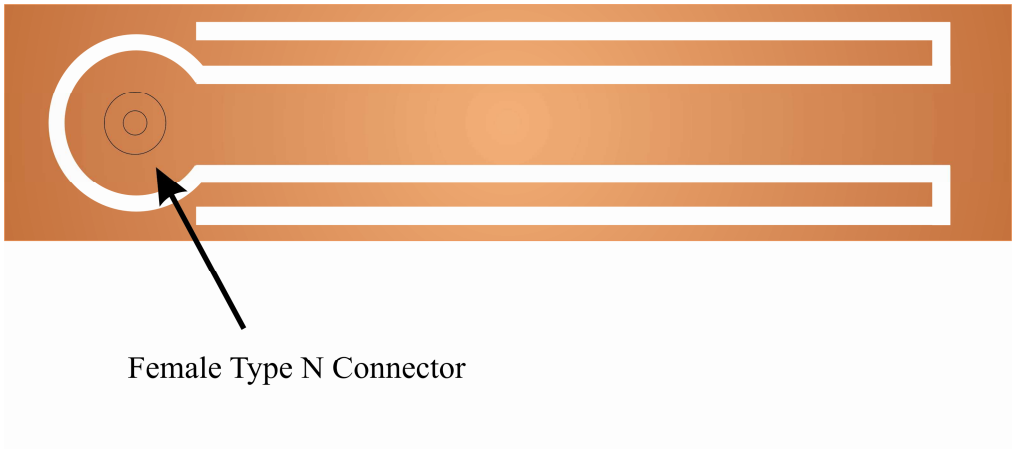


Figure 2.2 A schematic diagram of the inside surface of a semi-cylindrical microwave radiator.

Microwaves with a frequency of 2.45 GHz are supplied from a Sairem microwave generator to the copper radiators *via* two Sucoflex wave guides. The lengths of these two waveguides are chosen to be different by half a wavelength, resulting in the microwaves arriving at each side of the copper radiator 180 ° out of phase.[6] The microwave power available from the microwave generator is adjustable up to 300 W, but in these experiments microwave powers of 200 W were used for atomic hydrogen and deuterium generation from $H_2$ and $D_2$ gas respectively, whilst 180 W were used for the generation of atomic oxygen from $O_2$ gas. These powers were chosen as they represented the values at which the reflected microwave power (i.e. that which is not coupled into the plasma) reached a minimum. The microwave generator is designed to operate safely with the reflected power up to 10 % of the output power. However, keeping the reflected power to a minimum is important as large reflected powers can shorten the life of the magnetron. Typically, the reflected power achieved in these experiments is less than 2 % of the output power.

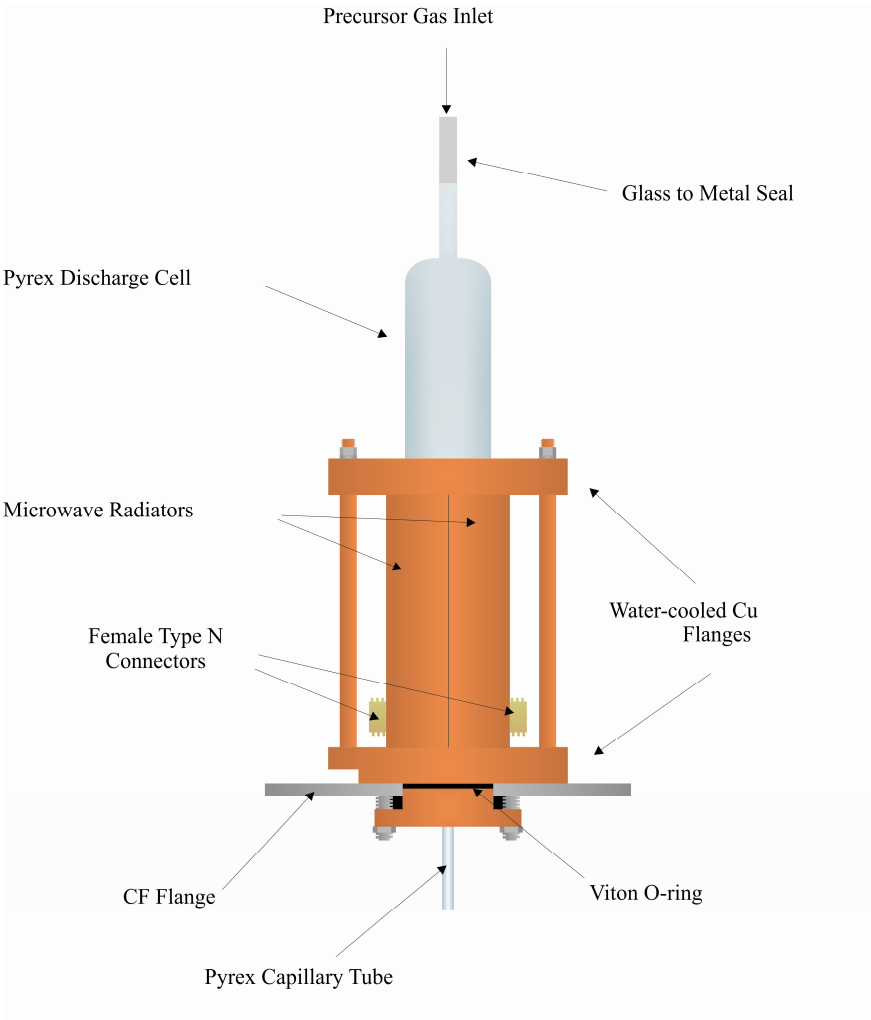


Figure 2.3 A schematic diagram of a microwave discharge source.

A schematic diagram of an entire microwave discharge source is shown in Figure 2.3. As shown in the diagram, the microwave discharge cell is cooled by being in thermal contact with a water cooled copper flange at either end. Sufficient cooling of the discharge cell is important for atom generation, as the atomic recombination efficiency on a Pyrex surface increases with increasing temperature.[7] The gas inlet line is connected to the glass to metal seal at the top of the discharge cell by a Cajon fitting, while the PTFE atom transport tube inside the vacuum chamber is simply pushed snugly over the end of the glass capillary of the discharge cell.

The precursor gases used for atomic oxygen, atomic hydrogen and atomic deuterium generation are oxygen ($O_2$) (99.5 %), hydrogen ($H_2$) (99.995 %) and deuterium ($D_2$) (99.9 %). In order to remove any contamination of the discharge cell by air, the gas inlet lines are flushed several times with the relevant precursor gas before being switched on. The source pressure at which the maximum flux of H or D atoms is achieved has previously been determined to be in the region of 0.4 – 0.6 Torr and so a source

pressure of 0.4 Torr is used in the current experiments in order to keep the pressure in the target chamber to a minimum. The dissociation efficiency and O atom intensity for an oxygen discharge, measured by recording electron ionization mass spectra of the gas effusing from the PTFE atom transport tube, is shown in Figure 2.4. Clearly dissociation efficiency increases at low pressures whilst overall O atom intensity increases towards high pressures. This is to be expected since at low pressures there are fewer collisions and so recombination of oxygen atoms is reduced, whilst at higher pressures the larger flux of $O_2$ results in the production of more O atoms, but at the same time reduces the ratio of $O:O_2$ and hence the dissociation efficiency. In these experiments as large a flux of O atoms as possible is required, albeit with a minimum amount of residual $O_2$. Hence an O atom source pressure of 0.20 Torr is used, where a compromise is reached between dissociation efficiency and overall O atom flux.

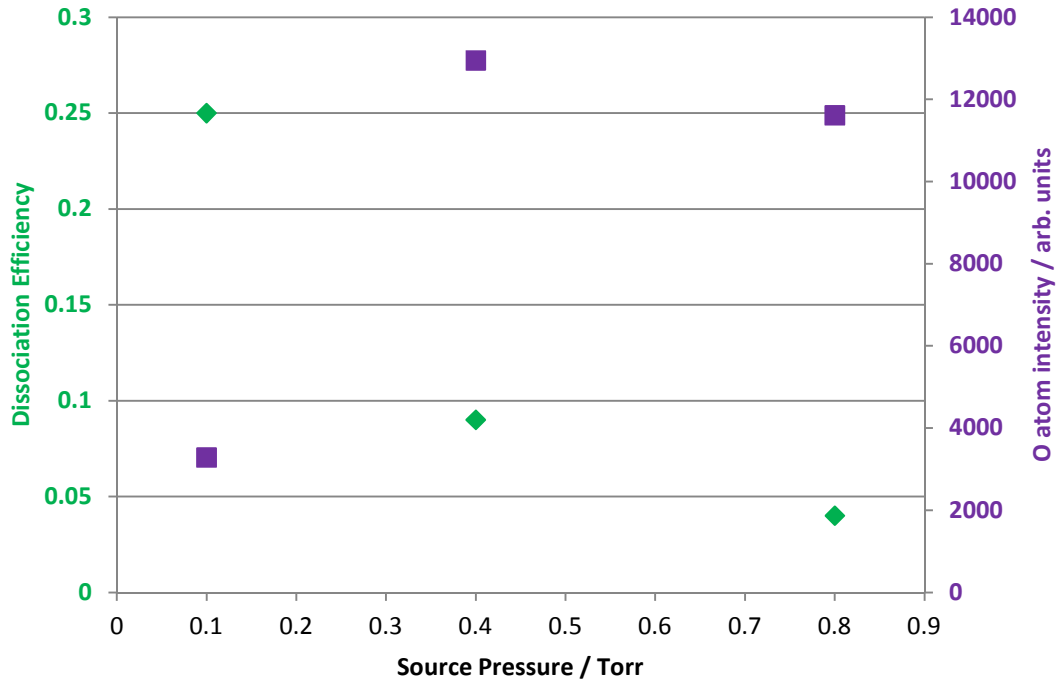


Figure 2.4 Graph showing the dependence of the O atom intensity (purple squares) and the dissociation efficiency (green diamonds) on the pressure of $O_2$ gas in the microwave discharge cell.

In order to ensure the atom source operates safely when unsupervised, gas cylinders are connected to the Pyrex discharge cell *via* a solenoid valve which automatically closes should certain conditions arise. These conditions are that the temperature of the discharge cell rises above 25 °C, the pressure in either chamber increases above $5 \times 10^{-5}$ Torr or the brightness of the light emitted by the plasma falls below a pre-determined level. These measures are particularly necessary for H or D atom generation

not only because the flammability of $H_2$ and $D_2$ means that a gas leak would be potentially dangerous, but also because the H or D atom source requires several hours for the flux to reach a maximum. This conditioning period can be attributed to impurities in the discharge cell, which condense onto the cooled cell walls whilst the discharge is off, taking some time to be consumed by reactions in the discharge. Consequently the D atom source is run continuously.

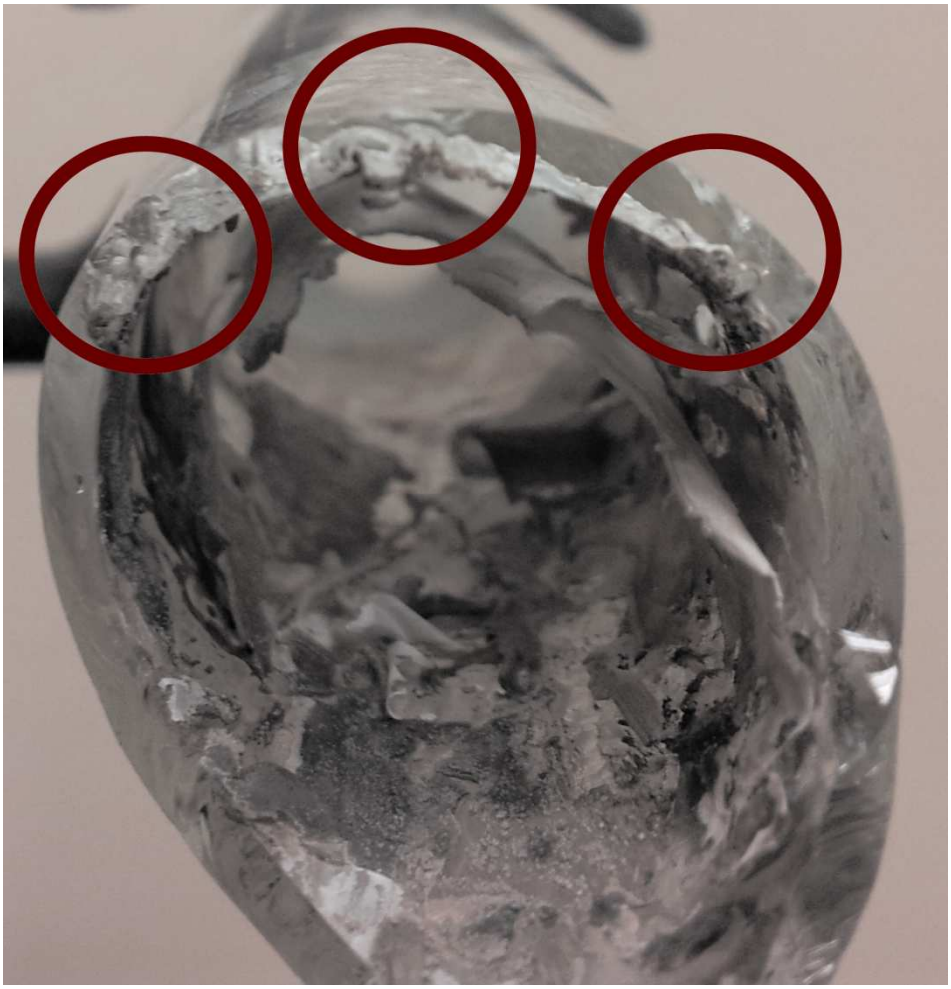

Figure 2.5 A photograph of a Pyrex microwave discharge cell which has cracked due to etching of the silicate by the hydrogen and oxygen plasmas. The red circles highlight areas where pitting of the glass along the crack line is clearly visible.

The Pyrex microwave discharge cells used in the current experimental setup have a limited lifetime due to etching of the borosilicate material by reactive species in the plasma. Figure 2.5 shows a photograph of a microwave discharge cell which had to be replaced after 18 months of use due to cracking. The cause of the crack appears to be a series of ‘pits’ or holes in the glass surface along the crack line. These pits have formed around the cell at the point where the microwave waveguides attach to the source, presumably because the plasma is most intense in this region. In addition to this pitting,

extensive processing of the Pyrex is visible throughout the cell, with thin sheets of borosilicate having peeled away from the glass surface. Surprisingly, this cell was able to produce abundant H and O atoms right up until the time when it cracked, implying that this etching does not have any effect upon the performance of the atom source. Given the extent of the etching of the cell, the potential for species originating from the Pyrex entering the gas phase and interfering with experiments needs to be considered. For example, when hydrogen atoms are produced in the cell, silanes and boranes might be expected to form from the reactions of H atoms with silicon and boron present in the Pyrex. However, no evidence of such gas phase species arising from the etching of the silicate has been observed and so it is assumed that this etching does not interfere with the experiments in any way.

## 2.4 Transport of Atomic Species

The O, H or D atoms are transported from the atom source to the HOPG surface in the target chamber *via* polytetrafluoroethylene (PTFE) tubing. PTFE tubing is used as it is both chemically inert and has an extremely low vapour pressure and can therefore be used safely under UHV conditions. The atom beams initially pass through the capillary of the Pyrex microwave discharge cell (1 mm internal diameter, 40 mm long) over which a length of PTFE tubing is pushed. The atoms then pass through this PTFE tubing to a cylindrical PTFE block located in the source chamber. This PTFE block is 10 cm long and has a channel drilled through the centre of it to allow atoms to pass through. A schematic diagram of the PTFE block can be seen in Figure 2.6.

As shown in Figure 2.6 the connection between the PTFE tube and the PTFE block is made *via* a PTFE plug. This PTFE plug features two 2 mm diameter ‘pumping holes’ at 180 ° to each other. The purpose of these pumping holes is to allow much of the gas passing through the atom transport tubes to escape, and be pumped away, in the source chamber. Pumping away most of the gas from the atom source in this manner allows the pressure in the discharge cell to be kept at the optimum for atom generation whilst keeping the pressure in the target chamber as low as possible. After having passed through the PTFE block, the gas from the atom source then passes through another PTFE plug, this time without pumping holes, which makes the connection to a further length of PTFE tubing. This PTFE tube passes through a hole in the brass plug which seals the connection between the source chamber and the target chamber (see Figure 2.1). This arrangement therefore allows only the gas in the tube to reach the target

chamber, thus precluding any species arising from gas phase interactions in the source chamber from arriving at the HOPG surface.

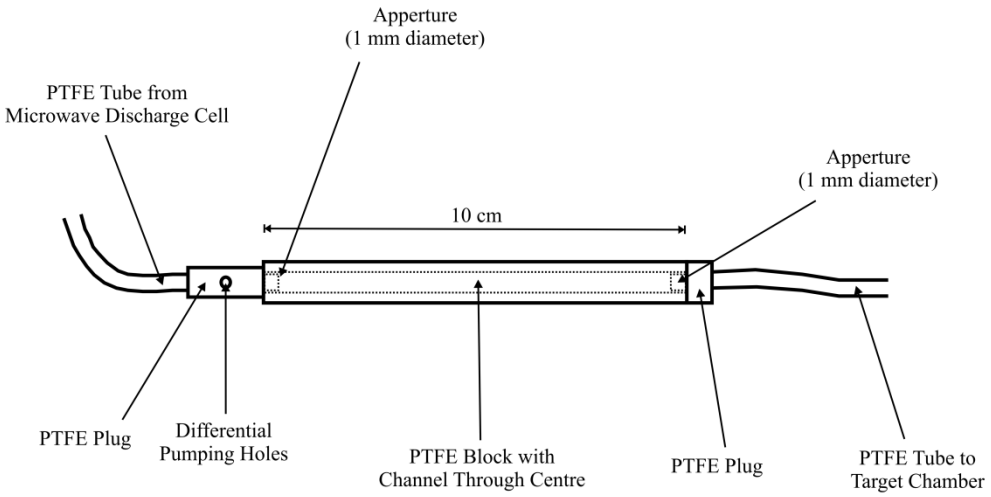


Figure 2.6 A schematic diagram showing the arrangement of the PTFE atom transport tubes in the source chamber. The diagram shows how PTFE plugs containing small 'pumping holes' are inserted into the atom transport line to allow most of the gas from the microwave discharge cells to escape in the source chamber.

Under normal operating conditions the atoms from the microwave discharge source are transported through PTFE tubes up to the HOPG target. However, in order to carry out diagnostic tests on the atom beam, it is sometimes necessary to arrange the PTFE tubes such that the atoms pass directly across the source region of the time of flight mass spectrometer (TOFMS). These two arrangements require different lengths of tube, hence in order to allow for the simple substitution of different lengths of tube the PTFE tube is broken inside the target chamber immediately after passing through the brass plug. The two separate lengths are then connected *via* a simple PTFE connector which is cylindrical in shape with a channel drilled through it which is sized such that the PTFE tubing fits securely inside. A final length of PTFE tubing then transports the atoms either to the TOFMS or, under normal experimental conditions, to the HOPG target. In the former operating mode the PTFE tubes are held in place by a PTFE block mounted on the repeller plate of the TOFMS, as shown in Figure 2.7.

In the latter case the tubes pass beneath the TOFMS assembly and are held in front of the HOPG target by stiff copper wire which is mounted on the radiation shield of the coldhead. This copper wire mount holds the PTFE tubes at approximately 10 mm from the HOPG target and at 45 ° to its surface.

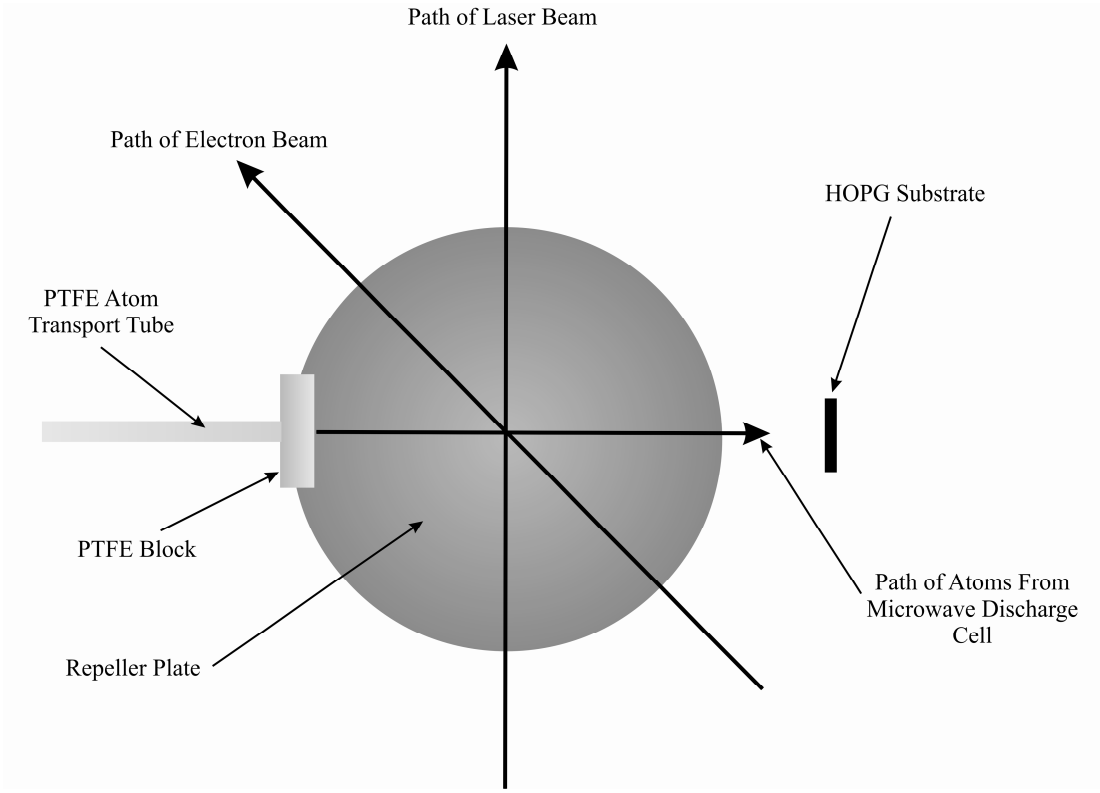


Figure 2.7 A schematic diagram showing the experimental geometry around the TOFMS. In this case the PTFE atom transport tube is held in a mount affixed to the repeller plate of the TOFMS. This arrangement is used for diagnostic experiments on the gases emerging from the microwave discharge.

An improved mount for the PTFE tubing has been designed and produced. A photograph of this mount is shown in Figure 2.8. Essentially, the mount consists of a circular aluminium plate with a rectangular 'window' cut through the centre. This plate is designed to bolt onto the end of the radiation shield of the coldhead such that the window sits exactly above the HOPG target. Either side of this window on the top side of the plate are wedge-shaped pieces of aluminium which slope upwards from the window edges. Channels are drilled through each of these aluminium wedges into which the PTFE atom transport tubes can be inserted. The overall result is that the PTFE tubes are held at 45 ° to the window so that atoms pass through the window and onto the HOPG surface. The advantages of this design are two-fold. Firstly this mount will inhibit the detection of species desorbing from the tantalum strip heater rather than the HOPG surface itself since only the latter will have a direct line of sight to the source region of the TOFMS. The very rapid heating of the tantalum strip at the start of a TPD experiment results in large desorption peaks occurring at the start of a TPD spectrum. Such early desorption peaks have the potential to interfere with the detection of very volatile species desorbing from the surface. The second advantage arises from the fact that the mount will be in thermal contact with the radiation shield of the coldhead which

and so can be cooled down to 30 K. Thus, if the PTFE tubes are not inserted fully into the aluminium channels but instead inserted a minimum amount so that species from the atom sources can collide with the aluminium, then traces of contaminant $H_2O$ ($D_2O$) in the H (D) atom beam may be frozen out in these channels before reaching the HOPG surface.

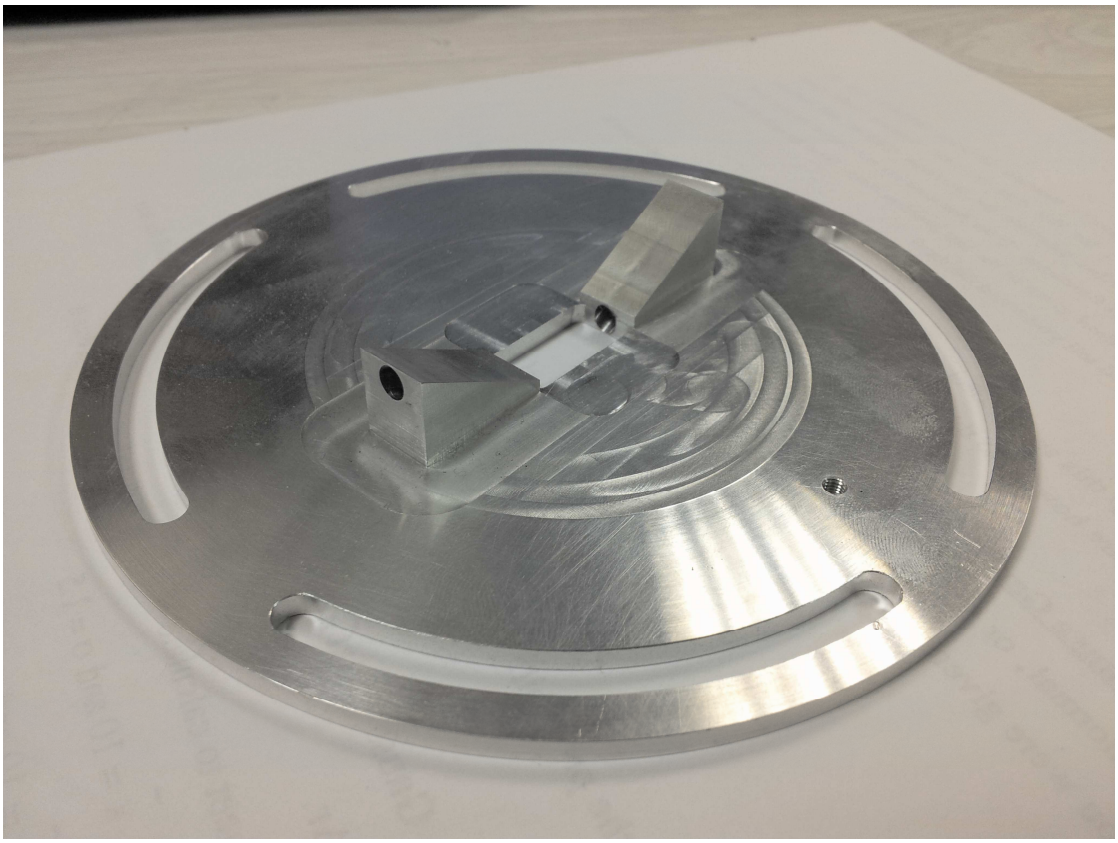

Figure 2.8 A photograph of the new mount for the PTFE atom transport tubes. The mount is designed to fit over the end of the radiation shield which surrounds the target mount.

## 2.5 Target Mount and Coldhead

The target mount used in the current experimental setup is fixed onto the cold head of a closed cycle helium cryostat which reaches a minimum temperature of 8 K during operation. The target mount is designed in such a way as to allow the HOPG target to be cooled to the region of 10 – 20 K to accurately represent the conditions of the interstellar medium, but also, to be heated to approximately 500 K to clean the surface with the coldhead still running. The HOPG surface is attached directly to a removable copper mount containing a tantalum strip heater held between two insulating pieces of aluminium nitride. By passing a constant current of 0 - 20 A through this tantalum strip heater, the temperature of the HOPG target can be controlled in the temperature range 10 – 500 K.

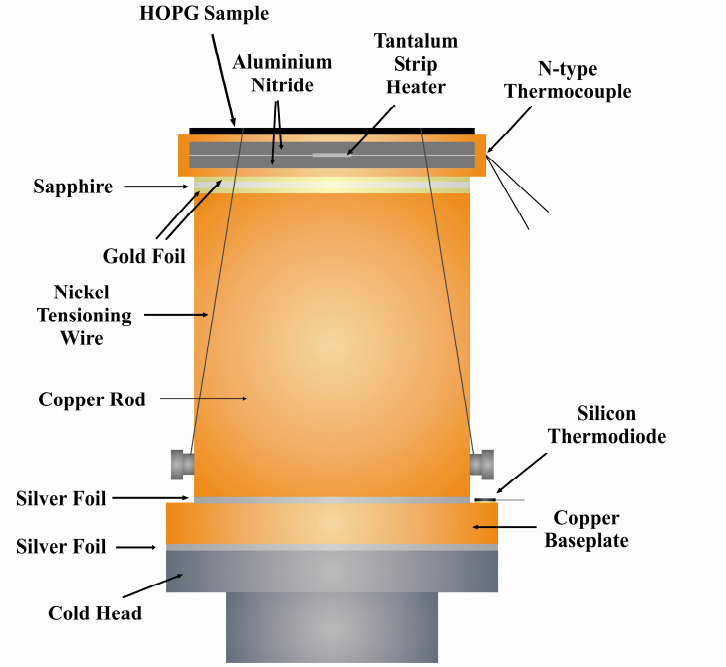


Figure 2.9 A schematic diagram of the target mount.

The coldhead and target mount must be installed in the vacuum chamber such that the HOPG target is as close to the source region of the TOFMS as possible in order to allow the efficient detection of desorbing species. In our experimental setup the HOPG surface is approximately 30 mm from the centre of the source region of the TOFMS with the centre of the HOPG target being equidistant between the planes of the repeller and middle plates of the TOFMS.

The thermal contact between the removable copper block and the coldhead is made *via* a copper rod. The removable copper block and HOPG surface are secured to the copper rod by two nickel tensioning wires. These wires are held tight by a tight by a sprung tensioning system which ensures that the HOPG target, copper block and copper rod remain in good thermal contact despite any thermal expansion and contraction which may take place during heating of the surface. The copper rod is mounted on a copper base-plate with silver foil between the two pieces. The silver foil improves thermal conductivity since it is soft enough to be pressed into crevices on the microscopically rough copper surfaces. The copper base-plate is bolted onto the cold-head, again *via* a layer of silver foil. Between the copper mount and copper rod there is a layer of sapphire between two layers of gold foil. The role of the gold foil is to ensure good thermal contact between the different components in the same manner as the silver foil mentioned above. The sapphire layer is a crucial part of the design of the target mount since it allows the HOPG target to be heated whilst the coldhead is still running. Under

normal circumstances any attempt to heat the target to high temperatures during operation of the cryostat would result in the thermal load becoming unacceptably high. However, the inclusion of the sapphire layer overcomes this problem since, whilst it is an excellent thermal conductor below 50 K, it is a poor thermal conductor at temperatures greater than 200 K. This property of sapphire allows the target mount to be heated whilst minimizing the heat flow to the coldhead and yet still provides for efficient cooling of the HOPG target when not heated.

The temperature of the copper base-plate is monitored using a silicon thermodiode, and is found to be efficiently cooled to 8 K. The temperature of the target can also be monitored independently *via* an n-type Nickel-Chromium-Silicon thermocouple attached to the removable copper mount.

The entire target mount is surrounded by a cylindrical aluminium radiation shield which is cooled to approximately 30 K during operation of the cryostat. The purpose of this radiation shield is to minimize heating by black body radiation originating from the warm chamber walls.

## 2.6 Electron Gun

In order to allow for simultaneous detection of all species desorbing from the HOPG surface, an electron gun has been installed in the target chamber. The electron gun consists of a V-shaped tungsten filament surrounded by a cylindrical piece of stainless steel. The tip of the filament is aligned with a small hole (2 mm Ø) in the top of the stainless steel cylinder. A current of approximately 2.5 A is continuously passed through the filament in order to maintain it at a sufficiently high temperature for thermionic emission to occur. In the experiments discussed in this thesis, the entire filament is lowered to a potential of either −200 V or −400 V relative to ground in order to produce 200 or 400 eV electrons respectively. The change in electron energies between the experiments discussed in Chapter 3 (400 eV) and those discussed in the remaining chapters (200 eV) was due to the necessary replacement of the electron gun power supply. A similar potential is applied to the stainless steel cylinder so that emission only occurs at the tip of the filament. After emerging from the stainless steel cylinder, electrons travel down a brass needle at 0 V to the source region of the TOFMS. Having crossed the source region of the TOFMS, the electrons impinge upon a copper ‘flag’ which has been installed in the vacuum chamber opposite the electron gun

needle. The purpose of the copper flag is to allow the electron current crossing the source region to be measured using a picoammeter. Typically electron currents of 50 – 200 nA are used in these experiments. Whilst higher currents up to tens of micro-amps are achievable, such a high current would result in the saturation of ion signals in the mass spectrum.

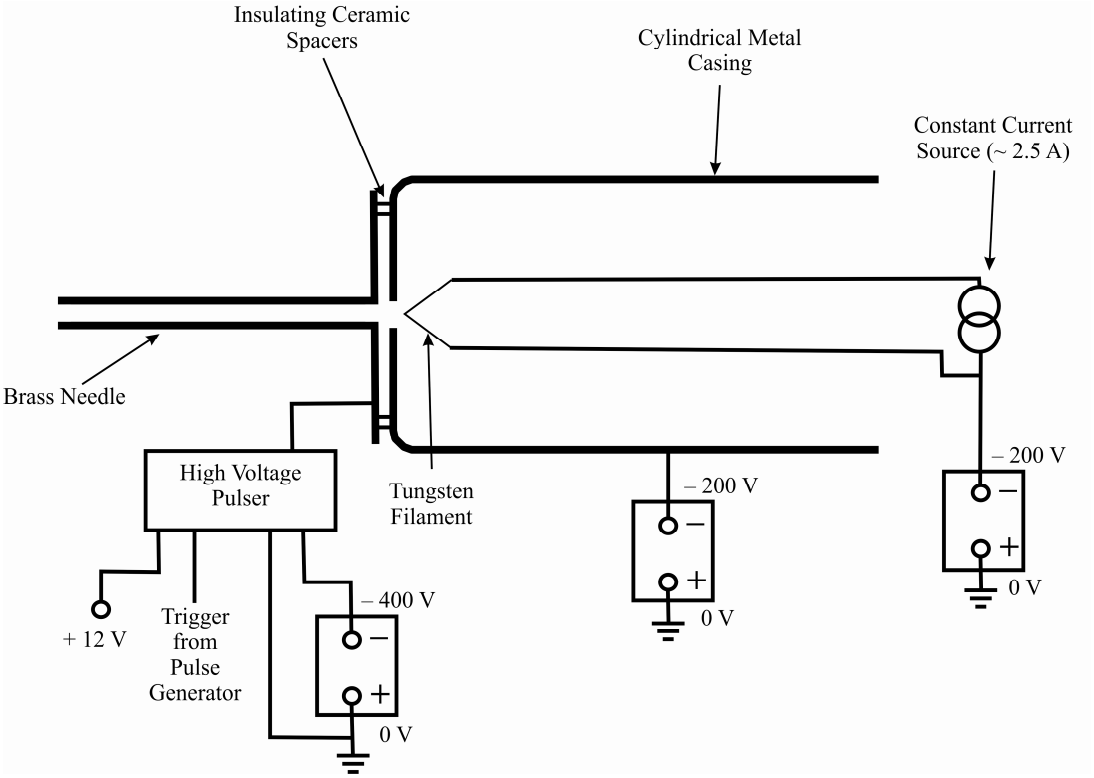


Figure 2.10 A schematic diagram of the electron gun.

In order to improve the signal to noise ratio in our mass spectra, the electron gun is pulsed ‘off’ during the time in which the TOFMS repeller plate potential is pulsed ‘on’ and the mass spectra recorded, as will be described in detail in Section 2.8. This is important for the reduction of noise in the mass spectra since any ions formed after the time of flight voltages were turned on would have longer than expected times of flight. Thus, continuous operation of the electron gun would give rise to ‘tailed’ ion peaks with an initial sharp peak of ions formed before the repeller plate potential was pulsed on followed by a tail of late arriving ions formed during the repeller pulse.

Pulsing of the electron beam is achieved by applying a stopping potential of −400 V to the brass needle whilst the mass spectrometer voltages are on. This negative potential on the brass needle eliminates or reverses the potential difference between the filament and the needle, thus suppressing emission from the filament. The pulse rate for the electron gun and mass spectrometer is 29 kHz.

## 2.7 Laser System

In the experiments discussed in this thesis, different molecules of the same mass, or different isomers of a desorbed molecule, can be distinguished by using a multi-photon ionization (MPI) scheme to selectively ionize them. In addition oxygen, hydrogen and deuterium atoms were detected using a (2+1) resonance enhanced multi photon ionization (REMPI) scheme in commissioning experiments. The ultraviolet photons required for all MPI experiments are provided by a tuneable dye laser pumped by a neodymium-doped yttrium aluminium garnet (Nd:YAG) laser.

### 2.7.1 Nd:YAG Laser

The lasing material in an Nd:YAG laser is a solid rod of yttrium aluminium garnet (YAG) doped with $Nd^{3+}$ ions which are randomly distributed throughout the YAG lattice at $Y^{3+}$ sites. The energy levels of the $Nd^{3+}$ ions are perturbed by the presence of the YAG crystal field. An Nd:YAG laser operates *via* a four level system involving the perturbed energy levels of the $Nd^{3+}$ ions. Two pulsed (10 Hz) Xenon flashlamps are used to pump the $Nd^{3+}$ ions from the ground $^4I_{9/2}$ level to the $^4F$ levels. The $^4F_{3/2}$ level is rapidly populated *via* non radiative transitions from the higher $^4F$ states. The most intense lasing transition then occurs from the $^4F_{3/2}$ to the $^4I_{11/2}$ level. The $^4I_{11/2}$ level is depopulated by non-radiative transitions to the ground $^4I_{9/2}$ level. This system produces infrared laser light at 1064 nm.

The power of the Nd:YAG laser beam can be varied using an electro-optic Q-switch provided by a Pockels cell. The Q-switching technique is used to generate intense laser pulses by reducing the quality factor of a laser cavity whilst pumping the lasing material. Reducing the quality factor in this way allows a strong population inversion to build up without lasing occurring. After a delay time from the start of the pumping flash-lamp pulse, the quality factor of the cavity is increased to produce a short intense pulse of laser light. Increasing the delay time of the Q-switch decreases the laser beam power because the population inversion starts to decay as the pump energy from the flash lamps decays, thus reducing the energy stored in the cavity. Conversely, a minimum delay time is required in order for a population inversion to build up initially.

The Nd:YAG laser has a pulse rate of 10 Hz with the duration of each pulse being 4 – 6 ns. In the experiments discussed in this thesis the third harmonic light of the Nd:YAG laser (355 nm) is used to pump a tuneable dye laser described in the following section.

To produce this third harmonic light, the fundamental beam is initially frequency doubled using a potassium dideuterium phosphate (KD*P) crystal. This second harmonic light is then mixed with the residual fundamental beam in a β-barium borate (BBO) crystal to produce the third harmonic light. The third harmonic beam has a maximum power of approximately 300 mJ per pulse. However, under normal operating conditions, the pulse energy of the Nd:YAG laser beam is kept below 100 mJ in order to reduce the degradation of the organic dyes used in the tuneable dye laser.

### 2.7.2 Tuneable Dye Laser

The lasing material in a tuneable dye laser is an organic dye dissolved in a solvent such as methanol. The laser system employed in a dye laser involves the initial excitation of the organic dye from the $S_0$ electronic state to the $S_1$, and possibly $S_2$ states. The $S_2$ state is then depopulated by internal conversion to high lying rovibrational levels of the $S_1$ state, which, in turn, undergo rapid non-radiative decay *via* collisional relaxation to the low lying rovibrational levels of the $S_1$ state. A population inversion is therefore produced between the $S_0$ and the $S_1$ electronic states. The lasing transitions arise from fluorescence from the low lying rovibrational levels of the $S_1$ state to the $S_0$ state. Organic dye molecules have an abundance of low-lying rovibrational states both in the $S_0$ and $S_1$ electronic states and consequently exhibit a broad quasi-continuous emission spectrum; a feature which allows the laser to be scanned over a narrow range of wavelengths (typically 20 – 40 nm) without the need to change laser dyes. Whilst triplet states of the organic dye molecules are not directly involved in the laser system, the non-radiative $S_1 \rightarrow T_1$ transition can reduce the gain of the laser. This problem arises because pumping of the $T_1 \rightarrow T_2$ transition can compete with pumping the $S_0 \rightarrow S_1$ transition. Such competition between different pumping processes is avoided by ensuring that the pumping duration is shorter than the time taken to build up a population in the $T_1$ electronic state and that the time between pumping pulses is sufficiently long to allow the $T_1 \rightarrow S_0$ non radiative transition to occur and thus depopulate the $T_1$ level.

Whilst organic laser dyes give rise to a broad quasi-continuous emission spectrum, as mentioned above, the optimum emission intensity of a particular dye occurs over a relatively narrow range of wavelengths. Therefore, in order to probe different species, different laser dyes must be used. In the experiments discussed here Coumarin laser dyes are used to provide wavelengths in the range of 440 – 500 nm. In order to pump

organic laser dyes the second (532 nm) and third (355 nm) harmonics of the Nd:YAG laser are typically used. Laser dyes which require pumping at 355 nm are available to cover the entire visible spectrum in addition to the near UV. However, dyes which are pumped at 532 nm are often used for wavelengths towards the red end of the spectrum since they offer higher conversion efficiencies. The Coumarin dyes used to produce laser light in the violet to green region of the spectrum in these experiments were all pumped by the third harmonic of the Nd:YAG fundamental beam.

The dye laser consists of an oscillator, a pre-amplifier and an amplifier. The oscillator and pre-amplifier stages take place within the same dye cell but at different vertical levels within that cell, whilst the amplification stage is contained within a separate dye cell. Laser light from the Nd:YAG laser is reflected into the dye laser *via* two UV mirrors. Inside the dye laser, a fraction of the light from the Nd:YAG laser is diverted by a partially reflecting mirror into an oscillator cell containing continuously flowing laser dye. A specific wavelength of light from the resulting fluorescence of the laser dye can be selected by adjusting a computer-controlled grating which acts as the rear mirror of the oscillator. The resulting monochromatic beam is then reflected into a pre-amplification stage which, as described above, is also housed in the oscillator cell. This pre-amplification stage is pumped by a further portion of the beam from the Nd:YAG laser. After the pre-amplification stage the dye laser beam is amplified in a separate dye cell. The amplification stage is pumped by the remainder of the Nd:YAG beam which accounts for approximately 70 % of the original Nd:YAG beam. After appropriate fine tuning of the alignment of the oscillator and amplifier dye cells, beam powers of approximately 3 mJ per pulse and 15 mJ per pulse can be achieved after the pre-amplification and amplification stages respectively at the peak output wavelength of the laser dye and using a Nd:YAG beam energy of 100 mJ per pulse.

### 2.7.3 Resonance Enhanced Multi-Photon Ionization

Resonance enhanced multi-photon ionization (REMPI) is a laser spectroscopic technique which allows selective ionization of individual electronic states of an atom or rovibronic states of a molecule.

In these experiments (2+1) REMPI schemes are employed in order to confirm the production of O $^3$P and H or D $^1$S atoms. REMPI offers particular advantages over electron ionization for these experiments since it allows the atom of interest to be detected without interference from ion fragments arising from dissociative ionization of

the precursor molecule. For example O atoms can be ionized and detected as $O^+$ without interference from $O^+$ arising from dissociative ionization of $O_2$. Furthermore, the state selectivity of REMPI means that the formation of atoms in their ground electronic state can be tested experimentally. In a (2+1) REMPI scheme, two photons are used to excite the species of interest from the ground electronic state to an excited electronic state, *via* a short lived virtual level. This virtual level is not an eigenstate of the atom and has a short lifetime ($10^{-15}$ s). However, the intense laser fields used mean that a second photon can be absorbed within the lifetime of this virtual level to reach the excited electronic state. The excited atom then absorbs a third photon and is ionized. The resulting ion can then be detected using the TOFMS.

### 2.7.4 Multi-Photon Ionization

Multi-photon ionization (MPI) can be used for the simple detection of molecules with low ionization energies. Two-photon ionization, for example, is a non-resonant process in which a molecule absorbs an initial photon and is excited to a short lived virtual level as for the (2+1) REMPI scheme outline above. However, in contrast to the (2+1) REMPI scheme, the second photon simply ionizes the molecule directly from this virtual level. Three-photon ionization is also possible in which the molecule is excited *via* two virtual levels. However, non-resonant three photon ionization is much less efficient than two photon ionization and so is impractical for detecting the small numbers of species produced in these experiments. MPI is much more suitable for use in conjunction with temperature programmed desorption techniques than REMPI because it is a non-resonant process and is therefore not state selective. A REMPI-TPD technique, for example, would only allow the detection of one rovibrational state of a desorbing molecule per experiment. Conversely, since MPI is not state selective, molecules in all rovibrational states can be detected simultaneously. In principle MPI can be used to detect any atom or molecule regardless of ionization energy. However, since three-photon ionization is inefficient and atoms and molecules with large ionization energies would require vacuum ultraviolet light for two photon ionization, MPI can only be used to detect those molecules which have ionization energies below 11.8 eV in the current experiments.

MPI can complement electron ionization experiments since different isomers can be distinguished from each other if they have different ionization energies. This is because in MPI experiments the ionizing energy is known exactly. Therefore, to differentiate

between two isomers with different ionization energies, the laser wavelength can firstly be set such that the two-photon energy lies between the two ionization energies, and then altered so that the two-photon energy lies above both ionization energies. In this way the two isomers can be distinguished since in the first case only the isomer with the lower ionization energy would be ionized, whereas in the second case both isomers would be ionized. In principle, such selective ionization could be using electrons by tuning the electron energy. However, the production of such low energy electrons is experimentally challenging because simply decreasing the filament potential to an appropriate value would result in an insufficient emission current for electron ionization experiments. Such a reduction in emission current stems from the fact that the barrier which electrons must overcome in order to escape from the tungsten filament increases with decreasing filament potential. Thus, this effect could be overcome by increasing the filament current, and hence filament temperature, but at the expense of filament lifetime. Furthermore, such low energy electrons would by greatly affected by stray magnetic fields, further reducing the electron beam current across the source region of the TOFMS.

## 2.8 Time of Flight Mass Spectrometer

As already discussed, any molecules which desorb from the HOPG surface during warming can be ionized and detected using time of flight mass spectrometry. The TOFMS used in these experiments is of a standard Wiley-McLaren[8] design. Time of flight mass spectrometers have the advantage of being able to simultaneously detect ions of all mass to charge ratios. One potential disadvantage of linear time of flight mass spectrometry is that the mass resolution is poor at large mass to charge ratios. However this decreased resolution for large ion masses is not a significant issue in the experiments reported in this thesis, which focus on the reactions of light (< 100 amu) atoms and molecules.

In a TOFMS ions formed in a ‘source region’ are accelerated by a series of electric fields towards a field free drift tube. The ions then travel at constant velocity through this drift tube towards a detector. Since the kinetic energy imparted to the ions in the electric fields of the TOFMS is related to the charge of the ion and the velocity of an ion is related to its kinetic energy and its mass, ions of different $m/z$ ratios will arrive at the detector at different times. It can be shown that the time of flight of an ion is related to its mass to charge ratio ($m/z$) by Equation 2.1.

$$t = k\sqrt{\frac{m}{z}} + c \qquad 2.1$$

The quantities *k* and *c* are constants. The constant *k* depends upon the magnitude of the electric fields as well as the length of the drift tube of the TOFMS, whilst the constant *c* is related to the electronic timing system. The values of *k* and *c* can be determined by measuring the times of flight of two species of known mass to charge ratio, for example $O^+$ and $O_2^+$ formed following ionization of $O_2$ gas.

The TOFMS used in these experiments consists of a 50 mm diameter repeller plate which is fixed 60 mm below the bottom of a drift tube *via* ceramic rods. This drift tube is 360 mm in length and has both ends covered with a fine nickel grid in order to avoid electric field penetration into the drift tube whilst still allowing for efficient transmission of ions. A middle plate is fixed to the ceramic rods equidistant between the drift tube and repeller plate. The middle plate consists of a stainless steel ring of 50 mm outer diameter and 32 mm inner diameter, with the centre of the ring being covered by a fine nickel grid which improves the homogeneity of the electric fields. The electric fields required for time of flight mass spectrometry when electron ionization is used are produced by applying potentials of +330 V, 0 V and −1000 V to the repeller plate, middle plate and drift tube respectively. Greater resolution was found to be achievable for laser ionization experiments by increasing the repeller plate potential to +730 V. When the laser is used for ionization these potentials are not pulsed. The temporal structure required for time of flight mass spectrometry is provided by the laser pulses. The small ionization volume inherent in laser ionization experiments ensures that a good mass resolution is achieved without the need to pulse the TOFMS voltages. However, the pulse length of the electron gun must be much longer than that of the laser in order to provide sufficiently high electron currents. Therefore, in electron ionization experiments, the pulsing of the electron gun does not provide sufficient time resolution and so in this case the repeller plate potential was also pulsed.

The TOFMS operates in two modes depending upon whether electron ionization or MPI is being used as the source of ions. As indicated above, when MPI is used, the laser pulse provides the start signal for the time to digital converter (TDC), with a reset signal being provided by a pulse generator after approximately 9 μs. These start and stop signals define a ‘look window’ for the TDC in which to ‘look for’ ion events. In this mode the TOFMS potentials are always on since the temporal resolution is provided by

the laser. Conversely, for the reasons discussed above, when electron ionization is used, the electron gun and TOFMS must be pulsed in sequence. Initially the electron gun is 'on' and the repeller plate of the TOFMS is at 0 V. At the start of a pulse sequence the electron gun is pulsed 'off'. After 21 ns the repeller plate is pulsed to +330 V and remains at this potential for 11 μs. The start signal for the time to digital converter (TDC) is in this case provided by the pulse generator 1 μs after the repeller pulse. A reset pulse is provided 30 ns after the end of the repeller plate pulse, turning the electron gun 'on' for 22 μs until the start of the next cycle and acting as a stop signal for the TDC.

The detector used in these experiments consists of a pair of micro channel plates (MCPs) in front of two perpendicular delay line anodes. The MCPs consist of an array of 10 μm glass channels. Ions colliding with the walls of these channels initiate an electron cascade resulting in approximately $10^4$ electrons being released per ion, and hence a total of $10^8$ electrons are released from the two MCPs. These electrons, which correspond to a current in the region of tens of pico-amps, then hit the delay line anodes and are detected. Each of the delay line anodes consists of two wires; a signal wire and a reference wire. The reference wire is negatively biased relative to the signal wire in order to force electrons onto the signal wire. Electrical signals travel along the signal wire at constant speed, resulting in the sum of the arrival times at each end of the wire having a constant value for all real ion detection events. Real signals can therefore readily be distinguished from those due to electrical noise.

In order for a mass spectrum to be recorded, the signals from the detector anode are passed through a series of amplification and counting electronics. The signal first passes through an impedance matching circuit followed by a pre-amplifier and amplifier before reaching a constant fraction discriminator (CFD). The CFD provides a pulsed signal for the TDC. The TDC counts are transferred to a PC for recording *via* a PCI interface. A schematic diagram of the timing and counting electronics can be seen below in Figure 2.11.

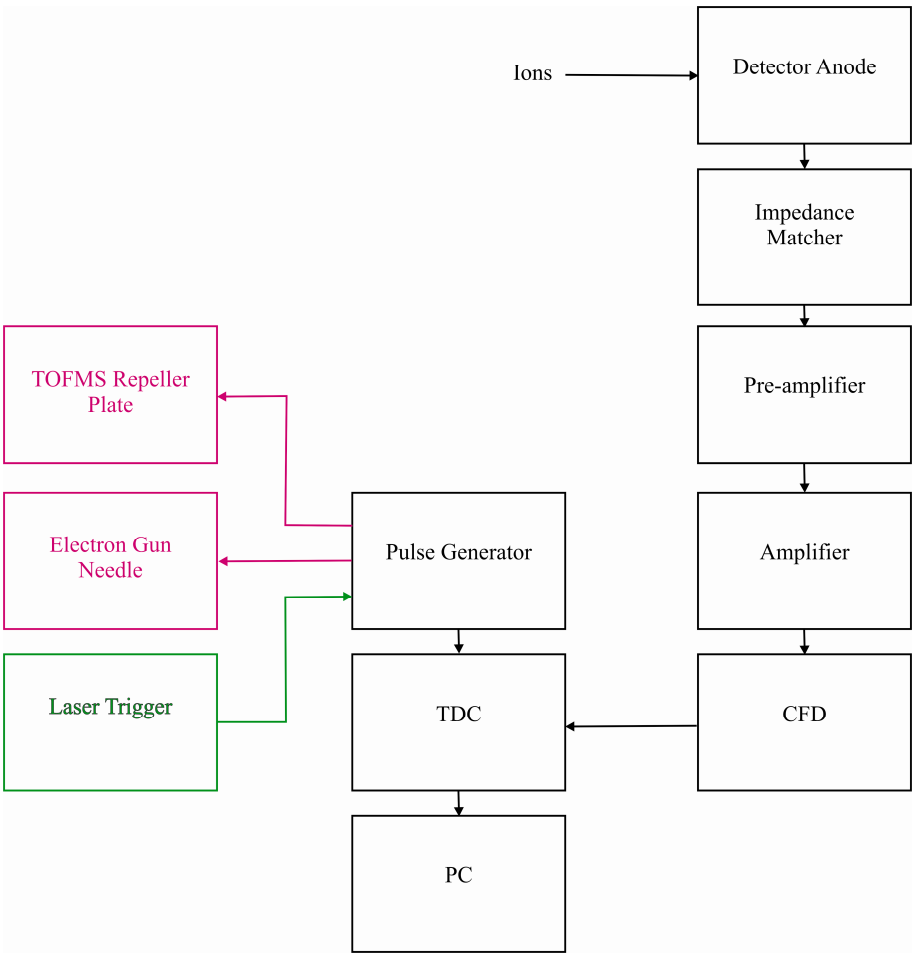


Figure 2.11 A block diagram of the timing electronics for the TOFMS. Pink; electron ionization mode only, green; laser ionization mode only, black; both ionization modes.

The mass resolution of the TOFMS is affected by two different factors. Firstly, the spatial spread of the ions formed in the source region can lead to peak broadening due to the ions being formed at different electrical potentials and hence acquiring differing kinetic energies. Secondly the spread in kinetic energies of the nascent ions can also reduce resolution in a TOFMS, since ions with large velocities towards the detector will arrive earlier than those which are travelling more slowly or away from the detector. The loss of resolution resulting from these two effects can be overcome by techniques known as space focussing and energy focussing respectively.

It is clear that if all ions were formed in a single plane perpendicular to the axis of the TOFMS then the spread in arrival times of ions of the same $m/z$ ratio would simply represent the initial spread in kinetic energies of the ions. This condition is in fact close to being met when the laser is used for ionization because the ions are only formed in the narrow focus of the laser beam. Consequently space focussing is not of great importance for laser ionization experiments. However, when the electron gun is used for

ionization, the spread in the initial positions of ions is much more significant due to the fact that the electron beam is relatively broad in relation to the laser focus. Therefore, for electron ionization experiments, space focussing is essential. The principle of space focussing can be understood by considering two ions, $X^+$ and $Y^+$, of identical *m*/*z* ratio and initial kinetic energies. The ion $X^+$ is formed in the source region at a position closer to the repeller plate than the middle plate whilst $Y^+$ is formed closer to the middle plate than the repeller plate. When the electric field is applied between the repeller and middle plates, $X^+$ will have a greater potential energy, and thus acquire greater kinetic energy, than $Y^+$. As a result $X^+$ will eventually overtake $Y^+$ as the ions move down the drift tube. Consequently, a plane will exist at which ions of the same *m*/*z* ratio and kinetic energy will arrive simultaneously regardless of their formation position in the source region. The position of this space focussing plane along the axis of the TOFMS can be altered by adjusting the electrical potentials applied to the repeller and middle plates and the drift tube. Thus, space focussing conditions are met when the space focussing plane is in the same plane as the detector, as shown in Figure 2.12.

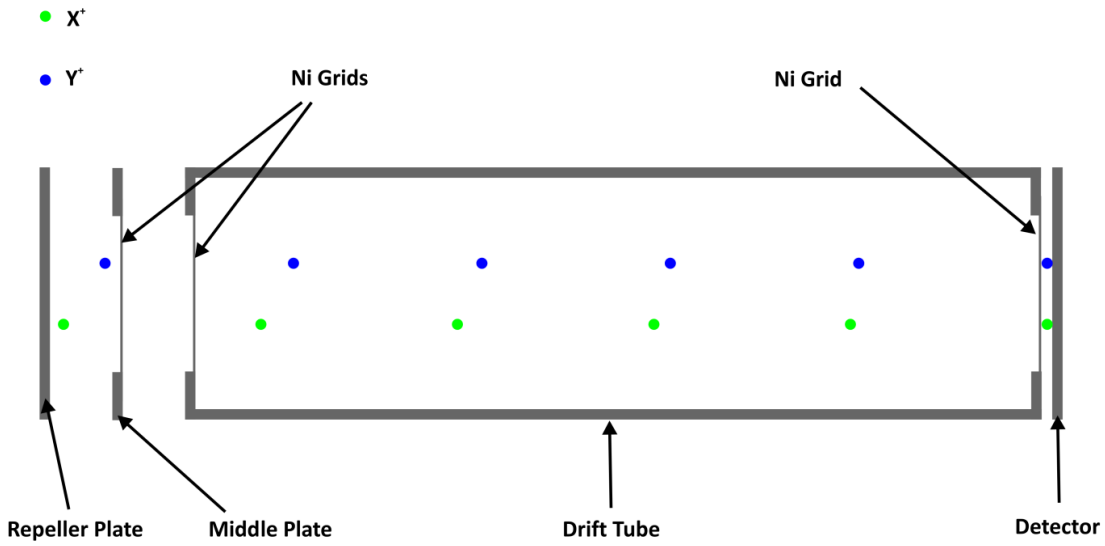


Figure 2.12 A schematic diagram of the TOFMS. The diagram shows two ions of identical *m*/*z* ratio, $X^+$ and $Y^+$, moving toward the detector of the TOFMS under space focussing conditions.

In practice ions formed in the source region of the TOFMS have a range of initial kinetic energies, and so even when space focussing conditions are met, ions of identical *m*/*z* ratios will still arrive at the detector with a spread of flight times characteristic of the spread of their initial kinetic energies. This effect can be understood by again considering the two ions, $X^+$ and $Y^+$, which are in this case formed at the same position in the source region of the TOFMS but with $X^+$ having an initial velocity towards the

detector and $Y^+$ having an initial velocity away from the detector. In this case, when the electric field is applied, $X^+$ is immediately accelerated towards the detector, whereas $Y^+$, which is moving away from the detector, must first be decelerated to a velocity of zero before being accelerated towards the detector. This 'turn-around time' causes a time lag to be observed between the detection of $X^+$ and $Y^+$ leading to a broadening of peaks in the mass spectrum. Energy focussing can be employed in order to attempt to overcome this loss of mass resolution. One technique which can provide some degree of energy focussing involves introducing an appropriate time delay between ion formation and application of an electric field. During this time delay ions with velocity components away from the detector move towards positions closer to the repeller plate and thus will have larger potential energies upon application of the electric field. Consequently such ions are accelerated in the electric field to a greater degree than those ions with velocity components towards the detector thus compensating for the turn-around time. However the time delay necessary to achieve energy focussing *via* this technique is dependent upon the *m*/*z* ratio of the ions and so energy focussing can only be achieved for ions with a narrow range of *m*/*z* ratios. Additionally, energy focussing can result in a loss of space focussing.[8] Energy focussing has therefore not been attempted in these experiments. Indeed, since most ions observed in our experiments are formed from desorbing molecules which are thermalised with the cold HOPG substrate, loss of mass resolution due to the thermal distribution of ion kinetic energies is minimal. Additionally, multiple ionization of small molecules typically represents a minor channel following electron ionization at the energies used in these experiments, hence energetic ion fragments formed from the Coulomb explosion of multiply charged precursors are not expected to represent a major contribution to our mass spectra.[9-11] Furthermore, in the experiments discussed in the following chapters, the yields of reaction products are, where possible, derived from the peak corresponding to the parent monocation of that product, thus avoiding any contribution arising from multiple ionization.

## 2.9 Data Acquisition

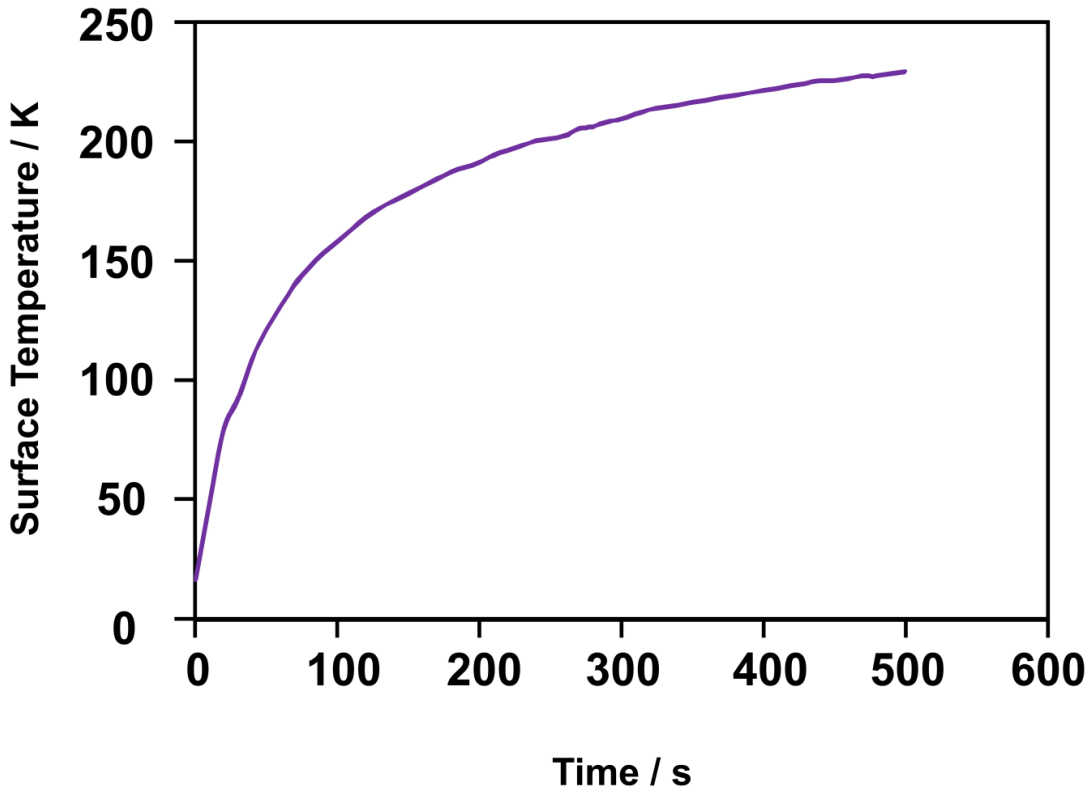


Figure 2.13 A graph showing the typical variation the surface temperature with time during the heating of the surface. The graph shown was recorded using a heater current of 15 A.

The experimental data consist of a series of short time-of-flight mass spectra recorded consecutively during warming of the HOPG surface at the end of an experiment. These mass spectra provide the yield of ions as a function of the ions mass to charge ratio, whilst the consecutive recording of mass spectra allows the ion yields to be monitored with function increasing surface temperature. The data are therefore displayed as a two dimensional histogram as shown in Figure 2.14. Whilst the temperature of the surface during the TPD phase of an experiment is not recorded directly, the mass spectrum number does provide a proxy for temperature since the surface is being continuously warmed during the recording of the consecutive mass spectra. Therefore, for simplicity, the axis in the two dimensional histogram, which strictly represents mass spectrum number, shall hereafter be referred to as the temperature axis.

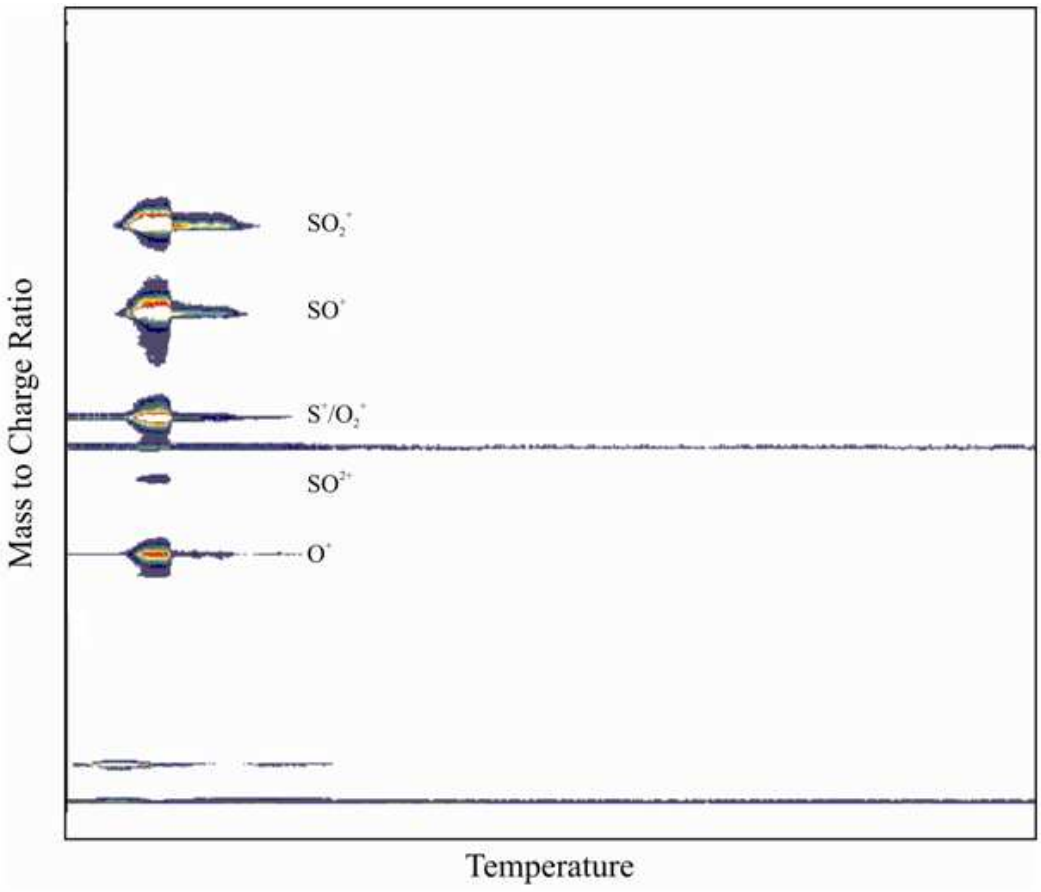


Figure 2.14 An example of a two dimensional histogram of ion counts recorded for the desorption of $SO_2$ ice. The ion fragments arising from $SO_2$ are labelled. Weak continuous signals can also be observed for background $N_2^+$ and $H^+/H_2^+$. The material which appears at low temperatures has desorbed from the strip heater and is disregarded.

Both temperature programmed desorption spectra for a particular mass to charge ratio and mass spectra for a particular desorption temperature can be extracted from the two dimensional dataset described above. Ions detected during the recording of mass spectra in these experiments are 'binned' according to their time of flight, with each bin representing a specific range of flight times. Thus in the two dimensional dataset each of these 'bins' represents one row of data and ions of particular mass to charge ratio will be recorded over a small range of rows. A temperature programmed desorption spectrum can therefore be obtained by summing the data in the rows representing flight times characteristic of a particular mass to charge ratio, thus providing a list of ion counts as a function of surface temperature during the temperature programmed desorption. Similarly a mass spectrum can be obtained for a particular range of desorption temperatures by summing the data in the columns representing that temperature range in the two dimensional dataset.

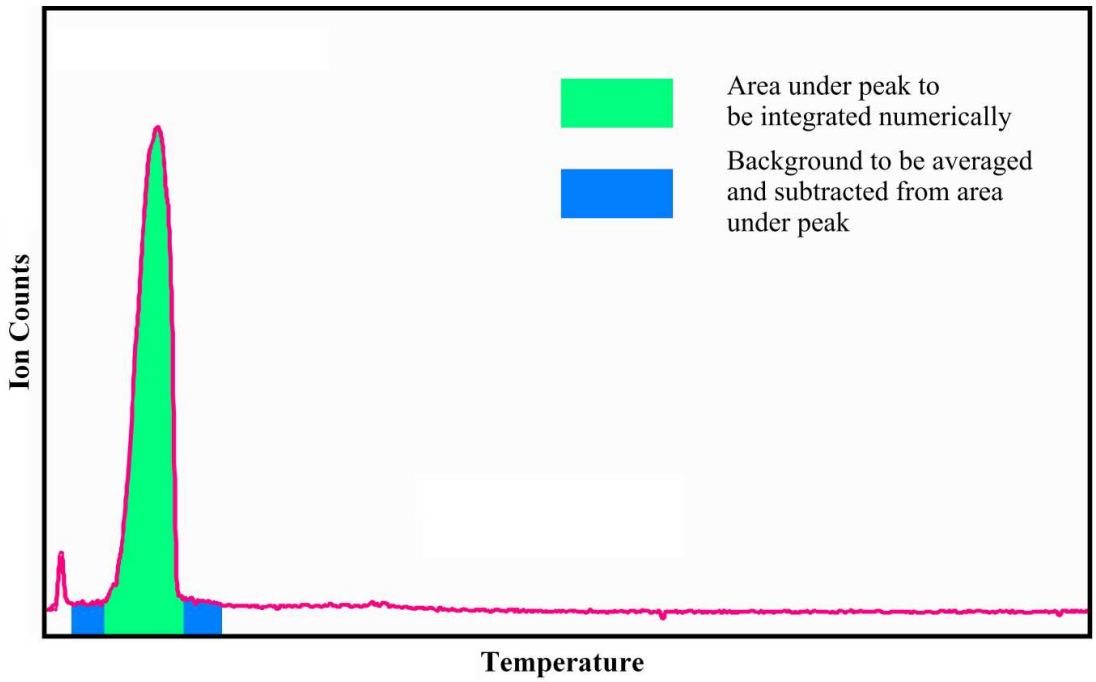


Figure 2.15 A typical TPD spectrum, in this case monitoring the m/z = 64 ion signal for $SO_2$ desorbing from the HOPG surface. The diagram also provides a pictorial representation of the analysis and background subtraction method.

A typical temperature programmed desorption spectrum derived from the above two-dimensional histogram is shown in Figure 2.15. In order to derive product yields from such a spectrum, the area under the peak is first integrated numerically. The background is then subtracted by averaging the background to the left and right of the product peak. In some cases, particularly for those reactions involving H or D atoms, the product of a reaction is similar in mass to the reactant. Consequently, the large peak in the mass spectrum for the reactant can sometimes cause an increase in the background of the mass spectrum beneath the product peak, resulting in a 'peak' in the TPD spectrum for the product at the temperature where the reactant desorbs. Clearly, this effect can complicate the background subtraction if the product and reactant desorb at similar temperatures. In these cases the background subtraction method has been modified in order to account for the interference from the desorption of the reactant. These modifications are discussed in more detail in the relevant chapters.

A single experiment in this thesis represents dosing reactants onto the HOPG surface for one hour and then warming the surface whilst recording consecutive mass spectra as described above. Such experiments are performed with the surface held at different temperatures during dosing, thus allowing a separate product yield to be obtained for each surface temperature investigated. In this manner, a complete temperature dependence of the product yield for a given reaction can be obtained. In order to provide

an estimate of the uncertainties in the product yields, experiments are repeated three times at each surface temperature. The uncertainties are estimated as the standard deviation of these repeated measurements.

## 2.10 Ion Signal Normalization

In order to derive absolute rate constants for a surface reaction, it is necessary to place the experimental results on an absolute scale of number of product molecules formed as a function of surface temperature during dosing. The detection efficiency of the experimental apparatus must therefore be known. This detection efficiency is determined by taking the measured total ion count of the major ion fragment of the molecular reactant, Y, for a given experiment and dividing this number by the number of Y molecules known to have built up on the surface during the one hour dosing period. The total number of Y molecules on the surface is determined from the flux of Y, $J_Y$, and assumes that the sticking probability of Y is unity. The values of the fluxes can be estimated from the pumping speed in the target chamber (400 l $s^{-1}$) and the pressure rise in the chamber due to the gases from the atom source and the co-reactant. It should be noted that in the case of O, H or D atoms, the flux of ($X + X_2$) where X = O, H or D is calculated initially. The flux of X atoms can then be estimated from the measured dissociation efficiency. Typically, when considering the deposition of species onto a surface, the number of available adsorption sites must be taken into account. Consideration of the number of adsorption sites is especially important when the adsorbates chemisorb onto, that is form a chemical bond with, the surface. In this case, an atom or molecule may only adsorb onto the surface at a site where a chemical bond can be formed. In contrast, atoms and molecules can physisorb onto the surface on top of previous adsorbates, forming physisorbed multi-layers. Thus, there is always an available site for an incoming gas phase species to adsorb. Since at temperatures relevant to interstellar dust clouds atoms and molecules can only physisorb onto the surface, an adsorption site is always available for a species arriving at the surface from the gas phase. Consequently, the number of molecules which can build up on the surface is unlimited and, assuming a sticking probability of unity, will be equal to the fluence. This assumption that the sticking probability is unity is justified on the basis that no pressure rise in the target chamber is observed upon admitting any of the molecular reactants discussed in this thesis into the chamber when the surface is cold. This procedure is repeated for every experiment to give a proportionality constant, $\alpha_Y$,

between the overall number of reactant, Y, molecules present and the number of $Y^+$ ions detected in that experiment. Using α, the background corrected yield of product ions can therefore be converted to an estimate of the number of product molecules present on the surface at the end of the reaction. In principle, a correction must be made for the partial ionization cross sections (PICS) for forming $Y^+$ by electron ionization of Y and similarly for forming the product parent ion *via* electron ionization of the product. However, in some cases no PICS are currently available in the literature to enable this correction to be made, whilst in other cases the product could not be identified or consists of a mixture of different isomers. The specific corrections for the PICS used to reveal the absolute ion yield for each reaction is therefore discussed in greater detail in the relevant chapters.

## 2.11 Kinetic Model

As described above, our experimental dataset is processed to give the yield of product as a function of the surface temperature during the dosing. To account for this experimental data a simple kinetic model has been developed which allows the surface processes occurring during an experiment to be quantified. In order to develop this kinetic model, the mechanisms by which surface reactions can take place must firstly be considered. The two limiting mechanisms for surface reactions were introduced in Chapter 1. These are the Eley-Rideal (ER) and Langmuir-Hinshelwood (LH) mechanisms.

In the ER mechanism a species from the gas phase X(g) reacts with an adsorbed partner Y(ads) without equilibrating with the surface:

$$X(g) + Y(ads) \rightarrow XY(ads) \qquad 2.2$$

In the LH mechanism both reactants initially adsorb and thermalize on the surface. In the low temperature regime applicable to the experiments discussed in this thesis, the adsorbates form a weak physisorption bond with the HOPG surface and so can readily diffuse on the surface. This diffusion of adsorbates on the surface may eventually lead to a mutual encounter, and reaction, between the two reactants.

$$X(ads) + Y(ads) \rightarrow XY(ads) \qquad 2.3$$

The kinetic model involves calculating the rate of the ER and LH reactions, at a given surface temperature, at regular time intervals throughout the dosing period and

integrating these rates to determine the total number of product molecules generated during the dosing period. In principle, very small time steps would be desirable in order to calculate the continuously changing surface concentrations and reaction rates as accurately as possible. However, for very small time steps the number of steps required to cover the one hour dosing period becomes unwieldy. In the kinetic model, 1 s time steps were found to provide a good compromise between the above two factors. The total number of product molecules predicted by the model can then be compared with the experimental product yields.

The relevant rate equations for the ER and LH mechanisms are given by Equation 2.4 and Equation 2.5 respectively:[12]

$$r_{ER} = k_{ER}[\mathrm{X}]_S F_\mathrm{Y} \qquad 2.4$$

$$r_{LH} = k_{LH}[\mathrm{X}]_S[\mathrm{Y}]_S \qquad 2.5$$

where $r$ is the rate of reaction, $[\mathrm{X}]_S$ and $[\mathrm{Y}]_S$ are the number of species adsorbed on the HOPG surface per unit area and $F_\mathrm{Y}$ is the fluence of Y molecules onto the surface. The 'surface concentrations', $[\mathrm{X}]_S$ can readily be calculated from the flux of the species onto the surface and the rate of desorption of the species from the surface.

The kinetic model allows both the ER and LH mechanisms to occur simultaneously. The resulting combined rate equation for product formation is given by Equation 2.6.[13]

$$r = \frac{d[\mathrm{Product}]}{dt} = (k_{ER}[\mathrm{X}]_S F_\mathrm{Y} + k_{LH}[\mathrm{X}]_S[\mathrm{Y}]_S) \qquad 2.6$$

The rate constants for the LH and ER reaction pathways are $k_i$ ($i$ = ER or LH), given by an Arrhenius expression:

$$k_i = A_i \exp\left(\frac{-E_i}{RT}\right) \qquad 2.7$$

where $A_i$ is the appropriate pre-exponential factor and $E_i$ is the relevant reaction barrier.

The yield of product is determined by integrating Equation 2.6 starting from the initial conditions $[\mathrm{X}]_s = [\mathrm{Y}]_s = 0$ at $t = 0$. In order to determine the surface concentrations of the reactants and products during this integration, three processes must be considered: the deposition of the species onto the surface, the consumption of the reactants *via* their mutual reaction and the rate of desorption of the reactants onto the surface.

As described above, in the physisorption regime in which these experiments operate, the rate of deposition of reactants onto the surface is simply equal to the flux of a reactant. However, the experimental fluxes are equivalent to a dosing rate of > 1 monolayer (ML) per second and so the surface coverages would reach values equivalent to several thousand monolayers after an hour of dosing. Using such surface concentrations directly in the kinetic model would be unrealistic since, in practice, only the surface layers would be available for reaction. The surface concentrations in the kinetic model are therefore typically limited to a few monolayers. The justification for the exact limit chosen in the case of a particular reaction will be discussed in the relevant chapter.

The desorption rate for a given species at a given surface temperature can readily be calculated using Equation 2.8.

$$r_{Des,X} = A_{Des,X} \exp\left(\frac{E_{Des,X}}{RT}\right)[\mathrm{X}]_S \qquad 2.8$$

The pre-exponential factor for the desorption process, $A_{Des,X}$ is commonly taken as the vibrational frequency of the adsorbate-surface bond. Strictly, in Equation 2.8 the value of $[\mathrm{X}]_S$ should be raised to the power of $n$ where $n$ represents the order of the desorption process. Equation 2.8 therefore assumes that desorption in these experiments is a first order process (i.e. $n = 1$). Typically desorption of physisorbed multilayer ices is found to be zero order.[14] However the use of a first order rate equation is justified in this case because the surface concentrations in the kinetic model are limited to a maximum of a few monolayers to reflect the penetration depths of H, D and O atoms into the ice. Thus, multilayer desorption when the coverage is greater than the penetration depth has no effect on the surface concentrations calculated in the model. Instead only desorption of the last few layers of ice would affect the surface concentrations; a regime likely to be governed by first order kinetics.

In view of the contribution of the processes outlined above to the number of species on the surface, rate of change of the surface concentrations of the reactants is given by:

$$\frac{d[\mathrm{X}]_S}{dt} = -r_{Des,X} - r + J_{\mathrm{X}} \qquad 2.9$$

The surface concentrations of each reactant can therefore be obtained by integrating Equation 2.9. Having calculated these surface concentrations, Equation 2.6 can be integrated to give the overall yield of the reaction product. The rate constants, $k_i$, of a

reaction at a particular temperature can then be determined by adjusting the rate constant used in the kinetic model until the product yield predicted by the model agrees with that determined experimentally. In this manner, effective rate constants can be determined for each surface temperature investigated experimentally. In principle, the resulting rate constants may then be used to produce an Arrhenius plot of ln($k$) against 1/$T$ in order to determine the reaction barriers $E_i$ and the Arrhenius pre-exponential factor, $A_i$. However, such an approach cannot be used to determine physically meaningful reaction barriers in practice because at certain surface temperatures the effective rate constants include factors such as desorption of a reactant or the desorption of the product itself, leading to strong deviations from Arrhenius behaviour. A more useful approach to determining reaction barriers is not to adjust the overall rate constant in the kinetic model to fit the experimental data at each temperature but rather to choose a barrier and a pre-exponential factor and calculate the rate constants from these parameters. Such an approach provides an entire temperature dependence of product yields based on ideal Arrhenius behaviour. This ideal temperature dependence can then be fitted to the experimental data. An example of such a fitting procedure is shown for the reaction of $C_2H_4$ with oxygen atoms in Figure 2.16.

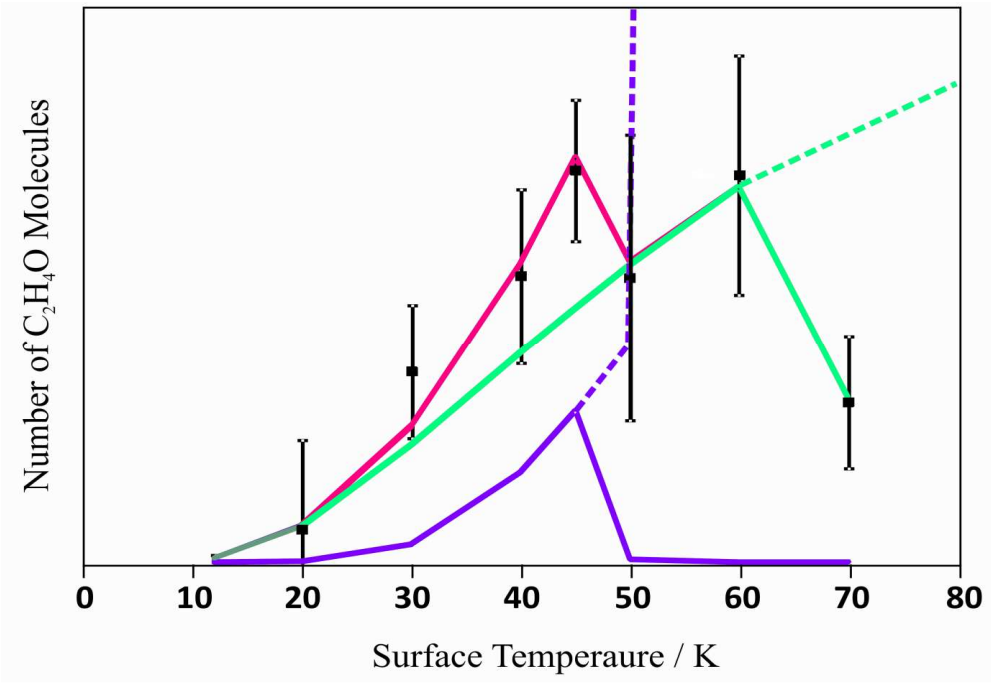


Figure 2.16 A typical temperature dependence of the yield of $C_2H_4O$ from the reaction of $C_2H_4$ with O atoms, obtained experimentally and fitted by kinetic modelling. The black squares represent the experimental data points. The contribution of the ER mechanism is represented by the green line and that from the LH mechanism by the purple line. The combined yield from both reaction mechanisms is shown in pink. The dashed sections show the predicted yield from each mechanism if desorption is disregarded.

Any deviations in the experimental data from ideal behaviour can then be addressed. For example in Figure 2.16, it can be seen that the experimental data fits an ideal Arrhenius ER reaction very well with the exception of two data points; those at 45 K and 70 K. In order to explain these deviations some observations can be made. Firstly, whilst for the ER mechanism only one reactant need adsorb onto the surface, at higher temperatures neither reactant will adsorb and so no surface reaction will occur. Secondly the reactants may stop adsorbing to the surface at either a higher or lower temperature than that at which the product desorbs upon formation and so the product yield may be limited at higher temperatures by both reactants not adsorbing, or by the product desorbing instantly upon formation. However, from the temperature programmed desorption spectrum it can be determined that in this case the $C_2H_4$ reactant desorbs at a lower temperature than the $C_2H_4O$ product and so this reaction must be limited by the desorption energy of either O or $C_2H_4$. From the literature O atoms are expected to have a lower binding energy to the surface than $C_2H_4$.[15,16] It is therefore clear that, since the reaction can proceed *via* the ER mechanism with only one reactant adsorbing onto the surface, the high temperature limit of the reaction must be defined by the desorption temperature of $C_2H_4$ because this species has a higher desorption energy than that of O. Therefore, by now adjusting the desorption energy of $C_2H_4$ such that the model output at 70 K fits the experimental data point, an estimate of this desorption energy may be obtained.

Now the data point at 45 K must be addressed. It is clear from figure that the product yield at this temperature is enhanced over that expected from the ER mechanism. The obvious conclusion is that the product yield at this temperature must include a contribution from another mechanism: the LH mechanism. In order for the LH mechanism to be able to explain this data point it is found that the reaction barrier for this mechanism must be higher than that for the ER mechanism. This higher barrier is physically realistic since in the LH mechanism the reactants must diffuse on the surface and so the LH reaction barrier also includes a barrier to this surface mobility. Additionally there must be a cut of for the LH mechanism above 45 K. This cut off can most simply be explained by the desorption of O atoms. Therefore, in a similar manner to before, the O atom desorption energy can be adjusted so that the contribution to the product yield from the LH mechanism predicted by the model agrees with the experimental data. Satisfyingly, as will be described in detail in chapter 3, this approach

yields desorption energies for both O and $C_2H_4$ that are in good agreement with the literature.

This approach clearly enables a great deal of information to be determined from the experimental data. However, it has unfortunately not been possible to follow this route in the case of every reaction discussed in this thesis. The problem arises from the fact that determination of the reaction barrier requires the onset temperature of the reaction to be known. However in the case of reactions involving H or D atoms the onset temperature appears to be below the lowest temperature which can be investigated using the current experimental setup, implying that the reactions of H and D atoms investigated here either have very small barriers or are barrierless. An alternative explanation is that H and D atoms are sufficiently light to be able to efficiently tunnel through any reaction barriers present. In either case, no onset can be observed in the experimental temperature dependences of the H and D atom reactions investigated here. Consequently it has, in these cases, been necessary to simply determine the apparent overall rate constants at individual temperatures. This procedure will be described in greater detail in the relevant chapters.

## 2.12 Summary

This chapter has provided a detailed description of the experimental apparatus employed in the experiments described in the succeeding chapters. Furthermore a broad overview of the kinetic modelling approach used to derive kinetic parameters from the experimental data has been presented. The following chapters will describe the results obtained using the experimental arrangement and data analysis procedures described here and will discuss their astrophysical implications.

## 2.13 References


(1) Perry, J. S. A.; Gingell, J. M.; Newson, K. A.; To, J.; Watanabe, N.; Price, S. D. *Measurement Science & Technology* **2002**, *13*, 1414.
(2) Williams, D. A. *Chemistry-a European Journal* **1997**, *3*, 1929.
(3) Higgins, D. P.; McCullough, R. W.; Geddes, J.; Woolsey, J. M.; Schlapp, M.; Gilbody, H. B. *Advances in Engineering Materials* **1995**, *99-1*, 177.
(4) McCullough, R. W. Characterisation and Applications of a New Reactive Atom Beam Source. In *Application of Accelerators in Research and Industry*; Duggan, J. L., Morgan, I. L., Eds.; AIP Press: New York, 1997; pp 275.
(5) Donnelly, A.; Hughes, M. P.; Geddes, J.; Gilbody, H. B. *Measurement Science & Technology* **1992**, *3*, 528.
(6) McCullough, R. W.; Geddes, J.; Donnelly, A.; Liehr, M.; Hughes, M. P.; Gilbody, H. B. *Measurement Science & Technology* **1993**, *4*, 79.
(7) Wise, H.; Wood, B. J. *Advances in Atomic and Molecular Physics* **1967**, *3*, 291.
(8) Wiley, W. C.; McLaren, I. H. *Review of Scientific Instruments* **1955**, *26*, 1150.
(9) Ward, M. D.; King, S. J.; Price, S. D. *Journal of Chemical Physics* **2011**, *134*, 10.
(10) Douglas, K. M.; Price, S. D. *International Journal of Mass Spectrometry* **2011**, *303*, 147.
(11) King, S. J.; Price, S. D. *International Journal of Mass Spectrometry* **2008**, *277*, 84.
(12) Harris, J.; Kasemo, B. *Surface Science* **1981**, *105*, L281.
(13) Readhead, P. A. *Vacuum* **1962**, *12*, 203.
(14) Burke, D. J.; Brown, W. A. *Physical Chemistry Chemical Physics* **2010**, *12*, 5947.
(15) Bergeron, H.; Rougeau, N.; Sidis, V.; Sizun, M.; Teillet-Billy, D.; Aguillon, F. *Journal of Physical Chemistry A* **2008**, *112*, 11921.
(16) Rubes, M.; Kysilka, J.; Nachtigall, P.; Bludsky, O. *Physical Chemistry Chemical Physics* **2010**, *12*, 6438.

# Chapter 3 – Reactions of Ethene and Propene with Oxygen Atoms

## 3.1 Introduction

Ethene, $C_2H_4$, and propene, $C_3H_6$, are the two simplest hydrocarbon molecules to contain a carbon-carbon double bond. Molecules with such unsaturated bonds are of considerable astrophysical interest since they are generally considered to exhibit a greater reactivity under the cold conditions of the interstellar medium than their fully saturated counterparts.[1] Extraterrestrial ethene was first observed in the circumstellar envelope of the supergiant star IRC +10216 by Betz[2], whilst interstellar propene was detected much more recently in the direction of the dark cloud TMC-1.[3] Although no detection of either of these molecules in interstellar ices has been reported in the literature, it has been shown experimentally that ethene is produced when ices containing a mixture of $H_2O$ and $CH_4$ are irradiated by electrons[4,5] and ultraviolet photons.[6] Therefore, given the prevalence of $CH_4$ in interstellar ices,[7-10] it is expected that ethene is also present, albeit in a low abundance of less than 1 %.[11] Whilst propene is expected to be even less abundant than ethene in interstellar ices, its inclusion in this study provides valuable insights into the effect of the carbon chain length on the interstellar heterogeneous reactivity of unsaturated carbon-carbon bonds in organic molecules. As discussed in Section 1.8.4, the reactivity of unsaturated hydrocarbons with hydrogen atoms has previously been the subject of astrochemical studies by Hiraoka and co-workers.[12,13] These studies show that both ethene and propene readily react with thermal hydrogen atoms to form the corresponding alkane. In contrast, little experimental attention has been devoted to the reactions of oxygen atoms with unsaturated organic molecules. This neglect of oxygen atom chemistry is surprising, both in view of the importance of oxygen bearing organic molecules in prebiotic chemistry, and the high elemental abundance of oxygen in the Universe. The experiments discussed in this chapter therefore investigate the reactivity of ethene and propene with thermal oxygen atoms under interstellar conditions.

In thermal reactions under the low temperature conditions of the interstellar medium, there is little energy available to break chemical bonds. Consequently, the interaction of thermal O atoms with ethene on a cold interstellar grain surface analogue could be expected to form products of chemical formula $C_2H_4O$. As shown in Figure 3.1, there

are three structural isomers with this empirical formula: ethylene oxide, acetaldehyde and vinyl alcohol. All three of these $C_2H_4O$ isomers have been detected in the interstellar medium. Acetaldehyde has been observed in translucent clouds,[14] cold molecular clouds[14,15] and star-forming regions.[16-22] Ethylene oxide has been detected toward hot cores[19,20,23] and has recently been proposed as a carrier of the unidentified infrared bands.[24] Vinyl alcohol has been observed in the hot core Sgr B2N,[25] a source in which all three of the $C_2H_4O$ isomers have been identified.


Figure 3.1 The structures of the three isomers of $C_2H_4O$.

A variety of mechanisms have been put forward for the formation of gas-phase acetaldehyde, ethylene oxide and vinyl alcohol, in the interstellar medium.[11] Consideration of these mechanisms, involving both ion-neutral and neutral-neutral chemistry, led Charnley to conclude that such gas-phase pathways cannot account for acetaldehyde and its isomers in star-forming regions.[17] The logical alternative formation mechanisms for $C_2H_4O$ isomers involve reactions on dust grain surfaces. Two series of thermal surface reactions are proposed by Charnley as possible acetaldehyde formation mechanisms. One of these two pathways involves the reduction of a ketyl, HCCO, radical by successive reactions with hydrogen atoms. This ketyl radical is itself formed from a CO molecule *via* an initial reaction with a hydrogen atom followed by the reaction of the resulting HCO radical with a carbon atom. The second pathway takes acetylene, $C_2H_2$, as a starting point and proceeds *via* an initial hydrogenation step to form a vinyl, $C_2H_3$, intermediate. This intermediate then reacts with an oxygen atom to produce a $C_2H_3O$ radical which can then be further hydrogenated to form any of the $C_2H_4O$ isomers. Charnley concludes that the greater abundance of acetaldehyde than ethylene oxide suggests that the reducing pathway (which only forms acetaldehyde) may dominate over the oxidizing pathway. The suggested greater contribution from the reducing pathway is rationalized in terms of the greater abundance of CO in icy mantles compared to $C_2H_2$.

Whilst little experimental effort has been directed towards understanding thermal routes to the $C_2H_4O$ isomers, non-thermal processing of ices to form these species under interstellar conditions has been the subject of several experimental investigations.[11,26,27] An early study of the $C_2H_4$ + O reaction involved irradiating an ice containing a mixture of ozone and $C_2H_4$, deposited at 15 – 20 K, with UV–visible photons.[26] Under these conditions the $O_3$ was photolysed to produce 'hot' O atoms which then reacted with adjacent $C_2H_4$ molecules in the ice. Infrared spectroscopy of the irradiated ices confirmed the formation of acetaldehyde, ethylene oxide, vinyl alcohol and ketene ($H_2CCO$). The formation of the three $C_2H_4O$ isomers following electron irradiation of mixed $CO_2$ and $C_2H_4$ ices has also been investigated in great detail. The electrons in this case were an analogue for charged cosmic ray particles in the interstellar medium.[11] This study again used infrared spectroscopy to detect any products of supra-thermal oxygen atoms, generated by the interactions of the electrons with $CO_2$ molecules, reacting with ethene molecules. These reactions formed ethylene oxide, by direct addition, and acetaldehyde *via* an oxirane intermediate. Additionally, a minor channel involving O atom insertion into a C-H bond to form vinyl alcohol was also observed.

The above studies of the reaction of $C_2H_4$ with supra-thermal O atoms under astrophysically relevant conditions demonstrate that the three $C_2H_4O$ isomers can be formed *via* non-thermal chemistry in mixed ices. However, such investigations offer little information on the kinetics and energetics of the surface reaction. For example, it is not possible to derive a reaction barrier from such supra-thermal studies, since the energy distribution of the reacting oxygen atoms is not well characterized. [11]

To date, no studies of the surface reactivity between $C_2H_4$ and *thermal* O atoms have been carried out under astrophysically relevant conditions. The absence of such studies has perhaps stemmed from an assumption that the significant reaction barrier to this reaction in the gas phase would preclude such a surface reaction having any astrophysical importance. [28,29] However, recent computational investigations have shown that atom-molecule reactions on model interstellar grain surfaces may proceed *via* pathways involving markedly lower barriers than those observed for the gas phase reaction.[30] Thus, given the neglect of the O + $C_2H_4$ pathway in the proposed thermal schemes for the formation of $C_2H_4O$ on interstellar surfaces,[17] this heterogeneous

reaction has been studied under thermalized and astrophysically relevant conditions. As will be described in detail, these experiments confirm that thermal O atoms react readily with $C_2H_4$ to form $C_2H_4O$, on a highly oriented pyrolitic graphite (HOPG) surface, at a range of temperatures down to 20 K. Modelling the experimental results allows the activation energies for the surface reactions to be extracted, as described in Section 2.11 and in Section 3.4. These activation energies are shown to be dramatically reduced in comparison with those controlling the gas-phase reactivity. In addition, in two-photon ionization experiments, the major product of the thermal $C_2H_4$ + O reaction has been identified as ethylene oxide, with acetaldehyde representing a minor product. These observations indicate that thermal routes for ethylene oxide and acetaldehyde formation are available on interstellar dust grains.

As mentioned above, these studies have also been extended to investigate the reactions of O atoms with propene, $C_3H_6$, on HOPG at interstellar temperatures. This reaction has also been widely studied in the gas phase (see, for example, refs 28,29,31-33) but no prior studies of this reaction on a surface have been carried out, under astrophysically relevant conditions. The experiments discussed in this chapter show that O atoms react efficiently with $C_3H_6$ on HOPG at astrophysical temperatures to generate $C_3H_6O$.

## 3.2 Experimental

The experimental apparatus and procedures used in these studies are described in detail in Chapter 2. The $C_2H_4$ and $C_3H_6$ gases used in these experiments were commercial samples of 99.99 % and 99 % purity respectively and were used without further purification. The fluxes of $C_nH_{2n}$ and O used in the present experiments were $1.2 \times 10^{15}$ $cm^{-2}$ $s^{-1}$ and $1.2 \times 10^{14}$ $cm^{-2}$ $s^{-1}$ respectively. These fluxes result in a $C_nH_{2n}$:O ratio of 10:1 during dosing. Ethene or propene was co-deposited with O atoms onto the HOPG substrate at various substrate temperatures in the range from 12 K – 90 K for 60 minutes in each experiment. Following this dosing period, the HOPG surface was warmed to approximately 200 K. Species desorbing from the HOPG surface during this warming phase of the experiment pass across the source region of the TOFMS, and, in these experiments, are ionized by 400 eV electrons. Consecutive 1 s duration mass spectra are recorded whilst the HOPG surface is warmed in order to obtain a two-dimensional histogram of ion time of flight against desorption temperature, as described in Section 2.9. These desorption spectra clearly show the formation of $C_2H_4O$ and $C_3H_6O$, from

the reaction of O atoms with $C_2H_4$ and $C_3H_6$, at temperatures below 70 K and 90 K respectively. The yield of $C_2H_4O$ ($C_3H_6O$) when dosing the HOPG at a given surface temperature is derived from the total ion counts detected for the corresponding parent ion in the TPD spectra, using the procedure described in Section 2.10.

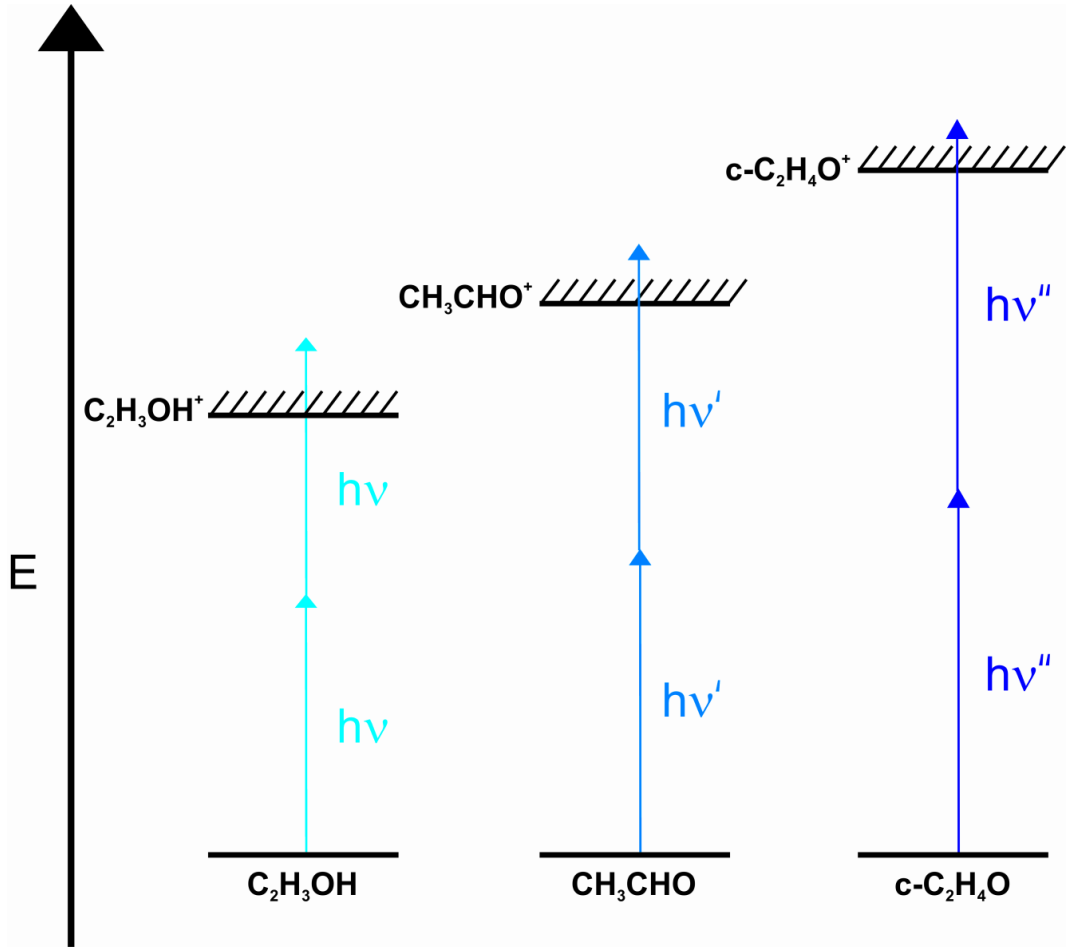


Figure 3.2 A diagram illustrating the use of MPI to distinguish between $C_2H_3OH$ (vinyl alcohol), $CH_3CHO$ (acetaldehyde) and c-$C_2H_4O$ (ethylene oxide). The wavelengths used in each case were hν = 245.0 nm, hν′ = 240.0 nm and hν″ = 234.0 nm.

In order to identify the isomeric form (Figure 3.1) of the $C_2H_4O$ product, separate experiments were carried out using the frequency-doubled output of a tuneable dye laser (Coumarin 480) to ionize the reaction products desorbing from the surface during warming.[34] The tunability of the laser photons allows the three different isomers of $C_2H_4O$ to be ionized selectively using two-photon ionization. The ionization energies of vinyl alcohol, acetaldehyde and ethylene oxide are 9.33 eV, 10.23 eV and 10.56 eV respectively.[35] By setting the wavelength of the dye laser such that the two-photon energy was slightly above each of these ionization energies, it is possible to ionize only vinyl alcohol, or vinyl alcohol and acetaldehyde, or all three isomers, respectively, as shown in Figure 3.2. This methodology allows for the identification of the isomers formed from the thermal $C_2H_4$ + O reaction.

The ionizing wavelengths used in these experiments were 245.0 nm (ionizes vinyl alcohol only), 240.0 nm (ionizes vinyl alcohol and acetaldehyde) and 234.0 nm (ionizes all three isomers). Given the low laser power used in these experiments (0.6 mJ per pulse) any contribution to the ion signal from three-photon ionization is negligible. Indeed, in separate experiments, acetaldehyde and ethylene oxide were separately admitted into the target chamber and two-photon ionization mass spectra recorded to confirm the specific ionization of the expected molecules at the above wavelengths. The laser ionization experiments were carried out after dosing for an hour at a surface temperature of 40 K, a temperature at which a good product yield is observed. Following deposition of the reactants, consecutive laser ionization mass spectra were taken whilst the surface was warmed to approximately 200 K. Due to the markedly lower laser pulse repetition rate (10 Hz) in comparison with the electron gun (29 kHz), longer duration (10 s) mass spectra were recorded in the laser ionization experiments.

Separate experiments were also carried out in which the relevant alkene was deposited onto the surface together with pure $O_2$ gas (i.e. with the microwaves to the O atom source turned off). These experiments confirmed that the formation of oxygenated products occurs specifically *via* the reaction of alkene molecules with O atoms.

## 3.3 Results

### 3.3.1 $C_2H_4$ + O

The dependence of the yield of the $C_2H_4O$ product, from the reaction of O with $C_2H_4$, on the temperature of the HOPG surface during dosing is shown in Figure 3.3. The product yield increases from 12 K, reaching a peak at 45 K, before appearing to decrease somewhat at 50 K. At 60 K, the product yield reaches a second peak before finally decreasing by more than 50 % at 70 K. As will be discussed below, the unambiguous double peak observed in the yield of $C_3H_6O$ from the reaction with propene, as well as the predictions of the kinetic model, strongly suggest that the double peak in Figure 3.3 is a real feature.

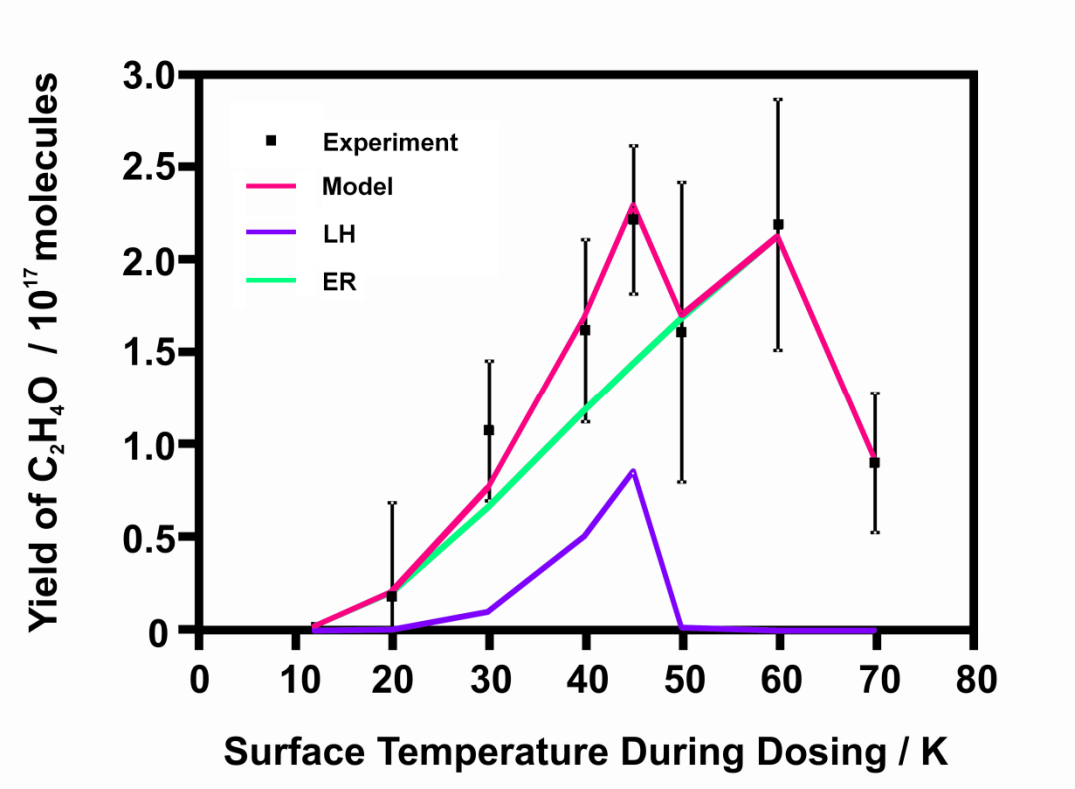


Figure 3.3 The temperature dependence of the yield of $C_2H_4O$ molecules from the surface reaction of $C_2H_4$ with thermal O atoms. The black squares represent the experimental data points and the pink line the yield predicted by the kinetic model. The green and purple lines represent the predicted individual contributions from the ER and LH mechanisms respectively.

As outlined in the experimental section, photoionization experiments have also been conducted at wavelengths of 245.0 nm (equivalent to a two-photon energy of 10.13 eV), 240.0 nm (10.34 eV) and 234.0 nm (10.61 eV) in order to determine the identity of the $C_2H_4O$ product from the reaction of O with $C_2H_4$. No ionized products were observed at 245.0 nm indicating that no vinyl alcohol is formed in the reaction of thermal O atoms with $C_2H_4$ under the present experimental conditions. At 240.0 nm a small but clear peak at *m*/*z* 44 is observed, which must be due to acetaldehyde, whilst at 234.0 nm a much larger peak at *m*/*z* 44 could be observed, indicating that the majority of the $C_2H_4O$ formed is the ethylene oxide isomer. This association of the yields of product photoions to the relative abundance of the different isomers of $C_2H_4O$ relies on the fact that no resonant ionization is occurring at 234.0 nm. Such resonant ionization would dramatically enhance the ionization of acetaldehyde this wavelength, a signal which would then be interpreted as ethylene oxide. The absence of any such resonant enhancement has been confirmed by recording photoionization spectra of acetaldehyde and ethylene oxide independently. These experiments show the ion yield from

ionization of acetaldehyde is similar at 240.0 nm and 234.0 nm and that ethylene oxide is only ionized at 234.0 nm.

### 3.3.2 $C_3H_6$ + O

Propene, $C_3H_6$, dosed onto the HOPG surface was found to react with oxygen atoms to form $C_3H_6O$ under astrophysically relevant conditions. The yield of this reaction as a function of surface temperature is shown in Figure 3.4. As for the reaction of O atoms with $C_2H_4$, the product yield generally increases with increasing surface temperature, up to 80 K, before decreasing at higher temperatures. However this trend is interrupted by a peak at 40 K which reaches approximately the same value as the peak at 80 K.

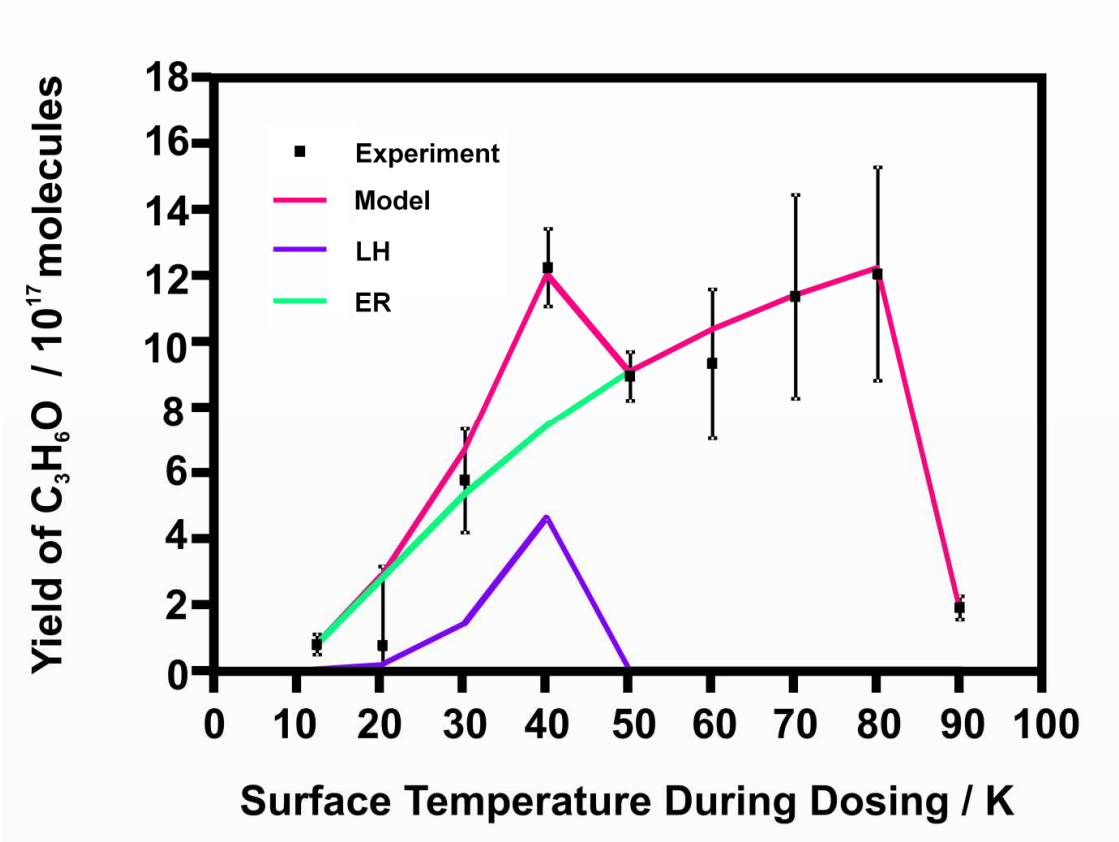


Figure 3.4 The temperature dependence of the yield of $C_3H_6O$ molecules from the surface reaction of $C_3H_6$ with thermal O atoms. The black squares represent the experimental data points and the pink line the yield predicted by the kinetic model. The green and purple lines represent the predicted individual contributions from the ER and LH mechanisms respectively.

Unfortunately there are eleven possible isomers of $C_3H_6O$, making laser ionization experiments to identify the structure of the product molecule impractical. However, by analogy with the $C_2H_4$ + O reaction, it seems reasonable to suggest that the major product is likely to be propylene oxide.

## 3.4 Data Analysis

The experimental dataset is processed to give the yield of oxygenated product ($C_2H_4O$ or $C_3H_6O$) as a function of the surface temperature during the dosing. Kinetic parameters such as the reaction barriers and Arrhenius pre-exponential factors can then be derived from the experimental data using the kinetic model described in detail in Section 2.11. In this kinetic model, the two prototypical mechanisms of a surface reaction, the ER and LH mechanisms, are treated separately.

From the temperature dependences shown in Figure 3.3 and Figure 3.4, it is clear that the reaction proceeds at temperatures substantially higher than the expected desorption temperature of oxygen atoms from a graphite surface (~ 45 K).[36] Furthermore, by inspection of the experimental data, all of the experimental data points, except those at 45 and 70 K in the case of the $C_2H_4$ reaction and at 40 and 90 K in the $C_3H_6$ reaction, appear to follow an underlying curve which broadly follows Arrhenius behaviour. This underlying curve is therefore expected to represent the contribution from a single reaction mechanism with a small positive activation energy. Since this curve extends to temperatures above the O atom desorption temperature, this reaction mechanism is identified as an ER mechanism in which a gas phase O atom reacts with an adsorbed alkene molecule. The kinetic model was therefore initially run considering only this ER mechanism. The reaction barrier of this ER mechanism was then adjusted to achieve a good agreement between the temperature dependence predicted by the kinetic model and the underlying curves observed in the experimental data.

The next stage in the modelling procedure was to address the highest temperature points investigated experimentally in each reaction: 70 and 90 K for the $C_2H_4$ and $C_3H_6$ reactions respectively. As shown in Figure 3.3 and Figure 3.4, the product yields at these temperatures are substantially reduced over those which could be expected from the simple extrapolation of the underlying trends in the respective temperature dependences. As described above, only the alkene species are expected to adsorb onto the surface at these temperatures. The obvious conclusion is that the substantial reduction in product yield at these temperatures corresponds to a decrease in the life time of the alkene molecules on the surface. The life time of a species adsorbed on a surface is governed by the desorption energy of that species. For example, the time taken for half the molecules on a surface to desorb, $t_{1/2}$, is given by Equation 3.1.

$$t_{\frac{1}{2}} = \frac{1}{A_{Des}} \exp\left(\frac{E_{Des}}{RT}\right) \quad 3.1$$

Therefore the temperatures at which the product yields decrease can be used to provide an estimate of the desorption energy of the relevant alkene.

Finally the enhancement in the yields of $C_2H_4O$ and $C_3H_6O$ at 45 and 40 K respectively must be accounted for. There are two remaining reaction pathways which may be invoked in order to explain these enhanced product yields: a second ER mechanism in which a gas phase alkene molecule reacts with an adsorbed oxygen atom, hereafter termed ER*, and an LH mechanism in which an adsorbed O atom reacts with an adsorbed alkene molecule. Both of these mechanisms are limited to temperatures below the desorption temperature of oxygen atoms. However, two arguments can be made in favour of attributing the enhanced product yields to a contribution from the LH mechanism. Firstly, given that the concentrations of species adsorbed onto the surface can reach much larger values than the fluxes of species arriving at the surface from the gas phase, it is expected that, at temperatures sufficiently low for O atoms to adsorb, the product yield from the LH mechanism would dominate any contribution from the ER* reaction. Secondly, the fact that the mechanism responsible for the peak at 40 K does not appear to make any contribution to the product yield at the lowest temperatures investigated implies that its activation energy is larger than that for the ER reaction between a gas phase O atom and an adsorbed alkene molecule. In the case of the LH mechanism such an increased reaction barrier can be understood in terms of an additional barrier to the mobility of O atoms in the ice. Conversely, since there is no analogous physical explanation for an increased reaction barrier for the ER* reaction, this mechanism would be expected to contribute to the product yield even at low temperatures.

As outlined above, the LH mechanism is limited to low temperatures by the desorption energy of O atoms. Consequently, in incorporating the LH mechanism into the kinetic model, an estimate of the desorption energy of O atoms can be derived from the data by fitting the high temperature limit of this mechanism. Therefore, by modelling the experimental data, an estimate of the desorption energies of both reactants can be obtained for the reactions discussed in this chapter.

The final step in modelling the experimental data is to place them onto an absolute scale, following the procedure described in Section 2.10. Unfortunately, the PICSs of

the major products (ethylene oxide and propylene oxide) are not available in the literature and so it was necessary to assume that they were identical to the relevant PICSs of the reactants. With the experimental results on an absolute scale it is possible to estimate the Arrhenius pre-exponential factors. In order to reduce the number of free parameters in the kinetic model, it is assumed that these pre-exponential factors are identical for the ER and LH mechanisms. This assumption is justified on the basis that neither reaction mechanism is expected to be sterically more favourable than the other.

## 3.5 Discussion

### 3.5.1 $C_2H_4$ + O

Fitting the experimental data with the kinetic model described above, allows the reaction barriers for both the ER and the LH pathways to be determined. The temperature dependence of the product yield, predicted by the kinetic model, can be seen overlaid on the experimental results in Figure 3.3. The values for the reaction barriers obtained from the kinetic modelling are: $E_{ER}/R$ = 70 ± 15 K and $E_{LH}/R$ = 190 ± 45 K. These barriers compare with an experimental gas phase barrier equivalent to 974 ± 48 K.[28] The fit to the experimental data also allows the determination of the desorption energies, as discussed in Section 2.11 and Section 3.4. The desorption energies ($E_{Des}/R$) derived by using the kinetic model to reproduce the experimental data are 2016 ± 12 K for $C_2H_4$ and 1455 ± 72 K for O atoms (16.8 kJ $mol^{-1}$ and 12.1 kJ $mol^{-1}$ respectively). Note that the uncertainty in the desorption energy of the O atom is significantly larger than that for $C_2H_4$ since this energy only affects the product yield from the LH mechanism, which only contributes a maximum of 40 % of the total product yield. Conversely, since varying the desorption temperature of $C_2H_4$ affects the product yields from the ER mechanism, which contributes 100 % of the product yield at the desorption temperature of $C_2H_4$, it is possible to determine this value more precisely. As discussed above, the desorption energies only affect the model output at specific temperatures, thus it is possible to extract the desorption energies from the fit to the experimental data whilst still allowing the reaction barriers to be determined. The data cannot therefore be fitted with an incorrect reaction barrier by manipulating the desorption energies.

Comparison of the desorption energies with adsorbate-surface interaction energies reported in the literature indicates that the values determined from the present experiments agree well with previous work. For example the interaction energy between

$C_2H_4$ and coronene (hollow site) is calculated to be 17.4 kJ $mol^{-1}$, equivalent to 2088 K,[37] and the interaction energy between O atoms and pyrene (bridge site) is calculated to be 11.6 kJ $mol^{-1}$,[36] equivalent to 1395 K. These calculated values agree well with those extracted from the current data. However, caution should be exercised in interpreting these experimental desorption energies as simple values for adsorption on a graphite substrate. This caveat is necessary as the high dosing rates in these experiments (> 1 monolayer per second) lead to the reaction taking place upon a layer of $C_2H_4$ ice after the initial stages of an experiment. Nevertheless, it is expected that the desorption energies of the reactants on the carbonaceous alkene ice would be broadly similar to the desorption energies on graphite, a prediction which is supported by the values extracted from the kinetic model.

Additionally, a fit to the absolute values of the product yield, as described in Section 2.11, results in a value of $A_{Rxn}$ of $(1.6 \pm 0.3) \times 10^{-15}$ $cm^2$ $molecule^{-1}$ $s^{-1}$. At 15 K the value of $k_{LH}$, derived from $A_{Rxn}$ and $E_{LH}/R$, is $5.0 \times 10^{-21}$ $cm^2$ $molecule^{-1}$ $s^{-1}$. The value of $k_{ER}$ at 15 K, $1.5 \times 10^{-17}$ $cm^2$ $molecule^{-1}$ $s^{-1}$ is considerably larger, but is perhaps of less astrophysical relevance since surface reactions in the ISM are considered to be dominated by the LH mechanism due to the low surface coverages.[38] The two rate constants are broadly comparable with rate constants extracted from studies of other astrophysically important surface reactions.[38]

It can be seen from Figure 3.3 that the modelling the experimental data with both a LH mechanism and an ER mechanism in which a gas phase O atom reacts with an adsorbed alkene molecule reproduces the double peak structure observed experimentally. Furthermore, as described above, this analytical approach results in desorption energies for O and the alkenes which are in good agreement with those reported in the literature, confirming that the double peak is a real feature and not a statistical anomaly. In Figure 3.3 the modelled yield from the LH and ER reactions are indicated separately. It is clear that the product yield from the ER mechanism increases with temperature up to 60 K, as the rate constant increases with temperature, before decreasing rapidly above 60 K. Since the ER reaction considered here involves the O atoms as the gas phase species, the desorption energy of O atoms has no influence upon the product yield from the ER mechanism. However, above 60 K the lifetime of $C_2H_4$ on the surface decreases rapidly leading to a lower concentration on the surface and thus reduced reaction rates. Consequently the product yield from the ER mechanism decreases rapidly above 60 K.

The contribution to the product yield from the LH mechanism on the other hand is critically dependent upon the desorption energy for O atoms and the associated reaction barrier. It should be noted that the barrier for the LH mechanism is somewhat larger than that for the ER mechanism. As discussed above, this is to be expected as the LH barrier incorporates any energy barriers to the diffusion of species on the surface. Conversely, no such barriers are involved in the ER mechanism. The result of the larger barrier for the LH mechanism and the lower desorption energy for O atoms is that, in the laboratory, the LH mechanism only contributes to the product yield at surface temperatures between 30 and 50 K. Below 30 K the reactants are too immobile on the surface to encounter each other on a laboratory timescale, whereas above 50 K the O atoms have a very short lifetime on the surface and consequently desorb before they have time to react *via* the LH mechanism. The peak in the overall model output at 45 K arises from the opportunity for the LH mechanism to contribute to the product yield around this temperature. The kinetic parameters derived for this system are summarized in Table 3.1.

| Reaction | $(E_a / R)$ / K | $A_{rxn}$ / $10^{15}$ cm$^2$ molecule$^{-1}$ s$^{-1}$ | $(E_{Des,O} / R)$ / K | $(E_{Des,CnH2n} / R)$ / K | $k_{rxn}$ / cm$^2$ molecule$^{-1}$ s$^{-1}$ (at 20 K) |
|---|---|---|---|---|---|
| $C_2H_4$(ads) + O(ads) | 190 ± 45 | 1.6 ± 0.3 | 1455 ± 72 | 2016 ± 12 | 1.20E−19 |
| $C_2H_4$(ads) + O(g) | 70 ± 15 | | | | 4.80E−17 |
| $C_3H_6$(ads) + O(ads) | 145 ± 10 | 4.8 ± 0.4 | | 2580 ± 4 | 3.40E−18 |
| $C_3H_6$(ads) + O(g) | 40 ± 5 | | | | 6.50E−16 |

Table 3.1 The reaction barriers, $E_a$, reaction pre-exponential factors, $A_{rxn}$, desorption energies, $E_{Des}$, estimated for the surface reactions of O atoms with $C_2H_4$ and $C_3H_6$. Rate constants for the reactions studied, $k_{rxn}$, have also been calculated for a surface temperature of 20 K. See text for details.

### 3.5.2 $C_3H_6$ + O

The output of the kinetic model for the O + $C_3H_6$ is shown overlaid upon the experimental results in Figure 3.4. From the kinetic modelling, the reaction barriers are determined to be equivalent to (40 ± 5) K for the ER reaction and (145 ± 10) K for the LH mechanism. The finding that both values are lower than those for ethene is perhaps not surprising since both reactions likely proceed *via* RHC—$CH_2O$ (where R = H or $CH_3$) intermediates. Such intermediates contain an electron deficient carbon atom which can be stabilised by electron releasing groups. The reduced barrier for the $C_3H_6$ + O reaction can therefore be explained by the fact that the electron releasing methyl group

present in propene can stabilise the reaction intermediate. For comparison the gas phase reaction barrier for the O + propene reaction has been reported to be equivalent to 517 ± 48 K.[28]

From the resolved contributions to the product yield from the ER and the LH mechanism (Figure 3.4) it can be seen that the ER mechanism alone can be used to fit all the data points, with the exception of the point at 40 K. The contribution of the LH mechanism between 30 and 50 K accounts for the increased yield at 40 K. Furthermore, the excellent fit to the O + $C_3H_6$ data uses the same desorption energy for the O atoms as used for modelling the $C_2H_4$ + O reaction, again supporting the identification of the secondary mechanism between 30 and 50 K as a LH mechanism. The desorption energy derived for $C_3H_6$ is 21.45 ± 0.03 kJ $mol^{-1}$ (2580 K). As would be expected, this desorption energy is slightly larger than that determined for the lighter ethene molecule. For the O + $C_3H_6$ reaction, a fit to the absolute values of the product yield, as described above, results in a value of $A_{Rxn}$ of (4.8 ± 0.4) × $10^{-15}$ $cm^2$ $molecule^{-1}$ $s^{-1}$. Again, the kinetic parameters derived for this system are summarized in Table 1.

## 3.6 Astrophysical Implications

The experimental results presented here show that, on an analogue of an interstellar dust grain and at temperatures similar to those in interstellar clouds, oxygen atoms can readily add to carbon-carbon double bonds to produce epoxide rings. The reaction of O atoms with $C_2H_4$ is detectable above a surface temperature of 12 K, with the reaction's efficiency peaking between 30 K and 50 K. In this latter regime the reaction is highly efficient with approximately 50 % of the incident O atoms reacting to form $C_2H_4O$. At a surface temperature of 20 K this efficiency is reduced to approximately 5 %. The reaction with propene is markedly more efficient, both at 12 K and in the 30-50 K regime. These observations indicate that thermal processing of alkene molecules by O atoms is viable in the interstellar medium, contrary to some earlier discussion.[25] Indeed, the rate constants derived in the experiments discussed in this chapter have been used by Occhiogrosso *et al* in an astrochemical model of the ethylene oxide abundance.[39] The abundance of ethylene oxide predicted by this model is in good agreement with observed column densities. Extrapolating the current results indicates that the thermal processing of longer chain alkenes by oxygen atoms should be highly efficient under conditions typical of dense interstellar clouds. The finding that increasing carbon chain length decreases the reaction barrier is of particular interest in view of the long carbon

chain ($C_n$) and cyanopolyyne ($HC_nCN$) molecules present in the interstellar medium.[40] The experimental results discussed in this chapter imply that such long chain polyunsaturated species may readily react with thermal O atoms and, perhaps, other species, to produce complex organic molecules.

The previous neglect in the literature of thermal reactions of adsorbed oxygen atoms is due to the large barriers of the equivalent reactions in the gas-phase. These large gas-phase barriers had been thought to indicate that the surface reactions would also have barriers that precluded them from occurring, without the intervention of cosmic rays or UV radiation, in interstellar environments. In fact, the reaction barriers determined for the $C_2H_4$ + O and the $C_3H_6$ + O reactions on a model dust grain surface are substantially smaller than the gas-phase values. These small barriers result in oxygen addition reactions occurring readily between surface species thermalised at temperatures relevant to the interstellar medium.

The major product of the surface reaction of O + $C_2H_4$ is ethylene oxide, a saturated molecule which is commonly considered unreactive with respect to further processing by reactive atoms on interstellar surfaces.[17] Chemists would, nevertheless, consider ethylene oxide to be potentially highly reactive due to the inherent ring-strain present in the molecule. Indeed, this potential reactivity has prompted an investigation of the ion-molecule chemistry of ethylene oxide as a potential route to pre-biotic species.[41]

By analogy with the results for O + $C_2H_4$, it is reasonable to assume that the reaction of O with $C_3H_6$ yields propylene oxide, but of course this product may readily isomerise to propanal or even acetone. To date, propylene oxide has not been detected in the ISM.[42] Gas-phase isomerisation of this epoxide to the more stable propanal appears to require significant activation in the gas-phase,[43] but may be promoted on grain surfaces by non-thermal routes. Propanal has been detected in the interstellar medium and its formation *via* reactions on grain surfaces has been proposed.[44]

The experiments discussed here are estimated to simulate the equivalent of about $10^5$ − $10^6$ years of exposure to O atoms. This time is of the same order as the lifetime of a typical molecular cloud. Thus, the transformation of ethene to ethylene oxide in these environments is entirely feasible over the lifetime of a cloud. Ethene is thought to be formed in ices as a secondary product of charged particle irradiation and photolysis of methane ices.[5] However, ethene does not appear to be a major component of interstellar

ice, and is likely present at unobservable concentrations of less than 1 % in interstellar ice mantles.[11] Despite its low abundance in ices, non-thermal routes for the formation of the isomers of $C_2H_4O$ from ethene have been proposed, and investigated, in detail, experimentally.[11] These experiments, which involved the irradiation of mixed CO and $C_2H_4$ ices, with the consequent reaction of O atoms with the alkene molecule, observed efficient formation of acetaldehyde and ethylene oxide, with vinyl alcohol a minor product. These non-thermal studies could, coupled with the observed efficacy of irradiation of mixed $CO_2$ and $CH_4$ ices which yields only acetaldehyde of the $C_2H_4O$ isomers, explain the interstellar excess of acetaldehyde over ethylene oxide.[19,20] However, Bennett *et al* note that there would be expected to be a strong temperature dependence of the formation routes, and hence the abundances, of the $C_2H_4O$ isomers, if thermalised oxygen atoms react with ethene to yield these species.[11] The experimental results presented here show that thermal reaction of O atoms with alkenes do indeed occur and can provide additional, temperature dependent, routes to interstellar epoxides, such as ethylene oxide. Indeed, these results indicate that in more quiescent and shielded regions, where the contribution of non-thermal pathways is likely to be reduced, a higher relative abundance of epoxides with respect to aldehydes might be expected.

The experiments of Bennett *et al*[11] indicated that given the astronomical observation of an abundance ratio [25] of ethylene oxide to vinyl alcohol of 1.5, a viable route for the interstellar formation of vinyl alcohol was required, given the low branching to form this molecule in their irradiation experiments. The laser ionization experiments discussed in above show no evidence of vinyl alcohol as a significant product from thermal reaction of O atoms with $C_2H_4$. Thus, it does not appear that thermal surface chemistry can account for the observed abundance of vinyl alcohol. It may be that, in the current experiments, any vinyl alcohol formed tautomerizes to acetaldehyde when the surface is warmed in the desorption phase. However, given the low desorption temperatures observed in the present experiments, this seems unlikely. An alternative explanation may be that there is a substantial barrier to forming vinyl alcohol on the surface. This barrier would be more readily surmounted by energetic O atoms than by thermalized O atoms.

## 3.7 Summary

The experimental results presented in this chapter show that both $C_2H_4O$ and $C_3H_6O$ are readily formed from reactions of ethene and propene molecules with thermalised oxygen atoms at temperatures in the range of 12 – 90 K. It is clear from these experiments that the reactions on a graphite surface proceed with significantly reduced reaction barriers compared with those for the gas phase reaction. Indeed, for both the $C_2H_4$ + O and the $C_3H_6$ + O reactions, the surface reaction barriers determined in the present studies are reduced by approximately an order of magnitude compared with the barriers in the gas-phase. The modelling of the experimental results also extracts desorption energies which agree well with literature values. Furthermore, major product from the O + $C_2H_4$ reaction has been determined to be ethylene oxide, with acetaldehyde representing a minor product. No vinyl alcohol could be observed to form from the reaction of O atoms with $C_2H_4$. Consequently, these experiments show that thermal heterogeneous pathways can contribute to the formation of the $C_2H_4O$ isomers in interstellar clouds and that an increased relative abundance of epoxides, relative to the corresponding aldehydes, could be an observational signature of this process.

## 3.8 References


(1) Wakelam, V.; Smith, I. W. M.; Herbst, E.; Troe, J.; Geppert, W.; Linnartz, H.; Oberg, K.; Roueff, E.; Agundez, M.; Pernot, P.; Cuppen, H. M.; Loison, J. C.; Talbi, D. *Space Science Reviews* **2010**, *156*, 13.

(2) Betz, A. L. *Astrophysical Journal* **1981**, *244*, L103.

(3) Marcelino, N.; Cernicharo, J.; Agundez, M.; Roueff, E.; Gerin, M.; Martin-Pintado, J.; Mauersberger, R.; Thum, C. *Astrophysical Journal* **2007**, *665*, L127.

(4) Wada, A.; Mochizuki, N.; Hiraoka, K. *Astrophysical Journal* **2006**, *644*, 300.

(5) Bennett, C. J.; Jamieson, C. S.; Osamura, Y.; Kaiser, R. I. *Astrophysical Journal* **2006**, *653*, 792.

(6) Oberg, K. I. R.; van Dishoeck, E. F.; Linnartz, H.; Andersson, S. *Astrophysical Journal* **2010**, *718*, 832.

(7) Sandford, S. A.; Allamandola, L. J.; Tielens, A.; Valero, G. J. *Astrophysical Journal* **1988**, *329*, 498.

(8) Boogert, A. C. A.; Schutte, W. A.; Tielens, A.; Whittet, D. C. B.; Helmich, F. P.; Ehrenfreund, P.; Wesselius, P. R.; deGraauw, T.; Prusti, T. *Astronomy and Astrophysics* **1996**, *315*, L377.

(9) Boogert, A. C. A.; Schutte, W. A.; Helmich, F. P.; Tielens, A.; Wooden, D. H. *Astronomy and Astrophysics* **1997**, *317*, 929.

(10) Boogert, A. C. A.; Helmich, E. P.; van Dishoeck, E. F.; Schutte, W. A. *Astronomy and Astrophysics* **1998**, *336*, 352.

(11) Bennett, C. J.; Osamura, Y.; Lebar, M. D.; Kaiser, R. I. *Astrophysical Journal* **2005**, *634*, 698.

(12) Hiraoka, K.; Takayama, T.; Euchi, A.; Handa, H.; Sato, T. *Astrophysical Journal* **2000**, *532*, 1029.

(13) Hiraoka, K.; Sato, T.; Sato, S.; Takayama, T.; Yokoyama, T.; Sogoshi, N.; Kitagawa, S. *Journal of Physical Chemistry B* **2002**, *106*, 4974.

(14) Turner, B. E.; Terzieva, R.; Herbst, E. *Astrophysical Journal* **1999**, *518*, 699.

(15) Matthews, H. E.; Friberg, P.; Irvine, W. M. *Astrophysical Journal* **1985**, *290*, 609.

(16) Bell, M. B.; Matthews, H. E.; Feldman, P. A. *Astronomy and Astrophysics* **1983**, *127*, 420.

(17) Charnley, S. B. Acetaldehyde in star-forming regions. In *Space Life Sciences: Steps toward Origin(S) of Life*; Bernstein, M. P., Kress, M., NavarroGonzalez, R., Eds.; Pergamon-Elsevier Science Ltd: Kidlington, 2004; Vol. 33; pp 23.

(18) Fourikis, N.; Sinclair, M. W.; Robinson, B. J.; Godfrey, P. D.; Brown, R. D. *Australian Journal of Physics* **1974**, *27*, 425.

(19) Ikeda, M.; Ohishi, M.; Nummelin, A.; Dickens, J. E.; Bergman, P.; Hjalmarson, A.; Irvine, W. M. *Astrophysical Journal* **2001**, *560*, 792.

(20) Nummelin, A.; Dickens, J. E.; Bergman, P.; Hjalmarson, A.; Irvine, W. M.; Ikeda, M.; Ohishi, M. *Astronomy and Astrophysics* **1998**, *337*, 275.

(21) Turner, B. E. *Astrophysical Journal Supplement Series* **1991**, *76*, 617.

(22) Ziurys, L. M.; McGonagle, D. *Astrophysical Journal Supplement Series* **1993**, *89*, 155.

(23) Dickens, J. E.; Irvine, W. M.; Ohishi, M.; Ikeda, M.; Ishikawa, S.; Nummelin, A.; Hjalmarson, A. *Astrophysical Journal* **1997**, *489*, 753.

(24) Bernstein, L. S.; Lynch, D. K. *Astrophysical Journal* **2009**, *704*, 226.

(25) Turner, B. E.; Apponi, A. J. *Astrophysical Journal* **2001**, *561*, L207.

(26) Hawkins, M.; Andrews, L. *Journal of the American Chemical Society* **1983**, *105*, 2523.

(27) Hudson, R. L.; Moore, M. H. *Astrophysical Journal* **2003**, *586*, L107.
(28) Atkinson, R.; Cvetanov.Rj. *Journal of Chemical Physics* **1972**, *56*, 432.
(29) Perry, R. A. *Journal of Chemical Physics* **1984**, *80*, 153.
(30) Adriaens, D. A.; Goumans, T. P. M.; Catlow, C. R. A.; Brown, W. A. *Journal of Physical Chemistry C* **2010**, *114*, 1892.
(31) Atkinson, R.; Pitts, J. N. *Chemical Physics Letters* **1974**, *27*, 467.
(32) Stuhl, F.; Niki, H. *Journal of Chemical Physics* **1971**, *55*, 3954.
(33) Knyazev, V. D.; Arutyunov, V. S.; Vedeneev, V. I. *International Journal of Chemical Kinetics* **1992**, *24*, 545.
(34) Islam, F.; Latimer, E. R.; Price, S. D. *Journal Of Chemical Physics* **2007**, *127*, 064701.
(35) Lias, S. G. Ionization Energy Evaluation. In *NIST Chemistry WebBook, NIST Standard Reference Database Number 69*; Linstrom, P. J., Mallard, W. G., Eds.; National Institute of Standards and Technology, 2011.
(36) Bergeron, H.; Rougeau, N.; Sidis, V.; Sizun, M.; Teillet-Billy, D.; Aguillon, F. *Journal of Physical Chemistry A* **2008**, *112*, 11921.
(37) Rubes, M.; Kysilka, J.; Nachtigall, P.; Bludsky, O. *Physical Chemistry Chemical Physics* **2010**, *12*, 6438.
(38) Awad, Z.; Chigai, T.; Kimura, Y.; Shalabiea, O. M.; Yamamoto, T. *Astrophysical Journal* **2005**, *626*, 262.
(39) Occhiogrosso, A.; Viti, S.; Ward, M. D.; Price, S. D. **2012**, In Preparation.
(40) Allamandola, L. J.; Hudgins, D. M.; Bauschlicher, C. W.; Langhoff, S. R. *Astronomy and Astrophysics* **1999**, *352*, 659.
(41) Jackson, D. M.; Adams, N. G.; Babcock, L. M. *Journal of the American Society for Mass Spectrometry* **2007**, *18*, 445.
(42) Cunningham, M. R.; Jones, P. A.; Godfrey, P. D.; Cragg, D. M.; Bains, I.; Burton, M. G.; Calisse, P.; Crighton, N. H. M.; Curran, S. J.; Davis, T. M.; Dempsey, J. T.; Fulton, B.; Hidas, M. G.; Hill, T.; Kedziora-Chudczer, L.; Minier, V.; Pracy, M. B.; Purcell, C.; Shobbrook, J.; Travouillon, T. *Monthly Notices of the Royal Astronomical Society* **2007**, *376*, 1201.
(43) Elango, M.; Maciel, G. S.; Palazzetti, F.; Lombardi, A.; Aquilanti, V. *Journal of Physical Chemistry A* **2010**, *114*, 9864.
(44) Hollis, J. M.; Jewell, P. R.; Lovas, F. J.; Remijan, A.; Mollendal, H. *Astrophysical Journal* **2004**, *610*, L21.

# Chapter 4 – Reaction of Nitric Oxide with Deuterium Atoms

## 4.1 Introduction

The simplest oxide of nitrogen, nitric oxide, NO, has been detected in relatively high abundance fractional in the interstellar medium. For example, in the dark cloud TMC-1, NO has been detected with a fractional abundance of $2.7 \times 10^{-8}$ with respect to $H_2$.[1] Additionally the fractional abundances of NO in Orion KL, Sgr B2(N), Sgr B2(OH), W33A, W51M and DR21(OH) have been measured to lie in the range $4.2 \times 10^{-9}$ to $1.1 \times 10^{-8}$.[2] This interstellar nitric oxide is believed to form *via* the gas phase reactions shown below:[3]

$$N + OH \rightarrow NO + H \quad 4.1$$

$$O + NH \rightarrow NO + H \quad 4.2$$

To date, no observation of nitric oxide in interstellar ices has been made. Nevertheless, there are several reasons why NO may be expected to be present in the icy mantles of interstellar grains. Firstly, laboratory experiments have shown that exposure of ice mixtures composed of mixtures of $H_2O$ and $N_2$ to energetic electrons results in the formation of nitric oxide, amongst other species.[4] Hence, processing of interstellar ices containing $H_2O$ and $N_2$ by cosmic rays may be expected to result in NO formation. Furthermore, the surface reaction of N and O atoms provides a possible thermal route to NO formation. Whilst no experimental studies of this N + O reaction have yet been carried out under astrophysical conditions, such a radical-radical reaction might be expected to proceed efficiently in the interstellar medium. Finally, given the prevalence of NO in the gas phase, it is likely that some will be frozen out onto the icy mantles of interstellar dust grains.[1] Thus, the solid state chemistry of nitric oxide is of considerable astrochemical interest.

The potential for hydrogenating nitric oxide to hydroxylamine ($NH_2OH$) is of particular interest in view of recent experimental results which show that hydroxylamine may be a key precursor to amino acid formation in the interstellar medium.[5,6] Whilst amino acids have yet to be detected in the interstellar medium,[7] they have been found in carbonaceous chondrite meteorites.[8] In particular glycine ($NH_2CH_2COOH$) and β-alanine ($NH_2CH_2CH_2COOH$) were the most abundant amino acids detected in the CI chondrites Orgueil and Ivuna.[8] Additionally the enantiomers of α-alanine

($CH_3CH(NH_2)COOH$), L-alanine and D-alanine, were also detected in the Orgueil meteorite, in a ratio of approximately 1:1, providing strong evidence that the amino acids present were extraterrestrial in origin. The ionized forms of glycine and β-alanine have been found by Blagojevic *et al* to be formed in the reactions of ionized hydroxylamine ($NH_2OH^+$) with acetic and propanoic acids respectively.[5] Similarly, these authors find that protonated hydroxylamine ($NH_3OH^+$) can also take part in these reactions in place of ionized hydroxylamine, correspondingly yielding the amino acids in their protonated forms. The reactions between propanoic acid and these hydroxylamine species show strong selectivity for forming β-alanine over α-alanine. Therefore, the 9:1 average ratio of β-alanine to α-alanine in Orgueil and Ivuna[5,6,8] provides strong support for these amino acids having formed *via* the reactions of protonated and ionized hydroxylamine. Hydroxylamine has yet to be detected in the interstellar medium, however an efficient interstellar formation mechanism for hydroxylamine would lend considerable support to the amino acid formation routes proposed by Blagojevic *et al* [5] and Snow *et al* [6]. The reaction of NO in molecular ices with hydrogen atoms is one of two reactions proposed by Blagojevic *et al* as possible routes to the formation of the $NH_2OH$ required in the authors' suggested route to interstellar amino acids.[5] Whilst the alternative production pathway of hydroxylamine suggested by Blagojevic *et al*, UV irradiation of mixed ammonia and water ices, has been investigated experimentally,[9] little attention had, until recently, been paid to the reaction of thermal hydrogen atoms with nitric oxide ice under interstellar conditions. However, during the preparation of this thesis, another experimental study of the surface hydrogenation reaction of NO was published by Congiu *et al* which demonstrated that hydroxylamine can be efficiently formed *via* this mechanism on both amorphous solid water and silicate substrates in the temperature range 10 – 15 K.[10] This chapter presents the results of experiments investigating the reaction of thermal deuterium atoms with nitric oxide molecules on an HOPG surface at temperatures in the range 15 – 60 K.

## 4.2 Experimental

The experimental apparatus used in the experiments discussed in this chapter has been described in detail in Chapter 2. The nitric oxide gas used in the current experiments was a commercial sample of 99.5 % purity and was used without further purification. Deuterium atoms were chosen for this study in place of hydrogen atoms in order to increase the mass separation between the reactant NO and the products as much as possible and hence alleviate any potential interference in the product desorption peaks

in the TPD spectra from the desorption of the reactant. In order to confirm the identity of the products of the NO + D reaction, additional experiments were performed in which the NO + H reaction was investigated.

The fluxes of reactants used in the present experiments were $9.6 \times 10^{14}$ $cm^{-2}$ $s^{-1}$ for NO and $1.9 \times 10^{14}$ $cm^{-2}$ $s^{-1}$ for D atoms resulting in a ratio of NO:D of approximately 5:1. The flux of NO molecules was simply calculated from the pressure rise in the target chamber when the NO supply was turned on with the HOPG surface warm. The estimation of the flux of D atoms will be discussed in more detail in Section 4.5 below. A single experiment consists of the co-deposition of NO and D atoms for one hour with the HOPG surface held at a constant temperature between 15 and 60 K. After dosing the reactants for one hour, the NO inlet line was evacuated and the surface allowed to cool briefly to 15 K. The surface was then heated to approximately 300 K by passing a constant current of 15 A through the tantalum strip heater. Any reactant and product molecules desorbing from the surface during this heating phase of the experiment were ionized by 200 eV electrons and detected by recording consecutive 1 s duration mass spectra. As described in the preceding chapters, this method of data collection yields a two-dimensional histogram of ion yield as a function of mass to charge ratio and surface temperature during heating.

## 4.3 Results

At all surface temperatures investigated, the reaction of NO with D atoms was found to result in a product with a mass of 36 which desorbed at a surface temperature slightly greater than the $D_2O$ desorption temperature of approximately 160 K.[11] Given the elements available from the reactants, there are three possible products with a mass of 36: deuterium peroxide, $D_2O_2$, deuterated hydrazine, $N_2D_4$, and deuterated hydroxylamine, $ND_2OD$. In supplementary experiments, in which hydrogen atoms were used in place of deuterium atoms, the product peak was found to shift to a mass to charge ratio of 33, confirming the product to be $ND_2OD$. The variation of the yield of $ND_2OD$ with the temperature of the HOPG substrate during dosing can be seen in Figure 4.1. The yield of $ND_2OD$ decreases sharply as the surface temperature increases from 15 to 20 K. Between 20 K and 50 K the yield of hydroxylamine decreases slowly with increasing temperature, before approaching zero at 60 K. The yield at 15 K is substantially enhanced in comparison to that which might be expected by simple extrapolation of the trend between 20 and 50 K. Given that H atoms are only expected

to adsorb to the surface below 20 K, this apparent enhancement at 15 K can be attributed to the contribution of the LH mechanism, whilst at higher temperatures only the ER reaction between an adsorbed NO molecule and a gas phase D atom occurs. In principle the alternative ER* mechanism, between an adsorbed D atom and a gas phase NO molecule may occur below 20 K in addition to the LH mechanism. However, the contribution of this ER* mechanism is expected to be negligible in comparison to that from the LH mechanism, due to the fact that the concentrations of species adsorbed onto the surface can reach much larger values than the fluxes of species arriving at the surface from the gas phase.

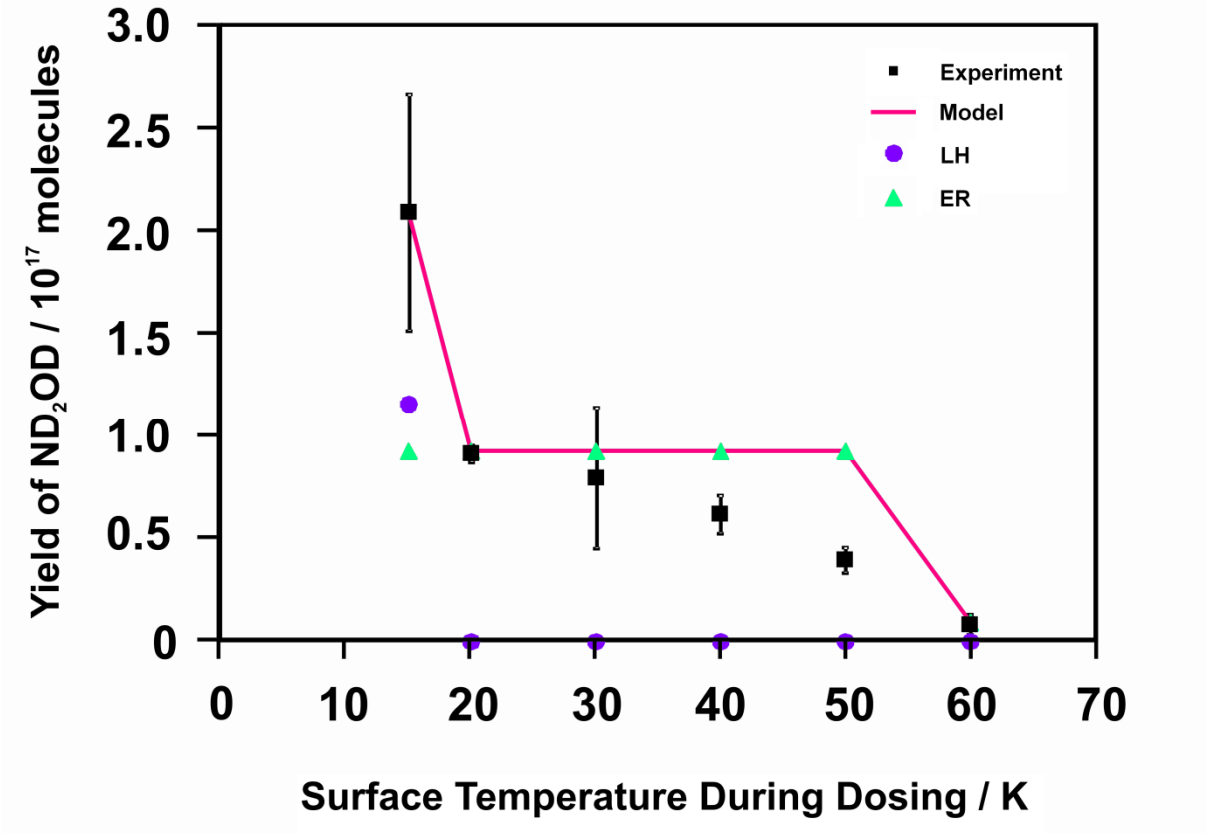


Figure 4.1 The temperature dependence of the yield of hydroxylamine ($ND_2OD$) formed from the reaction of NO with D atoms. The experimental data are represented by the black squares. The yield predicted by the kinetic model using $E_{LH} = E_{ER} = 0$ (see text) is shown by the pink line. The individual contributions from the LH and ER mechanism are shown by the purple circles and green triangles respectively.

An additional desorption peak, corresponding to a species with a mass of 64, was also observed. This desorption peak occurred at a temperature higher than that for both $D_2O$ and $ND_2OD$. Again, given the available reactants, this mass would be consistent with either deuterated nitric acid, $DNO_3$, or deuterated hyponitrous acid, $D_2N_2O_2$. When hydrogen atoms were used in place of deuterium atoms, the peak for this product shifted to a mass to charge ratio of 62, clearly indicating the presence of two hydrogen or

deuterium atoms. This product is therefore identified as $D_2N_2O_2$. The yield of this product appears to be largely independent of the surface temperature during dosing and shows no enhancement at 15 K. As was observed for hydroxylamine, the yield of $D_2N_2O_2$ falls to zero at 60 K.

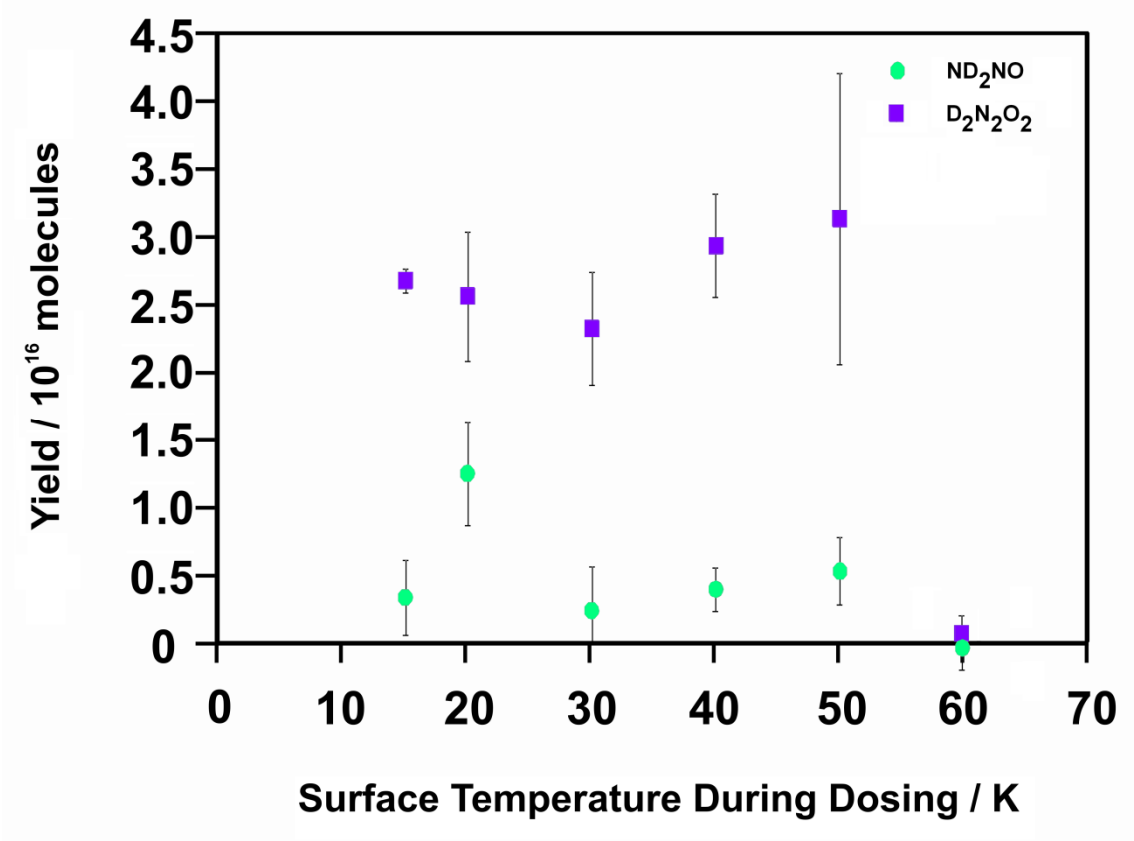


Figure 4.2 The temperature dependences of the yields of $ND_2NO$ (green circles) and $D_2N_2O_2$ (purple squares) formed by the reaction of NO with D atoms.

A third product was observed with a mass of 48 which desorbed at the same temperature as $D_2O$. This mass is consistent with the product being deuterated nitrosamine, $ND_2NO$. An alternative plausible product with a mass of 48 would be ozone, $O_3$. However, in previous experiments studying the reactions of O atoms, ozone has been observed to desorb at temperatures much lower than the ~ 160 K desorption temperature of water. Furthermore, when NO was reacted with H atoms, this product peak moved to mass 46, again indicating the presence of two H or D atoms. It is therefore clear that this product is deuterated nitrosamine. The yield of $ND_2NO$ is again broadly independent of the surface temperature during dosing with the exception of the yield at a surface temperature of 20 K. At this temperature the yield of $ND_2NO$ appears to be somewhat enhanced over that at other temperatures in the range 15 – 50 K. The yield of $ND_2NO$ again falls to zero at 60 K.

## 4.4 Data Analysis

Kinetic parameters such as reaction barriers and Arrhenius pre-exponential factors can be derived from the experimental data using the simple kinetic model described in detail in Section 2.11. Briefly, this kinetic model considers both the Eley-Rideal (ER) mechanism, in which a gas phase atom or molecule reacts directly with a species adsorbed onto a surface, and the Langmuir-Hinshelwood mechanism, in which two adsorbed species react. As described in Section 2.11, the kinetic model involves calculating the rates of the ER and LH reactions, at a given surface temperature, at regular time intervals throughout the dosing period. These rates are then integrated in order to determine the total number of product molecules generated during the dosing period. For a given rate constant, the number of product molecules can therefore be calculated for each surface temperature investigated, thus providing the temperature dependence of a product yield which can be compared with that measured experimentally.

In principle two separate ER mechanisms are available for the surface reaction between NO and D atoms: one in which a gas phase D atom reacts with an adsorbed NO molecule and a second in which a gas phase NO molecule reacts with an adsorbed D atom. Hereafter these mechanisms will be termed ER and ER* respectively. In the present experiments, the ER* reaction is disregarded since at temperatures low enough for D atoms to adsorb, NO molecules will also adsorb and the LH mechanism will be available. The contribution from this LH mechanism is likely to be much larger than that from the ER* mechanism due to the much larger concentrations available on the surface in comparison with those in the gas phase.

In order to separate out the contributions to the product yield from the ER and LH mechanisms, the desorption energy of D atoms must first be considered. Clearly, at higher temperatures where only NO molecules can adsorb onto the surface, only the ER mechanism will be available. Conversely at lower temperatures both NO and D atoms can adsorb onto the surface and so there may be an additional contribution from the LH mechanism. Ghio *et al* have determined the desorption energy of D atoms from graphite to be approximately 3.4 kJ $mol^{-1}$.[12] Given this desorption energy, deuterium atoms are not likely to adsorb onto the surface at temperatures higher than 15 K. Consequently, at 20 K and above, the product yield must arise solely from the ER mechanism. The

experimental data points in the temperature range 20 – 50 K are therefore used to derive kinetic parameters for the ER reaction.

The penetration depth of atoms into a molecular ice is finite, thus, when thick molecular ices are used, as in the experiments discussed here, the lower layers of the ice will not be available for reaction. Therefore, in modelling the experimental data, the penetration depth of D atoms into the NO ice must be considered. Unfortunately, no previous estimations of this penetration depth are available in the literature. However, Fuchs *et al*, who studied the reaction of H atoms with CO ices at 12 K, found that the yields of $H_2CO$ and $CH_3OH$ were independent of the ice thickness for coverages greater than 4 monolayers, indicating that the penetration depth of H atoms in CO ice is 4 monolayers.[13] Given that NO is sterically very similar to CO, the penetration depth of D atoms in NO ice might be expected to be similar to that for H atoms in CO ice. A penetration depth of 4 monolayers has therefore been assumed for the purposes of modelling the experimental data. It should be noted that in reality this penetration depth is likely to increase with increasing surface temperature, as species adsorbed onto the surface become more mobile. However, in the absence of any experimental data indicating the nature of the temperature dependence of the penetration depth, it seems to be no more justifiable to attempt to replicate this temperature dependence than to approximate it to a constant value. It must be emphasized that the penetration depth affects only the estimation of the pre-exponential, $A_{Rxn}$, and has no impact upon the determination of the reaction barriers or desorption energies.

## 4.5 Discussion

As outlined above, the experimental data shows that the reaction between NO and D atoms to form deuterated hydroxylamine proceeds efficiently at 15 K. The yield of $ND_2OD$ at 20 K is less than 50 % of that at 15 K and shows a mild decrease with increasing temperature between 20 and 50 K. At 60 K the yield of hydroxylamine falls to almost zero. In contrast, the yields of $D_2N_2O_2$ and $ND_2NO$ are broadly independent of temperature between 15 and 50 K. The temperature dependence observed for the reaction of NO with deuterium atoms is in good agreement with the observation by Congiu *et al* that NO reacts efficiently with hydrogen atoms at 10 and 15 K.[10]

The most obvious mechanism for the formation of $ND_2OD$ from the reaction of deuterium atoms with NO is the stepwise addition of D atoms to the NO molecule to saturate the N=O bond:

$$NO \xrightarrow{D} DNO \xrightarrow{D} ND_2O \text{ or } DNOD \xrightarrow{D} ND_2OD \qquad 4.3$$

Given the fact that the formation of hydroxylamine in these experiments is most efficient at 15 K, it is likely that none of these sequential deuteration reactions have a significant barrier. Alternatively, hydrogen and deuterium atoms may efficiently tunnel through any barriers present. However, Congiu *et al* observe that NO reacts with hydrogen and deuterium atoms at similar rates.[10] This finding suggests that the reaction does not proceed *via* a tunnelling mechanism, which would be expected to be slower in the case of the heavier deuterium atoms.

In the Congiu *et al* experiments, hydrogen atoms were found to react with NO molecules with an efficiency of approximately unity, an observation which provides a convenient method for estimating the flux of deuterium atoms in the current experiments.[10] To calculate this flux, it is assumed that every D atom impinging upon the surface at 15 K reacts and thus is contained within a product molecule at the end of the experiment. Thus, by summing the total number of molecules of each product species, multiplied by the number of deuterium atoms that species contains, an estimate of the total fluence of deuterium atoms can be obtained. Finally this fluence can simply be divided by the dosing time (3600 s) in order to derive the flux of D atoms. This calculation provides an estimate of the D atom flux of $1.9 \times 10^{14}$ $cm^{-2}$ $s^{-1}$. The combined flux of ($D + D_2$) can also be estimated from the pressure rise in the target chamber when the D atom source is turned on with the HOPG surface warm. Hence, from comparison of these two fluxes, a value for the dissociation efficiency of 25 % can be derived. These values of the D atom flux and $D_2$ dissociation efficiency are in good agreement with previous estimates for the current experimental setup.[14] It is important to note, however, that this estimate of the flux represents a lower limit for several reasons. Firstly, the reaction efficiency of D atoms with NO molecules may be slightly less than unity, resulting in some D atoms not being detected as constituents of product molecules. Secondly, products other than those detected in the present experiments may be formed resulting in the D atoms in those products not being counted. For example, another potential product from the reaction of D atoms with NO molecules is $D_2O$. However, the presence of background traces of $D_2O$ in the gas from the deuterium atom source in these experiments means that it was not possible to definitively determine whether $D_2O$ was also formed in the reaction of NO with D atoms. Finally the exothermicity of the reactions may result in a proportion of the intermediate products (for example DNO) being ejected into the gas phase and thus not detected in the present

experiments. As described in Section 4.4 above, the estimated flux of deuterium atoms can be used in the kinetic model, along with the other required parameters, to estimate overall rate constants for the conversion of nitric oxide to deuterated hydroxylamine by reaction with thermal D atoms.

As discussed above, deuterium atoms are only expected to be able to adsorb onto the surface at temperatures below 20 K. Furthermore, since all of the observed products desorb at temperatures much higher than NO, the substantial decrease in product yield between surface temperatures of 50 and 60 K is most likely due to a reactant or intermediate desorbing at these temperatures. Therefore, initially only the experimental data points between 20 and 50 K were modelled using an ER reaction in which a gas phase D atom reacts with an adsorbed NO molecule. The reaction barrier required to fit the experimental data points at these temperatures was $E_{ER} / R = -21$ K. The negative sign of the reaction barrier is a consequence the fact that the product yield decreases with increasing temperature. Apparent negative activation energies are commonly observed for gas phase ion-neutral reactions in which the attractive Coulombic interactions result in enhanced collision rates at lower temperatures.[15] Such negative activation energies are also observed in some gas phase neutral-neutral reactions. In this case, the negative activation energy is interpreted in terms of an excited reaction intermediate which may decompose to either the products or the reactants. For example, consider an intermediate, B, which may decompose either to reactant, A, or product, C.

$$B \rightarrow A \qquad 4.4$$

$$B \rightarrow C \qquad 4.5$$

If reaction 4.4 has a larger positive activation energy than reaction 4.5, the formation of product C would be favoured at lower temperatures and so the yield of product C would show a negative temperature dependence. However, any excited intermediates formed in a surface reaction would be very rapidly stabilised by the cold surface, rendering any potential reverse reaction, to reform the reactants, endothermic and hence unfeasible under the cold conditions of the current experiments. Thus, a more plausible explanation than that invoked in gas phase reactions, is that at higher temperatures a competing pathway forming another product becomes more efficient, thus reducing the hydroxylamine yield. Such competing pathways, forming nitrosamine and hyponitrous acid, will be discussed in more detail below. It is therefore unlikely that the negative activation energy is an inherent feature of the hydroxylamine formation mechanism, but

rather a consequence of side reactions being available at the high NO concentrations used in the current experiments. Nevertheless it is clearly evident that there is no substantial barrier to forming $ND_2OD$ *via* the reaction of D with NO on the surface. Thus, given the arguments above, in order to derive a realistic estimate of the pre-exponential factor for the reaction, the barrier $E_{ER}/R$ was set to zero. The pre-exponential factor was then adjusted to fit the experimental data point at 20 K. Using the data point at this temperature ensures that the effect of any competing reaction pathways was minimal. The value of $A_{Rxn}$ required to produce a good fit between the model output and the experimental data was $(3.4 \pm 0.1) \times 10^{-17}$ cm$^2$ molecule$^{-1}$ s$^{-1}$.

Next, a LH mechanism was introduced into the model in order to reproduce the data point at 15 K. The yield of hydroxylamine produced *via* the LH mechanism depends on the D atom desorption energy as well as the barrier to the LH reaction. Therefore, in order to reduce the number of free parameters in the model, the barrier, $E_{LH}$, was set to zero. The data point at 15 K can therefore be fitted by adjusting only the D atom desorption energy. The best fit to the experimental data was achieved with $E_{Des,\ D} / R$ = 429 ± 42 K ($E_{Des,\ D}$ = 3.66 ± 0.35 kJ mol$^{-1}$). This desorption energy is in excellent agreement with that determined for D atoms on graphite by Ghio *et al* (3.42 kJ mol$^{-1}$). It is important to note that due to the high deposition rates in the present experiments, the reaction takes place upon a layer of predominantly NO ice during the majority of the dosing period. Nevertheless, the excellent agreement between the D atom desorption energy estimated here and that determined for a graphite surface does suggest that the assumption that the LH mechanism has a zero reaction barrier is justified.

The decrease in the yield of hydroxylamine at 50 and 60 K is attributed to the decreased lifetime of NO molecules on the surface at these temperatures. The desorption of one of the intermediates in the reaction sequence at these temperatures represents an alternative explanation for this declining hydroxylamine yield. However, the polar N—H and O—H bonds in these intermediates would be expected to result in larger desorption energies for these species compared to that for NO. The desorption temperature of NO, $E_{Des,NO}$, can therefore be determined by adjusting this value in the model until the predicted yield at 50 K fits the experimental data point. The value of $E_{Des,NO}/R$ was determined to be 1744 ± 12 K ($E_{Des,NO}$ = 14.0 ± 0.1 kJ mol$^{-1}$). Few previous measurements of the NO-graphite interaction energy in the physisorption regime are reported in the literature. However, Brown and Hall report adsorption energies for NO physisorbed onto a

graphtized carbon black sample at low coverage, obtaining values of approximately 12 kJ $mol^{-1}$ at coverages close to zero, rising to approximately 18 kJ $mol^{-1}$ at monolayer coverage.[16] These values suggest that the value of $E_{Des,NO}$ determined from the current experiments represents a reasonable estimate for the NO-graphite physisorption energy. However, it must again be emphasized that the value determined in this study is not directly comparable with that determined by Brown and Hall due to the difference in coverages between the two studies.

Any further reactions of the hydroxylamine product with D atoms have been disregarded in this study. This neglect of secondary reactions is justified on the basis of the relative concentrations of NO and $ND_2OD$ in the ice. The ratio of $ND_2OD$:NO is approximately 0.06, thus a D atom is almost 17 times more likely to collide with an NO molecule than a $ND_2OD$ molecule. It would, in principle, be possible to confirm this assumption experimentally, by co-depositing hydroxylamine with H or D atoms. Hydroxylamine is available commercially as a 50 % aqueous solution. However, when a mass spectrum was recorded from the vapour of this solution, only $H_2O$ was observed along with some $N_2O$, which, presumably, is one of the decomposition products of hydroxylamine. In principle, the hydroxylamine solution could be dried and the solid hydroxylamine residue used as a source of $NH_2OH$ molecules. However, solid $NH_2OH$ decomposes rapidly and such an approach would likely yield only the gas phase decomposition products.[17]

A second product observed following the reaction of NO with deuterium atoms was deuterated nitrosamine, $ND_2NO$. The reaction mechanism leading to the formation of this product is less clear than in the case of hydroxylamine formation. Nevertheless, some indication of the reaction mechanism can be gained by considering the gas phase enthalpies of formation of the reactants and potential intermediates in the reaction. Consideration of these formation enthalpies indicates whether or not a particular reaction is exothermic, and, hence, viable under the low temperature conditions of these experiments. Of course, some caution is required in using gas phase energies to interpret the mechanism of a surface reaction. However, given that physisorption energies are small compared to the reaction enthalpies discussed below, it is unlikely that physisorption onto a surface would affect the sign of the enthalpy of a given reaction. The equivalent hydrogenated species are considered here because the relevant data for the deuterated intermediates is not available in the literature.

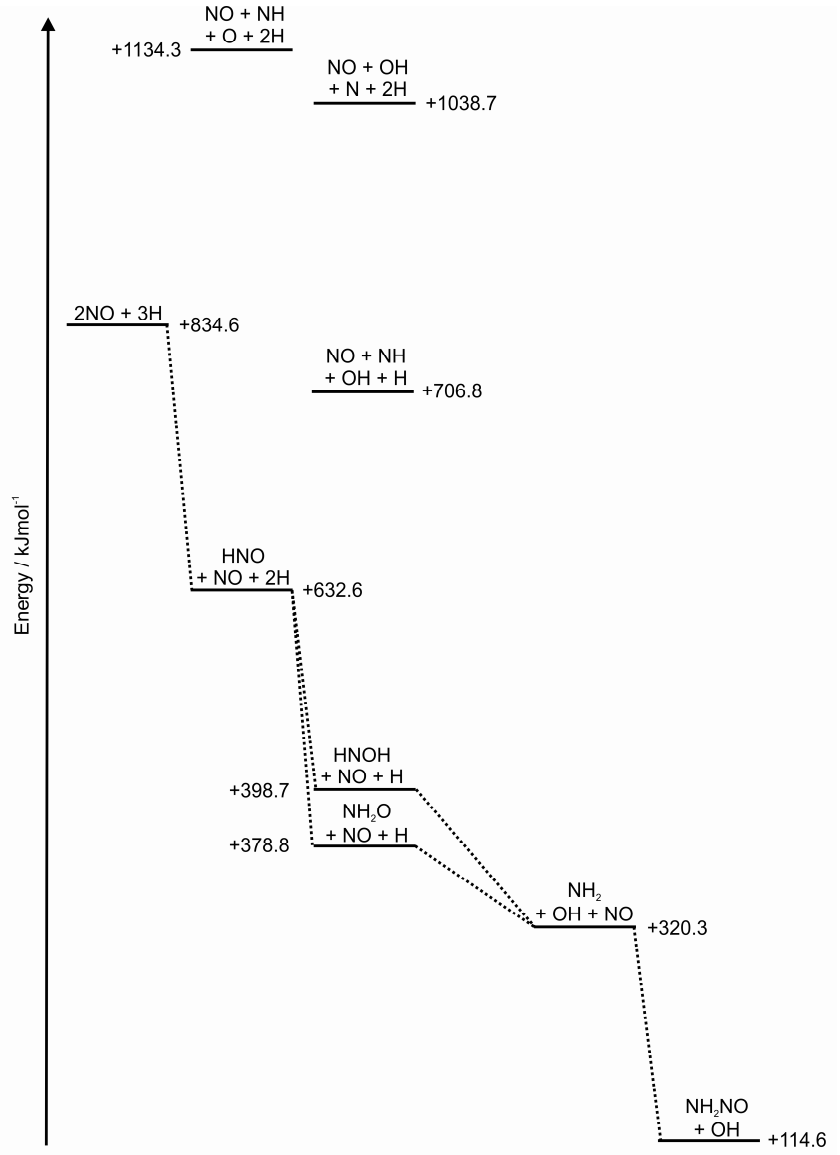


Figure 4.3 An energy level diagram showing the gas phase enthalpies of formation (in kJ $mol^{-1}$) of some possible intermediates in the formation of nitrosamine ($NH_2NO$). The dotted lines indicate the simplest exothermic reaction sequence. The enthalpies of formation are taken from Ref (18).

Clearly, the formation mechanism of nitrosamine involves cleavage of an N—O bond. Two ways in which the N—O bond can be cleaved are *via* the abstraction of either an N or an O atom from an NO molecule by an H atom as shown below:

$$NO + H \rightarrow NH + O \qquad 4.6$$

$$NO + H \rightarrow N + OH \qquad 4.7$$

However, as can be seen from Figure 4.3, both of these abstraction reactions are strongly endothermic in the gas phase. Alternatively dissociation of the N—O bond may take place after the initial hydrogenation step to form HNO, as shown below:

$$HNO + H \rightarrow NH + OH \quad 4.8$$

As shown in Figure 4.3, the overall conversion of 2NO + 3H to NO + NH + OH + H is exothermic. However, the reaction step shown in Equation 4.8 is endothermic. Thus, given that HNO is expected to rapidly thermalise with the surface upon formation, this mechanism is perhaps not a viable route to nitrosamine formation under the current experimental conditions. The simplest exothermic route to forming nitrosamine is, therefore, as follows:

$$NO + D \rightarrow DNO \quad 4.9$$

$$DNO + D \rightarrow D_2NO \text{ or } DNOD \quad 4.10$$

$$(D_2NO \text{ or } DNOD) + D \rightarrow ND_2 + OD \quad 4.11$$

$$ND_2 + NO \rightarrow ND_2NO \quad 4.12$$

It must be emphasised again that the energies shown in Figure 4.3 are for the species in the gas phase and thus the reaction enthalpies may be altered in the solid phase. Furthermore, there are other exothermic pathways involving reactions with additional D atoms. Consequently, the formation mechanism of nitrosamine cannot be definitively identified as that given above. Nevertheless, this mechanism does provide one plausible explanation for the formation of nitrosamine in the present experiments.

The temperature dependence of the yield of nitrosamine shows no enhancement at 15 K as was observed in the case of hydroxylamine. As described above, the enhanced yield of hydroxylamine at 15 K can be explained by an LH mechanism becoming available at this low temperature. However, at low temperatures, the formation of nitrosamine is likely to be inhibited by the requirement for two molecular species to interact. For example, in the reaction scheme proposed above, amino, $ND_2$, radicals must react with an NO molecule, yet these large species are likely to be quite immobile at low temperatures. The fact that the yield of nitrosamine appears to be broadly independent of temperature can therefore be explained as being a consequence of two competing factors. At 15 K the deuteration reactions to form $ND_2$ are very efficient but the reaction of $ND_2$ with NO is slow, whilst at higher temperatures $ND_2$ may efficiently react with NO but the $ND_2$ is less efficiently formed. If these two factors are approximately self-compensating over the range of temperatures investigated, one would expect the yield of $ND_2OD$ to be broadly independent of surface temperature. From Figure 4.2, there is some evidence of a mild enhancement in the nitrosamine yield at 20 K. However, in view of the estimated uncertainties, this enhancement is perhaps very small and should

not be overstated. Any small enhancement in the nitrosamine yield at 20 K could perhaps be explained by the possibility that this temperature is still low enough for deuterium atom addition reactions to occur efficiently and produce $ND_2$ but warm enough that this $ND_2$ is sufficiently mobile to react with NO molecules.

A similar temperature dependence is observed for the formation of hyponitrous acid, $D_2N_2O_2$. In this case the yield is essentially constant between 15 and 50 K and decreases to approximately zero at 60 K. Hyponitrous acid is known to be the product of dimerization of the nitroxyl (HNO) molecule and is most likely formed in these experiments from the reaction of two DNO molecules. The temperature dependence is again explicable in terms of a D atom addition reaction which is enhanced at 15 K and a DNO + DNO reaction which is more favourable at higher temperatures.

Unfortunately, the complexity of the reaction mechanisms for forming nitrosamine and hyponitrous acid precludes the determination of meaningful kinetic parameters. Specifically, the temperature dependences of the product yields in these two cases are superficially consistent with a barrier of approximately zero in each case. However, in reality these temperature dependences are probably the sum of contributions with different activation energies as discussed above. In any case, the involvement of two NO molecules in the formation mechanisms of $D_2N_2O_2$ and $ND_2NO$ suggests that these pathways are unlikely to be significant in interstellar ices where the concentration of NO is very low.

## 4.6 Astrophysical Implications

Assuming a fractional abundance of $10^{-4}$ $n_H$ for atomic hydrogen in dense interstellar clouds [19], the total fluence of D atoms in one of the current experiments is estimated to be equivalent to $10^6 – 10^7$ years of exposure to H atoms in a such a cloud. This time is of the same order as the lifetime of a typical interstellar cloud. The experimental results discussed in this chapter therefore indicate that the reaction of thermal hydrogen atoms with nitric oxide at interstellar dust grain surfaces represents a highly efficient route to the formation of hydroxylamine in the interstellar medium. This finding is of significant astrobiological importance because, as outlined in Section 4.1, both ionized hydroxylamine ($NH_2OH^+$) and protonated hydroxylamine ($NH_3OH^+$) have been found by Blagojevic *et al* to react with acetic acid to form the simplest amino acid, glycine, in its ionized and protonated forms respectively.[5] Similarly these same hydroxylamine species also react with propanoic acid to produce β-alanine, again in its ionized and

protonated forms. The plausibility of this proposed route to amino acid formation in the interstellar medium is further supported by hydroxylamine's low ionization energy (10.06 eV)[20] and high proton affinity (~ 8.4 eV).[21] Furthermore a theoretical study by Largo *et al* [22] indicates that neither hydroxylamine in its protonated nor ionized forms will react with molecular hydrogen under interstellar conditions due to the presence of substantial activation energies for the exothermic pathways. Consequently the formation of $NH_3OH^+$ and $NH_2OH^+$ from neutral hydroxylamine is expected to be efficient in the interstellar medium.

Nitrosamine and hyponitrous acid were also observed to form in the surface reaction of H and D atoms with nitric oxide. However, the formation mechanisms of these two species require two NO molecules to exist in close proximity in the ice; a situation which would be rare in interstellar ices. Consequently, the formation of nitrosamine and hyponitrous acid is considered to be unlikely to occur in the interstellar medium. Nevertheless, the formation of these species in the current experiments does offer some insight into the reactivity of $NH_2$ and HNO in interstellar ices. For example, it appears that NH2 can react with NO molecules to produce nitrosamine, NH2NO, whilst HNO can dimerize to produce hyponitrous acid, $H_2N_2O_2$. The formation and consequent reactions of the amino group is of astrochemical interest because its reactions with organic molecules may represent simple thermal routes to amines and amino acids. However, experimental astrochemical investigations into the reactivity of species such as $NH_2$ and HNO are non-trivial, due to the difficulty in producing clean beams of such molecular radicals. For example $NH_2$ may, perhaps, be produced in a microwave discharge in ammonia, but it would be difficult to distinguish between the reactions of $NH_2$ and other species produced such as NH. However, in view of the results obtained in the current experiments, it may be possible to gain some limited insight into the possible reactions of $NH_2$ by mixing a potential co-reactant with NO and dosing the mixed ice with H atoms.

## 4.7 Summary

In this chapter experiments investigating the reactions of D atoms with nitric oxide have been discussed. These experiments show that hydroxylamine may readily be formed *via* the surface reaction of NO with thermal H atoms under interstellar conditions. In its ionized or protonated forms, this hydroxylamine was observed to react with acetic and propanoic acids to produce glycine and β-alanine respectively. As already discussed in

Section 4.1, nitric oxide has yet to be detected in interstellar ices. The confirmation of the existence of nitric oxide in interstellar ices would therefore confirm the plausibility of the hydroxylamine mediated route to interstellar amino acids and hence would be of considerable astrobiological interest.

## 4.8 References


(1) Gerin, M.; Viala, Y.; Casoli, F. *Astronomy and Astrophysics* **1993**, *268*, 212.
(2) Ziurys, L. M.; McGonagle, D.; Minh, Y.; Irvine, W. M. *Astrophysical Journal* **1991**, *373*, 535.
(3) Jorfi, M.; Honvault, P.; Halvick, P. *Journal of Chemical Physics* **2009**, *131*, 8.
(4) Zheng, W. J.; Kim, Y. S.; Kaiser, R. I. *Physical Chemistry Chemical Physics*, *13*, 15749.
(5) Blagojevic, V.; Petrie, S.; Bohme, D. K. *Monthly Notices of the Royal Astronomical Society* **2003**, *339*, L7.
(6) Snow, J. L.; Orlova, G.; Blagojevic, V.; Bohme, D. K. *Journal of the American Chemical Society* **2007**, *129*, 9910.
(7) Lattelais, M.; Pauzat, F.; Pilme, J.; Ellinger, Y.; Ceccarelli, C. *Astronomy & Astrophysics* **2011**, *532*, 7.
(8) Ehrenfreund, P.; Glavin, D. P.; Botta, O.; Cooper, G.; Bada, J. L. *Proceedings of the National Academy of Sciences of the United States of America* **2001**, *98*, 2138.
(9) Nishi, N.; Shinohara, H.; Okuyama, T. *Journal of Chemical Physics* **1984**, *80*, 3898.
(10) Congiu, E.; Fedoseev, G.; Ioppolo, S.; Dulieu, F.; Chaabouni, H.; Baouche, S.; Lemaire, J. L.; Laffon, C.; Parent, P.; Lamberts, T.; Cuppen, H. M.; Linnartz, H. *Astrophysical Journal Letters* **2012**, *750*.
(11) Burke, D. J.; Wolff, A. J.; Edridge, J. L.; Brown, W. A. *Physical Chemistry Chemical Physics* **2008**, *10*, 4956.
(12) Ghio, E.; Mattera, L.; Salvo, C.; Tommasini, F.; Valbusa, U. *Journal of Chemical Physics* **1980**, *73*, 556.
(13) Fuchs, G. W.; Cuppen, H. M.; Ioppolo, S.; Romanzin, C.; Bisschop, S. E.; Andersson, S.; van Dishoeck, E. F.; Linnartz, H. *Astronomy & Astrophysics* **2009**, *505*, 629.
(14) Perry, J. S. A.; Gingell, J. M.; Newson, K. A.; To, J.; Watanabe, N.; Price, S. D. *Measurement Science & Technology* **2002**, *13*, 1414.
(15) Meotner, M.; Field, F. H. *Journal of the American Chemical Society* **1975**, *97*, 2014.
(16) Brown, C. E.; Hall, P. G. *Journal of Colloid and Interface Science* **1973**, *42*, 334.
(17) Cisneros, L. O.; Rogers, W. J.; Mannan, A. S. *Thermochimica Acta* **2004**, *414*, 177.
(18) Dean, A. M.; Bozzelli, J. W. Combustion Chemistry of Nitrogen. In *Gas-Phase Combustion Chemistry*; Jr., W. C. G., Ed.; Springer, 2000; pp 125.
(19) Cuppen, H. M.; Herbst, E. *Astrophysical Journal* **2007**, *668*, 294.
(20) Lias, S. G.; Bartmess, J. E.; Liebman, J. F.; Holmes, J. L.; Levin, R. D.; Mallard, W. G. *Journal of Physical and Chemical Reference Data* **1988**, *17*, 1.
(21) Boulet, P.; Gilardoni, F.; Weber, J.; Chermette, H.; Ellinger, Y. *Chemical Physics* **1999**, *244*, 163.
(22) Largo, L.; Rayon, V. M.; Barrientos, C.; Largo, A.; Redondo, P. *Chemical Physics Letters* **2009**, *476*, 174.

# Chapter 5 – The Reaction of Carbon Disulfide with Oxygen Atoms

## 5.1 Introduction

The discrepancy between the elemental abundance of sulfur in the universe and the gas phase abundances of sulfur bearing molecules in interstellar clouds has prompted increasing interest in the chemistry of sulfur on interstellar dust grains. Specifically, whilst the interstellar elemental abundance of sulfur, relative to hydrogen, has been calculated to be in the region of $10^{-5}$,[1-3] the sulfur abundances required to explain the gas phase column densities of sulfur-containing species in dense interstellar clouds ($T \approx$ 10 – 20 K) are much lower, typically $10^{-7}$ – $10^{-9}$.[4-7] An obvious conclusion is that a significant proportion of sulfur in dense interstellar clouds must be contained in the icy mantles of interstellar dust grains.[8] However, to date, only two sulfur containing molecules have been identified in interstellar ices: sulfur dioxide ($SO_2$) and carbonyl sulfide (OCS).[9-12] The presence of hydrogen sulfide ($H_2S$) in grain mantles has also been suggested, *via* observations of the embedded protostar W33A,[13] but the definitive detection of $H_2S$ is complicated by the overlap of its main infrared band with an infrared feature of methanol.[8] The above deduction of a significant abundance of sulfur-containing molecules in the icy mantles on interstellar grains indicates there is potentially a rich sulfur chemistry in this environment, a conclusion reached, for example in accounting for the abundance of OCS in hot cores ($T \approx$ 100 – 300 K).[4,14,15]

Studies of the surface chemistry of sulfur containing species, under interstellar conditions, have so far been restricted to work involving non-thermal processing, where ices containing sulfur are activated by irradiation. Experiments studying the non-thermal processing of $SO_2$ and $H_2S$ containing mixed ices by energetic (200 – 800 keV) protons have been performed, and indicate such interactions provide routes to OCS.[8,16] However, in both of these studies, significant amounts of carbon disulfide ($CS_2$) were also detected following the irradiation of ice mixtures of CO and $H_2S$; the $CS_2$ perhaps being formed by the processing of the primary OCS product. Indeed, for ice mixtures of CO and $H_2S$, Garozzo et al.[8] report that more $CS_2$ is formed than OCS. Hence, these authors suggest that $CS_2$ may act as a reservoir of sulfur on interstellar grain surfaces. So far, however, $CS_2$ has not been detected in interstellar ices. This failure to observe $CS_2$ in ice mantles is perhaps due to the fact that the main infrared band of $CS_2$, at

around 6.60 μm, overlaps with other spectral features.[8] Alternatively, the reactivity of $CS_2$ may be such that it is rapidly converted to other sulfur containing species. Either way, the fate of $CS_2$ on interstellar dust grain surfaces is of considerable interest in developing a complete picture of the surface chemistry of sulfur containing species in the ISM.

Recently, investigations of UV-processing of $H_2S/H_2O$ ices have revealed the eventual formation of $S_2$, and by implication other $S_n$ surface species.[17] These refractory polymeric sulfur species have also been proposed as a sulfur reservoir on the dust grains in dense interstellar clouds.

The non-thermal reactivity of sulfur bearing ices may well be markedly different to that resulting from thermal processes, where the reacting system is not activated by an incident particle or photon. In view of the fact that both sulfur containing species confirmed to exist in interstellar ices to date ($SO_2$, OCS) contain oxygen, this chapter presents the results of experiments studying the reaction between $CS_2$ and oxygen atoms on a highly-oriented pyrolitic graphite (HOPG) surface under astrophysically relevant conditions. In these experiments, $CS_2$ and oxygen atoms are co-deposited onto the HOPG substrate at a range of different surface temperatures, between 15 and 70 K. Temperature-programmed desorption (TPD), coupled with time-of-flight mass spectrometry (TOF-MS), is then used to detect any products formed. Carbonyl sulfide, OCS, is readily formed across the range of surface temperatures investigated. In order to derive rate constants for the reaction between oxygen atoms and $CS_2$, the experimental results are fitted with the simple kinetic model described in Section 2.11.

## 5.2 Experimental

The experimental arrangement used for the experiments discussed in this chapter is described in detail in Chapter 2. The source of $CS_2$ molecules was the vapour above a liquid sample of $CS_2$ (99.9 %) held at 0 $^{o}$C. Any volatile impurities were first removed from this liquid sample of $CS_2$ by pumping on it at 0 °C. The fluxes of $CS_2$ and O used in these experiments were $7.4 \times 10^{14}$ cm$^{-2}$ s$^{-1}$ and $1.2 \times 10^{14}$ cm$^{-2}$ s$^{-1}$ respectively, resulting in a ratio of $CS_2$ to O of approximately 6:1.

$CS_2$ and O atoms were simultaneously dosed for one hour in each experiment whilst the HOPG surface was held at a fixed temperature between 15 K and 70 K. After the one hour dosing the supply of both reactants was turned off, the supply lines evacuated and

the surface cooled to 15 K. The HOPG surface was then warmed to approximately 200 K by applying a constant current to a tantalum strip heater housed beneath the HOPG substrate. During this warming period, any species desorbing from the surface are ionized, using 200 eV electrons from a pulsed electron gun (29 kHz), and detected using the TOF mass spectrometer. As described in Section 2.9, the dataset generated from dosing at a given surface temperature (e.g. 20 K) is a two-dimensional histogram of ion intensity as a function of ion mass to charge ratio and the surface temperature during the desorption cycle. As shown below, such a set of experiments allows the temperature dependence of the surface reaction rates to be determined.

In the current experiments multi-photon ionization (MPI) can also be employed, in place of electron ionization, to distinguish between different ions of identical mass to charge ratios. Specifically, MPI is used in these experiments to distinguish between $SO^+$ and $O_3^+$. This selectivity is possible because SO and $O_3$ have different ionization energies (10.29 and 12.53 eV respectively).[18] Therefore by using photons of a wavelength such that the two-photon energy is intermediate between these two values, one molecule can be selectively ionized without interference from the other.[19] In the experiments discussed here 224.800 nm photons are used (two-photon energy 11.05 eV). The duration of the consecutive mass spectra recorded during warming is longer (10 s *vs.* 1 s) when laser ionization is used in order to compensate for the much lower pulse frequency of the laser (10 Hz) in comparison with the electron gun. The same heating current, and hence temperature ramp, was used in both the electron ionization and MPI experiments.

## 5.3 Results

Following the dosing of $CS_2$ and O atoms onto the HOPG surface, the formation of carbonyl sulfide (OCS) is observed at surface temperatures between 15 and 70 K. Additional experiments where $CS_2$ and pure $O_2$ (i.e. the microwaves were turned off to the O atom source) were co-deposited onto the HOPG substrate at 20 K did not give any OCS signals, confirming OCS is formed by the reaction of O atoms with $CS_2$.

The temperature dependence of the OCS yield on surface temperature is shown in Figure 5.1. At 70 K the OCS yield decreases markedly despite the fact that a large desorption peak for $CS_2$ is still observed at this temperature, indicating that the surface is still cold enough for $CS_2$ to adsorb onto it. It therefore seems clear that at this

temperature the lifetime of OCS on the surface is short enough that the molecule can desorb before the TPD spectrum is recorded. At 15 K and 20 K the yield of OCS seems to be greater than at 25 K. As discussed in detail below, this enhancement in OCS yield suggests that a separate reaction mechanism is available at these low temperatures but is inhibited above 20 K.

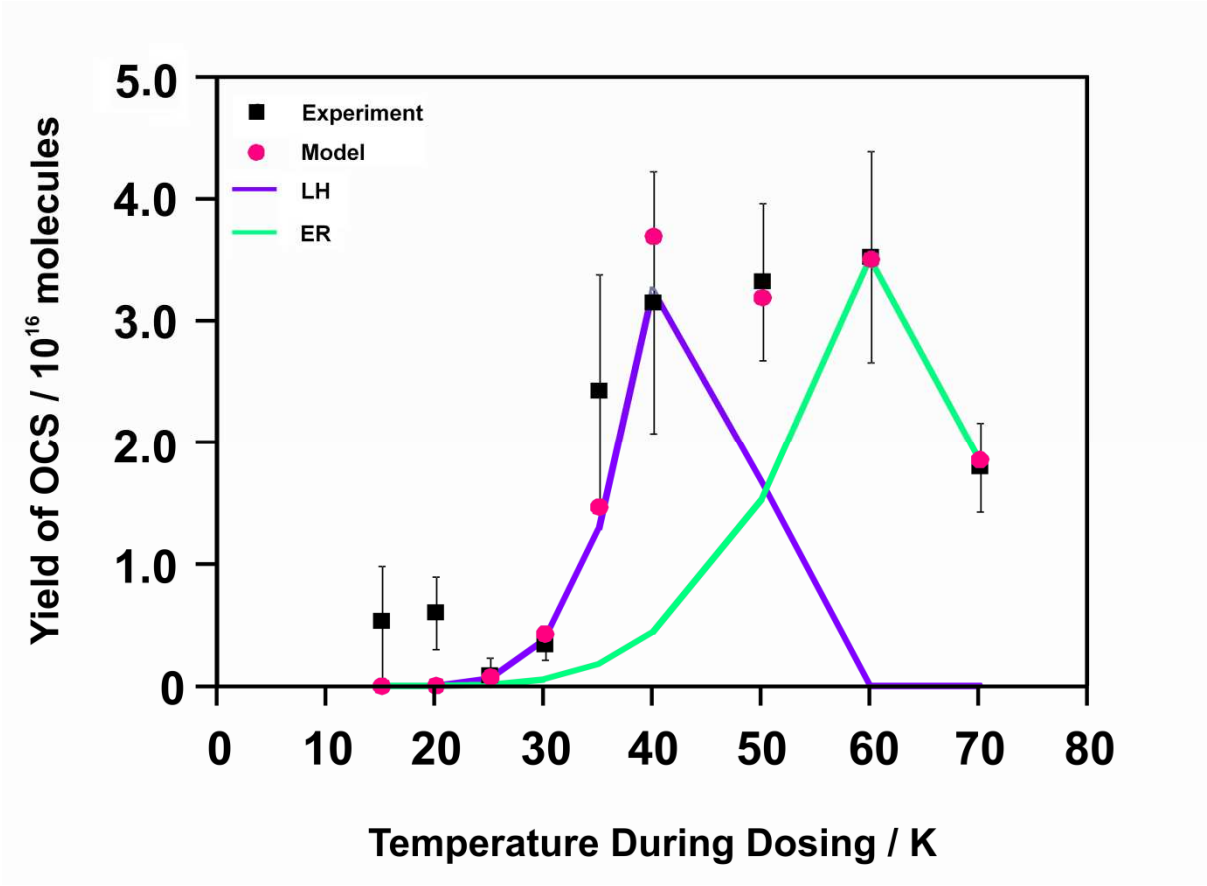


Figure 5.1 The temperature dependence of the yield of OCS formed from the surface reaction of $CS_2$ with O atoms. The experimental data points are represented by the black squares with the pink circles representing the yield predicted by the kinetic model. The green and purple lines represent the individual contributions to the product yield from the ER and LH mechanisms respectively.

At low surface temperatures sulfur monoxide (SO) was also detected from the reaction of O atoms with $CS_2$. Definitive identification of the mass spectral signal at $m/z$ = 48 as SO, instead of $O_3$ for example, was performed using multi-photon ionization (MPI) as described above. This MPI technique is required because, with conventional electron ionization, it is not possible to distinguish between SO, formed *via* a reaction between O and $CS_2$, and potential traces of $O_3$ formed *via* the possible reaction between O and residual $O_2$ molecules from the O atom source.

## 5.4 Data Analysis

The TPD data is integrated to give the total yield of carbonyl sulfide (OCS) from the reaction of $CS_2$ with O atoms as a function of the surface temperature during the dosing. In order to estimate the rate constants for reactions taking place on the surface, the experimental data have been fitted using the simple kinetic model described in detail in Section 2.11. For clarity, the key features of this kinetic model, as applied to the $CS_2$ + O, are reiterated here.

The kinetic model considers both of the prototypical surface reaction mechanisms: the Eley-Rideal (ER) mechanism and the Langmuir-Hinshelwood (LH) mechanism. The rates of both the ER reaction and LH reaction are calculated at each time step throughout the dosing period at a given surface temperature. Given that both of these processes can occur simultaneously, the overall rate of reaction is simply the sum of the rates of the ER and LH mechanisms. The total number of product molecules formed can therefore be calculated by integrating this rate over the entire dosing period.

As noted in the preceding chapters, there are in principle two ER reactions which can occur simultaneously. In the case of the surface reaction of $CS_2$ and O atoms, one of these ER reactions involves a gas phase O atom reacting with an adsorbed $CS_2$ molecule, whilst in the alternative ER mechanism, a gas phase $CS_2$ molecule reacts with an adsorbed O atom. Here, only the ER process for the reaction of O atoms from the gas-phase reacting with an adsorbed $CS_2$ molecule is considered. This neglect of the alternative O(ads) +$CS_2$(g) ER reaction is justified because this mechanism will only be available at temperatures low enough for O atoms to adsorb onto the surface. At these low surface temperatures $CS_2$ molecules will also stick and hence the LH mechanism is also available. Any contribution to the product yield from an O(ads) + $CS_2$(g) ER process is thus likely to be insignificant in comparison to that from the LH mechanism, due to the enhanced concentrations of reactants available for the LH process.

It should also be noted that the above rate equation assumes that the OCS product does not react further with O atoms or $O_2$. This can be justified by considering the relative concentrations of $CS_2$ reactant and OCS product on the surface. Specifically, the maximum $[OCS]_S$:$[CS_2]_S$ ratio observed in the present experiments is 0.007. Clearly then interactions of incident oxygen atoms with $CS_2$ will be more than 100 times more frequent than those with OCS, and even if some of these collisions were reactive the

effect on the OCS yield would be negligible. Unfortunately, experimentally confirming the absence of this secondary reaction is very difficult. Specifically, the product of an OCS + O reaction is, by analogy with $CS_2$ + O, likely to be $CO_2$, which has a very similar desorption temperature to OCS. This similarity in desorption temperatures of OCS and $CO_2$ then presents difficulties in distinguishing between small numbers of $CO_2^+$ ions ($m/z$ = 44) formed from ionization of any $CO_2$ product and the large numbers of $CS^+$ ions ($m/z$ = 44) formed from dissociative ionization of the plentiful OCS reactant. In principle MPI might be used to provide a definitive detection of $CO_2$. However, two-photon ionization of $CO_2$ requires photons of wavelengths (≤ 180 nm) inaccessible to the current laser configuration.

To determine the predicted yield of OCS from the kinetic model for comparison with the experimental values, the overall rate equation is integrated numerically starting from the initial conditions $[O]_s = [CS_2]_s = 0$ at $t = 0$. The surface concentrations of O atoms and $CS_2$ molecules can be calculated at each time step by considering their flux onto the surface, their rate of desorption from the surface at the relevant temperature and their consumption *via* mutual reaction as described in Section 2.11. The flux of O atoms and $CS_2$ molecules has been estimated to be $1.2 \times 10^{14}$ molecules $cm^{-2}$ $s^{-1}$ and $7.4 \times 10^{14}$ molecules $cm^{-2}$ $s^{-1}$ respectively as described in Chapter 2. The desorption rate for a given species at a given surface temperature can readily be calculated using Equation 5.1 and, as described below, the desorption energies of O and OCS, $E_{\mathrm{Des,O}}$ and $E_{\mathrm{Des,OCS}}$, can readily be determined by fitting the model output to the experimental data.

$$r_{Des,X} = A_{Des,X} \exp\left(\frac{E_{Des,X}}{RT}\right)[\mathrm{X}]_S \qquad 5.1$$

The pre-exponential factor for the desorption process, $A_{Des,X}$ (Eq. 5) is often similar to the vibrational frequency of the adsorbate-surface bond.[20] Since no determinations of $A_{Des,O}$ for desorption from graphite or $CS_2$ ice are available in the literature, the vibrational frequency of an O atom adsorbed at a bridge site of pyrene ($3.10 \times 10^{12}$ $s^{-1}$) is used for $A_{\mathrm{Des,O}}$.[21] Also, in the absence of any literature value for $A_{Des,OCS}$, the value for a $CO_2$ monolayer physisorbed on HOPG ($5.3 \times 10^{14}$ $s^{-1}$) is used.[22] It should be noted that the rate of $CS_2$ desorption is set to zero in the model, at all surface temperatures. This negligible desorption rate is clearly supported by the experiments, where no evidence of significant $CS_2$ desorption is observed at any of the substrate temperatures

investigated. This observation confirms that, as expected, the desorption energy of $CS_2$ is larger than that of OCS.[23]

The penetration depth of O atoms in the present experiments is set to one monolayer. This assumption that O atoms do not penetrate the ice is supported by previous diagnostic experiments studying the reaction $^{16}O$ with a pre-deposited $^{18}O_2$ ice. In these experiments, it was found that rather than penetrating the $^{18}O_2$ ice to produce the ozone isotopologue $^{16}O^{18}O_2$, the $^{16}O$ predominantly reacted with $^{16}O_2$ ice which accumulated on the surface during dosing of the $^{16}O$ atoms. These observations clearly indicate that the penetration depth of O atoms is minimal, at least for $O_2$ ice. It is reasonable to assume that the penetration depth of O atoms into ices composed of bulky $CS_2$ molecules is not greater than that into ice composed of $O_2$.

In order to derive reaction barriers for the ER and LH mechanisms, ($E_{LH}$ and $E_{ER}$) and the relevant desorption energies ($E_{\mathrm{Des,O}}$ and $E_{\mathrm{Des,OCS}}$), the barrier heights are adjusted in the model to achieve the best fit between the temperature dependence predicted by the kinetic model and that observed in the experimental data. The product yield is strongly affected by the desorption energy of O atoms (which determines the maximum temperature at which the LH mechanism can proceed efficiently; in this case approximately 50 K) and the desorption energy of OCS (which determines the temperature at which the contribution to the measured yield from the ER mechanism starts to decrease; in this case approximately 70 K). However, it is important to note that the effect of these desorption energies on the OCS yield is limited to a restricted set of data points, close to the desorption energies, and does not affect the entire temperature dependence. Therefore, both the reaction barriers and the desorption energies can be extracted robustly from a normalized fit to the experimental data.

Absolute rate constants for the $CS_2$ + O reaction can be derived by placing the experimental data on an absolute scale as described in Section 2.10. Rescaling the experimental results in this way has no effect upon the form of the temperature dependence. Thus the pre-exponential factor for the reaction can be determined independently of the reaction barriers. Following the procedure described in Section 2.10, the experimental data can be plotted as the number of molecules formed against surface temperature. The output of the kinetic model is also in these units and can be fitted to the experimental data, using the reaction barriers and desorption energies

obtained as described above, by setting $A_{Rxn} = (5.5 \pm 1.0) \times 10^{-15}$ cm$^2$ molecule$^{-1}$ s$^{-1}$. The kinetic parameters derived using the kinetic model are summarized in Table 5.1.

## 5.5 Discussion

As described above, reaction barriers for both the ER and the LH pathways can be determined by fitting the experimental data with the kinetic model. Such a fit is shown in Figure 5.1. Clearly above 25 K there is good agreement between the experimental results and the model output. However, it is not possible to fit the product yield at 15 and 20 K with the model used whilst still maintaining a good fit at higher temperatures. This difficulty in fitting the entire temperature dependence suggests that there is more than one reaction pathway involved in the formation of OCS from the reaction of $CS_2$ with O atoms. Indeed, as discussed below, the experimental data clearly support the operation of two pathways forming OCS: a low temperature pathway occurring below 25 K and a high temperature pathway occurring above 25 K.

Unfortunately, given just two data points, it is not possible to derive any statistically meaningful kinetic parameters for the reaction pathway occurring at 15 and 20 K. However, some empirical observations can be made. Firstly, it seems clear that the reaction pathway responsible for OCS formation at these temperatures has a much lower barrier than that taking place at higher temperatures. Secondly, the near-zero product yield at 25 K implies that there is some 'cut off' for this mechanism between 20 and 25 K. One explanation for this behaviour is that the reaction proceeds *via* an intermediate which, at temperatures above 20 K, does not remain adsorbed onto the surface long enough for the reaction to proceed to OCS. One reaction pathway consistent with this explanation involves $CS_2$ initially reacting with O to form carbon monosulfide (CS) and sulfur monoxide (SO):

$$CS_2 + O \rightarrow CS + SO \qquad 5.2$$

Providing the CS radical remains adsorbed on the surface, it may then undergo reaction with a further oxygen atom to form OCS. This mechanism would be consistent with the decrease in OCS yield at 25 K because the desorption energy for CS on a graphite surface has been calculated to be 6.3 kJ mol$^{-1}$ ($E_{Des}/R$ = 758 K).[24] The desorption energy is related to the time taken for half the molecules on a surface to desorb, $t_{1/2}$, by Equation 5.3.

$$t_{\frac{1}{2}} = \frac{1}{A_{Des}} \exp\left(\frac{E_{Des}}{RT}\right) \quad 5.3$$

Thus, given the calculated desorption energy, and assuming the pre-exponential factor for desorption to be $1 \times 10^{12}$ $s^{-1}$, the approximate half-life of CS on the surface can be calculated to be several hours at 20 K and a few seconds at 25 K. Clearly, the lifetime of CS on the surface at or below 20 K will not be a limiting factor in the product yield. However, at surface temperatures of 25 K and above, the concentration of CS on the surface would not build up sufficiently to yield a detectable amount of OCS. Further support for this low-temperature reaction pathway comes from multi-photon ionization (MPI) experiments following co-deposition of $CS_2$ and O at a surface temperature of 15 K. These experiments were carried out with photons of wavelength 224.800 nm such that the two photon energy was above the ionization energy for SO but below that for $O_3$. In these MPI experiments a clear desorption peak for SO was observed at $m/z$ = 48, providing clear evidence that at low surface temperatures $CS_2$ initially reacts with O to form SO and CS. Unfortunately it was not possible to definitively detect the accompanying CS molecules, since the ionization energy of CS is higher than that of $CS_2$. Therefore, in MPI experiments aimed at detecting CS, $CS_2^+$ ions will be produced, which at these photon energies may be photodissociated by absorption of a single further photon to produce both CS + $S^+$ and $CS^+$ + S. Consequently, $CS^+$ ions formed from photodissociation of $CS_2^+$ ions would interfere with the detection of $CS^+$ ions from two-photon ionization of CS.

Given the above analysis, the observation of OCS formation at 15 and 20 K may be explained in terms of an oxygen atom reacting initially with $CS_2$ to form SO and CS. At 15 and 20 K, the CS radical may remain on the surface for long enough to react with a further O atom to form OCS. At surface temperatures of 25 K and above, the lifetime of the CS radical on the surface is too short for it to react further to form OCS and this channel is closed.

At surface temperatures greater than 20 K, it is clear that the general trend is one of increasing OCS yield with increasing surface temperature up to 60 K, before the yield decreases substantially at 70 K. This higher temperature data has been fitted with the kinetic model outlined above, the output of which can be seen overlaid on the experimental results in Figure 5.1. It is clear from Figure 1 that temperature dependence of the OCS yield is a direct consequence of the simultaneous occurrence of the Eley-

Rideal and Langmuir-Hinshelwood mechanisms; it is not possible to replicate the OCS yield as a function of temperature without involving both mechanisms. The reaction barriers ($E/R$) derived from this fitting procedure were 260 ± 5 K for the Langmuir-Hinshelwood mechanism and 250 ± 14 K for the Eley-Rideal mechanism. Clearly, these values result in excellent agreement between the model output and the experimental results.

| Reaction | $(E_a/R)$ / K | $A_{Rxn}$ / $10^{-15}$ $cm^2 molecule^{-1} s^{-1}$ | $(E_{Des,O}/R)$ / K | $(E_{Des,OCS}/R)$ / K | $k_{Rxn}$ / $cm^2 molecule^{-1} s^{-1}$ (at 20 K) |
|---|---|---|---|---|---|
| $CS_{2(ad)} + O_{(ad)}$ | 260 ± 5 | 5.5 ± 1.0 | 1504 ± 12 | 2430 ± 24 | 1.24E−20 |
| $CS_{2(ad)} + O_{(g)}$ | 250 ± 14 | | | | 2.05E−20 |

Table 5.1 Summary of the reaction barriers ($E_a$), reaction pre-exponentials ($A_{Rxn}$) and desorption energies ($E_{Des}$), estimated for the surface reactions of O atoms with $CS_2$. Rate constants for the reactions studied ($k_{rxn}$) have also been calculated for a surface temperature of 20 K.

As noted above, the fitting procedure also yields values for the desorption energies of O and OCS. The desorption energy for O is found to be 12.5 ± 0.1 kJ $mol^{-1}$ ($E_{Des}/R$ = 1504 K). This value is comparable with the O atom interaction energy at the bridge site of pyrene calculated by Bergeron *et al* (11.6 kJ $mol^{-1}$, $E_{Des}/R$ = 1395 K), and is in excellent agreement with the previous determinations of the O atom desorption energies in reactions with ethene and propene (see Chapter 3) (12.1 ± 0.6 kJ $mol^{-1}$, $E_{Des}/R$ = 1455 K).[21] It is important to note that beyond the initial stages of the experiments, reactants are deposited onto a layer of ice composed primarily of the co-reactant, in this case $CS_2$, which will have built up on the graphite surface. Therefore, caution should be exercised in comparing the current values directly with those for O atom physisorption on graphite. Nevertheless, the present results do suggest that O atom physisorption energies are comparable for both graphite and substrates consisting of non-polar molecular ices. The desorption energy for OCS was found to be 20.2 ± 0.2 kJ $mol^{-1}$ ($E_{Des}/R$ = 2430 K). This compares with a value measured by Burke & Brown ([22]) of 28.6 ± 1.3 kJ $mol^{-1}$ ($E_{Des}/R$ = 3440 K) for the desorption of OCS from bulk OCS ice (multilayer desorption). This comparison indicates that, as expected, the desorption energy of OCS from non-polar $CS_2$ ice is somewhat smaller than that from polar OCS ice.

## 5.6 Astrophysical Implications

In studies of the irradiation of mixed $H_2S$ and CO ices, both OCS and $CS_2$ have been observed as reaction products.[8,16] However, whilst OCS has been observed in icy

mantles of interstellar dust grains, $CS_2$ so far has not been detected in the interstellar medium. This non-detection of $CS_2$ may be due to difficulties in its spectroscopic identification, leaving open the possibility that $CS_2$ could account for some of the 'missing' sulfur in the interstellar medium.[8] However, for $CS_2$ to account for a significant proportion of the sulfur reservoir, which would explain the discrepancies between astrochemical models and observed elemental abundances, $CS_2$ ices must be relatively inert under the conditions of the interstellar medium. At the very least it seems clear that thermal reactions with abundant species such as H, O, C and N would inhibit the build up of any $CS_2$ reservoir. However, the experimental results presented here indicate that, rather than being inert under interstellar conditions, $CS_2$ ice does indeed react with thermal O atoms and is readily converted to OCS. The experimental results discussed in this chapter also show that this reaction occurs even at temperatures as low as 15 K. The fluence of O atoms in these experiments is approximately equivalent to the exposure to O atoms over the lifetime of a typical dense interstellar cloud ($10^5$ – $10^6$ years). Therefore, the implication of the present results for sulfur chemistry in the interstellar medium is to reveal that, whilst $CS_2$ may be formed together with OCS by energetic processing of sulfur, carbon and oxygen containing ices, any $CS_2$ is readily converted back to OCS by thermal processes.

The experimental results presented in this chapter therefore represent a means of reconciling experimental studies of the energetic processing of sulfur containing ices with astrophysical observations. Specifically, the non-detection of $CS_2$ in interstellar ices despite its abundant production in energetic processing experiments, can be explained by efficient thermal reactions of $CS_2$ with O atoms. If this argument is correct, the effective yield of OCS from energetic processing of sulfur bearing ices would be substantially larger than previously predicted. For example, in the experiments of Garozzo *et al* on the energetic processing of CO ices containing a small amount of $H_2S$, $CS_2$ is formed with an abundance approximately 4 to 6 times higher than that of OCS.[8] Consequently, thermal reactions of this $CS_2$ with oxygen atoms may be expected to enhance the abundance of OCS by a factor of approximately 5 over that which would be expected from energetic processing alone.

## 5.7 Summary

The experiments discussed in this chapter demonstrate for the first time that carbon disulfide ($CS_2$) can readily react with oxygen atoms (O) to form carbonyl sulphide

(OCS) on an HOPG surface under astrophysically relevant conditions. The reaction of $CS_2$ and O has been studied at surface temperatures in the range 15 – 70 K and OCS is observed to form *via* two distinct mechanisms. Furthermore, one of these mechanisms proceeds even at the lowest temperature investigated, 15 K. The discussion of the experimental results presented in this chapter also illustrates that the surface temperature dependence of the yield of OCS can be explained by invoking the simultaneous occurrence of the ER and LH mechanisms. Kinetic parameters for the calculation of rate constants for the reaction of $CS_2$ with O *via* both of these mechanisms have also been derived.

## 5.8 References


(1) Lodders, K. *Astrophysical Journal* **2003**, *591*, 1220.
(2) van Steenbergen, M. E.; Shull, J. M. *Astrophysical Journal* **1988**, *330*, 942.
(3) Sofia, U. J.; Cardelli, J. A.; Savage, B. D. *Astrophysical Journal* **1994**, *430*, 650.
(4) Herbst, E.; van Dishoeck, E. F. Complex Organic Interstellar Molecules. In *Annual Review of Astronomy and Astrophysics, Vol 47*, 2009; Vol. 47; pp 427.
(5) Garrod, R. T.; Wakelam, V.; Herbst, E. *Astronomy & Astrophysics* **2007**, *467*, 1103.
(6) Millar, T. J.; Herbst, E. *Astronomy and Astrophysics* **1990**, *231*, 466.
(7) Doty, S. D.; van Dishoeck, E. F.; van der Tak, F. F. S.; Boonman, A. M. S. *Astronomy & Astrophysics* **2002**, *389*, 446.
(8) Garozzo, M.; Fulvio, D.; Kanuchova, Z.; Palumbo, M. E.; Strazzulla, G. *Astronomy & Astrophysics* **2010**, *509*, 9.
(9) Boogert, A. C. A.; Schutte, W. A.; Helmich, F. P.; Tielens, A.; Wooden, D. H. *Astronomy and Astrophysics* **1997**, *317*, 929.
(10) Palumbo, M. E.; Geballe, T. R.; Tielens, A. *Astrophysical Journal* **1997**, *479*, 839.
(11) Palumbo, M. E.; Tielens, A.; Tokunaga, A. T. *Astrophysical Journal* **1995**, *449*, 674.
(12) Zasowski, G.; Kemper, F.; Watson, D. M.; Furlan, E.; Bohac, C. J.; Hull, C.; Green, J. D. *Astrophysical Journal* **2009**, *694*, 459.
(13) Geballe, T. R.; Baas, F.; Greenberg, J. M.; Schutte, W. *Astronomy & Astrophysics* **1985**, *146*, L6.
(14) Charnley, S. B. *Astrophysical Journal* **1997**, *481*, 396.
(15) Charnley, S. B.; Ehrenfreund, P.; Millar, T. J.; Boogert, A. C. A.; Markwick, A. J.; Butner, H. M.; Ruiterkamp, R.; Rodgers, S. D. *Monthly Notices of the Royal Astronomical Society* **2004**, *347*, 157.
(16) Ferrante, R. F.; Moore, M. H.; Spiliotis, M. M.; Hudson, R. L. *Astrophysical Journal* **2008**, *684*, 1210.
(17) Jimenez-Escobar, A.; Caro, G. M. M. *Astronomy & Astrophysics* **2011**, *536*, A91.
(18) Lias, S. G. Ionization Energy Evaluation. In *NIST Chemistry WebBook, NIST Standard Reference Database Number 69*; Linstrom, P. J., Mallard, W. G., Eds.; National Institute of Standards and Technology.
(19) Ward, M. D.; Price, S. D. *The Astrophysical Journal* **2011**, *741*, 121.
(20) Wagner, S.; Ostrom, H.; Kaebe, A.; Krenz, M.; Wolf, M.; Luntz, A. C.; Frischkorn, C. *New Journal of Physics* **2008**, *10*, 125031.
(21) Bergeron, H.; Rougeau, N.; Sidis, V.; Sizun, M.; Teillet-Billy, D.; Aguillon, F. *Journal of Physical Chemistry A* **2008**, *112*, 11921.
(22) Burke, D. J.; Brown, W. A. *Physical Chemistry Chemical Physics* **2010**, *12*, 5947.
(23) Collings, M. P.; Anderson, M. A.; Chen, R.; Dever, J. W.; Viti, S.; Williams, D. A.; McCoustra, M. R. S. *Monthly Notices of the Royal Astronomical Society* **2004**, *354*, 1133.
(24) Adriaens, D. A.; Goumans, T. P. M.; Catlow, C. R. A.; Brown, W. A. *Journal of Physical Chemistry C* **2010**, *114*, 1892.

# Chapter 6 – Reactions of Carbon Disulfide and Sulfur Dioxide with Deuterium Atoms

## 6.1 Introduction

As discussed in Chapter 5, the chemistry of sulfur in the interstellar medium has so far received little attention in relation to other light elements such as hydrogen, carbon, nitrogen and oxygen. This neglect of interstellar sulfur chemistry perhaps reflects its low elemental abundance compared with H, C, N and O. However, the discrepancy between the estimated elemental abundance of sulfur relative to hydrogen ($1 \times 10^{-5}$)[1-3] and that implied by the observed abundances of gas phase sulfur species ($10^{-7} – 10^{-9}$)[4-6] suggests that much of the sulfur in the interstellar medium may be in the form of molecules frozen out onto dust grain surfaces, hinting at a rich solid state sulfur chemistry in interstellar dust clouds. Indeed, van der Tak *et al* state that approximately 90 % of the interstellar sulfur must be in an as yet undetected solid form, assuming all gas phase sulfur species have been detected.[7] To date only sulfur dioxide ($SO_2$) and carbonyl sulfide (OCS) have been definitively identified in interstellar ices.[8] The presence of hydrogen sulphide ($H_2S$) in interstellar ices is also suspected,[9] however, its main infrared band overlaps with a weak IR feature of methanol.[8,10] Furthermore, a very simplistic estimate of the $H_2S$ ice abundance relative to $H_2O$ ice would be 3 % based on the cosmic S:O ratio,[11] thus combined with the weak band strength of $H_2S$, this low abundance is likely to mean that any $H_2S$ bands are below the detection limit of most observations.[11] Whilst carbon disulfide has not yet been detected in interstellar ices, it has been observed to form following irradiation of mixed CO/$H_2S$ ices by energetic (200 – 800 keV) protons.[8,12] Furthermore, Garozzo *et al* suggest that carbon disulfide, along with solid sulfur, may account for part of the undetected interstellar sulfur.[8] Indeed, recent investigations of the ultraviolet processing of mixed $H_2O/H_2S$ ices demonstrated the formation of refractory sulfur polymers up to $S_8$.[11]

In view of the suggestion that solid $CS_2$ may account for some of the undetected sulfur in the interstellar medium, the experiments discussed in Chapter 5 were carried out to investigate the reaction of $CS_2$ with thermal oxygen atoms. In these experiments it was found that $CS_2$ readily reacts with oxygen atoms to produce OCS at interstellar temperatures, suggesting that $CS_2$ is too reactive to build up in interstellar ices in

significant quantities. Consequently, it appears unlikely that $CS_2$ could account for a significant proportion of the sulfur residing in icy mantles in the interstellar medium. This conclusion would be further supported if $CS_2$ showed significant reactivity toward hydrogen atoms.

Reactions of $CS_2$ ice with hydrogen atoms at astrophysical temperatures have been observed previously by Bohn and co-workers.[13] In this previous study $CS_2$ contained in a solid Ar matrix at 12 K was dosed with H atoms and the products detected by infra-red spectroscopy. However, the primary focus of this previous study was to investigate the structure of the HSCS radical. Consequently, whilst the authors comment that the activation energy for forming HSCS must be very low, they do not derive any kinetic data for the reaction. The previous study of the reactions of $CS_2$ with oxygen atoms, discussed in Chapter 5, has therefore been extended to investigate the reactions of D atoms with $CS_2$. Additionally, the results of experiments carried out to investigate the surface reactions of the $SO_2$ with D atoms are presented and discussed in this chapter.

In the present experiments deuterium atoms are used in place of hydrogen atoms in order to provide the maximum possible mass separation between the reactant and any possible products. In the reaction of $CS_2$ with D atoms, the formation of $D_2S$, as well as deuterated isotopomers of organic species bearing the thiol (-SD) functional group, is observed. Following the $SO_2$ + D reaction, the formation of $D_2S$ is again observed in addition to $D_2O_2$. Estimates of the rate constants for these reactions are obtained by fitting the experimental results with a simple kinetic model.

## 6.2 Experimental

The experimental apparatus used in the experiments discussed in this chapter has been described in detail in Chapter 2 and so only the key features are presented here. Either $CS_2$ or $SO_2$ have been co-deposited with deuterium atoms onto a highly oriented pyrolitic graphite (HOPG) substrate at fixed surface temperatures between 15 and 60 K. Dosing of $CS_2$ or $SO_2$ was stopped after 60 minutes and the surface was allowed to cool briefly to 15 K. Any products formed are then thermally desorbed by heating the HOPG to approximately 300 K. Consecutive 1 s duration mass spectra are recorded during this heating of the surface, as described in Chapter 2. The experimental data are therefore in the form of a two dimensional histogram of ion yield as a function of both mass to

charge ratio, *m*/*z*, and surface temperature, *T*, during heating, as described in Section 2.9.

The source of $CS_2$ molecules was the vapour above a liquid sample of $CS_2$ (99.9 %) held at 0 $^{o}$C which had initially been pumped on to remove any volatile impurities. The $SO_2$ used in the present experiments was taken from a commercial sample of 99.9 % purity and used without further purification. The flux of the $CS_2$ or $SO_2$ used in these experiments was $9.6 \times 10^{14}$ cm$^{-2}$ s$^{-1}$, whilst the flux of D atoms was approximately $1.9 \times 10^{14}$ cm$^{-2}$ s$^{-1}$.

Separate experiments were also carried out in which $CS_2$ and $SO_2$ were co-deposited with pure $D_2$ to confirm that neither of these molecules react with residual $D_2$ from the D atom source. Additionally experiments were conducted in which D atoms were dosed onto the bare HOPG surface at 15 K to verify that the species identified as reaction products do not in fact arise from contaminants in the microwave discharge. Both of these experiments demonstrate that the observed products do indeed arise from the reaction of $CS_2$ or $SO_2$ with D atoms.

## 6.3 Results

### 6.3.1 $CS_2$

Following the reaction of $CS_2$ with D atoms, signals are observed in the TPD spectra for ions with mass to charge (*m*/*z*) ratios of 36, 52 and 84. Given the available elements, C, S and D, the corresponding products with masses of 36 and 52 can be unambiguously identified as deuterium sulfide ($D_2S$) and deuterated methanethiol ($CD_3SD$) respectively. The observation of a *m*/*z* = 84 ion is consistent with a product arising from the addition of four deuterium atoms to $CS_2$; a finding supported by complementary experiments using H atoms, in which the ion peak for this product shifted to *m*/*z* = 80. Given the 4 % natural abundance of $^{34}S$, the stoichiometry $CD_4S_2$ would be expected to give rise to a peak at *m*/*z* = 86, with an intensity of approximately 8 % of that at *m*/*z* = 84, corresponding to the $CD_4{}^{32}S^{34}S$ isotopomer. Indeed, such a peak at *m*/*z* = 86 is observed, providing further evidence that the product with a mass of 84 results from the addition of four D atoms to $CS_2$. Two species are consistent with the empirical formula $CD_4S_2$: deuterated methanedithiol, $CD_2(SD)_2$, and deuterated methyl persulfide, $CD_3SSD$. In our ~200 eV electron ionization mass spectrum of this product, two strong

peaks of approximately equal intensity are observed at $m/z$ = 84 ($CD_4S_2^+$) and $m/z$ = 50 (loss of SD), along with weaker peaks at $m/z$ = 48 ($D_2CS^+$), $m/z$ = 46 ($DCS^+$) and $m/z$ = 34 ($SD^+$). Unfortunately, no reference mass spectrum appears to be available in the literature for methanedithiol. However, it is clear that such a fragmentation pattern is inconsistent with that observed for methyl persulfide using 70 eV electrons, in which the parent ion peak is approximately 10 % of that of the largest peak (at $m/z$ = 46 for $H_2CS^+$).[14] Of course, care should be taken in directly comparing the current spectra with this reference spectrum due to the differing ionizing electron energies used. Nevertheless, such a large difference in relative fragment ion yields as the ionizing electron energy increases from 70 eV to 200 eV would be very unusual.[15-17] It is therefore reasonable to conclude that the mass spectra observed for the $CD_4S_2$ product do not support its identification as methyl persulfide. Hence, the $CD_4S_2$ product is identified as being methanedithiol. This assignment, based upon the mass spectra, is further supported by the fact that methanedithiol can simply be produced by sequential addition of H atoms to $CS_2$, whereas methyl persulfide would require substantial rearrangement of the molecule, a process disfavoured at the low temperatures of the present experiments.

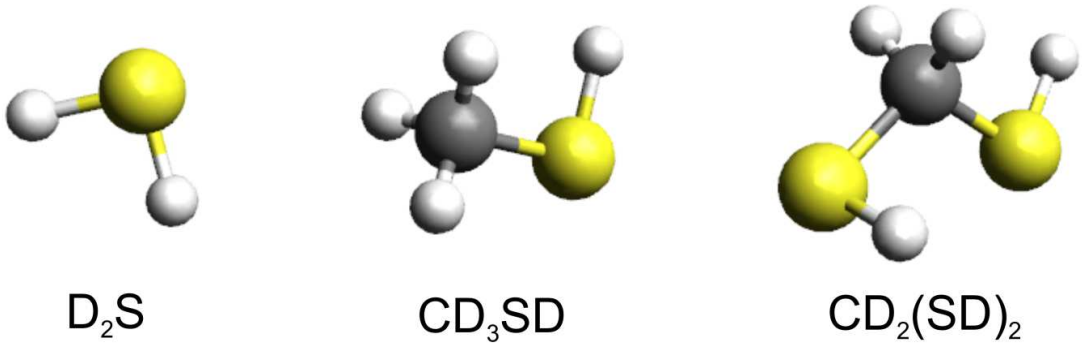


Figure 6.1 The primary products of the surface reaction of $CS_2$ with D atoms.

A very small desorption peak at $m/z$ = 100 was also observed following the reaction of $CS_2$ with D atoms. In complementary experiments with H atoms, this desorption peak shifted to $m/z$ = 94, indicating the presence of six H or D atoms in the molecule. These masses are consistent with the stoichiometry $C_2H_6S_2$. There are several conceivable species with this stoichiometry, including 1,1-ethanedithiol ($CH_3CH(SH)_2$), 1,2-ethanedithiol ($CH_2(SH)CH_2(SH)$), dimethyl disulfide ($CH_3SSCH_3$) and methyldithiomethane ($CH_3SCH_2(SH)$). Unfortunately the very low yield of this product

made its definitive identification difficult and precluded any statistically meaningful kinetic analysis.

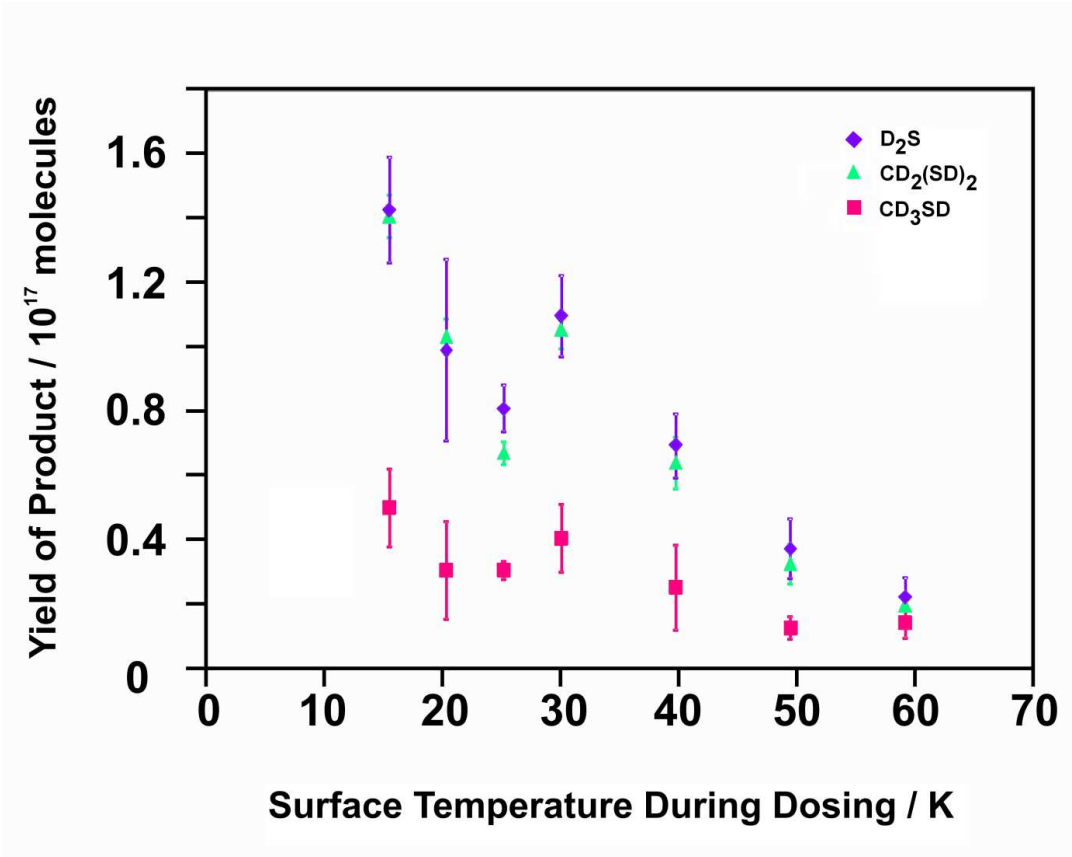


Figure 6.2 The temperature dependences of the yields of $D_2S$, $CD_2(SD_2)$ and $CD_3SD$ from the surface reaction of $CS_2$ with D atoms.

The temperature dependence of the yields of $D_2S$, $CD_3SD$ and $CD_2(SD)_2$ are shown in Figure 6.2. As can be seen from Figure 6.2, the temperature dependences of all three species follow a similar trend. Overall, there is clearly a strong inverse relationship between the yield of product and the surface temperature during the dosing of the reactants. However, the yields of all three species increase as the surface temperature is increased from 25 to 30 K.

### 6.3.2 $SO_2$

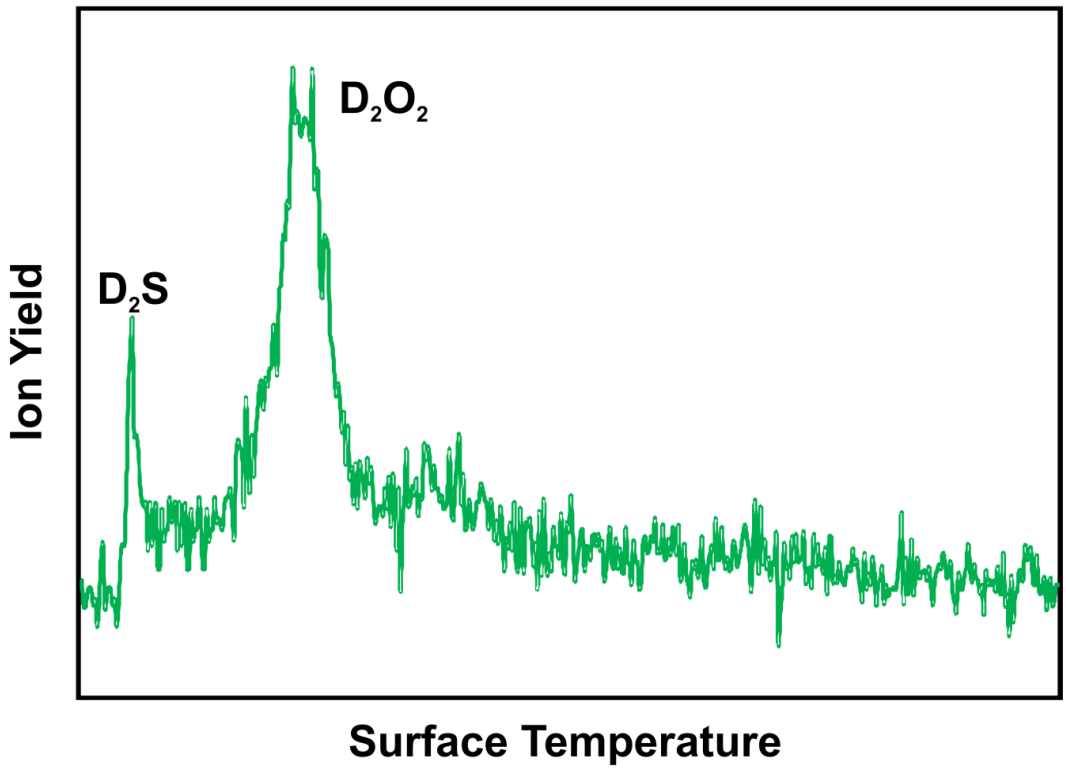


Figure 6.3 A typical TPD spectrum at *m*/*z* = 36. This TPD spectrum was taken following the co-deposition of $SO_2$ and D atoms at 15 K for 60 minutes.

As shown in Figure 6.3, two desorption peaks at *m*/*z* = 36 are observed at different temperatures in the TPD experiments following the co-deposition of $SO_2$ molecules and D atoms. The low temperature desorption peak occurs at the same surface temperature as the *m*/*z* = 36 peak observed in the $CS_2$ + D experiments discussed above. Thus, this low temperature *m*/*z* = 36 peak is clearly attributable to the desorption of deuterium sulfide, $D_2S$. The high temperature *m*/*z* = 36 desorption peak occurs at a temperature similar to the desorption temperature of water. Hence, one possibility is that this high temperature peak is due to $D_2S$ becoming trapped in background $D_2O$ ice on the surface and then co-desorbing with this $D_2O$. To test whether $D_2S$ could become trapped in $D_2O$ ice in the presence of $SO_2$, separate experiments were carried out in which $H_2S$ and $SO_2$ were co-deposited onto the surface at 15 K, along with background water. However, in these experiments, only a single desorption peak for $H_2S$ is observed, indicating that $H_2S$ is not readily trapped in water ice in the presence of $SO_2$. Instead, the high temperature *m*/*z* = 36 peak in the TPD spectra is attributed to the desorption of $D_2O_2$. If $D_2O_2$ is indeed formed in the reaction of $SO_2$ and D atoms, one may also expect to observe the formation of $D_2O$. However, given that there is always some background

$D_2O$ formed in the D atom source, the definitive identification of $D_2O$ arising from the reaction is difficult. Nevertheless, the yield of $D_2O$ desorbing from the surface following the reaction of D atoms with $SO_2$ is substantially larger than that observed following the $CS_2$ + D reaction. Thus, given that no adjustment was made to the D atom source between the $CS_2$ + D experiments and the $SO_2$ + D experiments, the enhanced yield of $D_2O$ in the latter experiments suggests that $D_2O$ is indeed formed in the reaction of $SO_2$ with D atoms.

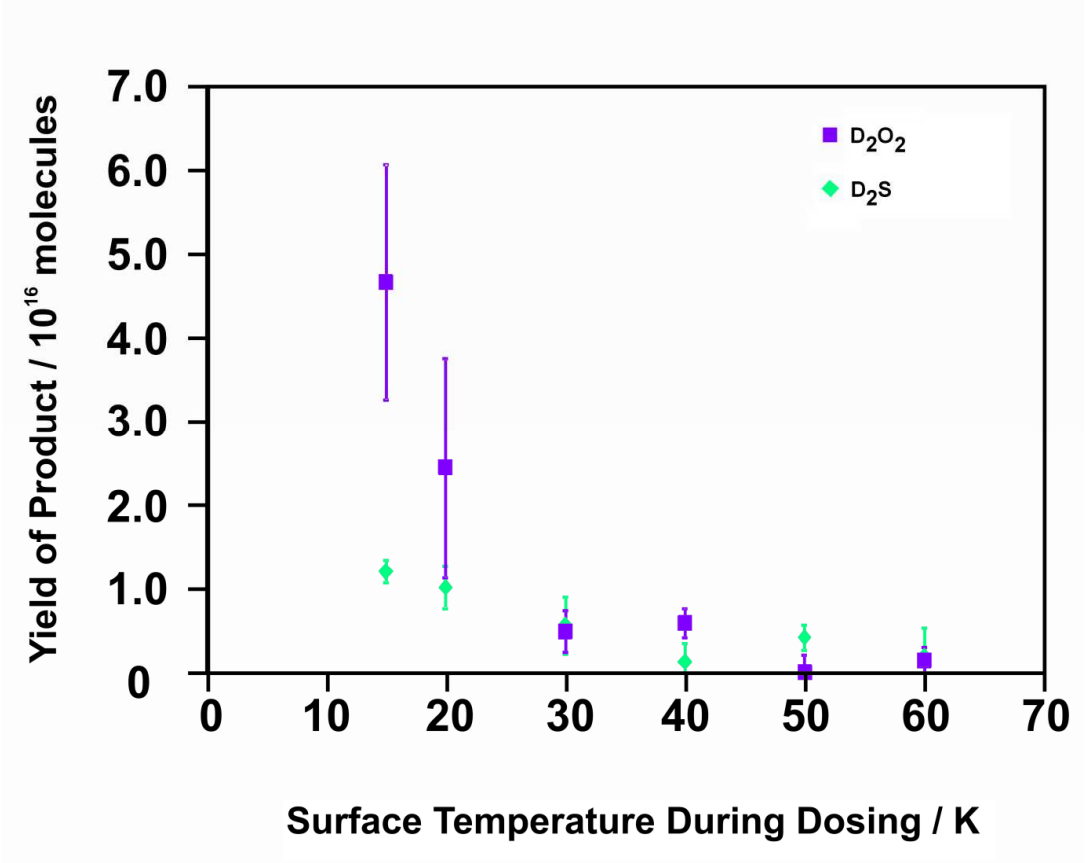


Figure 6.4 The temperature dependences of the yields of $D_2O_2$ and $D_2S$ from the surface reaction of $SO_2$ with D atoms.

As was the case for the product yields from the reaction of $CS_2$ with D atoms, the yields of both $D_2S$ and $D_2O_2$ decrease with increasing surface temperature between 15 and 60 K. This decrease in the product yield with increasing temperature appears to be stronger in the case of $D_2O_2$ formation than for $D_2S$ formation. It is also interesting to note that, in contrast to the experimental results for the $CS_2$ reaction, there is no enhancement in the yield of either $D_2S$ or $D_2O_2$ at 30 K. The temperature dependences of the yields of both $D_2S$ and $D_2O_2$ from the surface reaction of $SO_2$ with thermal D atoms are shown in Figure 6.4.

## 6.4 Data Analysis

As described in detail in Section 2.11, and in Chapters 3 – 5, the kinetic model used to derive kinetic parameters from the experimental data considers two limiting mechanisms for a surface reaction. These two mechanisms are an ER mechanism, in which a gas phase species reacts directly with an adsorbed species, and an LH mechanism, in which two adsorbed species react. Provided that the relative importance of the ER and LH mechanisms in contributing to the product yield at a specific temperature is known, the rate constants, $k_{ER}$ and $k_{LH}$, can be adjusted until the product yield predicted by the model agrees with that observed experimentally. At temperatures above the desorption temperature of D atoms it is clear that only the ER mechanism will contribute to the product yield. If it is assumed that the desorption temperature of D atoms from $CS_2$ and $SO_2$ ice is approximately similar to that for NO ice, (~3.6 kJ mol$^{-1}$, determined in Chapter 4), or for graphite (3.4 kJ mol$^{-1}$ [18]), the D atom half-life on the surface would decrease from a few seconds at 15 K to a few milliseconds at 20 K. Thus, it is clear that the LH mechanism would only have the potential to contribute significantly to the product yield at 15 K. Of course, it must be emphasized that the desorption energy of D atoms from molecular ices of $CS_2$ or $SO_2$ may be different to that determined for NO ice in Chapter 4 or to that determined for graphite by Ghio *et al.*[18] Nevertheless, previous experimental determinations of the desorption energy of oxygen atoms on molecular ices of $C_2H_4$, $C_3H_6$ and $CS_2$ (see Chapters 3 and 5) suggest that the physisorption energy of an atomic species on an ice composed of small molecules is broadly independent of the constituents of that ice. Additionally, these desorption energies for molecular ice surfaces have previously been found to be similar to those for graphite. Therefore, the assumption that the D atom desorption energy for ices composed of $CS_2$ or $SO_2$ molecules is similar to that for ice composed of NO molecules, or for graphite, is reasonable. Having established, then, that the contribution from the LH mechanism at surface temperatures of 20 K and above is likely to be negligible, the contribution from the LH mechanism at 15 K must be considered. From the temperature dependences shown in Figure 6.2 and in Figure 6.4, it is clear that there is no enhancement above the general trends at 15 K in any of the product yields. Thus, it can be concluded that there is also no significant contribution from the LH mechanism at 15 K. Consequently, in modelling the experimental results, only the ER mechanism involving D atoms as the gas phase species, is considered.

As discussed previously, hydrogen and deuterium atoms can penetrate into molecular ices and react with molecules beneath the surface layer. The penetration depth of D atoms into the ice must therefore be estimated in order to derive estimates of the rate constants. No previous determinations of the penetration depth of D atoms into either $CS_2$ or $SO_2$ ice appear to have been reported in the literature. Therefore, as described in detail in Chapter 4, the penetration depth measured by Fuchs *et al* for H atoms on CO ice (4 monolayers) has been taken as an approximate estimate.[19]

In order to obtain estimates for the rate constant of the reaction at a specific temperature the experimental results are placed on an absolute scale as described in Section 2.10. In principle, this normalization procedure must include a correction for the different partial ionization cross sections (PICS) for forming the reactant parent ion and the product parent ions by electron ionization. Previous experimental determinations of the PICSs of hydrogenated and deuterated isotopomers of ammonia and water indicate that they do not, in general, exhibit a significant isotope effect.[20,21] The PICSs for $H_2S$ are therefore used to perform the correction to the $D_2S$ yield. However, whilst these PICSs are available in the literature for $SO_2$, $CS_2$ and $H_2S$,[22,23] there have been no measurements to date of the those for $CH_3SH$, $CH_2(SH)_2$ or $H_2O_2$. Thus, for the former two molecules it is assumed that the PICSs are the same as for $CS_2$, whilst for $D_2O_2$ it is assumed that the PICS is the same as for $SO_2$.

## 6.5 Discussion

### 6.5.1 $CS_2$

As can be seen in Figure 6.2, the overall trend in product yield, following the reaction of $CS_2$ molecules with D atoms, is one of decreasing product yield with increasing surface temperature. However, in contrast to this general trend, the product yields at 30 K are all greater than those at 25 K. There are two possible interpretations of the temperature dependences shown in Figure 6.2. For example, they may be interpreted in terms of an underlying decreasing trend with the product yields at 30 and 40 K being enhanced in comparison to this trend by some other process. An alternative interpretation is that there is a change in mechanism between 25 and 30 K and that consequently the data points at 30 K and above follow a separate trend to those between 15 and 25 K. An obvious way of establishing which of the above interpretations is correct is to estimate the rate constants, $k_{ER}$, for forming each product, at each surface temperature

investigated, and to produce an Arrhenius plot of ln($k_{ER}$) against 1/$T$ for the formation of that product. If the interpretation that the data points at 30 and 40 K are enhanced above an underlying trend is correct, such an Arrhenius plot would be expected to show a single linear relationship between ln($k_{ER}$) and 1/$T$, with only the values of ln($k_{ER}$) corresponding to the rate constants at 30 and 40 K deviating from this trend. Alternatively, if the experimental data in fact follow separate trends above and below 30 K, one would expect to see two separate linear relationships in the Arrhenius plot. Estimates of $k_{ER}$ are obtained by adjusting the value of $k_{ER}$ in the model until predicted yield agrees with that determined experimentally. This procedure provides estimates of $k_{ER}$ for each product, at each surface temperature investigated experimentally. These values of $k_{ER}$, along with their associated uncertainties, are presented in Table 6.1. Figure 6.5 shows a typical Arrhenius plot of ln($k_{ER}$) against 100/$T$ for $D_2S$ formation. It is clear from this Arrhenius plot that there are two separate linear trends, highlighted by the different colours in Figure 6.5, indicating that there is a change in reaction mechanism, and hence reaction barrier, as the surface temperature is increased from 25 to 30 K. A similar change in mechanism is also observed in similar Arrhenius plots for $CD_3SD$ and $CD_2(SD)_2$. The physical origin of this change in reaction mechanism is ambiguous, but some possible explanations will be discussed below.

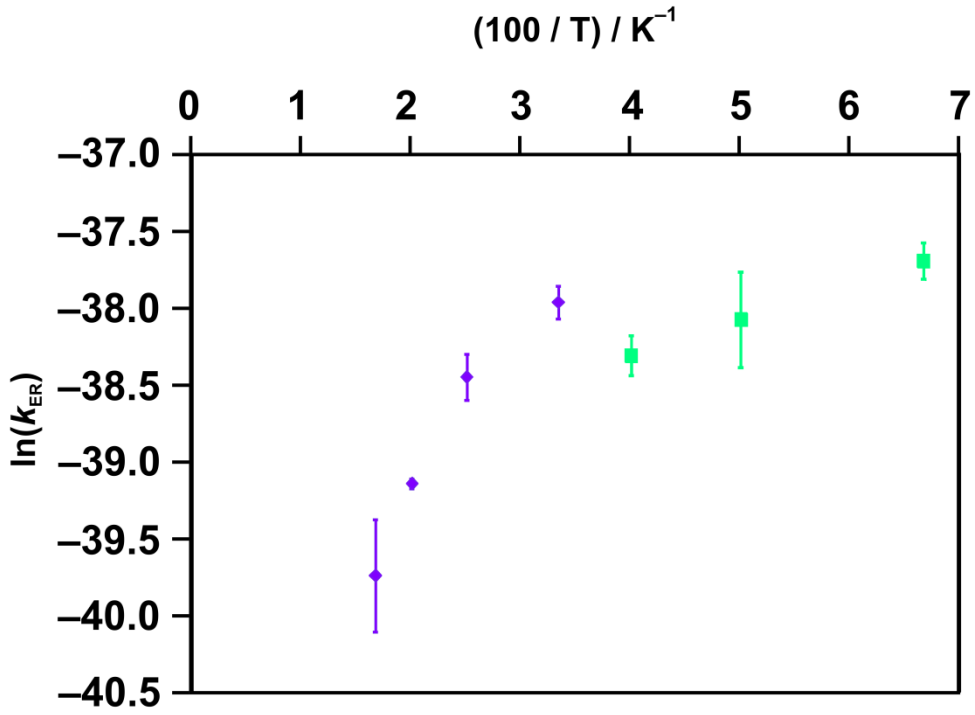


Figure 6.5 Arrhenius plot of ln($k_{ER}$) against 100/$T$ for the formation of $D_2S$ from the surface reaction of $CS_2$ with D atoms. The data points corresponding to temperatures below 30 K are shown in green whilst those corresponding to temperatures of 30 K and above are shown in purple.

Estimates of the activation energy for each reaction pathway, forming $D_2S$, $CD_3SD$ and $CD_2(SD)_2$, can also be obtained from the respective Arrhenius plots of $\ln(k_{ER})$ against $100/T$. Due to the apparent change in mechanism above 30 K, two estimates of the activation energy for each product forming channel are obtained: one for the reaction at 15 – 25 K and one for the reaction at 30 K and above. At surface temperatures below 30 K, all three product forming channels have apparent activation energies ($E/R$) in the range −22 to −29 K. At 30 K and above, the activation energies for forming each product lie in the range −89 to −113 K. This finding, that the activation energies for forming $D_2S$, $CD_3SD$ and $CD_2(SD)_2$ both above and below 30 K are very similar, strongly indicates that the mechanisms for the formation of all three of these species share the same rate determining step. This rate determining step must therefore be the initial addition of a hydrogen atom to the $CS_2$ molecule to form the radical with the stoichiometry $HCS_2$ since this is the only step which all three product forming channels can share in common.

| T/K | $k_{ER}$ / $10^{-18}$ cm$^2$ molecule$^{-1}$ s$^{-1}$ | | |
|---|---|---|---|
| | $D_2S$ | $CD_2(SD)_2$ | $CD_3SD$ |
| 15 | 43 ± 5 | 42 ± 2 | 14 ± 4 |
| 20 | 29 ± 9 | 3 ± 2 | 8 ± 4 |
| 25 | 23 ± 3 | 19 ± 1 | 8 ± 1 |
| 30 | 33 ± 4 | 30 ± 2 | 11 ± 3 |
| 40 | 20 ± 3 | 18 ± 2 | 7 ± 4 |
| 50 | 10 ± 1 | 8 ± 2 | 3 ± 1 |
| 60 | 6 ± 2 | 45 ± 2 | 3 ± 2 |

Table 6.1 The values of $k_{ER}$ for the formation of $D_2S$, $CD_2(SD)_2$ and $CD_3SD$ from the surface reaction of $CS_2$ with D atoms.

Despite the formation of $CD_3SD$ and $CD_2(SD)_2$, no unsaturated intermediates, such as the thioformaldehyde and dithioformic acid isotopomers, $D_2CS$ and DCSSD, are observed in the current experiments. It is clear therefore that, under the present experimental conditions, the rates of deuteration of $D_2CS$ and DCSSD are faster than the rate of deuteration of $CS_2$, providing further support for the argument that the rate limiting step in the formation of $D_2S$, $CD_3SD$ and $CD_2(SD)_2$ is the elementary D + $CS_2$ reaction. The non-observation of DCSSD is nevertheless somewhat surprising given that this species was observed to form from the thermal reaction of D + $CS_2$ at 12 K by Bohn *et al*.[13] Furthermore Bohn *et al* do not report the formation of either $CD_3SD$ or $CD_2(SD)_2$. However, these discrepancies between the Bohn *et al* study and the present

experiments can simply be attributed to the different concentrations of reactants used. In the Bohn *et al* experiments, both reactants were typically diluted by a factor of 100 in an argon matrix. In contrast, the reactants are not diluted in the present experiments. Clearly then, the probability of reactive collisions in the earlier study would have been greatly reduced compared to those in the present experiments, thus limiting the products in the previous study to those containing only one or two hydrogen atoms.

Inverse temperature dependences have been observed for some surface reactions of H atoms with molecular ices by Hiraoka and co-workers.[24-27] In particular, the yields of products from the reactions of H atoms with CO, $C_2H_2$, $C_2H_4$, $C_3H_6$ and $SiH_4$ have been observed to increase with decreasing surface temperature. The experiments discussed here confirm that such behaviour also extends to reactions of deuterium atoms.

For low temperature surface reactions (below 20 K), the most commonly proposed explanation for an increasing product yield with decreasing temperature is the reduced sticking probability of H atoms at higher temperatures.[24] However, this explanation may be discounted as an explanation for the present results for several reasons. Firstly, the binding energy of a physisorbed D atom on a graphite surface is approximately 3.4 kJ $mol^{-1}$ and appears to be similar for physisorption on molecular ices (see Chapter 4).[18] Consequently the half life of D atoms on the surface drops from a few seconds at 15 K to a few milliseconds at 20 K and to a few microseconds at 30 K. Therefore, above 20 K, deuterium atoms can react with the molecular ice solely *via* an ER mechanism. In this case then, where the only available reaction is that between gas phase D atoms and adsorbed sulfur bearing species, the sticking probability should have no effect on the reaction rate. Despite this restriction of any effect of the D atom sticking probability to low temperatures, the present experimental results demonstrate that the negative temperature dependence continues up to 60 K.

Hiraoka *et al* propose an alternative explanation for the product yield decreasing with increasing surface temperature. These authors argue that the quasi-continuous set of vibrational energy levels arising from the many adsorbate-surface bonds acts as an energy sink promoting the exothermic forward reaction.[28] Furthermore, they suggest that the suppression of thermal fluctuations results in the ability of these adsorbate-surface bonds to act as an energy sink being enhanced at low temperatures. The nature of the thermal fluctuations they consider is not clear. However, one possibility is that at higher temperatures, adsorbates surrounding a reactive site are in more excited

vibrational states and so are able to remove less of the energy released by the reaction. Logically this line of reasoning should apply to any exothermic reaction, including those involving oxygen atoms instead of H or D atoms. However, only positive temperature dependences are observed in the reactions of O atoms with $C_2H_4$, $C_3H_6$ and $CS_2$, (see Chapters 3 and 5). Nevertheless the presence of non-zero reaction barriers, and the low probability of tunnelling through them in the case of heavier atoms such as oxygen, may mask this effect and so these previous observations for O atom reactions do not disprove the explanation proposed by Hiraoka *et al*.

A simpler explanation of the negative temperature dependences of the product yields is that discussed in Chapter 4. In this explanation, an apparent negative temperature dependence arises from the existence of reaction pathways, which compete with the product forming reaction. For example, if a reaction pathway forming a given product has a smaller positive reaction barrier than a pathway which consumes that product, the apparent yield of the product would decrease with increasing temperature. Unfortunately, without knowledge of the radicals and intermediates formed in the ice during the reaction, it is not possible to determine conclusively what these competing reaction pathways might be in the present reaction. Nevertheless an obvious explanation is that at higher temperatures, the sulfur-bearing radical intermediates may become more mobile on the surface and polymerize. The polymerization products would not be expected to be observed in the TPD spectra since they are likely to have very high desorption temperatures. Indeed, a yellow-white residue was observed on the HOPG surface during routine maintenance of the experimental apparatus following the experiments discussed in this chapter. This residue may well be composed of such sulfur bearing polymers. However, further experiments would be required in order to determine which reactions produced this residue and to determine its composition.

The origin of the apparent enhancement in product yield at and above 30 K is also unclear. One possibility is that the $CS_2$ molecules within the ice are more mobile at higher temperatures and so pathways for D atoms to penetrate further into the bulk ice can open up. An alternative explanation may be that at higher temperatures D atoms have sufficient energy to ‘hop’ between $CS_2$ molecules, resulting in deuterated radical intermediates buried in the bulk ice being able to effectively migrate to the surface layers of the ice where they can then undergo further deuteration.

In the current experiments, the formation of $CD_3SD$ and $CD_2(SD)_2$ most likely proceeds *via* $D_2CS$ and DCSSD intermediates respectively. Thus, it is clear that the reactivity of these intermediates, is markedly different to that observed for the oxygenated analogues formaldehyde, $H_2CO$, and formic acid, HCOOH. Specifically, formaldehyde has been observed to form in the reaction of CO ice with H atoms, with a yield of more than 50 % at 15 K relative to that of methanol, $CH_3OH$.[19] In the same experiments the barrier (*E*/*R*) to the addition of a hydrogen atom to $H_2CO$ is estimated to be approximately 470 K. In contrast, HCOOH does not appear to react with H atoms at any appreciable rate under interstellar conditions.[29] Such comparisons suggest that sulfur-containing organic molecules have a distinctly enhanced thermal reactivity over their oxygen containing analogues and so the potential for the existence of a very broad range of sulfur bearing species in interstellar ices is clear.

### 6.5.2 $SO_2$

The yields of the $D_2S$ and $D_2O_2$ products following the reaction of $SO_2$ with D atoms are largely independent of temperature at temperatures of 30 K and above. At low temperatures, however, there is a marked enhancement in the yield of $D_2O_2$ and a milder enhancement in the yield of $D_2S$. The yield of $D_2S$ obtained from the reactions of D atoms with $SO_2$ is substantially lower than that from the reaction with $CS_2$; the $D_2S$ yield from the $SO_2$ reaction is less than 13 % of that from the $CS_2$ reaction at all of the temperatures investigated experimentally.

| T/K | $k_{ER}$ / $10^{-19}$ cm$^2$ molecule$^{-1}$ s$^{-1}$ | |
|---|---|---|
| | $D_2S$ | $D_2O_2$ |
| 15 | 9 ± 1 | 34 ± 10 |
| 20 | 7 ± 2 | 18 ± 9 |
| 30 | 4 ± 3 | 4 ± 2 |
| 40 | 1 ± 2 | 4 ± 2 |
| 50 | 3 ± 1 | 0 ± 2 |
| 60 | 2 ± 3 | 1 ± 1 |

Table 6.2 The values of $k_{ER}$ for the formation of $D_2S$ and $D_2O_2$ from the surface reaction of $SO_2$ with D atoms.

The observation that the product yields are broadly independent of temperature in the range 30 – 60 K whilst they are enhanced at 15 – 20 K, could, in principle, be explained by a barrierless ER reaction involving gas phase D atoms reacting with adsorbed $SO_2$ molecules combined with a barrierless LH mechanism operating at the lowest

temperatures investigated. However, attempting to fit the experimental data by using such a reaction scheme in the kinetic model indicates that a rather large and unrealistic barrier to D atom desorption of approximately 5 kJ $mol^{-1}$ would be required. Additionally, in order to fit the experimental data with this model, different pre-exponential factors for the LH and ER mechanism would be required. It therefore seems unlikely that the interpretation of barrierless ER and LH mechanisms occurring simultaneously is correct. Indeed, when the experimental data points are fitted individually with only an ER mechanism, Arrhenius plots of $\ln(k_{ER})$ against $100/T$ are approximately linear, as would be expected if the reaction were following the same pathway. The apparent reaction barriers derived from these plots are approximately −30 ± 20K for $D_2S$ and −55 ± 10 K for $D_2O_2$, indicating that the formation mechanisms of both products share the same rate limiting step. The rate constants determined at each temperature for the formation of $D_2O_2$ and $D_2S$ are shown in Table 6.2.

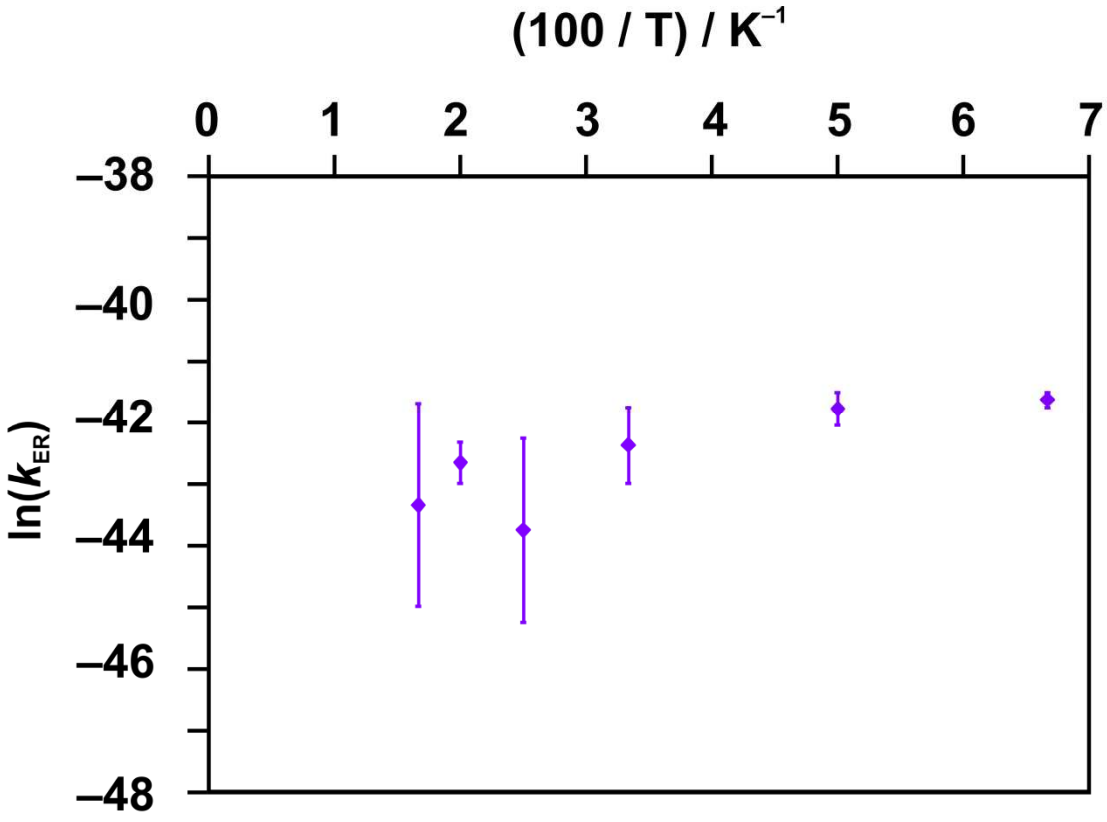


Figure 6.6 Arrhenius plot of $\ln(k_{ER})$ against $100/T$ for the formation of $D_2S$ from the surface reaction of $SO_2$ with D atoms.

Again the most likely explanation of the inverse temperature dependence of the yields of $D_2S$ and $D_2O_2$ is a competing reaction which is more efficient at high temperatures. Specifically, in the case of $D_2O_2$, $H_2O_2$ is known to react with H atoms to produce water

with this reaction having a positive activation energy.[30] Therefore the inverse temperature dependence of the yield of $D_2O_2$ may be a consequence of the reaction of this $D_2O_2$ with D atoms, producing $D_2O$, becoming increasingly efficient at higher temperatures. However, it is less clear whether there is a similar competing reaction in the case of $D_2S$. One possibility is that reactions of $D_2S$ with D atoms ultimately cause polymerization reactions, producing refractory solid sulfur which, of course, would not be detected in the current experiments. Some evidence to support such a polymerization reaction again comes from the fact that, as discussed above, a small amount of yellow-white residue was observed on the HOPG substrate following experiments on sulfur bearing species. Clearly, it is possible that this residue is composed of sulfur polymers formed from reactions of H and O atoms with sulfur bearing species. Again, further experiments would be required in order to confirm the origin of this residue.

## 6.6 Astrophysical Implications

The experimental results discussed in this chapter clearly indicate that both $CS_2$ and $SO_2$ present in interstellar ices can readily be converted to hydrogen sulfide. Additionally the reaction products of $CS_2$ and hydrogen atoms include a variety of organic thiols. The rate constants of the reactions of $CS_2$ and $SO_2$ with hydrogen atoms appear to increase at lower temperatures, with the product yields reaching a maximum at the lowest temperature investigated, 15 K. Therefore given that the total fluence of hydrogen or deuterium atoms in these experiments is similar to that expected over the lifetime of a typical dense interstellar cloud, it appears that $CS_2$ and $SO_2$ could be expected to react with hydrogen atoms quite readily in the interstellar medium. Indeed, in these laboratory experiments, it appears that, at 15 K, nearly 100% of the D atoms react.

When considered together with the results of the study presented in Chapter 5, on the reaction of oxygen atoms with $CS_2$, it seems clear that $CS_2$ itself is rather too reactive to represent a significant proportion of the 'missing' sulfur in the interstellar medium. However, given that the reaction of H atoms with $CS_2$ produces organic sulfur bearing species, it may be that these species can account in part for the under-abundance of sulfur bearing molecules in the gas phase. It therefore seems reasonable to suggest that whilst $CS_2$ may not itself be present in significant quantities in interstellar ices, it may be an important intermediate in the formation of complex sulfur bearing organics which

could then partially account for the under-abundance of sulfur bearing molecules in the gas phase.

As explained in detail by Garozzo *et al*, there are spectroscopic reasons which may explain why $CS_2$ has not so far been detected in interstellar ices.[8] Briefly, the main band of $CS_2$ at approximately 6.60 μm overlaps with other well known spectral features at 6.00 and 6.85 μm. However, given the experimental results described here, the presence of $CS_2$ in interstellar ices could perhaps be determined using one of the thiol containing species as a proxy. Furthermore, if $CS_2$ is indeed produced by the energetic processing of sulfur-bearing ices, then the yield of OCS in a specific interstellar cloud may be expected to show some dependence on the ratio of O atoms to H atoms in that cloud. For example, in regions where the O:H ratio is higher, most of the $CS_2$ formed in interstellar ices might be expected to react with O atoms, thus increasing the abundance of OCS, whereas in regions with lower O:H ratios, $CS_2$ may predominantly react with H atoms to produce $H_2S$ and thiols.

The observation that both $CS_2$ and $SO_2$ react with D atoms to produce $D_2S$ has interesting implications for the potential presence of $H_2S$ in icy mantles. The experimental results discussed suggest that $H_2S$ should indeed be present in astrophysical ices. However, the current non-detection of $H_2S$ in these ices perhaps implies that it has a rich chemistry itself under interstellar conditions and is readily converted into other species. The thermal reactivity of $H_2S$ under interstellar conditions is therefore of considerable interest and will be the subject of a future study.

## 6.7 Summary

In this chapter the results of experiments investigating the surface reactions of both carbon disulfide, $CS_2$, and sulfur dioxide, $SO_2$, with thermal deuterium atoms have been discussed. These experiments show $CS_2$ readily reacts with D atoms to form a variety of products including $D_2S$ and the thiol containing species $CD_3SD$ and $CD_2(SD)_2$. A key consequence of these findings for sulfur chemistry in the interstellar medium is that part of the ‘missing’ sulfur in the interstellar medium may be present in interstellar ices in the form of of a range of organic thiols. Additionally $H_2S$ may readily form from the reaction of H atoms with $CS_2$ formed in energetic processing of interstellar ices. Hence, the fact that $H_2S$ has yet to be observed in interstellar ices, may imply that it readily undergoes chemical reactions and is converted into other species. The experiments

discussed in this chapter also show that $SO_2$ reacts with D atoms to produce both $D_2S$ and $D_2O_2$. Additionally, it is likely that the reaction of $SO_2$ with D atoms also produces $D_2O$. Rate constants for these reactions have also been estimated.

## 6.8 References


(1) Lodders, K. *Astrophysical Journal* **2003**, *591*, 1220.
(2) van Steenbergen, M. E.; Shull, J. M. *Astrophysical Journal* **1988**, *330*, 942.
(3) Sofia, U. J.; Cardelli, J. A.; Savage, B. D. *Astrophysical Journal* **1994**, *430*, 650.
(4) Garrod, R. T.; Wakelam, V.; Herbst, E. *Astronomy & Astrophysics* **2007**, *467*, 1103.
(5) Millar, T. J.; Herbst, E. *Astronomy and Astrophysics* **1990**, *231*, 466.
(6) Doty, S. D.; van Dishoeck, E. F.; van der Tak, F. F. S.; Boonman, A. M. S. *Astronomy & Astrophysics* **2002**, *389*, 446.
(7) van der Tak, F. F. S.; Boonman, A. M. S.; Braakman, R.; van Dishoeck, E. F. *Astronomy & Astrophysics* **2003**, *412*, 133.
(8) Garozzo, M.; Fulvio, D.; Kanuchova, Z.; Palumbo, M. E.; Strazzulla, G. *Astronomy & Astrophysics* **2010**, *509*, 9.
(9) Geballe, T. R.; Baas, F.; Greenberg, J. M.; Schutte, W. *Astronomy & Astrophysics* **1985**, *146*, L6.
(10) Jimenez-Escobar, A.; Caro, G. M. M. *Astronomy & Astrophysics*, *536*, 11.
(11) Jimenez-Escobar, A.; Caro, G. M. M. *Astronomy & Astrophysics* **2011**, *536*.
(12) Ferrante, R. F.; Moore, M. H.; Spiliotis, M. M.; Hudson, R. L. *Astrophysical Journal* **2008**, *684*, 1210.
(13) Bohn, R. B.; Brabson, G. D.; Andrews, L. *Journal of Physical Chemistry* **1992**, *96*, 1582.
(14) NIST Mass Spec Data Centre; S. E. Stein; director. NIST Chemistry Webbook. In *NIST Standard Reference Database Number 69*; Linstrom, P. J., Mallard, W. J., Eds.; National Institute of Science and Technology, Gaithersburg MD, 20899; Vol. "Mass Spectra".
(15) Ward, M. D.; King, S. J.; Price, S. D. *Journal of Chemical Physics* **2011**, *134*, 10.
(16) Douglas, K. M.; Price, S. D. *International Journal of Mass Spectrometry* **2011**, *303*, 147.
(17) King, S. J.; Price, S. D. *International Journal of Mass Spectrometry* **2008**, *277*, 84.
(18) Ghio, E.; Mattera, L.; Salvo, C.; Tommasini, F.; Valbusa, U. *Journal of Chemical Physics* **1980**, *73*, 556.
(19) Fuchs, G. W.; Cuppen, H. M.; Ioppolo, S.; Romanzin, C.; Bisschop, S. E.; Andersson, S.; van Dishoeck, E. F.; Linnartz, H. *Astronomy & Astrophysics* **2009**, *505*, 629.
(20) Rejoub, R.; Lindsay, B. G.; Stebbings, R. F. *Journal of Chemical Physics* **2001**, *115*, 5053.
(21) Straub, H. C.; Lindsay, B. G.; Smith, K. A.; Stebbings, R. F. *Journal of Chemical Physics* **1998**, *108*, 109.
(22) Lindsay, B. G.; Rejoub, R.; Stebbings, R. F. *Journal of Chemical Physics* **2003**, *118*, 5894.
(23) Lindsay, B. G.; Straub, H. C.; Smith, K. A.; Stebbings, R. F. *Journal of Geophysical Research-Planets* **1996**, *101*, 21151.
(24) Hiraoka, K.; Takayama, T.; Euchi, A.; Handa, H.; Sato, T. *Astrophysical Journal* **2000**, *532*, 1029.
(25) Hiraoka, K.; Sato, T.; Sato, S.; Takayama, T.; Yokoyama, T.; Sogoshi, N.; Kitagawa, S. *Journal of Physical Chemistry B* **2002**, *106*, 4974.
(26) Hiraoka, K.; Sato, T.; Sato, S.; Hishiki, S.; Suzuki, K.; Takahashi, Y.; Yokoyama, T.; Kitagawa, S. *Journal of Physical Chemistry B* **2001**, *105*, 6950.

(27) Hiraoka, K.; Sato, T.; Sato, S.; Sogoshi, N.; Yokoyama, T.; Takashima, H.; Kitagawa, S. *Astrophysical Journal* **2002**, *577*, 265.
(28) Hiraoka, K.; Sato, T.; Takayama, T. *Science* **2001**, *292*, 869.
(29) Bisschop, S. E.; Fuchs, G. W.; van Dishoeck, E. F.; Linnartz, H. *Astronomy & Astrophysics* **2007**, *474*, 1061.
(30) Ioppolo, S.; Cuppen, H. M.; Romanzin, C.; van Dishoeck, E. F.; Linnartz, H. *Physical Chemistry Chemical Physics* **2011**, *12*, 12065.

# Chapter 7 – Reactions of Acrylonitrile with Hydrogen and Oxygen Atoms

## 7.1 Introduction

Several of the approximately 160 interstellar molecules detected to date contain a C≡N triple bond within their structure.[1] These C≡N containing molecules range from the simplest, the cyano radical, CN, to long chain cyanopolyynes, $HC_nN$.[2-7] Additionally, the simplest closed shell C≡N containing molecule, HCN, is believed to be an important constituent of interstellar ices.[8-12] The thermal reactivity of the C≡N triple bond under interstellar conditions is therefore of considerable astrochemical interest, especially given the importance of the C—N linkage in prebiotic molecules such as amino acids. Acrylonitrile, $C_2H_3CN$, also known as vinyl cyanide or propenenitrile, is a convenient model system for studying the reactivity of the C≡N triple bond compared with that of the better characterized C=C double bond.[13,14]

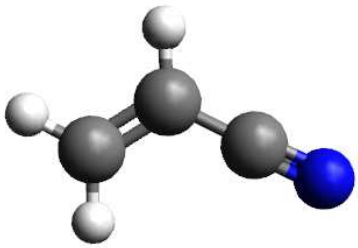

Figure 7.1 The molecular structure of acrylonitrile.

Acrylonitrile has been detected in the interstellar medium both toward Sgr B2 (15) and in the cold dark cloud TMC-1 (16). Additionally acrylonitrile has been observed in the circumstellar envelope of the carbon rich star IRC+10216.[17] Therefore, whilst acrylonitrile has yet to be detected in interstellar ices, its reactions under interstellar conditions are themselves of astrophysical interest. Nevertheless the purpose of the experimental investigations of the reactions of acrylonitrile with H and O atoms is primarily to elucidate the general reactivity of the C≡N bond with respect to the C=C bond under interstellar conditions.

Some previous experimental studies have investigated the chemistry of the C≡N bond under interstellar conditions. However, as discussed in Section 1.8.4, only those studies

carried out by Theule *et al* and Hiraoka *et al* have considered the reactions of the C≡N group with thermal species.[8,18] In the study by Theule *et al*, the authors investigated the reaction of HCN with thermal hydrogen atoms on a copper surface at 15 K. The HCN ice was initially deposited onto the copper surface and then dosed with a total fluence of H atoms of approximately $10^{18}$ $cm^{-2}$ $s^{-1}$. Both infrared spectroscopy and temperature programmed desorption were used to detect any products of the reaction of H atoms with HCN. However, reaction products could only be detected using the more sensitive thermal desorption technique. Specifically, the authors observed the formation of methylamine, $CH_3NH_2$. Clearly the yield of the methylamine product was so low that it was below the detection limit of the IR spectrometer used. The implication is that HCN only reacts with H atoms very slowly. Conversely the fact that the intermediate imine species, $CH_2NH$, was not detected suggests that C=N double bonds react with H atoms much more rapidly than C≡N triple bonds.

The results of the experiments carried out by Theule *et al* support those of an earlier study by Hiraoka *et al*.[18] In this earlier study, Hiraoka and co-workers investigated the surface reaction of D atoms with CN radicals in the temperature range 10 – 20 K. Whilst the authors observe the formation of DCN and DNC molecules following this reaction, they do not report the formation of any species arising from the further deuteration of these species.

In contrast to the thermal reactions of hydrogen atoms with species containing the C≡N group, several previous studies have shown that HCN can readily be saturated by suprathermal H atoms produced by energetic processing of astrophysical ice mixtures. For example, Elsila *et al* studied the processing of an ice containing a 20:2:1 mixture of $H_2O$, $CH_3OH$ and HCN by UV light at wavelengths of 121.6 nm and 140 – 180 nm.[10] This energetic processing of the ice was found to result in the production of measurable amounts of the amino acids glycine, alanine and serine. Energetic processing of HCN containing ices has also been studied by Gerakines *et al*, who investigated the processing of an ice containing various mixtures of $H_2O$, $NH_3$ and HCN by 0.8 MeV protons.[11] These authors find that when ices containing mixtures of $H_2O$ and HCN are bombarded by energetic protons, formamide, $HCONH_2$, is formed. Additionally, Gerakines *et al* find that when ices containing mixtures of $NH_3$ and HCN are irradiated in a similar way, various imine ($H_2C$=N-) containing species are formed, indicating the partial saturation of the C≡N bond.

Clearly, whilst the C≡N bond can readily be saturated by suprathermal hydrogen atoms, it only reacts slowly with thermal H atoms. One might therefore expect thermal hydrogen atoms to react with acrylonitrile preferentially at the C=C bond. However, since the thermal studies discussed above only consider very small C≡N containing species such as CN and HCN, it is not clear what effect, if any, the presence of the vinyl group in the acrylonitrile molecule has on the reactivity of the C≡N bond. For example, in Chapter 3 it was shown that the barrier to reaction of alkenes with O atoms decreased with increasing carbon chain length, and so the reactivity of the C≡N group may be greater in the acrylonitrile molecule than in either CN or HCN. In order to confirm that under interstellar conditions, the C=C bond is indeed more reactive with respect to thermal H atoms than the C≡N bond, experiments investigating the reaction of thermal hydrogen atoms with acrylonitrile on an HOPG substrate have been carried out at temperatures between 14 and 70 K. Additionally, this chapter reports the results of similar experiments studying the reaction of acrylonitrile with thermal oxygen atoms between 14 and 100 K.

## 7.2 Experimental

The experimental arrangement used for the experiments discussed in this chapter is described in detail in Chapter 2. The acrylonitrile was taken from the vapour above a liquid commercial sample, of greater than 99 % purity, at approximately 25 °C. Any volatile impurities were previously removed from this liquid sample of acrylonitrile by subjecting it to several freeze-pump-thaw cycles. Commercial samples of acrylonitrile contain approximately 35 – 45 ppm of monomethyl ether hydroquinone in order to inhibit polymerization of the sample. However, the presence of this inhibitor does not interfere with the current experiments in any way due to its low concentration and vapour pressure. In order to further limit polymerization of the acrylonitrile sample, it was stored on the inlet line in a glass vial from which ambient light was excluded.

In the experiments studying the reactions of acrylonitrile with oxygen atoms, the fluxes of reactants used was $4.4 \times 10^{14}$ cm$^{-2}$ s$^{-1}$ and $1.2 \times 10^{14}$ cm$^{-2}$ s$^{-1}$ respectively. For the hydrogen atom reaction experiments, the fluxes were again $4.4 \times 10^{14}$ cm$^{-2}$ s$^{-1}$ for acrylonitrile and $2.4 \times 10^{14}$ cm$^{-2}$ s$^{-1}$ for hydrogen atoms. Consequently the ratio of acrylonitrile to oxygen atoms was approximately 7:2 whilst the ratio of acrylonitrile to hydrogen atoms was approximately 2:1. In a typical experiment acrylonitrile was co-deposited with either hydrogen or oxygen atoms at a specific surface temperature for

one hour. At the end of this dosing period, the supply of reactants was turned off and the surface warmed to approximately 400 K in order to desorb the reactants as well as any products formed. Any species desorbing from the surface during this heating phase were ionized using 200 eV electrons and detected by recording consecutive 1 s time of flight mass spectra as described in detail in Section 2.9. The product yields were derived from the resulting desorption spectra following the procedure also described in Section 2.9.

## 7.3 Results

### 7.3.1 $C_2H_3CN + H$

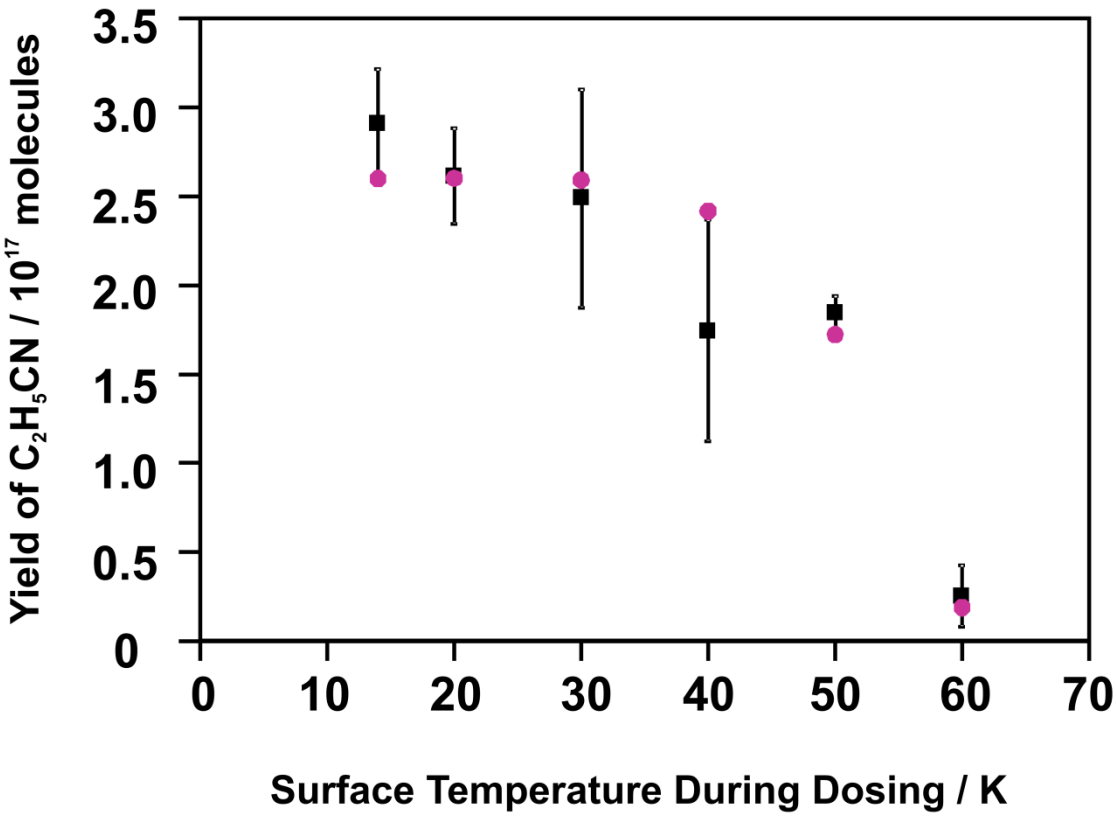


Figure 7.2 The temperature dependence of the yield of $C_2H_5CN$ from the reaction of $C_2H_3CN$ with H atoms. The experimental data are represented by black squares and the model output is represented by pink circles.

The surface reaction of acrylonitrile with H atoms was investigated at surface temperatures between 14 and 60 K. The temperature dependence of the product yield derived from these experiments can be seen in Figure 7.2. The reaction of H atoms with acrylonitrile was found to yield a single product with a mass of 55 at all temperatures investigated. Thus, given that acrylonitrile has a mass of 53, it seems clear that this product arises from the addition of two hydrogen atoms to an acrylonitrile molecule and therefore has an empirical formula $C_3H_5N$. The yield of $C_3H_5N$ is largest at the lowest

surface temperature investigated, 14 K, and decreases approximately linearly with increasing surface temperature up to 50 K. At 60 K the product yield deviates substantially from this linear trend, falling to approximately 10 % of that at 50 K. This substantial decrease in product yield between 50 and 60 K initially appears to indicate the desorption of either the acrylonitrile reactant or the $C_3H_5N$ product at 60 K. However, as discussed in Section 7.5, this explanation is not consistent with the TPD data. Instead the decrease in propanenitrile yield at 60 K is most likely an extension of the decreasing yield observed between 15 and 50 K. Assuming that H atoms have a similar desorption energy from acrylonitrile ice to the D atom desorption energy determined in Chapter 4 for NO ice, one would expect any contribution from a LH mechanism, or from an ER mechanism in which the H atom is the adsorbed species, to be observed in the form of an enhanced product yield at 15 K. Thus, given that there is no obvious enhancement above the general trend at 15 K, it appears that only the ER mechanism in which a gas phase H atom reacts with an adsorbed acrylonitrile molecule contributes significantly to the product yield.

### 7.3.2 $C_2H_3CN + O$

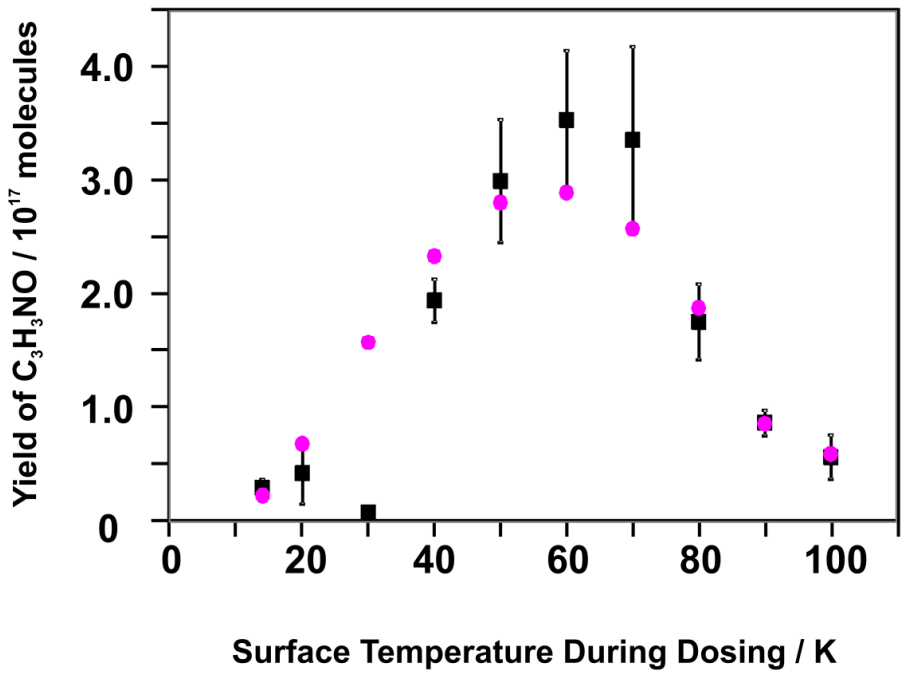


Figure 7.3 The temperature dependence of the yield of $C_3H_3NO$ from the reaction of $C_2H_3CN$ with O atoms. The experimental data are represented by black squares and the model ouput is represented by pink circles.

In the experiments investigating the reaction of acrylonitrile with O atoms, two products were observed to form with masses that were 16 and 32 atomic mass units higher than

that of acrylonitrile itself. These masses clearly represent products resulting from the addition of one and two oxygen atoms to the acrylonitrile molecule respectively. These oxygenated products therefore have the empirical formulae $C_3H_3NO$ and $C_3H_3NO_2$ respectively. The temperature dependence of the yield of $C_3H_3NO$ is shown in Figure 7.3. Broadly, the yield increases with increasing temperature up to a maximum at 60 K before decaying exponentially above this temperature. However, the yield of $C_3H_3NO$ at 30 K does not appear to follow the general trend; indeed, the yield reaches a minimum at this temperature. It is emphasized here that the experimental data shown in Figure 7.2, Figure 7.3 and Figure 7.4 represents the average of three measurements with the error bars representing one standard deviation in this average. Thus, it appears that the low yield of $C_3H_3NO$ at 30 K is a genuine feature of the reaction scheme and is not a statistical anomaly. Some possible explanations of this decreased $C_3H_3NO$ yield at 30 K will be discussed below. There does not appear to be any enhancement in the product yield at 30 – 50 K in the case of this reaction, again indicating that there is no contribution from either a Langmuir-Hinshelwood mechanism or an Eley-Rideal mechanism in which a gas phase acrylonitrile reacts with an adsorbed O atom.

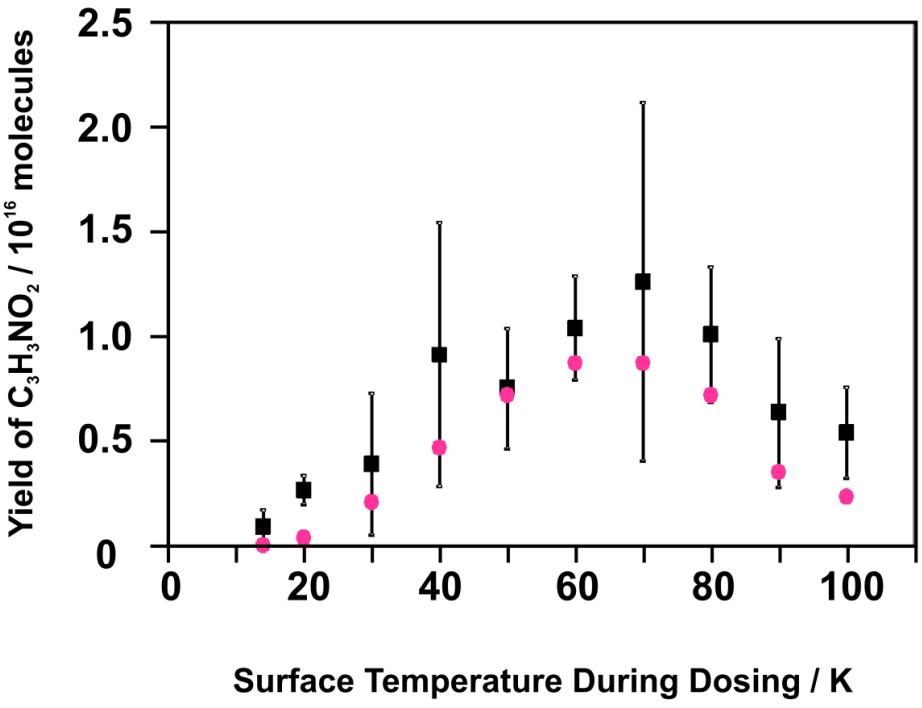


Figure 7.4 The temperature dependence of the yield of $C_3H_3NO_2$ from the reaction of $C_2H_3CN$ with O atoms. The experimental data are represented by black squares and the model ouput is represented by pink circles.

The variation of the yield of $C_3H_3NO_2$ with surface temperature is shown in Figure 7.4. The yield of this doubly oxygenated product appears to follow an approximately linear

trend, increasing with increasing surface temperature up to 70 K. In a similar way to the yield of the $C_3H_3NO$ product, the yield of $C_3H_3NO_2$ follows an approximately exponential decay above 70 K. Whilst there appears to be a small enhancement in the yield of $C_3H_3NO_2$ at 40 K, this enhancement lies within the experimental uncertainties. Consequently, the temperature dependence of the $C_3H_3NO_2$ product yield is again consistent with there being no contribution from a LH mechanism or from an ER mechanism involving an acrylonitrile molecule as the gas phase species.

## 7.4 Data Analysis

The kinetic model used to derive kinetic parameters from the experimental data has been described extensively in Section 2.11 and in Chapters 3 – 6. Therefore, only the key features concerning the modelling of the experimental data described in this chapter are outlined here.

As previously described, the kinetic model can in principle account for the simultaneous operation of an ER mechanism, in which a gas phase species reacts directly with an adsorbed species, and an LH mechanism, in which two adsorbed species react. However, as outlined above, there is no evidence of a substantial contribution to the product yield from an LH mechanism in either the H atom reaction or O atom reaction described here. Thus, in modelling the present experiments only an ER reaction is considered. Specifically, the ER reaction used to model the experimental data involves a gas phase hydrogen or oxygen atom reacting with an adsorbed acrylonitrile molecule. The alternative ER reaction in which a gas phase acrylonitrile molecule reacts with an adsorbed hydrogen or oxygen atom is not considered because the operation of such a mechanism would again be expected to cause an observable enhancement in product yield at temperatures low enough for the atomic species to adsorb onto the surface.

In modelling these reactions, the penetration depth of O and H atoms into the ice must be considered. In the case of O atoms this penetration depth is assumed to be one monolayer; that is to say the oxygen atoms do not penetrate the ice surface. Such an assumption is supported by previous experiments carried out using the present experimental arrangement, which studied the reaction of $^{16}O$ atoms with $^{18}O_2$ ice. As described in Chapters 3 and 5, the major product of this surface reaction was $^{16}O_3$ with $^{16}O^{18}O_2$ representing only a minor product. These results indicate that $^{16}O$ atoms react mainly with the newly deposited $^{16}O_2$ molecules coming from the O atom source rather than penetrating into the ice and reacting with the underlying $^{18}O_2$. Similar

measurements are less straightforward for H atoms using the present experimental apparatus because the H atom source takes several hours before a usable flux of H atoms is produced. Therefore the H atom source could not be turned off during dosing of the underlying reactant. In this case, the penetration depth measured by Fuchs *et al* for H atoms on CO ice (4 monolayers) is used as an approximate estimate in the absence of any previous determinations of the penetration depth of H atoms on hydrocarbon ices.[19]

## 7.5 Discussion

### 7.5.1 $C_2H_3CN$ + H

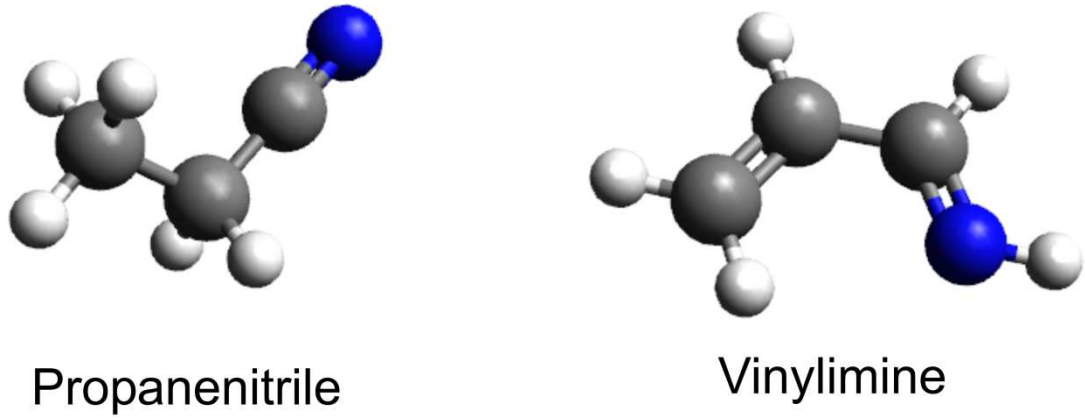


Figure 7.5 The molecular structures of the possible $C_3H_5N$ product formed from the reaction of acrylonitrile with H atoms.

As discussed above, a product with the empirical formula $C_3H_5N$ is formed in the surface reaction of thermal hydrogen atoms with acrylonitrile. The two hydrogen atoms which add to the acrylonitrile reactant to form this product can, in principle, add to either the C=C double bond or the C≡N triple bond. If the two hydrogen atoms add to the C=C double bond, the product would be expected to be propanenitrile, $CH_3CH_2CN$. Conversely, if the two hydrogen atoms add to the C≡N triple bond, the product would be vinylimine, $CH_2CHCHNH$. However, previous experiments by Theule *et al*, studying the reaction of HCN with H atoms under interstellar conditions, show that hydrogen atom addition continues until the C≡N bond is completely saturated, producing methylamine, $CH_3NH_2$.[8] Furthermore, these authors do not detect the intermediate imine species, $CH_2NH$, in infrared spectra of the ice during the reaction, indicating that hydrogenation of the C=N double bond proceeds much more quickly than that of the C≡N triple bond. Consequently, if in the current reaction the two

hydrogen atoms reacted at the C≡N triple bond, one would expect the vinylimine product to react rapidly with a further two hydrogen atoms to produce vinylamine, $CH_2CHCH_2NH_2$. The $C_3H_3N$ product is therefore identified as propanenitrile arising from hydrogenation of the C=C double bond.

As discussed above, the yield of propanenitrile from the reaction of H atoms with acrylonitrile decreases with increasing surface temperature. The possible causes of such negative temperature dependences in surface reactions have been outlined in both Chapter 4 and Chapter 6 and thus a detailed discussion is not repeated here. Briefly, however, it seems likely that the negative temperature dependences observed in some of the reactions discussed in this thesis arise from a combination of a barrierless reaction which produces the product of interest and a competing reaction with a positive activation energy which reduces the yield of that product. This argument may be understood simply by considering the two reactions:

$$A \rightarrow B \qquad 7.1$$

$$B \rightarrow C \qquad 7.2$$

The temperature dependence of the yield of B would be expected to be negative if reaction 7.1 is barrierless and reaction 7.2 has a positive activation energy. In terms of the current reaction of acrylonitrile with two hydrogen atoms to produce propanenitrile, a similar argument can be constructed as follows. The two consecutive hydrogen addition reactions are either barrierless or have a barrier which hydrogen atoms may tunnel through. However, the intermediate radical (either $\dot{C}H_2CH_2CN$ or $CH_3\dot{C}HCN$) may perhaps undergo a polymerization reaction which has a positive activation energy to form a heavy product which is not detected under the current experimental conditions. No evidence of the formation of species with higher masses is observed in the TPD spectra. However, it is likely that heavy polymeric species would desorb at temperatures well above those which can be investigated using the current experimental arrangement. It must, therefore, be emphasized that such a reaction mechanism is, at this stage, purely speculative and simply represents one way of explaining the experimental data.

Whilst the exact competing reaction mechanism which gives rise to the apparent negative temperature dependence is not definitively known, for the purposes of modelling the experimental data, it is assumed that this competing reaction is the

polymerization reaction suggested above. The fact that the formation of propanenitrile is observed, even at temperatures as low as 14 K, suggests that the product forming reaction is either barrierless or has a barrier through which hydrogen atoms can tunnel. The experimental data are therefore initially modelled with an ER reaction in which gas phase hydrogen atoms react with adsorbed acrylonitrile molecules with zero activation energy. Clearly, when only a barrierless product forming reaction is included in the kinetic model, the predicted product yield is independent of temperature and depends only upon the pre-exponential factor for the reaction. Given that the competing reaction appears to have the least effect upon the propanenitrile yield at 14 K, the pre-exponential factor for the reaction is determined by fitting the initial flat temperature dependence to the experimental data point at 14 K. At this stage a competing reaction is introduced into the model. In order to reduce the number of free parameters, the pre-exponential factor for the competing reaction is assumed to be equal to that for the product forming reaction. The barrier of the competing reaction is then adjusted until a best fit is achieved between the temperature dependence predicted by the model and that measured experimentally. The pre-exponential factor for both reactions was then re-adjusted to improve the fit between the predicted and experimental temperature dependences. After several iterations of this procedure, the best fit was achieved with a pre-exponential factor for the reaction of $(7.4 \pm 0.9) \times 10^{-17}$ cm$^2$ molecule$^{-1}$ s$^{-1}$ and a barrier ($E/R$) for the competing reaction of 355 ± 5 K. The temperature dependence predicted by this model is shown in Figure 7.2. As can be seen in Figure 7.2, the fit to the experimental data achieved when a competing reaction is included in the kinetic model is very good, indicating that such a competing reaction pathway is a likely explanation for the inverse temperature dependence of the yield of propanenitrile.

In principle, the product yield at the highest temperatures investigated could be affected by the desorption of either the acrylonitrile reactant or the propanenitrile product, thus resulting in an overestimation of the contribution of the competing reaction. However, desorption peaks for acrylonitrile are observed for temperatures up to 100 K in the experiments studying its reactions with oxygen atoms, suggesting that acrylonitrile adsorbs onto the surface at temperatures higher than 60 K. Furthermore, in the TPD spectra, propanenitrile is observed to desorb at a higher temperature than acrylonitrile. Therefore, it is not believed that desorption of either acrylonitrile or propanenitrile plays any in the reaction kinetics at any of the temperatures investigated experimentally.

### 8.1.1 $C_2H_3CN + O$

As outlined above, two products are observed following the reaction of acrylonitrile with O atoms. Given that these two products have masses that are 16 and 32 atomic mass units larger than that of the acrylonitrile reactant, it is clear that they have empirical formulae of $C_3H_3NO$ and $C_3H_3NO_2$ respectively. The temperature dependences of the yields of these products are shown in Figure 7.3 and Figure 7.4 respectively.

Firstly considering the yield of $C_3H_3NO$, it is clear that the general trend is one of increasing yield with increasing temperature between 14 and 60 K. Such a temperature dependence indicates that the reaction has a small positive energy barrier associated with it. As discussed above the absence of any enhancement in product yield in the region of 30 – 50 K, as has been observed in previous studies of O atom reactions (see Chapters 3 and 5), indicates that there is no significant contribution to the product yield from either a LH mechanism or an ER mechanism in which a gas phase acrylonitrile molecule reacts with an adsorbed O atom. The temperature dependence is therefore modelled with an ER mechanism in which the oxygen atom is the gas phase species. Setting the reaction barrier for this ER mechanism to $E_{ER}/R$ = 50 ± 10 K was found to produce the best fit (shown in Figure 7.3) to the experimental temperature dependence between 14 and 60 K. By placing the experimental data on an absolute scale as described in Section 2.10, an estimate of the Arrhenius pre-exponential factor for the reaction, $A_{Rxn}$, can also be derived. This pre-exponential factor was estimated to be (5.0 ± 0.8) × $10^{-16}$ $cm^2$ $molecule^{-1}$ $s^{-1}$.

The fit to the experimental data obtained as described above can be seen in Figure 7.3. It is clear that there are some discrepancies between the model output and the experimental data. In particular the model cannot explain the fact that the yield of $C_3H_3NO$ at 30 K is substantially lower than would be expected by inspection of the general trend. In attempting to explain the low yield of $C_3H_3NO$ at 30 K, it is helpful to consider the yield of $C_3H_3NO_2$. The yield of this doubly oxygenated species shows no such decrease at 30 K and instead increases in an approximately linear fashion to 60 – 70 K. Thus, since the formation of this doubly oxygenated product must proceed *via* the singly oxygenated species, an obvious conclusion is that the observed yield of the singly oxygenated product does not represent the actual amount of singly oxygenated product formed in the reaction. Instead, the singly oxygenated product is consumed in some

other process which is particularly efficient at 30 K. Of course one process which would consume the singly oxygenated product in this way is the reaction with a second O atom to produce $C_3H_3NO_2$. Indeed, when the yield of $C_3H_3NO$ predicted by the kinetic model outlined above is used to model a second ER oxygenation step, with an identical reaction barrier and pre-exponential factor, the temperature dependence of the predicted yield of $C_3H_3NO_2$ is in good agreement with that observed experimentally (Figure 7.4). Whilst these findings are encouraging, they do not satisfactorily explain the decreased yield of $C_3H_3NO$ at 30 K since, if the second oxygenation reaction has the same reaction barrier as the first oxygenation step, the secondary reaction should consume the same proportion of the singly oxygenated product at all temperatures below 60 K. An alternative explanation that could be invoked would attribute the enhanced depletion of $C_3H_3NO$ at 30 K to the availability of a LH mechanism in the case of the second oxygenation step. However, there are several reasons why this argument may be discounted. Firstly, the lack of an LH pathway in the first oxygenation step is presumably due to the immobility of O atoms in the acrylonitrile ice; there is no reason why this should be different in the case of the second oxygenation step. Secondly, for the LH mechanism to be most efficient at 30 K, as opposed to 40 – 50 K observed for other O atom reactions (see Chapters 3 and 5), would require a substantially reduced physisorption energy for O atoms on acrylonitrile ice. Whilst it is plausible that interaction energies of O atoms would be different on different ice surfaces, it is not clear why there should be such a marked reduction for acrylonitrile ice given the similarity in these O atom interaction energies for ethene, propene and carbon disulfide ices. Finally, such an LH mechanism might be expected to produce an enhancement in $C_3H_3NO_2$ yield at 30 K, yet no such enhancement is observed experimentally. Perhaps the most plausible explanation for the decreased $C_3H_3NO$ yield at 30 K is that there is a 'window of opportunity' for a competing reaction to occur at this temperature. Such a competing reaction would have to have a small positive reaction barrier in order to explain why it does not occur at the lowest temperatures investigated. Additionally there would need to be some reason why the competing reaction does not occur at temperatures above 40 K. One type of reaction which may fit these criteria is a polymerization reaction which proceeds *via* a weakly bound complex, for example a $(C_3H_3NO)_2$ dimer. At very low temperatures this dimer may not be formed due to the presence of a positive activation energy for its formation, whereas, at high temperatures, the dimer may simply decompose back to two $C_3H_3NO$ monomers. Whilst, in principle,

this dimerization pathway could be included in the kinetic model to reproduce the experimental data at 30 – 40 K, including such a pathway would introduce two free parameters to model two data points and, thus, offers little insight into whether this dimerization reaction can help explain the experimental data. Clearly, further experiments are required in order to confirm the presence of a polymerization reaction at 30 K.

At temperatures higher than 60 K the yields of both the singly and doubly oxygenated products decrease with increasing temperature. A decrease in product yield at high temperatures can often be attributed to the non-adsorption of both reactants or the desorption of the nascent products. However, as discussed above, acrylonitrile is observed to adsorb onto the surface at temperatures up to and including 100 K, whilst the TPD spectra indicate that the oxygenated products desorb at even higher temperatures. Thus, it seems that the decrease in the yields of the oxygenated products at temperatures above 60 K cannot be explained by the desorption of either the reactants or products. Instead, it is likely that there is again some competing reaction reducing the yield of these products at high temperatures. Again, the most obvious candidate for such a competing reaction is a polymerization reaction. A competing reaction has been included in the kinetic model in order to test whether such a reaction can account for the observed reduction in $C_3H_3NO$ yield. The predicted temperature dependence when this competing pathway has a barrier ($E/R$) of 250 ± 10 K and an Arrhenius pre-exponential factor of (3.3 ± 0.2) × $10^{-15}$ $cm^2$ $molecule^{-1}$ $s^{-1}$ is shown in Figure 7.3. It is clear that, when such a competing pathway is introduced, the model reproduces the decrease in product yield at high temperature reasonably well. It should be noted, however, that to fit the experimental data point at 100 K, a desorption energy for acrylonitrile of 23.7 ± 0.3 kJ $mol^{-1}$ was required. No previous measurements of the physisorption energy of acrylonitrile either on graphite or on molecular ices appear to be available in the literature. However, this desorption is intermediate between that measured for OCS (see Chapter 5) and that for $H_2O$ as would be expected given the position of the desorption peak for acrylonitrile in the TPD spectra recorded in the present experiments.[20] Thus, modelling the experimental data does suggest that a competing reaction is a plausible explanation for the decreasing yield of $C_3H_3NO$ above 60 K.

Unfortunately, it has not been possible to determine the structures of the products of the reaction of thermal O atoms with acrylonitrile in the current experiments. In principle

multi-photon ionization could be used to distinguish between different isomers of $C_3H_3NO$ and $C_3H_3NO_2$ as described in previous chapters. However, in practice there are many different possible isomers of these species, some of which have very poorly characterized ionization energies. Consequently, the definitive identification of these products in this way would be very difficult. Nevertheless, some empirical suggestions can be made as to the structures of the products. For example, given that H atoms were found to react with acrylonitrile at the C=C bond rather than the C≡N bond, it may be expected that oxygen atoms would also preferentially react with the C=C bond. Thus, if the C≡N bond is assumed to be inert with respect O atoms under the current experimental conditions, the $C_2H_3CN$ + O system is analogous with the $C_2H_4$ + O system described in Chapter 3. The primary product of the reaction of O atoms $C_2H_4$ was ethylene oxide, thus, the reaction of O atoms with acrylonitrile would be expected to produce cyanoethylene oxide, c-$C_2H_3(CN)O$. However, this analogy with the $C_2H_4$ + O reaction is clearly limited because in the reaction of acrylonitrile with O atoms, a doubly oxygenated product, $C_3H_3NO_2$, is observed, whereas ethylene oxide was found not to undergo further reaction with O atoms under conditions relevant to the interstellar medium. It is not clear whether this second oxygenation reaction indicates that the cyano group does in fact react with oxygen atoms or whether the presence of the electron withdrawing cyano group destabilizes the epoxide ring and renders it susceptible to further attack by oxygen atoms. The site of the second oxygenation reaction could be tested by investigating the reaction of an analogous epoxide such as fluoroethylene oxide with O atoms. This molecule contains an electron withdrawing fluorine atom in place of the cyano group. It is very unlikely that this fluorine atom would be susceptible to attack by O atoms under the cold conditions of these experiments due to the strong nature of the C—F bond, thus any doubly oxygenated product in this case would arise from the effect of an electron withdrawing group on the epoxide ring.

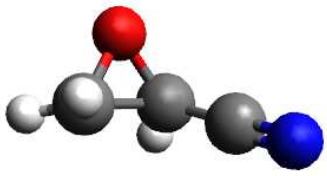

Figure 7.6 The molecular structure of cyanoethylene oxide.

## 8.2 Astrophysical Implications

Despite the fact that there are clearly still many questions to be addressed in fully characterising the reactions of acrylonitrile with oxygen and hydrogen atoms, some conclusions can still be drawn regarding the implications of the present results for chemistry in the interstellar medium. For example, it is clear from these experiments that thermal hydrogen atoms preferentially react with C=C double bonds over C≡N triple bonds under the cold conditions of the interstellar medium. This finding is in agreement with the observation by Theule *et al* that the reactions of hydrogen atoms with HCN to produce methylamine are very slow.[8] Conversely experiments by Elsila *et al* studying the irradiation of ices containing mixtures of HCN, $H_2O$ and $CH_3OH$ by UV photons show that energetic processing can readily saturate C≡N bonds.[10] Similarly, Gerakines *et al* found that species containing saturated C—N bonds, such as formamide, $HCONH_2$, were formed when ices composed of various mixtures of HCN, $H_2O$ and $NH_3$ were exposed to 0.8 MeV protons. These differences between thermal reactions and reactions initiated by energetic processing offer a potential observational indication of the relative importance these two types of reaction in complex molecule formation. Specifically, if thermal reactions are dominant one would expect to see only amines in which the carbon chain is fully saturated. By contrast, an abundance of unsaturated amines would imply that reactions initiated by energetic processing of interstellar ices played an important role.

Unfortunately in the absence of definitive structures of the products of the reaction of acrylonitrile with oxygen atoms, it is not yet possible to draw a similar conclusion with regard to oxygenated amine species. Nevertheless, the formation of a species containing all four elements necessary for amino acid formation, H, C, N and O is interesting in its own right. Furthermore the doubly oxygenated species contains C, N and O in the same ratio as alanine (3:1:2). The identification of this product would therefore be of considerable astrochemical interest since it may be that further thermal reactions of this species with H atoms could produce alanine.

## 8.3 Summary

This chapter has discussed the results of preliminary experimental investigations of the surface reactions of acrylonitrile with both H and O atoms under interstellar conditions. These experiments demonstrate that in reactions with H atoms, the C=C double bond in acrylonitrile is saturated whilst the C≡N triple bond does not appear undergo any

detectable reaction on the present experimental timescale. The product of the reaction of acrylonitrile with H atoms is therefore propanenitrile, $C_2H_5CN$. With oxygen atoms, acrylonitrile appears to undergo two stepwise oxygen addition reactions to form both singly and doubly oxygenated products. However, further experiments would be required in order to identify these products. Estimates of both the reaction barriers and pre-exponential factors for these reactions have also been determined.

## 8.4 References


(1) Kwok, S.; Zhang, Y. *Nature* **2011**, *479*, 80.
(2) Bell, M. B.; Feldman, P. A.; Travers, M. J.; McCarthy, M. C.; Gottlieb, C. A.; Thaddeus, P. *Astrophysical Journal* **1997**, *483*, L61.
(3) Bell, M. B.; Watson, J. K. G.; Feldman, P. A.; Travers, M. J. *Astrophysical Journal* **1998**, *508*, 286.
(4) Broten, N. W.; Macleod, J. M.; Avery, L. W.; Irvine, W. M.; Hoglund, B.; Friberg, P.; Hjalmarson, A. *Astrophysical Journal* **1984**, *276*, L25.
(5) Broten, N. W.; Oka, T.; Avery, L. W.; Macleod, J. M.; Kroto, H. W. *Astrophysical Journal* **1978**, *223*, L105.
(6) Cherchneff, I.; Glassgold, A. E.; Mamon, G. A. *Astrophysical Journal* **1993**, *410*, 188.
(7) Knight, J. S.; Freeman, C. G.; McEwan, M. J.; Smith, S. C.; Adams, N. G.; Smith, D. *Monthly Notices of the Royal Astronomical Society* **1986**, *219*, 89.
(8) Theule, P.; Borget, F.; Mispelaer, F.; Danger, G.; Duvernay, F.; Guillemin, J. C.; Chiavassa, T. *Astronomy & Astrophysics* **2011**, *534*.
(9) Lakhlifi, A.; Killingbeck, J. P. *Surface Science*, *604*, 38.
(10) Elsila, J. E.; Dworkin, J. P.; Bernstein, M. P.; Martin, M. P.; Sandford, S. A. *Astrophysical Journal* **2007**, *660*, 911.
(11) Gerakines, P. A.; Moore, M. H.; Hudson, R. L. *Icarus* **2004**, *170*, 202.
(12) Woon, D. E. *Computational and Theoretical Chemistry*, *984*, 108.
(13) Hiraoka, K.; Takayama, T.; Euchi, A.; Handa, H.; Sato, T. *Astrophysical Journal* **2000**, *532*, 1029.
(14) Hiraoka, K.; Sato, T.; Sato, S.; Takayama, T.; Yokoyama, T.; Sogoshi, N.; Kitagawa, S. *Journal of Physical Chemistry B* **2002**, *106*, 4974.
(15) Gardner, F. F.; Winnewisser, G. *Astrophysical Journal* **1975**, *195*, L127.
(16) Matthews, H. E.; Sears, T. J. *Astrophysical Journal* **1983**, *272*, 149.
(17) Agundez, M.; Fonfria, J. P.; Cernicharo, J.; Pardo, J. R.; Guelin, M. *Astronomy & Astrophysics* **2008**, *479*, 493.
(18) Hiraoka, K.; Ushiama, S.; Enoura, T.; Unagiike, H.; Mochizuki, N.; Wada, A. *Astrophysical Journal* **2006**, *643*, 917.
(19) Fuchs, G. W.; Cuppen, H. M.; Ioppolo, S.; Romanzin, C.; Bisschop, S. E.; Andersson, S.; van Dishoeck, E. F.; Linnartz, H. *Astronomy & Astrophysics* **2009**, *505*, 629.
(20) Bolina, A. S.; Wolff, A. J.; Brown, W. A. *Journal of Physical Chemistry B* **2005**, *109*, 16836.

# Chapter 8 – Conclusions and Further Work

## 8.1 Conclusions

In this thesis, the results of laboratory experiments studying the reactions of oxygen and hydrogen atoms with various astrophysically relevant molecular ices under interstellar conditions have been presented. Specifically, the temperature dependences of the product yields of these reactions have been recorded and used to derive estimates of the respective rate constants. These experimental studies indicate that the energy barriers to surface reactions are often substantially lower than the barriers to the corresponding gas phase reactions, meaning that reactions which in the gas phase would have too large an activation energy to proceed under the low temperature conditions of the ISM may, in fact, proceed on dust grain surfaces. A second key observation to arise from the experiments discussed in this thesis is that separate contributions to product yields from the ER and LH surface reaction mechanisms can be observed for many reactions.

A major focus of the experimental studies presented in this thesis is the surface chemistry of sulfur under interstellar conditions. Until now, all previous astrochemical studies of sulfur chemistry had focussed on those reactions initiated by energetic processing of sulfur bearing ices by UV photons or energetic electrons. The studies discussed in Chapters 5 and 6 represent the first experimental investigations of the thermal reactivity of sulfur bearing ices and suggest that sulfur exhibits a very rich solid state thermal chemistry under interstellar conditions, perhaps helping to explain the apparent depletion of gas phase sulfur bearing molecules in the ISM.

Other experimental studies presented in this thesis have been directed towards reactions which form potential precursors of prebiotic molecules such as those containing carbonyl and amine groups. Again, the results of these studies suggest that thermal reactions at grain surfaces in the interstellar medium potentially play a greater role in the formation of complex molecules than previously anticipated.

The reactions discussed in Chapters 3 – 7 are those which have been found to produce observable yields of reaction products under the current experimental conditions and do not represent a complete list of all of the reactions investigated during this work. Some potential reactions were investigated which did not produce any observable products. In

the interests of brevity, these reactions were not discussed in this thesis. Nevertheless, the following list of those reactions which were investigated but for which no products were observed may be useful:

$CH_4 + O$

$NH_3 + O$

$CO + O$

$SO_2 + O$

$CH_3OH + O$

$c\text{-}C_2H_4O + O$

$CH_3CHO + O$

$CH_3CN + O$

$HCOOH + O$

$CH_3COOH + O$

$CH_4 + H$

$NH_3 + H$

$CH_3OH + H$

$CH_3CN + H$

$HCOOH + H$

$CH_3COOH + H$

$HCOOCH_3 + H$

It is important to emphasize that under the current experimental arrangement only closed shell species can be detected efficiently, thus the presence of a reactant pair in the above list does not imply that no reaction occurs between them, only that any reaction does not give rise to detectable amounts of a closed shell product. Furthermore, if no reaction product was observed at a surface temperature of either 15 or 40 K, the

investigation of that reaction was not pursued further. Therefore, the formation of a product at other surface temperatures cannot be definitively discounted.

## 8.2 Further Studies of the Reactions of Oxygen and Hydrogen Atoms

In the previous chapter, the reactions of acrylonitrile with both thermal hydrogen and oxygen atoms was studied with a view to exploring some broad trends in the reactivity of unsaturated bonds under interstellar conditions. In particular, this reaction provided a convenient system for comparing the reactivity of C=C double bonds with C≡N triple bonds. However, as discussed in the previous chapter, the kinetics of the reaction of acrylonitrile with oxygen atoms, as well as the products which this reaction forms, are still not clear. An obvious first step in any follow up work is therefore to attempt to identify the oxygenated products of the reaction of acrylontirile with O atoms and also to try to separate the kinetics of the first oxygenation step and those of the second oxygenation step. Some insight into the site of the reaction of the initial O atom with acrylonitrile could be gained by studying the reaction of O atoms with propanenitrile. In the propanenitrile molecule, the CN group is bonded to a fully saturated ethyl ($C_2H_5$-) group as opposed to the vinyl ($C_2H_3$-) group present in acrylonitrile. One would therefore expect that any oxygenation reaction with propanenitrile would occur at the unsaturated C≡N bond rather than at the relatively inert alkyl group. Thus, the absence of a reaction between propanenitrile and O atoms would indicate that oxygen atoms react with acrylonitrile at the C=C bond. Such an indication of the site of reaction of the first oxygen atom would eliminate some of the possible isomers of the $C_3H_3NO$ product and perhaps make it feasible to calculate the ionization energies of the remaining isomers and hence perform MPI experiments to identify the product.

If the singly oxygenated product of the reaction of acrylonitrile with O atoms could be identified, it would in principle be possible to study the reaction of this species with oxygen atoms separately. Studying the separate oxygenation steps in this way would allow the kinetics of the second oxygenation step to be deconvoluted from those of the first oxygenation step. Consequently, it would be possible to determine the barriers for each reaction step definitively.

It would be valuable to extend this work on the relative reactivity of different unsaturated bonds to include the C≡C triple bond. Alkynes are abundant in the

interstellar medium, particularly in the form of long chain cyanopolyynes such as $HC_{11}N$. To this end some preliminary investigations have been carried out on the reaction of O atoms with propyne, $C_3H_4$. This reaction was studied at 40 K and was found to produce both a singly and doubly oxygenated product. However, some caution is required in interpreting this result as indicating that the C≡C bond reacts with O atoms because materials such as $SiO_2$ catalyse the tautomerization of propyne into propadiene.[1] Clearly then, given that the propyne passes through the Pyrex capillary of the microwave discharge cell before it reaches the HOPG surface, one may expect some propadiene to be present in the ice. Thus, it is possible that oxygen atoms in fact react with the two C=C double bonds in propadiene instead of the C≡C triple bond of propyne. It would therefore be preferable to study the reaction of acetylene with O atoms. Additionally, given the prevalence of cyanopolyynes in the interstellar medium, studies of the reactivity of molecules containing both C≡C and C≡N bonds under interstellar conditions would also be of particular interest. Whilst long chain cyanopolyynes are unstable under terrestrial conditions, some of the shorter chain species such as cyanoacetylene, $HC_3N$, can be synthesized and stored for several weeks.[2,3] Cyanoacetylene would therefore be a convenient analogue for longer chain species found in the interstellar medium for use in laboratory studies.

In addition to studying the astrochemical surface reactions of alkyne derivatives, it would also be worthwhile extending the studies of C=C double bond containing molecules presented in this thesis to include aromatic species. If aromatic C=C bonds are found to be reactive under interstellar conditions, it may be expected that the polyaromatic hydrocarbons present in the interstellar medium would also undergo reactions with atomic species such as O atoms. Again, a preliminary experiment has been carried out in which the reaction of toluene with O atoms at 40 K has been studied. This preliminary investigation showed that a singly oxygenated product is formed. Unfortunately, any potential doubly or triply oxygenated products would have been outside the mass range investigated in this experiment, but could easily be detected in future experiments by extending the mass range of the mass spectra.

## 8.3 Further Studies of the Reactions of Other Atoms and Radicals

The studies discussed in this thesis have all focussed on the reactions of oxygen and hydrogen (or deuterium) atoms. Oxygen and hydrogen atoms were chosen for these

studies because they are the first and third most abundant elements in the Universe and as such the reactions of these atoms might be expected to play a particularly significant role in the chemistry of the interstellar medium. However carbon and nitrogen have similar, if slightly lower, abundances to oxygen and so one possible future direction for the work presented in this thesis is to investigate surface reactions of C and N atoms. Some effort has already been directed toward producing a sufficient flux of nitrogen atoms for experimental investigations of their reactions to be carried out. In these experiments, nitrogen atoms were produced by using $N_2$ gas in the microwave discharge. Whilst many investigators produce N atom beams using simple microwave discharge cells in this way without modification, McCullough *et al* show that an enhanced dissociation efficiency can be obtained by applying an axial magnetic field to the discharge cell.[4] Therefore, in order to obtain the maximum possible flux of N atoms, an axial magnetic field to the discharge cell by passing an electrical current through a coil of wire wrapped around the atom source. However, a rather low dissociation efficiency of a few percent was obtained for N atoms. Whilst the exceptionally strong N≡N bond in $N_2$ is undoubtedly a factor in this low dissociation efficiency, it was also discovered that N atoms were efficiently scavenged by traces of oxygen containing species in the discharge to produce NO. Clearly then considerable effort will be required in order to purify the $N_2$ prior to it reaching the microwave discharge cell. Production of carbon atoms using the current experimental arrangement, whilst simple in principle, also presents some experimental challenges. These difficulties arise due to the fact that whichever gas phase precursor is used for carbon atom production, other reactive species will also be present. For example, microwave discharges in CO are sometimes used to produce carbon atoms, but these will of course also produce abundant O atoms.[5] These O atoms may preferentially react with the co-reactant or alternatively they may recombine with C atoms on the surface reducing the amount of C atoms available for reaction.

A similar problem is faced when one considers the production of sulfur atoms. The reactions of sulfur atoms would be a logical extension of the studies of thermal sulfur chemistry on grain analogue surfaces presented in this thesis. However, as is the case for carbon atoms, the obvious gas phase precursors would produce other reactive species which may complicate product identification. For example, if $SO_2$ were to be used it would be difficult to distinguish between the addition of one sulfur atom or two oxygen atoms to the co-reactant molecule. In principle the $^{34}S$ peaks may be used to

distinguish between these two processes, but, in practice, product yields are typically too small for the naturally occurring isotopomers to be detected. The prospects for studying the reactions of sulfur atoms using the current experimental arrangement are somewhat better than in the case of carbon atoms due to the higher vapour pressure of elemental sulfur. When heated to approximately 115 °C, the vapour pressure of $S_8$ is sufficiently high that it can be diluted in argon and used directly in a microwave discharge to produce sulfur atoms.[6] However, even this method would likely produce several reactive sulfur species such as $S_2$ and $S_3$ in addition to S atoms. Such polymerization reactions could be reduced by increasing the dilution of sulfur vapour in argon but only at the expense of reducing the flux of sulfur atoms.

It is clear from the above discussion that microwave discharge sources are most suited to producing atomic species from homonuclear diatomic precursors such as $H_2$, $N_2$, $O_2$, and $X_2$ (where X is a halogen atom). What is really required in order to effectively study the reactions of atoms such as S and C, as well as molecular radicals such as CN, is a means of producing clean beams of radicals. An experimental apparatus which enable the surface reactions of clean beams of radicals to be investigated is currently under development at UCL. Briefly, this apparatus would produce clean beams of radicals by first mass selecting a beam of an appropriate anion and then using a laser to detach the electron to leave a mass selected beam of neutral radicals. In addition to studying the surface reactions of radical species such as S, C and CN, such an experimental apparatus will also be valuable in providing greater insight into reaction mechanisms. For example, the formation of nitrosamine, $NH_2NO$, in the reaction of NO with H atoms could be further elucidated by studying the reaction of amino radicals, $NH_2$ with nitric oxide, NO, ice. If this reaction between NO and $NH_2$ proceeds under interstellar conditions, it would provide strong evidence that in the reaction of NO and H atoms, nitrosamine is formed *via* the initial formation of $NH_2$ followed by its reaction with an NO molecule. More generally, this technique will allow the kinetics of the different reaction steps of an overall reaction scheme to be deconvoluted from each other and, in some cases, enable the definitive determination of the rate determining step.

## 8.4 Summary

This chapter has provided an overview of some of the potential future directions for the work presented in this thesis. Some of these potential future studies would involve

directly extending the current work on the reactions of oxygen and hydrogen atoms, both to study their reactions with other astrophysically relevant molecules and to provide a more detailed understanding of the reactions discussed in Chapters 3 – 7. Alternatively, the techniques used in the experiments discussed in the preceding chapters could be extended and adapted to study the reactions of other atoms such as C, N and S and molecular radicals such as CN and OH. In any case it is clear that with more sensitive telescopes, such as the Atacama Large Millimetre Array (ALMA) and the James Webb Space Telescope (JWST), coming online over the next few years, the number of molecules detected in interstellar ices, and with them the number of questions to be addressed by laboratory astrochemistry experiments, is only likely to rise.

## 8.5 References


(1) Cordes, J. F.; Gunzler, H. *Chemische Berichte-Recueil* **1959**, *92*, 1055.
(2) Miller, F. A.; Lemmon, D. H. *Spectrochimica Acta Part a-Molecular Spectroscopy* **1967**, *A 23*, 1415.
(3) Clarke, D. W.; Joseph, J. C.; Ferris, J. P. *Icarus* **2000**, *147*, 282.
(4) Geddes, J.; McCullough, R. W.; Higgins, D. P.; Woolsey, J. M.; Gilbody, H. B. *Plasma Sources Science & Technology* **1994**, *3*, 58.
(5) Hiraoka, K.; Miyagoshi, T.; Takayama, T.; Yamamoto, K.; Kihara, Y. *Astrophysical Journal* **1998**, *498*, 710.
(6) Hassanzadeh, P.; Andrews, L. *Journal of Physical Chemistry* **1992**, *96*, 79.

# Appendix A – Generation of Higher Harmonic Light

For both the MPI and REMPI schemes used in the experiments discussed in this thesis, ultraviolet (UV) photons are required. The visible beam (440 – 500 nm) from the tuneable dye laser is therefore frequency doubled to give photons with wavelengths in the range 225 – 250 nm. A non-linear crystal of barium borate (β-$BaB_2O_4$, BBO) is used to produce the frequency doubled light. This section provides a brief overview of the principle of frequency doubling.

A beam of light propagating through a non-linear crystal such as BBO induces electric dipoles in the solid crystal which interact with the oscillating electric field of the electromagnetic wave. The induced dipole moment, $\mu$, is given by a power series, as shown in Equation A.1:

$$\mu = \alpha E + \frac{1}{2}\beta E^2 + \frac{1}{6}\gamma E^3 + \ldots \quad \text{A.1}$$

where $E$ is the magnitude of the oscillating electric field, and α, β and γ are the polarizability, hyperpolarizability and second order hyperpolarizability of the medium respectively. Additionally, the magnitude of the electric field, $E$, at a given time, $t$, is given by:

$$E = E_0 \sin(\omega t) \quad \text{A.2}$$

where $E_0$ is the amplitude of the oscillation of the electric field and $\omega$ is the angular frequency. Therefore, from standard trigonometric relationships, the $E^2$ term in Equation A.1 can be written as:

$$E^2 = \frac{1}{2}E_0^2(1 - \cos(2\omega t)) \quad \text{A.3}$$

Combining Equations A.1 and A.3, and assuming γ is negligible, the induced dipole is given by:

$$\mu \approx \alpha E + \frac{1}{4}\beta {E_0}^2 - \frac{1}{4}\beta {E_0}^2 \cos(2\omega t) \quad \text{A.4}$$

From Equation A.4, the induced dipole moment has a contribution from a term with angular frequency double that of the incoming electromagnetic radiation and so the second harmonic of the laser light is emitted. It should also be noted that given the

power series above, the induced dipole moment would also have higher harmonic contributions. However, these contributions are small and so have been disregarded here for clarity. Second harmonic generation may only take place in non-centrosymmetric crystals which have a non-linear response to an applied field.

The second harmonic light produced in a non-linear crystal will be an extraordinary ray (with an electric field vector parallel to the optic axis of the crystal) if the incident light is an ordinary ray (with an electric field vector perpendicular to the optic axis). The refractive index of the crystal is isotropic for the ordinary ray but anisotropic for the extraordinary ray. The coherence length, the length for which the incident wave and the second harmonic wave remain coherent, is inversely proportional to the difference in refractive indices of the crystal for the ordinary and extraordinary rays, $\Delta n$. Hence, if, as shown in Figure A.1, the incident beam enters the crystal at angle $\theta$, $\Delta n$ becomes approximately zero and the waves are phase-matched. Under phase-matching conditions the coherence length is greatly increased and the yield of second harmonic light is enhanced.

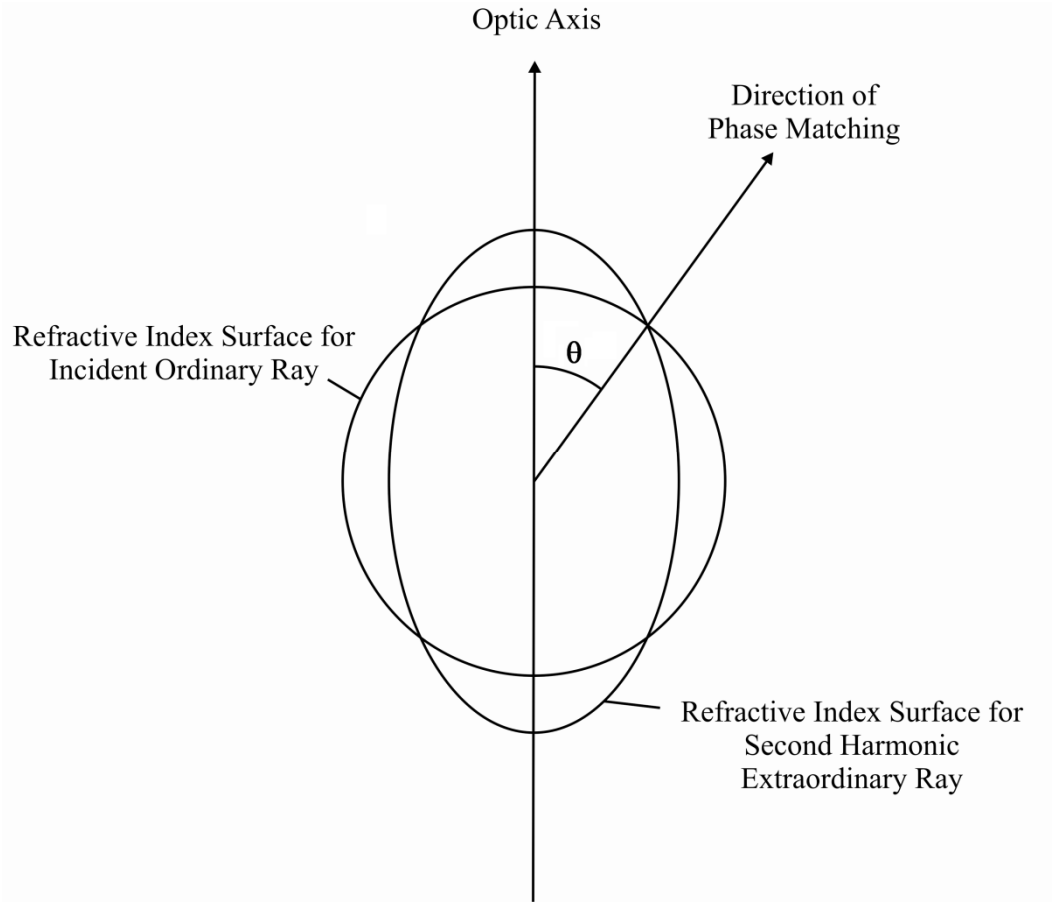


Figure A.1 A diagram showing the origin of the angular dependence for phase matching conditions.

The angle, $\theta$, at which $\Delta n$ reaches a minimum is dependent upon the wavelength of the fundamental beam. Thus, in order to ensure that the laser power remains constant when the wavelength is changed, for example during a REMPI scan, the BBO crystal is mounted on computer controlled motors which adjust the angle of the crystal according to user defined 'look up tables'. These look up tables are essentially plots of the motor position at which the optimum second harmonic beam power is obtained against wavelength and are created by the user simply by optimising the motor position, and hence second harmonic generation, at several wavelengths throughout the range required.

After having passed through the BBO crystal both the fundamental and frequency doubled beams pass through a compensator crystal. This crystal is necessary to correct for the refraction of the beam by the BBO crystal. Both beams then pass into a prism box in which the fundamental beam is diverted to a beam dump. The prism box contains four Pellin-Broca prisms whose orientations are adjusted such that only the second harmonic light is diverted around the four prisms. The second harmonic light leaves the prism box on the same path on which it entered. The beam is then reflected into the UHV chamber by two UV steering mirrors.

The maximum UV beam power achievable when the dye laser is pumped with 100 mJ per pulse light from the Nd:YAG laser is typically 2 mJ per pulse giving an overall conversion efficiency of approximately 2 %. Immediately before entering the UHV chamber the beam is focussed down to an intense waist by a UV lens with a 30 cm focal length. The focus of the beam has a minimum radius of 0.15 mm. The maximum power density per pulse for a typical 4 ns pulse can therefore be calculated as follows:

$$\frac{2 \times 10^{-3}}{4 \times 10^{-9}} \cdot \frac{1}{\pi(0.15 \times 10^{-3})^2} = 7.1 \text{ TW m}^{-2} = 0.71 \text{ GW cm}^{-2} \qquad \text{A.5}$$

This power density is more than sufficient for multi photon ionization experiments.[1,2]

## References

(1) Rebentrost, F.; Benshaul, A. *Journal of Chemical Physics* **1981**, *74*, 3255.
(2) Charalambidis, D.; Xing, X. *Journal of Physics B-Atomic Molecular and Optical Physics* **1991**, *24*, 127.